

12



SOLID STATE ELECTRONICS LABORATORY

STANFORD ELECTRONICS LABORATORIES
DEPARTMENT OF ELECTRICAL ENGINEERING
STANFORD UNIVERSITY · STANFORD, CA 94305

STUDY OF THE ELECTRONIC SURFACE STATES
OF III-V COMPOUNDS AND SILICON

Annual Technical Report

1 October 1980 to 30 September 1981

Principal Investigators:

W. E. Spicer
I. Lindau

Telephone: (415) 497-4643

Office of Naval Research
Department of the Navy
Arlington, Virginia 22217

Sponsored by

DEFENSE ADVANCED RESEARCH PROJECTS AGENCY
DARPA Order No. 3564
Program Code No. HX1241

Contract No. N00014-79-C-0072

Effective: 1 October 1980

Expiration: 30 September 1981 (237,629)

Stanford Electronics Laboratories
Stanford University
Stanford, California 94305

DISTRIBUTION STATEMENT A

Approved for public release;
Distribution Unlimited

82 05 17 181

DTIC
ELECTE
JUN 7 1982
S H D

AD A115208

DTIC FILE COPY

STUDY OF THE ELECTRONIC SURFACE STATES OF III-V COMPOUNDS AND SILICON

Annual Technical Report
1 October 1980 to 30 September 1981

Principal Investigators:

W. E. Spicer
I. Lindau

Telephone: (415) 497-4643

Office of Naval Research
Department of the Navy
Arlington, Virginia 22217

Sponsored by

DEFENSE ADVANCED RESEARCH PROJECTS AGENCY
DARPA Order No. 3564
Program Code No. HX1241

Contract No. N00014-79-C-0072

Effective: 1 October 1980

Expiration: 30 September 1981 (237,629)

Stanford Electronics Laboratories
Stanford University
Stanford, California 94305

The views and conclusions contained in this document are those of the authors and should not be interpreted as necessarily representing the official policies, either expressed or implied, of the Defense Advanced Research Projects Agency or the U.S. Government.

Contents

	<u>Page</u>
I. OVERVIEW	1
II. SUMMARY OF SELECTED TOPICS	2
A. Mechanism of Oxygen Chemi- sorption on GaAs	2
B. The Interaction of Oxygen with Si (111) Surfaces	3
III. ARTICLES PUBLISHED DURING PERIOD	5
APPENDICES	7

Chapter I

OVERVIEW

Our work during the past year has progressed in several areas. We list here the topics that comprise the majority of our efforts.

- (1) Si-Metal Contacts: We have investigated a number of transition metals (Ni, Pd, Pt, Ag) on Si to determine both the abruptness of the interface and the nature of the chemical bonding between Si and the metal. We have also examined in some detail the removal of the surface states on a cleaved Si surface by oxygen, cesium, and transition metals. These studies have advanced our understanding of the mechanism of Schottky barrier formation on Si.
- (2) Laser Enhanced Oxidation of GaAs (110): We have demonstrated an increase in the oxygen sticking probability on the GaAs (110) surface by exposure to low-intensity ($\leq 3 \text{ W/cm}^2$) laser radiation. We believe this enhancement is due to an increase in the density of free electrons at or near the surface.
- (3) Oxygen Chemisorption on GaAs (110): New valence band measurements, sensitive to very low (< 0.001 monolayer) oxygen coverages, have revealed that the chemisorbed state of oxygen on GaAs (110) consists of an oxygen bonded to a surface As in addition to an oxygen bridging between that As and a next nearest Ga.
4. Interface Between GaAs-Cs, O, and Vacuum in NEA Photocathodes: We have completed work which gives fundamental insight into the GaAs-Cs-O interface region and opens new possibilities for reducing the threshold of response (by using 3-5 semiconductor alloys) of negative electron affinity photocathodes, as well as making stable cathodes at lower wavelengths.
5. Interaction of Oxygen with Si (111): We have investigated the oxygen adsorption properties on both the Si surface cleaved at room temperature (which exhibits a 2×1 reconstruction) and the annealed surface (7×7 reconstruction). Our results have shown unambiguous support for the defect type model of the 7×7 surface.
6. Adsorption of Column III and V Elements on GaAs: We have found that the column III elements studied (Ga and Al) appear to form a metallic bond to the surface, thus forming two-dimensional "rafts" randomly oriented on the GaAs surface. In contrast, the column V element (Sb) gives evidence of a directional bond, resulting in an ordered overlayer.



Accession For	DTIC GRA&I	DTIC TAB	Unannounced	Justification	By	Distribution/	Availability Codes	Avail and/or	Dist	Special
	<input checked="" type="checkbox"/>	<input type="checkbox"/>	<input type="checkbox"/>	<i>See</i>	<i>See</i>					
										A

Chapter II

SUMMARY OF SELECTED TOPICS

Brief summaries of the aforementioned topics (3) and (5) are included here; summaries of the other topics will be found in our reports of the past year. More detailed accounts of our work in these areas appear in the appendices of this report as well as the appendices of previous and upcoming reports. Further information will be found in our proposal for the renewal of Contract No. N00014-79-C-0072 for the period 1 October 1981 to 30 September 1982.

A. Mechanism of Oxygen Chemisorption On GaAs

For both fundamental and practical reasons, we consider it very important to obtain a definitive understanding of the chemisorbed phase of oxygen on GaAs. This is the phase obtained with unexcited oxygen characterized by a completely resolved 2.9 eV As-3d shift and an asymmetric broadening of the Ga-3d peak (with a Ga shift of at most 0.7 eV). These shifts correspond to those obtained by Goddard's group (JVST 16, 1178 (1979)) for oxygen attached to a surface As without breaking any back bonds. This was also our original suggestion for the chemisorbed oxygen. Problems with this model involved the dynamics of the breakup of the O₂ molecule.

Goddard et. al. (private communication) and Mark et. al. (Thin Solid Films 56, 19 (1979); Crit. Rev. Solid State Sci. 5, 189 (1975)) suggested that this was done at defect sites with the oxygen uptake spreading outward from these sites. Our recent work shows that this is not the case. In addition, we have given definitive evidence that the model of Brundle et. al. (JVST 16, 1186 (1979)), which assumes that there is no chemisorbed state--only clusters of As₂O₃ and Ga₂O₃--is not correct. Finally, we have new

evidence for a second major adsorption site where, in addition to an oxygen bonded to an As, there is an oxygen bridging between that As and a next nearest Ga.

Essential to arriving at these conclusions have been extensive experiments. Included are the development of new valence band spectroscopy techniques in which very low concentrations of oxygen can be detected (<0.001 monolayer), thermal desorption, studies of the valence bands of Ga_2O_3 and As_2O_3 , and adsorption of oxygen on disordered sputtered Ga-rich GaAs (110) surfaces.

B. The Interaction of Oxygen with Si (111) Surfaces

It is well known that the Si (111) surface exhibits a 2×1 reconstruction after cleaving at room temperature and transforms to a 7×7 reconstruction after annealing at elevated temperatures ($>200^\circ$). Understanding the nature of these reconstructions is important in understanding the covalent bonding on the Si surface. Direct determination of the structure of the 7×7 reconstruction has so far been prohibited because of its complexity. During this reporting period, we have attempted to distinguish various models for the 7×7 reconstruction through detailed comparisons of the oxygen adsorption properties on the 2×1 and 7×7 surfaces. Our results have shown unambiguous support for the defect type model of the 7×7 surface.

We have also made progress in understanding the room-temperature oxygen adsorption configuration on the Si (111) 2×1 surface. By examining the evolution of the chemical shifts in Si 2p of oxygen-covered surfaces under heat treatments, we have eliminated many possibilities and have narrowed the choice to a few possible Si-O bonding configurations. These results suggest that more systematic studies of the annealing effects may be very important in understanding the Si-O bonding.

This work is not only important for gaining fundamental understanding of the Si surfaces but is also important in understanding the initial steps in oxidation of Si in VLSI applications.

Chapter III

ARTICLES PUBLISHED DURING PERIOD

1. Photoemission as a Tool to Study Solids and Surfaces, I. Lindau and W. E. Spicer, Chapter 6 in "Synchrotron Radiation Research", edited by H. Winnick and S. Doniach, Plenum Press (1980), pp. 159-221.
2. Column III and V Elements on GaAs (110); Bonding and Adatom-Adatom Interaction, P. Skeath, C. Y. Su, I. Lindau, and W. E. Spicer, J. Vac. Sci. Tech. 17(5), (Sept.-Oct. 1980), pp. 874-879.
3. Si-Pd and Si-Pd Interfaces, J. N. Miller, S. A. Schwarz, I. Lindau, and W. E. Spicer, J. Vac. Sci. Tech. 17(5), (Sept.-Oct. 1980), pp. 920-923.
4. Photoemission Investigation of the Temperature Effect of Si-Au Interfaces, I. Abbati, L. Braicovich, A. Franciosi, I. Lindau, P. R. Skeath, C. Y. Su, and W. E. Spicer, J. Vac. Sci. Tech. 17(5), (Sept.-Oct. 1980), pp. 930-935.
5. Oxygen Adsorption of the GaAs (110) Surface, C. Y. Su, I. Lindau, P. W. Chye, P. R. Skeath, and W. E. Spicer, J. Vac. Sci. Tech. 17(5), (Sept.-Oct. 1980), pp. 936-941.
6. Systematics on the Electron States of Silicon d-Metal Interfaces, L. Braicovich, I. Abbati, J. N. Miller, I. Lindau, S. Schwarz, P. R. Skeath, C. Y. Su, and W. E. Spicer, J. Vac. Sci. Tech. 17(5), (Sept.-Oct. 1980), pp. 1005-1018.
7. Unified Defect Model and Beyond, W. E. Spicer, I. Lindau, P. Skeath, C. Y. Su, J. Vac. Sci. Tech. 17(5), (Sept.-Oct. 1980), pp. 1019-1022.
8. Fermi Level Pinning at 3-5 Semiconductor Interfaces, W. E. Spicer, P. Skeath, C. Y. Su, and I. Lindau, Proc. of the XV International Conf. on the Physics of Semiconductors, Kyoto (Sept. 1980); J. Phys. Soc. Japan 49, (1980), Supp. A, pp. 1079-1087.
9. Oxidation of Si (111), 7 x 7 and 2 x 1, a Comparison, C. Y. Su, P. Skeath, I. Lindau, and W. E. Spicer, Proc. of the 27th National Vacuum Symposium, (Oct. 1980); JVST 18(3), (Mar.-Apr. 1981), Part II.
10. The Nature of the 7 x 7 Reconstruction of Si (111): As Revealed by Changes in Oxygen Sorption from 2 x 1 to 7 x 7, C. Y. Su, P. R. Skeath, I. Lindau, and W. E. Spicer, Surf. Sci. 107 (1981), L 355.
11. Nature of the Valence States in Silicon Transition Metal Interfaces, G. Rossi, I. Abbati, L. Braicovich, I. Lindau, and W. E. Spicer, Sol. State Commun. 39, (1981), p. 195.

12. New Fermi Energy Pinning Behavior of Au on GaAs (110) Suggesting Increased Schottky Barrier Heights on n-Type GaAs, P. Skeath, C. Y. Su, I. Hino, I. Lindau, and W. E. Spicer, Appl. Phys. Lett. 39(4), (1981), p. 349.
13. The Adsorption of Oxygen on the GaAs (110) Surface, I. Lindau, C. Y. Su, P. R. Skeath, and W. E. Spicer, Proc. Fourth International Conf. on Solid Surfaces and the Third European Conf. on Surface Science, 22-26 September 1980, Cannes, France, Supplement a la Revue "Le Vide, Les Couches Minces", No. 201, 1980, p. 979, edited by D. A. Degas and M. Costa.

APPENDICES

- A. I. Abbati, G. Rossi, L. Braicovich, I. Lindau, and W. E. Spicer, "Reactive Germanium/Transition Metal Interfaces Investigated with Synchrotron Radiation Photoemission: Ge/Ni and Ge/Pd," Appl. Surf. Sci. 9, 000 (1981).
- B. Perry Skeath, C. Y. Su, I. Lindau, and W. E. Spicer, "Experimental Determination of the Bonding of Column 3 and 5 Elements on GaAs," J. Cryst. Growth 56, 505 (1982).
- C. W. E. Spicer, "Use of Photoemission with Synchrotron Radiation to Probe Surfaces on an Atomic Scale," in Surfaces and Interfaces in Ceramic and Ceramic-Metal Systems, edited by Joseph Pask and Anthony Evans (Plenum, 1981), p. 51.
- D. C. Y. Su, Ph.D. Dissertation (Stanford, 1981).

APPENDIX A

Reactive Germanium/Transition Metal Interfaces
Investigated with Synchrotron Radiation Photo-
emission: Ge/Ni and Ge/Pd

I. Abbati, et. al.

Published in Appl. Surf. Sci. 9, 000 (1981)

REACTIVE GERMANIUM/TRANSITION METAL INTERFACES
INVESTIGATED WITH SYNCHROTRON RADIATION PHOTOEMISSION:
Ge/Ni AND Ge/Pd

I. ABBATI*, G. ROSSI, L. BRAICOVICH†, I. LINDAU and W.E. SPICER
Stanford Electronics Laboratories, Stanford University, Stanford, CA 94305, USA

Received 6 July 1981

Revised manuscript received 29 September 1981

We report the first photoemission studies of the electronic structure at the interface between Ge(111) and d-metal overlayers at monolayer coverages. Two systems are discussed, Ge(111)/Pd and Ge(111)/Ni. In the case of Ge(111)/Pd a broad, reacted germanide-like phase is formed with similar electronic features to the Si(111)/Pd interface. In the Ge(111)/Ni case an evolution of the valence band structure versus coverage from a reacted situation to a metal rich situation is found, indicating a strong gradient of concentration. The interface is narrower than for Ge/Pd. Photoemission spectra of the valence band at $h\nu = 80$ eV are presented as well as core line data of the Ge 3d which show the trends in binding energy shifts and the changes in the relative intensities as a function of metal coverage. The discussion is carried out on the differences in the growth of these interfaces and comparisons are made to the correspondent silicide/metal systems.

1. Introduction

The study of Si d-metal interfaces with photoelectron spectroscopy and other techniques of electron spectroscopy has provided an extraordinary amount of information about the electronic structure [1-10]. The interaction processes taking place in the interface region have been elucidated and the connection between interface reaction products and bulk silicides is now basically understood. Moreover the nature of the chemical bond in silicides has been examined in detail at least in the case of Ni, Pd [1] and Pt, i.e. the transition metals next to the noble metals in the periodic table [1,4]. These investigations have been pursued in close collaboration between theory and experiment.

Nevertheless an extensive systematic understanding of the interfaces between elemental group IV semiconductors and d-metals is still lacking basically for two reasons:

* Permanent address: Istituto di Fisica del Politecnico, Milano, Italy.

74305

(i) The study of the interfaces between Si and refractory d-metals is still at the beginning [6].

(ii) No spectroscopic information on Ge d-metal interfaces is available at present (in particular no reactive Ge transition metal interface has been studied with photoemission).

A wide empirical basis is of paramount importance to establish the trends of the electron states when the semiconductor (Si or Ge) or the d-metal are changed. The knowledge of these trends is extremely useful for a better understanding of the interface formation mechanism and to discriminate between different models for the interface growth. The present paper should be regarded as a step forward in this direction since it is the first presentation of photoemission results from reactive Ge d-metal interfaces. We present here results on Ge(111)-Ni and Ge(111)-Pd interfaces. We point out analogies and differences with respect to Si(111)-Ni and Si(111)-Pd interface and show the usefulness of a comparison between the silicon and Ge interfaces.

Photoemission results were obtained on cleaved Ge(111) covered with increasing amounts of Ni and of Pd. Since this is the first presentation of results for Ge interfaces of this kind the present paper is centered on the general trends of the electron states seen at increasing coverages θ (hereafter measured in monolayer units). A more detailed study of the θ -dependence at very low coverages comparable to those in the Si case [5], has been left for future investigations.

2. Experimental

N-type Ge(111) samples were cleaved in UHV (operative pressure $< 10^{-10}$ Torr) and the metal depositions were made thermally from high purity Pd and Ni thin wires at pressures within the 10^{-10} Torr range. The cleanliness of the sample was checked by XPS analysis. The angle integrated photoelectron spectra were recorded with a double pass cylindrical mirror analyzer with the axis normal to the sample surface. The light source was synchrotron radiation (SR) from the SPEAR storage ring at SSRL and a "grasshopper" monochromator was used for the monochromatization. The light was striking the sample at grazing incidence with an angle of 15° relative to the sample surface. Both valence band photoemission and Ge 3d core line photoemission were carried out with excitation energies giving kinetic energies of the photoelectrons close to the minimum of the escape depth. The two sets of measurements thus have the same degree of surface sensitivity and are directly comparable.

The excitation energies used were $h\nu = 80$ eV for the valence band which, in addition to the short escape depth, gives a high sensitivity of the d-contribution to the energy distribution curves (EDC's). Photoemission at the 4d Cooper minimum [4,5] in the Pd case to recover the sp contribution in the valence band EDC of Ge has been left to future investigations.

The Ge 3d core lines with a binding energy of about 30 eV were measured with $h\nu = 120$ eV which is the best compromise between intensity, cross section (surface sensitivity) and instrumental (escape depth) resolution.

3. Results

The relevant experimental information is summarized in a synthetic way in the figures. The valence band EDCs for Ge(111)-Pd and Ge(111)-Ni are given as a func-

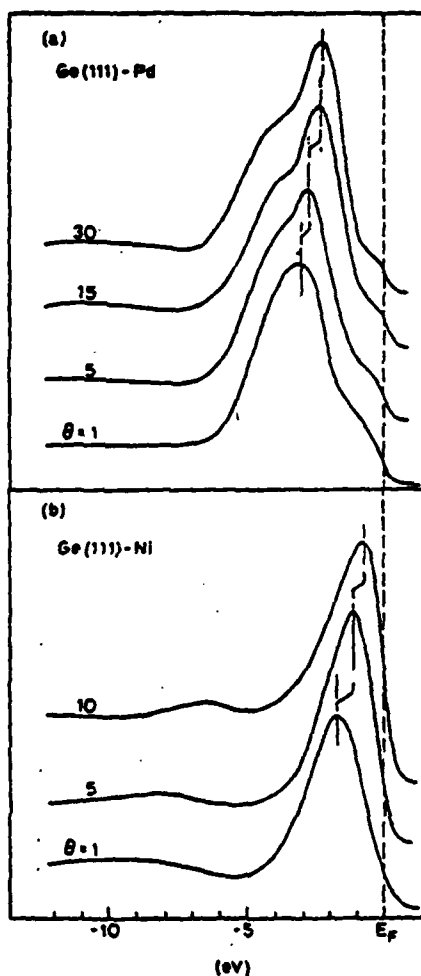


Fig. 1. Angle integrated valence photoelectron spectra ($h\nu = 80$ eV) from Ge(111) at increasing Pd (a) and Ni coverages (b); coverages in monolayer units.

tion of θ in fig. 1a and 1b, respectively. The dominant feature in these spectra is the d contribution. In fig. 2b we give the ratio R of the counting rates from the valence band d-metal and from the Ge 3d lines. The counting rate from the metal is taken from the peak of the valence states where the d-contribution is dominant since no deeper lying metal core lines could be used with sufficiently good resolution and intensity due to the limitation in the grasshopper output above the carbon-edge. The ratio R is given in arbitrary units since an absolute calibration was not possible due to the lack of knowledge of the 3d photoionization cross section in Ge-metal mixed systems. In fig. 2a is plotted the variation of the Ge 3d binding energy versus metal coverage by taking as a reference point the position at $\theta = 1$ where a superficial metallic phase is already developed (see the valence band EDCs in fig. 1). With this treatment of the data the core line position is referred to a metallic situation and no ambiguities due to band bending effects are present in the analysis in the interval covered in the present investigation ($\theta \geq 1$).

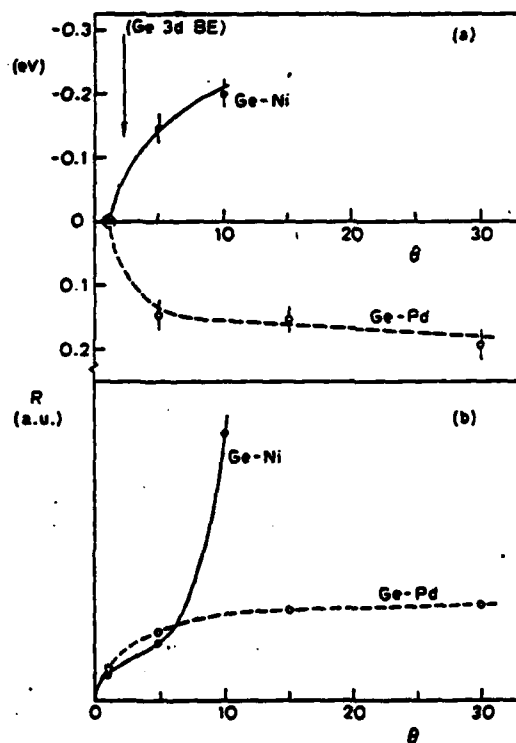


Fig. 3. Coverage dependence of the Ge 3d core line binding energy shift (referred to the $\theta = 1$ core line position) in Ge-Ni and Ge-Pd as a function of coverage θ in monolayer units (a). The ratio R (in arbitrary units) between the metal and Ge concentrations in Ge-Ni and Ge-Pd (b).

Before proceeding to the discussion it is important to note the following aspects of the experimental results: (i) The shape of the valence band density of states is very similar to that of the corresponding Si(111)-Pd and Si(111)-Ni interfaces [5]. In particular in the Ge(111)-Pd case the shape of the EDC is germanide-like also at the higher θ . (ii) The θ dependence of the ratio R between metal and Ge is considerably different in the two cases. In the Ni case R increases considerably while in Pd it levels off to an almost constant value (see fig. 2b). (iii) The Ge core level shift is opposite in the two interfaces (see fig. 2a), With the trend being towards lower binding energies in Ni and towards higher binding energies in Pd.

4. Discussion

The similarity between the valence band density of states in Ge and Si interfaces is not surprising, since the nature of the chemical bond [5] between the last column transition metal and the two elemental group IV semiconductors (Si and Ge) is expected to be the same. In this connection it is interesting to note that in Ge-Pd the composition of the reaction products reaches a nearly constant value indicating that even at room temperature something very similar to a well defined compound is formed, only a very small concentration gradient exists along the normal to the interface corresponding to a metal concentration increase. It is further well established [13] that in germanide formation the first nucleated compound is Pd_2Ge . Thus we attribute the plateau of fig. 2b to the formation of a Pd_2Ge -like interface in close analogy to Si-Pd interfaces. The important difference with respect to the Si-Pd case is the fact that higher coverages are required in Ge-Pd to reach the germanide-like situation. This point waits for a detailed thermodynamical investigation. For the time being we can rely upon the well recognized importance of condensation energy of the metal in promoting the intermixing [9,11,12]. The requirement of a greater coverage could be connected to a larger condensation energy of Pd on Ge i.e. a larger amount of energy release due to the Pd-Ge bond formation with respect to the Pd-Si case causing a stronger disruption in the interface region with a greater penetration of Pd into the substrate. Thus higher θ would be necessary to reach a Pd_2Ge -like situation. This is only a conjecture since the values of the condensation energy of these systems are not known at the present time. Another important point is the fact that the eutectic temperatures [15] in Ge are lower than in Si, thus indicating that intermixing at RT before Pd_2Ge formation could be easier in Ge-Pd than in Si-Pd.

The much higher concentration gradient in Ge-Ni than in Ge-Pd has its counterpart in Si-Ni and Si-Pd interfaces. In fact two possible models have been suggested for the Si systems. One of these modes is based on the much higher degree of order of Pd_2Si overgrowth as compared to Si-Ni due to the good lattice matching of Pd_2Si overgrowth as compared to Si-Ni due to the good lattice matching of Pd_2Si

and Si. Pd_2Si and Si are known to form rather sharp interfaces [1]. The barrier to interdiffusion in Si-Ni could be ascribed to the difficulty of mass transport across a disordered system [13]. Another possibility is the higher heat of formation of Si-Ni compounds makes it more difficult to create defects in the intermixed Si-Ni region so that defect assisted diffusion is less pronounced. For Ge it should be noted that the mismatch to hexagonal Pd_2Ge is higher than in the Si- Pd_2Si case and a lower degree of order is found as pointed out in [14]. Thus the different behavior of R in Si and Ge is a strong indication in favour of the fact that the degree of order is not the essential point. The poor knowledge of thermodynamical data (e.g. the heat of formation) on the Ge-transition metal compounds makes the discussion on this point difficult. Nevertheless we speculate, on the basis of Andrews and Phillips' [16] correlation between Schottky-barrier heights and heats of formation of silicides, that the Ni-Ge compounds have a higher heat of formation than to the Pd-Ge compounds.

Following this tentative speculation the defect formation energy, which is proportional to the heat of formation, would be higher for Ge-Ni than for Ge-Pd playing an important role in the interdiffusion. The lower barrier height of Ge-Ni is also consistent with the higher eutectic temperature if the same correlation with temperature as is assumed for Si [17].

The last thing we would like to point out is the opposite trend observed for the binding energy shifts of the Ge core lines (see fig. 2a). It is worthwhile noting that a similar behaviour has been found in the corresponding Si interfaces [2,5].

Our results for the Ge(111)-Ag interface, reported elsewhere [19], give the same trend as seen for Ge(111)-Ni with a chemical shift of the Ge 3d line signal towards the lower binding energies. In the interpretation of a small core line shift it is necessary to avoid oversimplified schemes based merely on charge transfer. In fact accurate calculations [18] of the valence states of Ni and Pd silicides show a charge transfer always from the metal to silicon in spite of the opposite trend of the Si 2p core lines. Presumably differences in relaxation energies, in the volume available to Si atoms and in the electron configuration can explain this behavior. For the present data it is thus premature to assess the charge transfer problem. Further theoretical work is required to put the available experimental results on a quantitative basis. We want to stress the importance of theoretical understanding of the core line chemical shifts since they may provide more information about the chemical bonding in the interface than the valence band structure.

5. Conclusion

In conclusion we have shown that in reactive Ge-Ni and Ge-Pd interfaces strong chemical interaction takes place also at room temperature with the formation of a germanide-like phase in Ge-Pd and with a rapidly varying concentration gradient in the Ge-Ni case. We have discussed the relevance of these results by a comparison of the available information on Ge and Si d-metal interfaces.

Acknowledgement

This work was supported by the GNSM of CNR, Italy and by ARPA of DOD monitored by ONR under contract No. N00014-79-C-0072. The experiments were done at SSRL which is supported by the National Science Foundation under Grant No. DMR77-27489 in collaboration with the Stanford Linear Accelerator Center and the Department of Energy.

References

- [1] G.W. Rubloff, P.S. Ho, J.L. Freeouf and J.E. Lewis, Phys. Rev. B 23 (1981) 4183.
- [2] P.J. Grunthaner, J. Grunthaner and J.W. Meyer, J. Vacuum Sci. Technol. 17 (1980) 924.
- [3] N.W. Cheung, R.J. Culberston, L.C. Feldman, P.J. Silverman, K.W. West and J.W. Meyer, Phys. Rev. Letters 45 (1980) 120.
- [4] G. Rossi, I. Abbati, L. Braicovich, I. Lindau and W.E. Spicer, Solid State Commun. 39 (1981) 195.
- [5] I. Abbati, G. Rossi, I. Lindau and W.E. Spicer, in: Proc. PCSI 8 Conf., J. Vacuum Sci. Technol. 19 (1981), 636.
- [6] A. Franciosi, D.J. Peterman and J.H. Weaver, to be published. *J. Vacuum Sci. Technol.* 19 (1981) 657.
- [7] P. Perfetti, S. Nannarone, F. Patella, C. Quaresima, A. Savoia, F. Cerrina and M. Capozzi, Solid State Commun. 35 (1980) 151.
- [8] L. Braicovich, C.M. Garner, P.R. Skeath, C.Y. Su, P.W. Chye, I. Lindau and W.E. Spicer, ~~J. Vacuum Sci. Technol. 17 (1980) 1005.~~ *Phys. Rev. B* 22 (1980) 22.
- [9] L. Braicovich, I. Abbati, J.N. Miller, I. Lindau, S. Schwarz, P.R. Skeath, C.Y. Su and W.E. Spicer, J. Vacuum Sci. Technol. 17 (1980) 1005.
- [10] I. Abbati, L. Braicovich, U. del Pennino, B. De Michelis and S. Valeri, in: Proc. 4th Intern. Conf. Solid Surfaces; Suppl. Le Vide et les Couches Minces n. 201 (Cannes, 1980) 1023.
- [11] I. Abbati, L. Braicovich, B. De Michelis and U. Del Pennino, J. Vacuum Sci. Technol. 17 (1980) 1003.
- [12] D. Gupta, K.N. Tu and K.W. Asai, Phys. Rev. Letters 35 (1975) 796.
- [13] G. Ottaviani and M. Costato, J. Crystal Growth 45 (1978) 365.
- [14] M. Hansen, Constitution of Binary Alloys (McGraw-Hill, New York, 1958).
- [15] J.M. Andrews and J.C. Phillips, Phys. Rev. Letters 35 (1975) 56.
- [16] G. Ottaviani, K.N. Tu and J.W. Mayer, Phys. Rev. Letters 44 (1980) 284.
- [17] O. Bisi and C. Calandra, private communication.
- [18] G. Rossi, I. Abbati, L. Braicovich, I. Lindau and W.E. Spicer, Phys. Rev. B., to be published.

OK!

1/11/81

APPENDIX B

Experimental Determination of the Bonding of Column 3
and 5 Elements on GaAs

P. Skeath, et. al.

Published in J. Cryst. Growth 56, 505 (1982)

EXPERIMENTAL DETERMINATION OF THE BONDING OF COLUMN 3 AND 5 ELEMENTS ON GaAs *

Perry SKEATH, C.Y. SU, I. LINDAU and W.E. SPICER **

Stanford Electronics Laboratories, Stanford University, Stanford, California 94305, USA

Following an introduction to the chemistry of the GaAs(110) surface, an experimental determination of the interfacial bond character between column 3 or column 5 elements and GaAs(110) is presented. The column 5-GaAs(110) bonds are directional (covalent) in character, while the column 3-GaAs(110) bonds are non-directional and apparently non-local in nature. Implications of these results for crystal growth are given. It is concluded that in 3-5 crystal growth, the column 5 atoms are expected to initiate the epitaxial alignment of a growing layer with the crystalline substrate.

1. Introduction

The microscopic processes which occur during the growth of a new lattice layer (single atomic or molecular layer) on a crystalline substrate are of fundamental interest. For example, surfaces of different crystallographic orientation on the same crystal may have different growth characteristics. This is due to the dependence of the surface layer's chemistry on the details of the bonding configuration of each atom within the surface unit cell. If the bonding configurations, and hence the chemistry, of a given surface lattice are well understood, then the bonding of crystal elements adsorbed on the surface may be investigated. From this, it may be learned which element is responsible for initiating the epitaxial growth of a new lattice layer. Subsequent steps in the growth of a lattice layer may then be studied.

In this paper we follow the sequence given above, first discussing the chemistry of the (110) surface of GaAs. Next, the bonding of column 3 (Al, Ga), and

column 5 (Sb) elements to GaAs(110) is examined, and finally the relationship of these data to GaAs (or more generally, 3-5 crystal) epitaxial growth is given.

2. Experimental

To gain an understanding of the microscopic processes which occur at a crystal surface during growth, it is necessary to use experimental techniques which will probe only the first atomic layer or two of the crystal surface. Photoemission electron spectroscopy (PES), supplemented by low energy electron diffraction (LEED), have been used in this work due to their high surface sensitivity. PES gives directly information on the bonding states at the surface [1] (both adsorbate and substrate), while proper analysis of LEED data (including multiple scattering effects) gives the crystal structure within the unit cell as well as the translational symmetry [2].

GaAs(110) crystal surfaces with low defect densities [3] and no contamination were prepared by cleavage under ultrahigh vacuum conditions (typically 10^{-10} Torr). After characterizing the clean surface with PES and/or LEED, adsorption of foreign materials was done by careful gas exposures [4] (O_2) or controlled evaporation from an elemental source (Al, Ga, Sb). PES and/or LEED measurements were typically repeated at several adsorbate coverages. Detailed descriptions of the experimental procedures may be found elsewhere [4-6].

* This work was supported by the Office of Naval Research under Contract No. N00014-75-C-0289 and by the Advanced Research Projects Agency of the Department of Defense (monitored by ONR) under Contract No. N00014-79-C-0072. Part of the work was performed at the Stanford Synchrotron Radiation Laboratory (SSRL) which is supported by the National Science Foundation, NSF DMR73-07692, in cooperation with the Stanford Linear Accelerator Center and the Department of Energy.

** Stanford W. Ascherman Professor of Engineering.

3. Background: the chemistry of GaAs(110)

LEED data have shown that the GaAs(110) non-polar surface has both the same translational symmetry (1×1 unit cell) and structure within the surface unit cell, regardless of whether it is prepared by cleaving, sputtering and annealing [3], or by molecular beam epitaxy [7] (MBE). However, it has been shown by LEED analysis [8,9] and by electron paramagnetic resonance measurements [10] that the structure within the surface unit cell is not the same as in the bulk. A reconstruction occurs such that the surface Ga atoms move 0.5 Å toward the crystal, and the surface As atoms move 0.2 Å away from the crystal [9].

This is understood on the basis of the chemistry of Ga and As [11,12]. The surface Ga atoms, having only three neighbors, tend toward a sp^2 hybridization, while the surface As atoms, also having a reduced coordination, tend to dehybridize toward

their atomic configuration. Both of these trends can be accommodated by a reconstruction of the surface lattice (see fig. 1).

Electronically, the reconstruction alters the partially occupied "dangling bond" states (sp^3) of the unreconstructed surface such that these states are shifted away from the band gap [11,13] (see fig. 1). The three valence electrons of the surface Ga atom are taken up in the three sp^2 bond orbitals, leaving an empty p_z state above the conduction band minimum (CBM). Thus, the partially occupied "dangling bond" state of the surface Ga atom shifts up in energy and becomes an empty p_z orbital. Of the five valence electrons on the surface As atoms, three are in p-like orbitals bonding to neighboring Ga atoms (back bonds), with the remaining two in an s-like "lone pair" configuration. Thus, the partially occupied "dangling bond" state of the surface As atom is replaced by a doubly occupied "lone pair" orbital, located well below the valence band maximum (VBM).

The effect of the reconstruction on the chemistry of the GaAs(110) surface is easily seen from studies of oxygen chemisorption. Considering only the properties of bulk Ga and As as separate elemental materials, one would expect oxygen to bind to the surface of bulk Ga in preference over the surface of bulk As. However, the Ga atoms on the reconstructed GaAs(110) surface do not have any nonbonding electrons available in a "lone pair" orbital. This suggests that oxygen atoms will adsorb on As sites in preference to Ga sites on a well-ordered reconstructed GaAs(110) surface [14], opposite to expectations based on bulk chemical thermodynamic properties of Ga and As.

Experimental data do, in fact, show a strong tendency for oxygen to bind to the surface As atoms. The chemical shift of the Ga 3d or As 3d core electrons gives a direct indication of the site and relative amount of oxygen adsorption on the surface. By performing photoemission electron spectroscopy (PES) using synchrotron radiation as a light source [15], the surface sensitivity of this measurement can be optimized such that only the first few lattice layers are sampled [1,15]. Chye et al. [16] have compared the oxidation of ordered vs disordered GaAs(110). In the case of a disordered (sputtered) surface, oxygen was found to bond to Ga in strong preference to As (ratio of oxidized Ga to oxidized As = 5 : 1), consistent with bulk thermodynamics. However, on the ordered

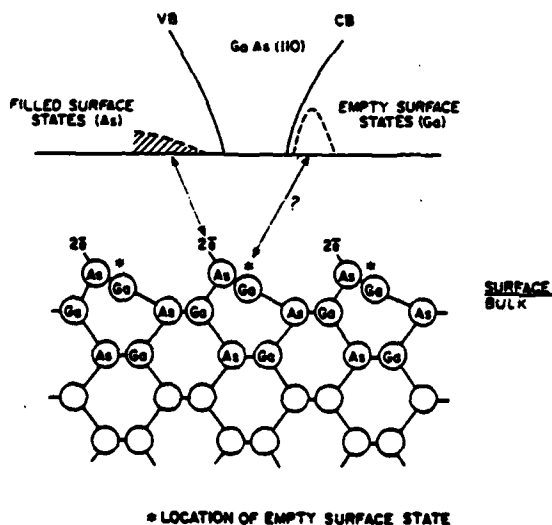


Fig. 1. A schematic illustration of the relationship between atomic and electronic structure of GaAs(110). The lower part of the figure shows a side view of the reconstructed surface, with two non-bonding electrons on the surface As atoms and an empty non-bonding orbital on each surface Ga atom. The density of electronic states versus energy is sketched in the upper half of the figure, showing occupied surface states below the valence band maximum and unoccupied surface states above the conduction band minimum. After Pianetta [26].

surface, a much stronger tendency for oxygen to bond to As is seen (ratio of chemically shifted As 3d to Ga 3d $\geq 1:1$, indicating that the chemical state imposed on the surface Ga and As atoms by the structure of the ordered surface has a strong influence on the surface chemistry).

Su et al. [17] have performed detailed experimental work involving thermally induced changes of the oxygen adsorption site on this surface and have examined several oxidation models based on their data. The interested reader is referred to their paper (and included references) for further analysis of oxygen adsorption on GaAs(110).

4. Results

4.1. Column 3 adatoms

Adsorption of both Al and Ga on GaAs(110) at room temperature was studied by PES and LEED. Only a brief summary of the data will be given here — more complete descriptions are available elsewhere [5,6,18,19].

Using an ultraviolet source (in this case, $h\nu = 21$ eV), detailed examination of the valence states of the semiconductor surface and the overlayer can be made. As increasing amounts of Ga were deposited on the surface, beginning with an average coverage (θ) of one-tenth monolayer (ML), attenuation of the photoemission EDC structure associated with the GaAs surface increased, indicating that the Ga overlayer was fairly uniform in thickness (see fig. 2). The early theoretical studies [20] of this system indicated that localized bonding of Al or Ga adatoms to the semiconductor surface lattice would produce new structure in the EDCs together with large changes in the surface lattice reconstruction. The absence of new peaks in the EDC as a function of coverage, together with a lack of qualitative change in the peaks of the clean surface, suggests that the bonding between Ga and GaAs is not of a localized, covalent nature and that the electronic states of the GaAs surface lattice are not strongly perturbed by the presence of a metallic overlayer. Similar results are obtained for Al overlayers [5]. LEED data have shown that the reconstruction of the GaAs(110) surface is unaffected by the presence of Al ($0.25 < \theta < 2$ ML)

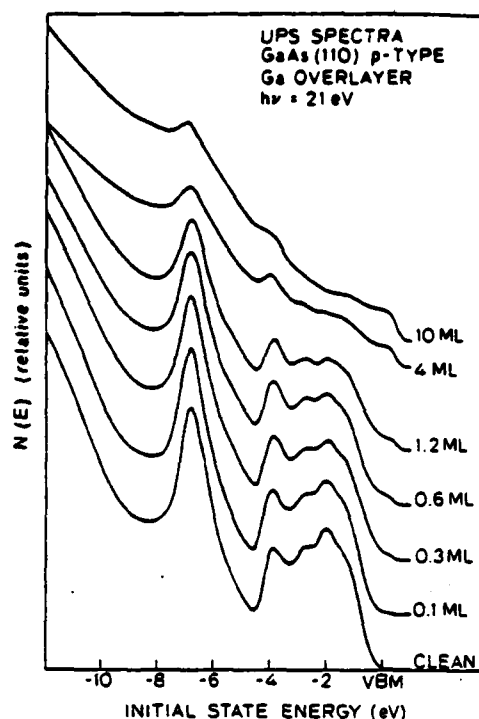


Fig. 2. UPS spectra showing emission from the valence electrons of GaAs + Ga adatoms for a series of Ga coverages. The lack of new structure in the upper valence band (-4 eV to VBM) indicates that a localized-bonding picture is not applicable here.

deposited at room temperature [21]. Preliminary LEED data of Ga on GaAs(110) also indicate a lack of change in surface reconstruction [22]. Neither Al [21] nor Ga [22] overlayers are epitaxial on GaAs(110) at room temperature. Al reacts with GaAs to form AlAs or AlGaAs below the surface at elevated temperatures (450°C), but still no epitaxy of the metal (Al/Ga) overlayer is seen ($0.25 < \theta < 2$ ML) [21].

It can be seen from the UPS data that the photoemission electron contribution from the Ga overlayer is relatively weak (see fig. 2). Difference curves, which eliminate the "background" of photoemission electrons from the GaAs, were obtained to examine the electronic structure of the overlayer in more detail (see fig. 3). These difference spectra are remarkably similar to one another and demonstrate that the overlayer is basically metallic or free-electron

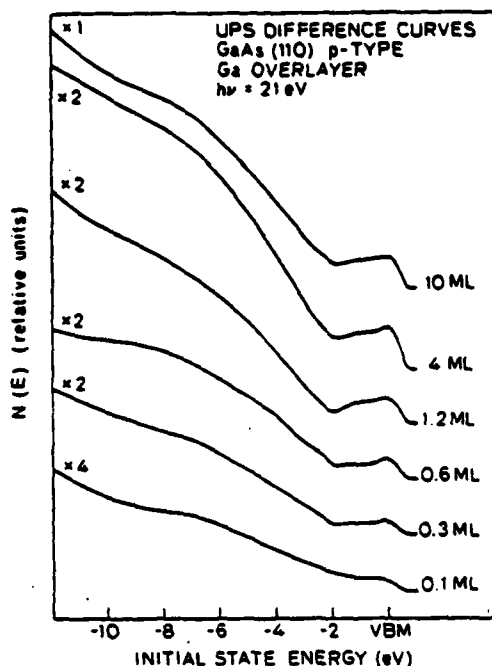


Fig. 3. Difference curves obtained by subtraction of a scaled clean-surface UPS spectrum of fig. 2 from each of the Ga-covered UPS spectra. The Ga overlayer is apparently free-electron-like even at submonolayer coverages. The strong resemblance between the difference curves for thick (10 ML) and thin (<1 ML) coverages also demonstrates the lack of change in the GaAs surface states.

like even at submonolayer coverages. This is most likely the result of clustering of the Ga on the surface. A more detailed analysis has shown that this clustering is mainly two dimensional or raft-like in nature [5,6].

In more recent theoretical work, Swarts has pointed out that column 3 adatoms will tend to bond weakly to the surface via the empty p_z orbital on the surface cations (in contrast to the early calculations), with negligible change in reconstruction [23]. Using this result, Chelikowsky has calculated a surface density of states for this system which shows less new electronic structure (and hence less EDS structure) than the early calculations [24]. In a critical review of the above theories, Zunger has rejected the idea of covalent or localized bonding between Al or Ga adatoms and GaAs(110) in favor of 3-dimensional metal cluster formation on top of the surface [25].

Although 3-dimensional clusters are quite likely the equilibrium state of the Al or Ga overlayer, the experimental data give strong support for raft formation (2-dimensional cluster) as a metastable state at room temperature.

4.2. Column 5 adatoms

Sb was used as a representative column 5 element. PES and LEED data of Sb adsorbed on GaAs have shown that the nature of the Sb-GaAs bond is fundamentally different from the Ga-GaAs or Al-GaAs bond. In contrast to the column 3 elements, Sb does produce first-order changes in the valence-band EDC structure (see fig. 4). Comparing the "clean" surface EDC to the "Sb covered" EDC, it is immediately clear that (a) attenuation of the peak at -6.75 eV has occurred, and (b) the "clean" surface peak at -2 eV has been removed. The attenuation of the -6.75 eV peak, which is associated mainly with bulk band structure, indicates that the Sb overlayer is fairly uniform in thickness, as with Ga and Al. The disappearance of the -2 eV peak indicates that,

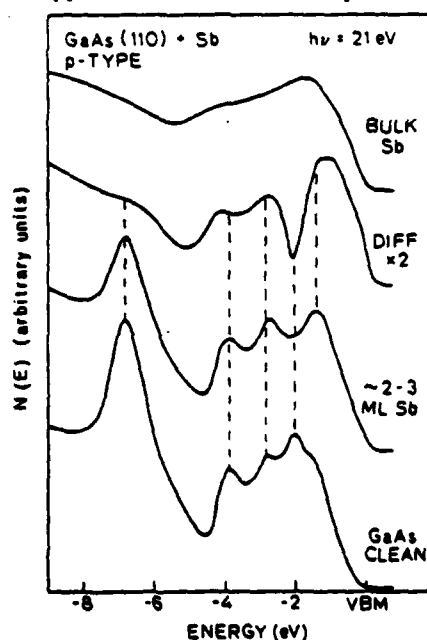


Fig. 4. UPS spectra showing emission from the valence electrons of GaAs + Sb adatoms. Note the change in upper valence band structure (-2 eV) which is particularly clear in the difference curve.

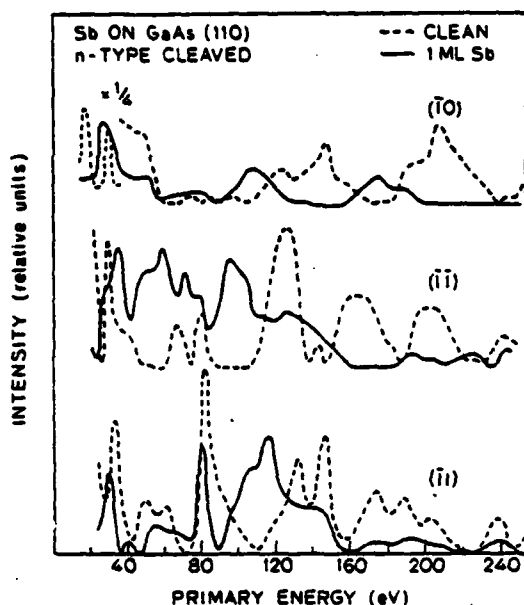


Fig. 5. LEED spot intensity versus primary energy data for Sb on GaAs(110). The surface unit cell size is (1×1) before and after Sb deposition. The structure in these data "fingerprint" the arrangement of atoms inside the surface unit cell.

unlike Ga, Sb adsorption has a strong effect on the GaAs states, due to a more localized, covalent bonding between the Sb adatoms and the GaAs surface lattice [6]. LEED data show that the translational symmetry (1×1) of the surface is unchanged by Sb deposition, but very strong changes in diffraction beam intensity versus voltage ($I-V$) characteristics, together with a low background intensity, are evidence of epitaxial growth of Sb on the surface (see fig. 5). Analysis of the structure of the Sb overlayers is given elsewhere [19].

5. Discussion

Deposited column 3 atoms (adatoms) may, at first thought, be expected to bond epitaxially to the (110) surface lattice As atoms via covalent bonds, as though beginning a new GaAs lattice layer. The data reported here, however, show that the Al or Ga overlayer on GaAs(110) is characterized by (a) a lack of epitaxy, (b) nonlocalized, nondirectional bonding, (c) a lack of change in GaAs surface electronic states and

atomic structure, and (d) a strong interaction between adatoms [5,6]. Thus the localized-orbital theoretical approach [20] is not expected to give an adequate description of the bonding between column 3 metals and the semiconductor.

A recent localized-orbital calculation does indicate that the localized-bond strength of Al on GaAs(110) is not large [23], in which case other (delocalized) bonding effects may dominate. Although it is quite clear that this calculation cannot describe the column 3-GaAs(110) bonds even qualitatively, it is instructive to consider the results of this calculation. The column 3 elements have a single p electron (less binding energy) and two s electrons (more tightly bound). It is thus anticipated that, in situations where a single (covalent) bond is to be formed, only the p states will be involved. Goddard has pointed out that bonding of column 3 elements to the surface As atoms is inconsistent with the chemistry of the reconstructed (110) surface [23]. Bonding may occur by the column 3 adatom donating its p electron into a bond orbital involving the empty p state on the surface lattice Ga atom. Their quantum chemical calculations of the bond strength for this configuration predict a weak bond (0.6 eV). Due to the weak directional bonding expected on the basis of theory, it is not surprising that adatom-adatom interactions are of first-order importance here, and that a delocalized character may dominate in the interfacial bonds.

In contrast to the column 3 elements, Sb does form an ordered overlayer. This has immediate implications for crystal growth and, in particular, molecular beam epitaxy. In MBE, the above results suggest that only the column 5 adatoms (but no column 3 atoms) will attach themselves epitaxially to the GaAs surface lattice. Thus the column 3 adatoms will be stabilized in epitaxial sites only when those sites have a sufficiently large number of neighboring column 5 atoms to favor hybridization (sp^2 or sp^3) of the column 3 valence orbitals.

These conclusions are also expected to apply to heteromolecule formation (e.g. $GaAs_2$, Ga_2As , etc.) on the surface prior to the incorporation of the adatoms into the lattice. Based on the above data, it seems safe to assume that the availability of a sufficient number of p electrons on the adatom or molecule is necessary for directional, covalent bonding to the (110) surface. It is anticipated that the column 3

atoms of a heteronuclear molecule will have its p electron (or all three valence electrons, depending on the molecule) taken up by bond orbitals *within* the molecule, while the column 5 atoms of the molecule may have p electrons available for bonding directionally to the semiconductor lattice. Thus again it is the column 5 element which is primarily responsible for establishing order in the overlayer with respect to the surface lattice. The relatively high temperature of MBE ($\sim 600^\circ\text{C}$) is believed necessary to dissociate both As₄ or other As molecules and to dissociate heteronuclear molecules which cannot otherwise be properly accommodated in the lattice.

In summary, we have determined experimentally the character of the bonds between column 3 (non-directional) or column 5 (directional) elements and GaAs(110). The column 5 element is expected to initiate the epitaxial alignment of a growing layer with the crystalline substrate.

References

- [1] W.E. Spicer, Bulk and Surface Ultraviolet Photoemission Spectroscopy, in: Optical Properties of Solids: New Developments, Ed. B.O. Seraphin (North-Holland, Amsterdam, 1976) p. 631.
- [2] J.B. Pendry, Low Energy Electron Diffraction (Academic Press, London, 1974);
F. Jona, J. Phys. C11 (1978) 4271;
C.B. Duke, Critical Rev. Solid State Mater. Sci. 8 (1978) 69.
- [3] P. Skeath, W.A. Saperstein, P. Pianetta, I. Lindau, W.E. Spicer and P. Mark, J. Vacuum Sci. Technol. 15 (1978) 1219.
- [4] P. Pianetta, I. Lindau, C.M. Garner and W.E. Spicer, Phys. Rev. Letters 37 (1976) 1166.
- [5] P. Skeath, I. Lindau, C.Y. Su, P.W. Chye and W.E. Spicer, J. Vacuum Sci. Technol. 17 (1980) 511.
- [6] P. Skeath, C.Y. Su, I. Lindau and W.E. Spicer, J. Vacuum Sci. Technol. 17 (1980) 874.
- [7] B. Kübler, W. Ranke and K. Jacobi, Surface Sci. 92 (1980) 519.
- [8] A.U. MacRae and G.W. Gobeli, J. Appl. Phys. 35 (1964) 1629.
- [9] A. Kahn, E. So, P. Mark, C.B. Duke and R.J. Meyer, J. Vacuum Sci. Technol. 15 (1978) 1223;
S.Y. Tong, A.R. Lubinsky, B.J. Mrstik and M.A. Van Hove, Phys. Rev. B17 (1978) 3303.
- [10] D.J. Miller and D. Haneman, J. Vacuum Sci. Technol. 15 (1978) 1267.
- [11] W.A. Harrison, Surface Sci. 55 (1976) 1.
- [12] C.A. Swarts, W.A. Goddard and T.C. McGill, J. Vacuum Sci. Technol. 17 (1980) 982.
- [13] D.J. Chadi, Phys. Rev. B18 (1978) 1800.
- [14] The suggestion that oxygen prefers to bind to the surface As atoms based on the non-bonding As electrons was first made by Gregory et al. [P.E. Gregory, W.E. Spicer, S. Ciraci and W.A. Harrison, Appl. Phys. Letters 25 (1974) 511]. The experimental data which Gregory et al. used to support this model were, however, not given proper interpretation. Much stronger experimental evidence for this model was obtained by Pianetta et al. [P. Pianetta, I. Lindau, C.M. Garner and W.E. Spicer, Phys. Rev. Letters 37 (1976) 1166], and a more complete theoretical basis has been provided by Barton et al. [J.J. Barton, W.A. Goddard and T.C. McGill, J. J. Vacuum Sci. Technol. 16 (1979) 1178].
- [15] I. Lindau and W.E. Spicer, Photoemission as a Tool to Study Solids and Surfaces, in: Synchrotron Radiation Research, Eds. H. Winick and S. Doniach (Plenum, New York, 1980) p. 159.
- [16] P.W. Chye, C.Y. Su, I. Lindau, P. Skeath and W.E. Spicer, J. Vacuum Sci. Technol. 16 (1979) 1191.
- [17] C.Y. Su, I. Lindau, P.R. Skeath, P.W. Chye and W.E. Spicer, J. Vacuum Sci. Technol. 17 (1980) 936.
- [18] P. Skeath, I. Lindau, P. Pianetta, P.W. Chye, C.Y. Su and W.E. Spicer, J. Electron Spectrosc. Related Phenomena 17 (1979) 259.
- [19] P. Skeath, I. Lindau, C.Y. Su and W.E. Spicer, J. Vacuum Sci. Technol., to be published.
- [20] D.J. Chadi and R.Z. Bachrach, J. Vacuum Sci. Technol. 16 (1979) 1159;
E.J. Mele and J.D. Joannopoulos, Phys. Rev. Letters 42 (1979) 1094;
J.R. Chelikowsky, S.G. Louie and M.L. Cohen, Solid State Commun. 20 (1976) 641.
- [21] A. Kahn, D. Kanani, J. Carelli, J.L. Yeh, C.B. Duke, R.J. Meyer and A. Paton, to be published;
C.B. Duke, A. Parton, R.J. Meyer, L.J. Brillson, A. Kahn, D. Kanani, J. Carelli, J.L. Yeh, G. Margaritondo and A.D. Katnani, Phys. Rev. Letters 46 (1981) 440.
- [22] P. Skeath, unpublished data.
- [23] C.A. Swarts, J.J. Barton, W.A. Goddard and T.C. McGill, J. Vacuum Sci. Technol. 17 (1980) 869.
- [24] J.R. Chelikowsky, J. Vacuum Sci. Technol., to be published.
- [25] A. Zunger, Phys. Rev. B24 (1981);
A. Zunger, private communication.
- [26] P. Pianetta, PhD Thesis, Stanford University (1977).

APPENDIX C

Use of Photoemission with Synchrotron Radiation to
Probe Surfaces on an Atomic Scale

W. E. Spicer

Published in Surfaces and Interfaces in Ceramic and
Ceramic-Metal Systems

From: SURFACES AND INTERFACES IN CERAMIC AND
CERAMIC-METAL SYSTEMS
Edited by Joseph Pask and Anthony Evans
(Plenum Publishing Corporation, 1981)

USE OF PHOTOEMISSION WITH SYNCHROTRON RADIATION TO PROBE SURFACES
ON AN ATOMIC SCALE[†]

W. E. Spicer

Stanford Ascherman Professor of Engineering
Department of Electrical Engineering
Stanford University, Stanford, California

ABSTRACT

The capabilities of synchrotron radiation are briefly reviewed with an emphasis on applications to photoemission spectroscopy. The physics of photoemission is also briefly reviewed with emphasis on the importance of the escape length of the photo-executed electron in determining the depth of material examined. Most of the text is utilized to demonstrate these techniques in the GaAs (110) - oxygen system and CuNi alloy - surface segregation studies. The relative importance of thermodynamic equilibrium and activation energies are discussed.

I. INTRODUCTION

I, and I hope others, sense an excitement in this meeting over our growing ability to probe down to an atomic level in investigating phenomena critical to the understanding of ceramic interfaces. These techniques will give us the ability to test the conclusions drawn from the established macroscopic methods, to choose between different models, and on occasion to uncover new phenomena. However, it must be recognized that each of these techniques has its own advantages

[†]This work was supported by the Office of Naval Research under Contract No. N00014-75-C-0289 and by the Advanced Research Projects Agency of the Department of Defense (monitored by ONR) under Contract No. N00014-79-C-0072. The experiments were performed at the Stanford Synchrotron Radiation Laboratory which is supported by the National Science Foundation under Grant No. DMR77-27489 in cooperation with the Stanford Linear Acceleration Center and the Department of Energy.

and disadvantages. Often it is essential to use them in concert. Above all, results and conclusions drawn from them must be tied to the existing macroscopic data.

These new "atomic" tools are expensive and increasingly available only as national facilities. Work tends to be led by physicists and chemists. For ceramics and related fields to fully profit from these developments, it is essential for the ceramicists to take an increasingly aggressive stance in first developing more collaborations with those using these facilities and/or ultimately developing their own programs making use of these capabilities. The NSF has structured national facilities such as the Stanford Synchrotron Radiation Laboratory (SSRL)¹ to facilitate such developments. In addition, NSF regional facilities such as the West Coast Surface Analysis Laboratory, Montana State University, Bozeman, Montana,² are being built up specifically to make expensive equipment accessible to outside groups.

In this paper, I will concentrate on the use of synchrotron radiation^{3,4,5} as a source in those photoemission experiments which, in my judgement, are most closely aligned to ceramic interfaces. Thus, this article should in no way be considered a survey of the capabilities of synchrotron radiation used in photoemission experiments. In addition, it should be emphasized that synchrotron radiation may be used with many techniques⁵ other than photoemission, and that these techniques may also be of use in ceramics. These include EXAFS (extended X-ray absorption fine structure)⁵ studies to determine, in a unique way, local configuration about a given element in an ordered or disordered lattice. There are other techniques which should be useful. Most importantly, given the special capabilities of synchrotron radiation, ceramicists may be able to devise new ways of using it which will give unique insights.

The most important characteristic of synchrotron radiation is that it provides the first, and a very intense, continuum of electron-magnetic radiation extending from the infrared to the hard X-ray region (Fig. 1).⁵ For most scientific studies, one wants monochromator radiation. Here nature is kind; the synchrotron radiation is strongly collimated in the forward direction,⁵ making it possible to monochromatize⁵ the radiation with minimal loss. Another important characteristic of the radiation is its natural polarization, although use is not made of this in the experiments described here.

II. FUNDAMENTALS OF THE PHOTOEMISSION PROCESS

The three-step model^{3,4,6,7} is an approximate description of the photoemission process which has proven extremely useful and has played a key role in the development of photoemission as a scientific tool. The reason for the success of this model has been its simplic-

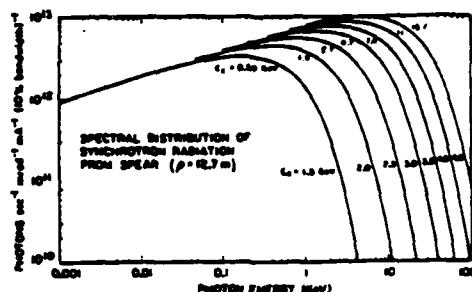


Fig. 1 The spectral distribution of the synchrotron radiation from the storage ring SPEAR at Stanford University for various energies of stored electron beam. The beam energy is indicated on each curve.

ity. It divides the photoemission process up into three successive events, each of which can be studied and treated simply and independently. Thus the essential parameters for each step can be determined and then applied to photoemission.

The three-step process is an approximation in that it treats each step as being independent. Ideally, they should be coupled and, in the extreme limit of photoelectrons originating only very close to the surface, the three processes must be treated as simultaneous,

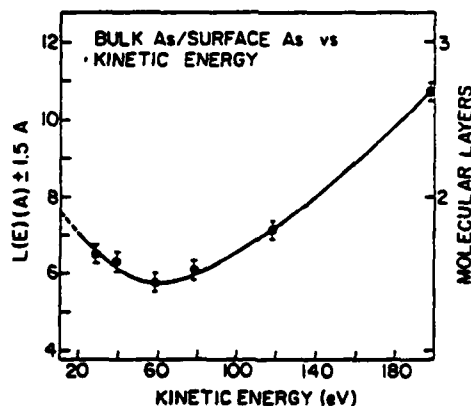


Fig. 2 The escape depth for photoelectrons from GaAs.

completely coupled events.^{7,8} In fact, experience has shown that the three-step model is very useful even in the limit of short escape depth.

Both theoretically and experimentally,^{6,7,9} it has been shown that the probability of the excited electron reaching the surface without appreciable energy loss is given by:

$$Q(E) = e^{-x/L(E)} \quad (1)$$

where $L(E)$ is the characteristic scattering probability of an electron excited to a final energy E . The escape depth versus energy curve for GaAs (corrected for geometry) is shown in Fig. 3. $L(E)$ for other materials can be found in the literature.

Equation (1) gives the probability of escape from a depth x without significant energy loss. The experimentally measured energy distribution, $N(E, h\nu)dE$, contains not only the electrons which escape without appreciable energy loss but also the distribution produced by the scattering process, $S(E, h\nu)dE$ (see Fig. 3). Thus,

$$N(E, h\nu)dE = P(E, h\nu)dE + S(E, h\nu)dE. \quad (2)$$

To first order, it is easy to separate the $P(E, h\nu)$ and $S(E, h\nu)$ in experimental data since $P(E, h\nu)$ usually gives strong structure which moves to higher energy as $h\nu$ is increased. In contrast, $S(E, h\nu)$ usually varies monotonically with energy without sharp structure (except for plasmon production).^{6,10} Normally, the distribution of scattered electrons tends to build up and peak near low energies.

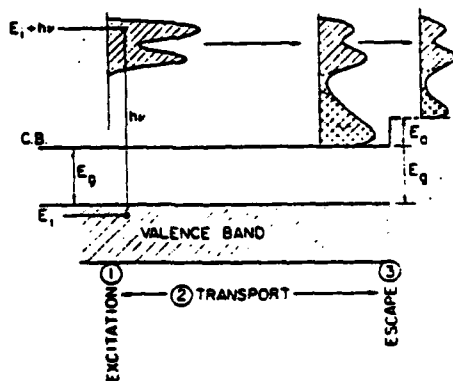


Fig. 3 A schematic diagram illustrating the three-step photo-emission process. An initial optically excited distribution is shown on the left. Changes in this distribution as it approaches the surface (due to inelastic scattering) and after it has escaped into the vacuum (due to the potential barrier at the surface) are indicated.

This is shown schematically in Fig. 3 for excitation from the valence band. Much more detail of the scattering processes can be found in the literature.^{7,11} Since synchrotron radiation is usually used for $h\nu > 12$ eV, the electron-electron (including plasmon creation) scattering event usually is dominant and will be of most importance for the work discussed here.

III. BENEFITS OF SYNCHROTRON RADIATION WITH PHOTOEMISSION

There are at least four primary advantages to be gained by having photon energies available over a wide energy range.

- 1) Providing the ability to examine core as well as valence states.
- 2) Being able to take maximum advantage of the photon dependence of the matrix elements to separate and identify levels which are degenerate in energy. The matrix elements for transitions from different quantum states may have quite different $h\nu$ dependencies. This is illustrated by Figs. 4 and 5. In these figures the absorption cross section giving the probability of producing a photoelectron with the energy characteristic of excitation from 3d (Fig. 4) or 4d and 5d (Fig. 5) core levels is presented. As can be seen from Figs. 4 and 5, the $h\nu$ dependence of the 3d and that of the 4 or 5d cross section are quite different. An example of the use of $h\nu$ dependence of matrix elements will be given in section VI.
- 3) Tuning the photon energy of a given transition in order to obtain the minimum escape depth (See Fig. 2) and thus maximize surface sensitivity, or conversely tuning to an energy where the escape depth is long to emphasize the bulk rather than the surface.
- 4) Tuning $h\nu$ to move along the $L(E)$ curve and thus probing the

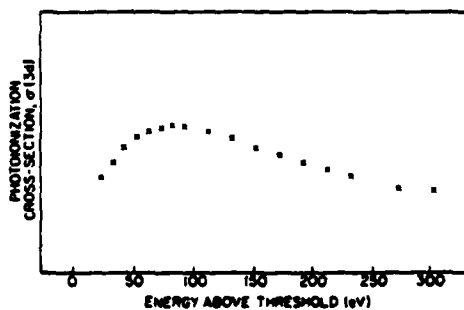


Fig. 4 Photoionization cross section versus $h\nu$ for exciting an electron from a 3d (Ga) core level.

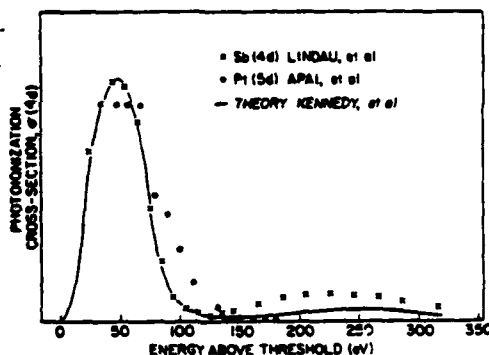


Fig. 5 Photoionization cross section versus $h\nu$ for exciting an electron from 4d and 5d levels. The strong minimum at 150 eV is due to the Cooper minimum.

composition of the sample on an atomic scale as a function of depth into the sample.

In the following section, we will illustrate these aspects of photoemission using synchrotron radiation. However, it should be kept in mind that these advantages are often interrelated. For example, one may choose a particular $h\nu$ to study adsorption of a foreign gas on a surface in order to get the proper compromise between minimum escape depth and maximum matrix element.

IV. GaAs SURFACE AND INTERFACE STUDIES

A. Use of Short Escape Depths

In section II, we introduced the concept of escape depth and in Fig. 2, indicated how escape depth varies as a function of electron energy. In this section, we will illustrate how the ability to tune the photon energy in order to minimize the escape depth can give very high surface sensitivity for core as well as valence states. The examples will be taken from studies of GaAs, which was one of the first materials for which these techniques were applied.

In Fig. 2, we present the escape depth versus electron energy as determined for GaAs. As can be seen, the escape depth goes through a shallow minimum at about 60 eV. The minimum falls at about one and a half molecular layers; thus, roughly half the emission will come from the first molecular layer and half from deeper in the sample.

We will examine two cases of the use of the surface sensitivity

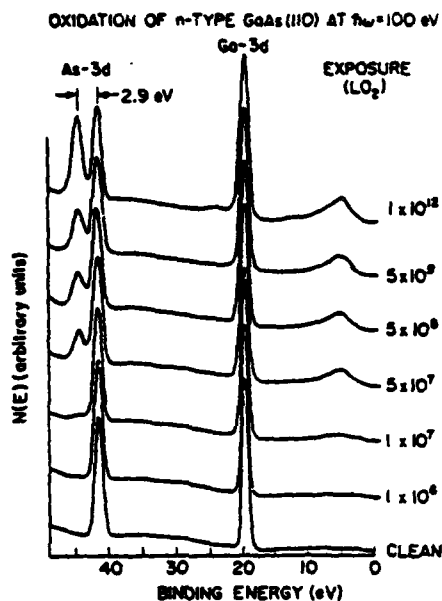


Fig. 6 The 3d core levels of Ga and As in GaAs as a function of exposure to oxygen in its ground state. Note the strong (2.9 eV) As 3d shift and the small broadening of the Ga 3d levels. This data is interpreted in terms of chemisorption of oxygen. The structure at about 6 eV which grows with increasing exposure is due to oxygen 2p levels.

given by a short escape depth. The first will be for the Ga and As 3d core states in which the shifts observed in these due to adsorption of oxygen is studied. The second will be a direct examination of the oxygen 2p states on the GaAs surface valence states. We will also illustrate matrix element effects by examining oxygen on GaAs.

In Fig. 6, we present spectra taken from the (110) GaAs face at $h\nu = 100$ eV as a function of oxygen exposure. (The exposure is indicated in terms of Langmuirs, L, on each curve. $1 \text{ L} = 10^{-6} \text{ torr-sec.}$) An atomically clean (110) surface was obtained by cleaving in a vacuum of 10^{-10} torr. In order to investigate the bonding of oxygen on an atomic scale, one wishes to see simultaneously the surface core states of both the Ga and As atoms. $h\nu = 100$ eV was chosen because the kinetic energy of the photoexcited As 3d electrons would be about 60 eV (which places it at the minimum of the escape depth curve); whereas the kinetic energy of the Ga 3d's is about 80 eV - close to the escape depth minimum. In addition, as can be seen from Fig. 4, the photoionization cross section, i.e. excitation probability for

the 3d peak, is reasonably close to its maximum value for each of these transitions. Whereas if we had used a small $h\nu$ (to get shorter escape depth for Ga 3d's), the As 3d cross section would have been noticeably decreased.

The benefit of examining the core levels at the surface is well illustrated by Fig. 6. As can be seen, there is a single new As peak shifted to higher binding energy which grows with oxygen exposure; whereas no shift is observed in the Ga peak. In Fig. 6, at approximately monolayer coverage (10^{12} L), the shifted and unshifted As peaks are about equal. If each gas atom stuck on the surface, 1 L would give approximately a monolayer. This shows that about half of the photoelectrons are coming from the surface As atoms. If the escape depth had been longer (as for example with $h\nu = 1.5$ KeV for XPS) it would have been much harder to see the chemical shift at low coverages, e.g. 10^6 L, since a much smaller fraction of the electrons would have come from the surface. If the resolution of the EDC's was poorer (as in XPS), it might have been impossible to distinguish the As 3d

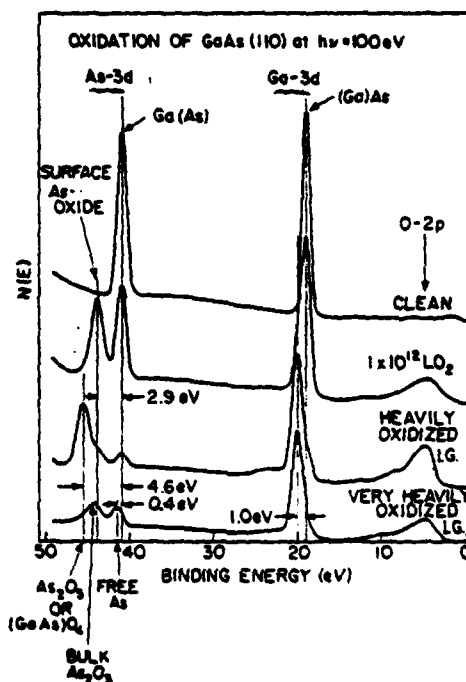


Fig. 7 The chemical shifts after heavy oxidation of GaAs. Note the various As shifts due to different chemical states as well as Ga shift corresponding to Ga_2O_3 . The heavily and very heavily oxidated curves were obtained using excited oxygen.

shift for this "chemisorbed" state from that for As_2O_3 formation.

The data of Fig. 6 gives definitive evidence that the oxygen removes electrons from the As in chemisorbing on the surface of the GaAs, since an As peak shift of 2.9 eV appears. Based on the chemistry of elemental As and Ga, it had been expected that oxygen would preferentially remove electrons from the Ga rather than the As. In fact, as Fig. 7 shows, this is what happens when one passes the chemisorption stage and breaks the GaAs covalent bonds in order to form bulk Ga and As oxides.

In order to limit the oxygen to chemisorption (Fig. 6) great care had to be taken¹⁴ that there was no excitation of the oxygen. This was done by turning or valving off all hot filaments, ion gauge or other possible sources of excitation. This is necessary even when the source of excitation is well-removed from (and well out of line of sight of) the sample under study. As can be seen from Fig. 6, only the As shift of 2.9 eV (which we associate with chemisorption) takes place, even when the GaAs is exposed to an atmosphere of pure, unexcited oxygen for about 15 minutes (10^{12} L).

In contrast (see Fig. 7), the bulk oxides are formed by orders of magnitude lower exposure (10^6 L) by simply turning on an ion gauge which is well out of line of sight of the GaAs, i.e. any oxygen excited by the ion gauge must be scattered from several metal surfaces before it can reach the GaAs. In order to understand this behavior, it is important to realize that oxygen has a very long-lived (15, min) excited state. Thus, even if oxygen ions or atoms cannot reach the sample, the long-lived oxygen excited states almost certainly can.

We can understand the behavior illustrated by Figs. 6 and 7 on the basis of the atomic and electronic rearrangement of the GaAs (110) surface. Knowledge of this has been developed in recent years¹⁵ through a combination of photoemission, LEED, and theoretical studies - details are given elsewhere. This knowledge is summarized schematically in Fig. 8. Figure 8 gives a schematic indication of our understanding of the GaAs (110) free (clean) surface. Although careful measurements and calculations have been made systematically only on GaAs (110), it is likely that the surface rearrangement is similar for other 3-5 compounds, and so is the effect of rearrangement on the the surface electronic structure for 3-5 materials (at least those with band gaps no greater than GaAs). Of critical importance is the rearrangement of the surface atoms. This is intimately connected with and in a certain sense driven by the electronic rearrangement.^{16,17,18,19} When one covalent bond of each of the surface atoms is broken to form the surface, the surface atoms tend toward their atomic configuration consistent with retention of the covalent bonds with each of their three remaining nearest neighbors. Thus, five electrons will be associated with the surface As and three with the surface Ga. It is this surface electronic rearrangement

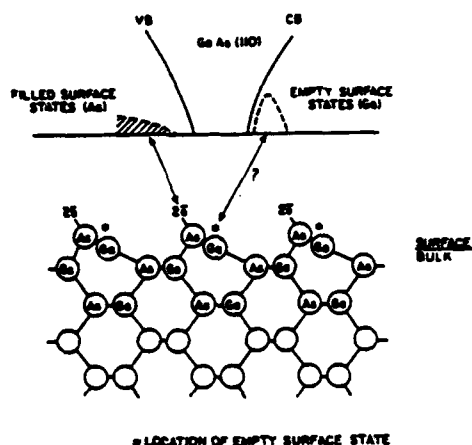


Fig. 8 Schematic of the surface electronic and lattice structure of (110) GaAs. Other 3-5 compounds are thought to be similar. Note the strong rearrangement of the surface atoms and that there are no intrinsic surface states in the band gap. Thus, there can be no intrinsic surface state pinning of the Fermi level. Note also that the nonbonding electrons are associated principally with the As surface atoms, whereas the empty surface states are predominantly associated with the Ga surface atoms.

which determines the final positions and bond configurations of the surface atoms to achieve the lowest energy state consistent with minimizing the bond and strain energies. The strain, which is large, is due to the lattice mismatch between the rearranged surface and the bulk lattice atoms.

As a result of the surface electronic rearrangement, the surface As and Ga atoms, respectively, move toward p^3s^2 and sp^2 configurations. In these configurations, there are five and three valence electrons associated with the surface As and Ga atoms, just as in the case of the free atoms. Thus, the Ga surface atom is constrained to move toward a sp^2 planar configuration because it must use all of its available electrons to form covalent bonds with its three remaining nearest neighbors. In contrast, the As surface atom needs only three of its five valence electrons to form covalent bonds with its three nearest neighbors. As Harrison²⁰ and others have shown, the lowest As bond energy is obtained by this electron taking up a s^2p^3 arrangement with the three p electrons forming the bonds and s electrons forming filled s^2 orbitals. As a result of the As bonding electrons moving toward a p^3 configuration and the Ga toward sp^2 , the As moves outward by about 0.5 Å and the Ga inward by about 0.3 Å. Low energy

electron diffraction (LEED) work^{21,22,23,24} has played the essential role in establishing the rearrangement of the surface atoms. Mark et al concluded from their LEED studies that the lattice distortions extend three molecule levels below the surface.²⁵ The filled "surface states" are associated principally with the As atoms and the empty states largely with the Ga atoms (see Fig. 8).

Even more important, independent confirmation for this model is found through the results of photoemission^{26,27,28} and contact potential^{29,30,31} measurements, followed by theoretical calculations³² of the electron structure. As can be seen, a striking feature of Fig. 8 is the lack of surface states in the band gap region. After much confusion due to the extrinsic surface states (i.e. states due to defects or impurities) and intrinsic surface states (i.e. states characteristic of the perfect rearranged surface), it was established through careful photoemission^{26,27} measurements that there were no surface states in the band gap in agreement with the original work of van Laar and Scheer²⁹ and van Laar and Huijser.^{31,32}

Examination of Fig. 8 leads to an understanding of the oxygen detachment data of Figs. 6 and 7. First recognize that there is an activation barrier to overcome in order to break the surface GaAs covalent bonds in order to form bulk oxides. With oxygen in the molecular ground state and the sample at room temperature (as was the case for the experiments of Fig. 6) the data of Fig. 6 indicates that this activation barrier cannot be overcome. Thus the major chemical shift is found on the As (2.9 eV) since only As s^2 electrons can be transferred to oxygen without breaking Ga-As bonds.^{12,14} However, this is an improbable event; thus, the sticking coefficient is very small (order 10^{-10}). It is about 0.1 for a metal. Since only a single monolayer of oxygen can be accommodated without breaking Ga-As bonds, the oxygen adsorption "saturates" at that coverage.¹⁴

Fig. 7 shows that with excited oxygen, the GaAs bonds can be broken and bulk As and Ga oxides formed. For Ga, only Ga_2O_3 is formed. With As, As_2O_5 or $(AsGa)_2O_4$ is first formed, then As_2O_3 which (being volatile) leaves the surface - reducing the As signal.¹⁴

As oxides are thermodynamically unstable in the presence of GaAs.³³ For example,



As a result, elemental As begins to appear after "very heavy oxidation." The systematics of such oxygen chemistry have been studied for GaSb, GaAs, and InP and found to proceed as would be expected in terms of the heat of formation of the compound semiconductor.^{34,35}

Making use of such studies (combined with photoemission measurements of the surface position of the Fermi level) as either oxygen or metal is added to an atomically clean surface, a unified model has

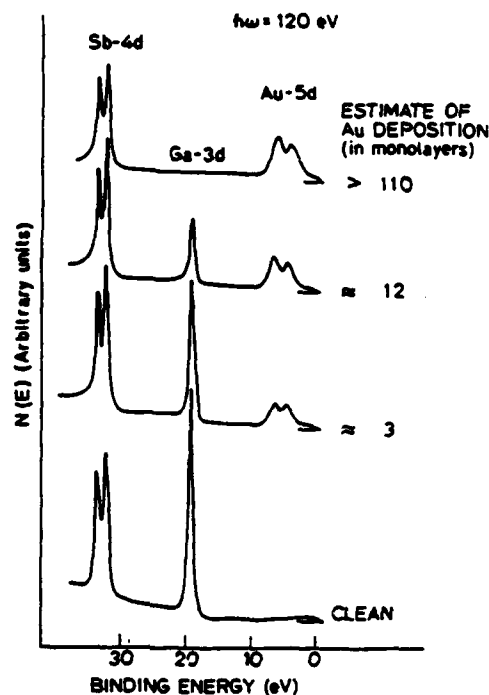


Fig. 9 Photoemission spectra taken at a photon energy of 123 eV for GaSb (110) exposed to different amounts of Au. Note the preferential movement of Sb to the surface.

been established for the formation of metal-semiconductor electrical contacts (Schottky barriers) and metal-oxide interface states.^{36,37} This is based on the formation of identical defect levels due to the deposition of metals or oxygen.

One important result which led to the unified model was the unexpected discovery that, even at room or lower temperature, semiconductor material is included in the metal. Fig. 9 shows an example of the core level results which established this.^{36,37,38} electron energies for the Sb and Ga d-levels are near the escape minimum (about two atomic layers); thus we are sensing the outer few layers. For Au, it is comparable or a little less, i.e. about 5 Å.^{39,40} Thus we are sampling only about two or three atomic layers into the Au.

The striking characteristic of Fig. 9 is that the Ga 3d peak drops relatively rapidly with Au coverage, whereas there is only a slight drop in the Sb peak even after over 100 monolayers of Au have been deposited. The conclusion is inescapable: Sb is being removed

from the interface and placed on the surface of the Au film. The fact that the Ga peak height is reduced by only a factor of 1/4 after 13 monolayers have been deposited indicates that some Ga is included in the Au, although there is not a heavy concentration near the surface as is the case for Sb. In fact, with an Au film of thickness greater than about 100 layers, no Ga can be detected within the escape depth, whereas the Sb intensity is diminished by less than a factor of two. These results have been confirmed by Sputter Auger measurements.^{37,38} The intermixing has since been established for a large number of semiconductor-metal systems^{37,38} - even when it is not favored by the bulk phase diagrams. It has been suggested that the activation energy necessary to place an occasional metal atom in the metal is supplied by the heat of adsorption of the metal^{36,37,38} on the semiconductor. Fig. 10 indicates the suggested mechanism. Detailed discussions can be found elsewhere.^{36,37,38}

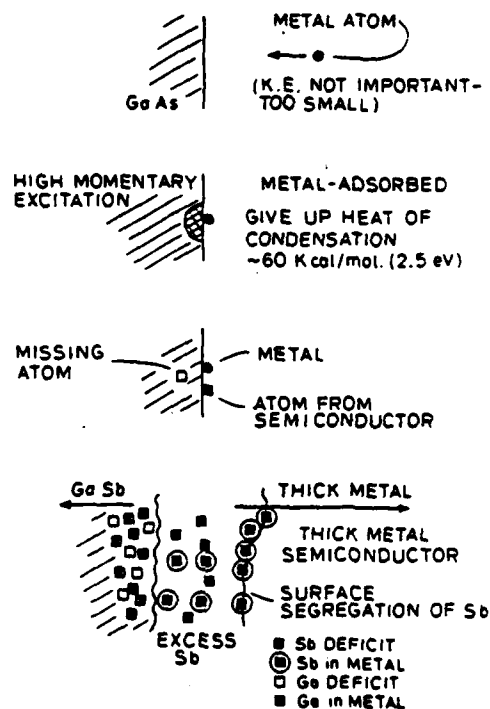


Fig. 10 Schematic diagram of suggested defect mechanism due to deposition of metal atoms on clean III-V surfaces. This process (i.e. a defect must be formed) need occur only about once for every hundred atoms striking the surface in order to explain the Fermi level pinning.

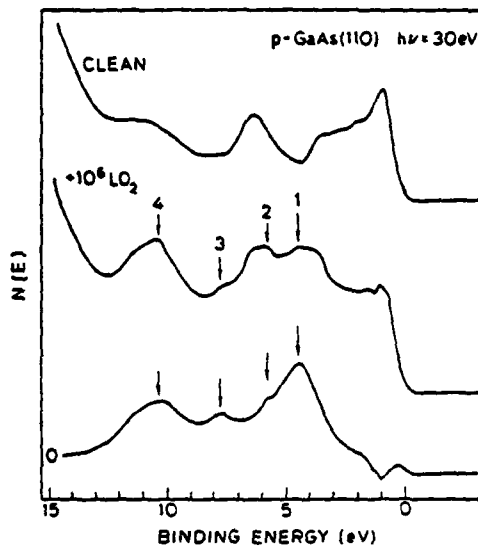


Fig. 11 EDC's of a clean p-GaAs (110) surface (top curve) and the same surface exposed to 10^6 L oxygen (center curve) taken at a photon energy of 30 eV. The bottom curve is their difference. As can be seen the oxygen spectra dominates, although only about 1% of a monolayer of oxygen is present.

B. Matrix Element Effects

In the last section some use of matrix element effects were evident. Here, for emphasis we will give other examples. In Fig. 11, we show data for oxygen adsorbed on GaAs.⁴¹ The matrix element for excitation from the valence band is reduced by several orders of magnitude by going to $h\nu = 30$ eV; however, the oxygen 2p matrix elements are little affected. Thus 1% of a monolayer of oxygen can be clearly separated from the GaAs valence band even though the density of oxygen electrons available for photoemission are about 200 times less than the number of GaAs electrons. This technique has been used for the following systems: oxygen⁴² and CO⁴³ on Pt, ~ 2% Cu alloyed in Pt,⁴⁴ and palladium silicides⁴⁵ (to separate the Pd d-electrons from the Si p and s electrons).

IV. USE OF SYNCHROTRON RADIATION TO OBTAIN "DEPTH PROFILES"

In recent years, Auger and photoemission measurements have been used to study the surface segregation in alloys and other systems. For example, in a CuNi alloy with 90% Ni bulk composition, the sur-

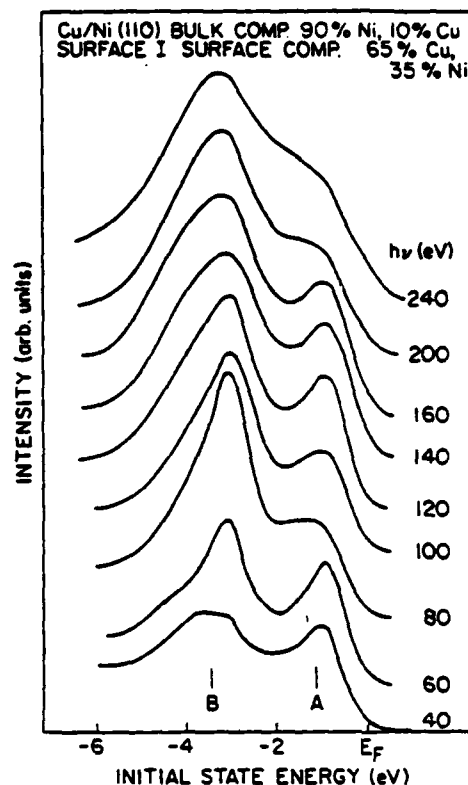


Fig. 12 Photoemission energy distribution curves from $h\nu = 40\text{--}240$ eV for Cu/Ni (110). The bulk atomic composition was 90% Ni, 10% Cu. The surface composition measured by AES was 65% Cu, 35% Ni.

face composition (as determined by Auger analysis) in "equilibrium" is 65% Cu; 35% Ni.⁴⁶ Methods have been devised to vary the surface composition between "equilibrium" and the bulk composition.⁴⁶ However, a critical consideration is the change in composition perpendicular to the surface. Making use of the tunability of the escape length in photoemission, this can be probed.

In Fig. 12 we present energy distribution curves (EDC's) for an "equilibrium" sample with surface composition 65% Cu; 35% Ni.⁴⁷ It had previously been established that the peak from the initial energy state at -1 eV (labeled "A") is due to Ni valence d-states and that the peak labeled "B" is due to Cu valence d-states. The EDC's in Fig. 12 are centered around the escape length minimum of about 4

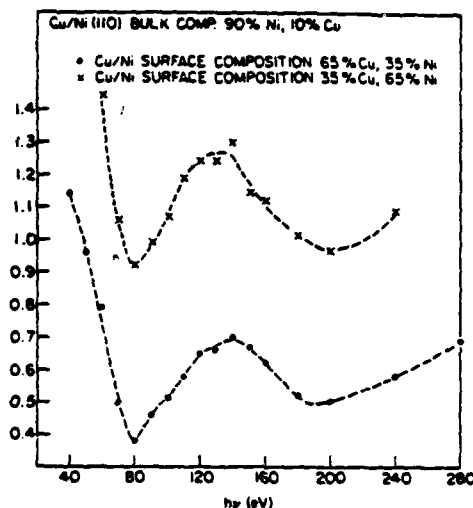


Fig. 13 Plot of r (ratio of Cu to Ni emission intensities) versus $h\nu$ (photon energy) for Cu/Ni (110). The dots are for the Cu/Ni I surface; 65% Cu, 35% Ni surface composition. The crosses are for the Cu/Ni II surface, ~65% Ni, ~35% Cu.

at 100 eV. The oscillations of strength of peaks A and B therefore indicate the change of composition with depth.

In Fig. 13 the ratio, r , of Cu to Ni emission intensity is plotted versus photon energy $h\nu$. Since the electrons are coming from the valence states $h\nu$ is within a few eV of the electron energy. As can be seen from Figs. 12 and 13, the Cu content does not decrease monotonically with depth. Rather, it goes through an oscillation with a peak at approximately 140 eV.

Precise analysis of the data is hindered because of the uncertainty in $L(E)$. However, within those limitations, it is clear that there must be a Cu enriched region 3 or 4 layers thick to produce the oscillation in Fig. 13. It should be emphasized that the occurrence of the oscillation has been confirmed by field emission field atom using stripping techniques.

A tentative explanation for these Cu-Ni results can be made. Ni and Cu are not miscible at sufficiently low temperatures (350 - 500°C); however, this is usually not important because the diffusion coefficient becomes very low before the miscibility gap is reached. Thus, the oscillation observed here can be due to the atomic jump probability near the surface being large enough to build up the al-

ternating Ni and Cu rich layers of a few atoms in thickness at the surface.

V. COMMENTS ON THERMODYNAMIC EQUILIBRIUM AND INTERFACES

It should be recognized that in all of the interfaces discussed here we have not been working under conditions of strict thermodynamic equilibrium. In fact, this departure from equilibrium is probably one property which characterizes most interfaces. In fact, one of the best characterized interfaces (to which a complete session of these proceedings is devoted) is Si:SiO₂. This is clearly only stable because the oxygen of the atmosphere is not able to penetrate the SiO₂ at room temperature to continue oxidation. Only under these conditions can the Si:SiO₂ interface be thought of as being in thermodynamic equilibrium. However, we would suggest that it is more useful to think in terms of activation energies rather than thermodynamic equilibrium. Thus, we would say that the Si:SiO₂ interfaces here are stable because the activation energy for bringing oxygen through the SiO₂ to the interface is too large for this to be an important process near room temperatures.

The Cu-Ni surface and near-surface oscillations mentioned in the last section are clearly non-equilibrium. Here the activation energy for movement of Ni and Cu atoms to take up positions of minimal energy is the limiting quantity.

In the case of the GaAs (110), it was the activation energy to break the Ga-As bonds which limited the uptake of oxygen for the unexcited molecular state (at room temperature) to the chemisorbed stage. However, this could be overcome by exciting the oxygen with an ion gauge and the interface could move toward equilibrium, as shown in Fig. 7

REFERENCES

1. Director: Prof. Arthur I. Bienenstock, SSKL, SLAC
Stanford University, Stanford, California 94305
2. Director: Prof. Gerald J. Lapeyre
Department of Physics
Montana State University, Bozeman, Montana 59717
3. W.E. Spicer, Electron and Ion Spectroscopy of Solids, p. 54,
L. Fierman, J. Vennik, and W. Dekeyser, eds., Plenum, New
York (1978), and references therein.
4. W.E. Spicer, Chapter 6, Nondestructive Evaluation of Semicon-
ductors, Jay N. Zemel, ed., Plenum, New York (1979).
5. H. Winick and S. Doniach, Synchrotron Radiation Research, Plenum,
New York and London (1980), and references therein.
6. W.E. Spicer, Phys. Rev. 112:114 (1958).

- C.N. Berglund and W. E. Spicer, Phys. Rev. 136:1030,1044 (1964).
7. M. Cardona and L. Ley, eds., Photoemission in Solids, I and II, Springer-Verlag, Berlin, Heidelberg, and New York (1979), and references therein.
8. P.J. Feibelman and D.E. Eastman, Phys. Rev. B 10: 4932 (1974).
9. W.E. Spicer, in Proc. Intern. Colloq. on Optical Properties and Electronic Structure of Metals and Alloys, 1965, Paris, ed. F. Ables, North Holland, Amsterdam; John Wiley, New York, pp. 296-315.
10. W.E. Spicer, Bulk and Surface Ultraviolet Photoemission Spectroscopy, Optical Properties of Solids - New Developments, B.O. Seraphin, ed., North Holland (1975).
11. T.H. DiStefano and W.E. Spicer, Phys. Rev. B 7:1554 (1973).
R. Powell and W.E. Spicer, G.B. Fisher, and P. Gregory, 8:3987 (1973).
12. W.E. Spicer, I. Lindau, J.N. Miller, D.T. Ling, P. Pianetta, P.W. Chye, and C.M. Garner, Physics Scripta 16:388 (1977).
13. G. Apai, P.S. Wehner, J. Stohr, R.S. Williams, and D.A. Shirley, Solid State Comm. 20:1141 (1976).
14. P. Pianetta, I. Lindau, C.M. Garner, and W.E. Spicer, Phys. Rev. 18:2792 (1978).
15. An excellent view of these developments can be obtained from the Proceedings of the Physics of Compound Semiconductor Interfaces, published as J. Vac. Sci. and Tech. 13, No. 4 (1976); 14, No. 4 (1977); 15, No. 4 (1978); 16, No. 4 (1979); and 18, No. 5 (1980); in view of this the number of individual references will be drastically limited.
16. R. Stuart, F. Wooten, and W.E. Spicer, Phys. Rev. B 4:4390 (1964).
17. I. Lindau and W.E. Spicer, J. Electron Spectroscopy 3:409 (1973).
18. T.H. DiStefano and W.E. Spicer, Phys. Rev. B 7:1554 (1973).
19. R.A. Powell, W.E. Spicer, G.B. Fischer, and P. Gregory, Phys. Rev. B 8:3987 (1972).
20. W.A. Harrison, Surf. Sci. 55:1 (1976); Proc. of 13th Intn. Conf. Phys. of Semicond. 111 (1976); J. Vac. Sci. and Tech. 14:883 (1977).
21. C.B. Duke, J. Vac. Sci. and Tech. 14:870 (1977); C.B. Duke, A. Lubinsky, B.W. Lee and P. Mark, J. Vac. Sci. and Tech. 13:761 (1976); P. Mark, G. Cisneros, M. Bonn, A. Kahn, C.B. Duke, G. Patton, and A.R. Lubinsky, J. Vac. Sci. and Tech. 14:910 (1977).
22. W.E. Spicer, I. Lindau, J.N. Miller, D.R. Ling, P. Pianetta, P.W. Chye, and C.M. Garner, Physica Scripta 16:388 (1978)
23. P. Mark, P. Pianetta, I. Lindau, and W.E. Spicer, Surf. Sci. 69:735 (1977); P. Skeath, W.A. Saperstein, P. Pianetta, I. Lindau, and W.E. Spicer, J. Vac. Sci. and Tech. 15:4 (in press).
24. S.Y. Tong, private communication; A. Kahn, E. So, P. Mark, C.B. Duke, and R. Meyer, J. Vac. Sci. and Tech. 15:4 (in press).
25. P. Mark et al, CRC Reviews in Solid State Physics, (in press).
26. W.E. Spicer, I. Lindau, P.E. Gregory, C.M. Garner, P. Pianetta,

Fig.

ity.
ever
dent
nineste;
the
the

- and P.W. Chye, J. Vac. Sci. and Tech. 13:780 (1976).
27. W. Gudat and D.E. Eastman, J. Vac. Sci. and Tech. 13:831 (1976).
28. C. Caroli, D. Lederer-Rozenblatt, B. Roulet, and D. Saint James, Phys. Rev. 138:4552 (1973); P.J. Feibleman, Phys. Rev. Lett. 34:1092 (1975); Phys. Rev. B 14:762 (1976).
29. J. van Laar and J.J. Scheer, Sur. Sci. 8:342 (1967).
30. J. van Laar and A. Huijser, J. Vac. Sci. and Tech. 13:769 (1976).
31. A. Huijser and J. van Laar, Sur. Sci. 52:202 (1976); J. van Laar, A. Huisjer, and T.L. von Rooy, J. Vac. Sci. and Tech. 14:894 (1977); W.E. Spicer, P. Pianetta, I. Lindau, and P.W. Chye, J. Vac. Sci. and Tech. 14:885 (1977).
32. J.R. Chelikowsky, S.G. Louie, and M.L. Cohen, Phys. Rev. B 14:894 (1977); D.J. Chadi, J. Vac. Sci. and Tech. (to be published);
33. G.P. Schwartz, C.D. Thurmond, C.W. Kamlott, and B. Schwartz, J. Vac. Sci. and Tech. 17:5 (1980) in press, and references therein.
34. W.E. Spicer, I. Lindau, P. Pianetta, P.W. Chye, and C.M. Garner, Thin Solid Films 56:1 (1979).
35. P.W. Chye, C.Y. Su, C.M. Garner, P. Pianetta and W.E. Spicer, Sur. Sci. 88:439 (1979).
36. W.E. Spicer, I. Lindau, P. Skeath, C.Y. Su, and P.W. Chye, Phys. Rev. Lett. 44:420 (1980), and references therein.
37. W.E. Spicer, P.W. Chye, P. Skeath, C.Y. Su, and I. Lindau, J. Vac. Sci. and Tech. 16:1422 (1979).
38. P.W. Chye, I. Lindau, P. Pianetta, C.M. Garner, C.Y. Su, and W.E. Spicer, Phys. Rev. 18:5545 (1978).
39. I. Lindau and W.E. Spicer, J. Electron Spectroscopy 3:409 (1973).
40. P. Pianetta, I. Lindau, C.M. Garner, and W.E. Spicer, Phys. Rev. B (in press).
41. C.Y. Su, I. Lindau, P. Skeath, P.W. Chye, and W.E. Spicer, J. Vac. Sci. and Tech. 5 (1980) in press.
42. J.N. Miller, D.T. Ling, M.L. Shek, D.L. Weissman, P.M. Stefan, I. Lindau, and W.E. Spicer, Sur. Sci. 94:16 (1980).
43. J.N. Miller D.T. Ling, I. Lindau, P. Stefan, and W.E. Spicer, Phys. Rev. Lett. 38:1419 (1977).
44. M.L. Shek, P.M. Stefan, D.L. Weissman, B.B. Pate, I. Lindau, and W.E. Spicer (to be submitted).
45. J.N. Miller, S.D. Schwartz, I. Lindau, W.E. Spicer, B. De Michelis, I. Abbati, L. Braicovich, J. Vac. Sci. and Tech. 5 (1980) in press.
46. K.Y. Yu, C.R. Helms, and W.E. Spicer, Solid State Comm. 18:1365 (1976); K.Y. Yu, D.T. Ling, and W.E. Spicer, J. of Catalysis 44:373 (1976) and references therein.
47. D.T. Ling, J.N. Miller, I. Lindau, W.E. Spicer, and P.M. Stefan, Sur. Sci. 612 (1978).
48. K.Y. Yu, C.R. Helms, W.E. Spicer, and P.W. Chye, Phys. Rev. 15:1629 (1977).

APPENDIX D

Ph. D. Dissertation (Stanford University, 1981)

C. Y. Su

PHOTOEMISSION STUDIES OF THE INTERACTION OF OXYGEN WITH SOLID SURFACES

A DISSERTATION
SUBMITTED TO THE DEPARTMENT OF ELECTRICAL ENGINEERING
AND THE COMMITTEE ON GRADUATE STUDIES
OF STANFORD UNIVERSITY
IN PARTIAL FULFILLMENT OF THE REQUIREMENTS
FOR THE DEGREE OF
DOCTOR OF PHILOSOPHY

By

Chung-Yi Su

August 1981

I certify that I have read this thesis and that in my opinion it is fully adequate, in scope and quality, as a dissertation for the degree of Doctor of Philosophy.

(Principal Adviser)

I certify that I have read this thesis and that in my opinion it is fully adequate, in scope and quality, as a dissertation for the degree of Doctor of Philosophy.

I certify that I have read this thesis and that in my opinion it is fully adequate, in scope and quality, as a dissertation for the degree of Doctor of Philosophy.

(Material Science and Engineering)

Approved for the University Committee
on Graduate Studies:

Dean of Graduate Studies & Research

ACKNOWLEDGEMENT

I wish to express my deepest appreciation to Professor William E. Spicer and Professor Ingolf Lindau for their guidance, encouragement and support. Professor Spicer is specially thanked for the extra time he spent in tutoring me English. Professor Lindau is specially thanked for leading me through my first series of graveyard shifts at SSRL.

I want to thank my associate dissertation adviser, Professor Gerald L. Pearson, for his warm encouragement throughout the years at Stanford.

I am grateful to Professor Clayton Bates Jr. for his many helpful suggestions and reading of this manuscript.

Special thanks must go to the members of the Stanford Tube Lab, completion of this dissertation work would have been impossible without their excellent technical support.

Thanks are also extended to the members of the photoemission group, for providing a stimulating and enjoyable working environment and, in particular, to Patrick Chye and Perry Skeath who have collaborated in a large part of the experimental work.

Attention should also be brought to my wife Chun-ling, a silent partner in this work, whose companionship and good spirit have made the otherwise difficult graduate student life memorable. Finally I want to thank our parents for their encouragement and support.

Financial support of this work was provided by the Advanced Research Project Agency of the Defense Department through the Office of Naval Research.

ABSTRACT

The interaction of oxygen with solid surfaces has been studied with angle-integrated photoelectron spectroscopic techniques using synchrotron radiation as light source. The systems studied include O/Si(111), O/GaAs(110), O/Cs, and oxygen adsorption on cesiated GaAs(110) surfaces. The results from these studies are applied to characterizing and understanding the (Cs,O) activated surfaces of GaAs negative electron affinity (NEA) photocathodes.

Room temperature adsorption of oxygen on 2x1 and 7x7 reconstructed Si(111) surfaces is shown by core level shift and sticking coefficients to proceed differently, indicating strongly different nature of the two reconstructions and supporting the defect type models for the 7x7 reconstruction. The bonding configuration of oxygen on the Si(111) 2x1 surface is studied by examining the effects of annealing on the shifts in Si-2p. Possible chemisorption configurations are discussed in terms of the new information gained and many possibilities are eliminated.

In the study of room temperature adsorption of oxygen on cleaved GaAs(110) surfaces, particular effort has been given to obtain the proper photoemission spectrum that represents the density of valence states (DOVS) of the oxygen bonded to GaAs(110). Simple theoretical interpretation, substantiated with comparison made between the DOVS of O/GaAs(110) and the experimental DOVS' of Ga₂O₃ and As₂O₃, of the DOVS

of $O/GaAs(110)$ has led to the proposal of a new adsorption model involving both nonbridging oxygen ($As=O$) and bridging oxygen ($Ga-O-As$). Another form of oxygen which saturates at relatively low oxygen which adsorbs at defect sites of the $GaAs(110)$ in the form of $Ga-O-Ga$ units was also observed. The role of oxygen adsorption at defect sites in the initial steps of adsorption, particularly the dissociation of oxygen molecules, is discussed. Such discussion is further substantiated by detailed studies of the oxygen adsorption on sputter-disordered $GaAs(110)$ surfaces.

In the studies of the oxidation of Cs, four different states of oxygen were observed. Definitive identification of three of the four oxygen states has been achieved by considering both the energy separations and the absolute binding energies of the multiplets originated from photoionizing the $O-2p$ subshell. The oxygen species identified are O^{2-} , O_2^{-2} and O_2^- .

In studying the interaction of (Cs,O) with $GaAs(110)$ surfaces, the bonding of oxygen to $GaAs$ is found to be drastically enhanced ($>10^7$ times) by the presence of one monolayer of Cs. On a monolayer-Cs-covered $GaAs$ surface, no oxygen can be incorporated into the Cs layer before a significant amount of oxygen species is bonded to $GaAs$ and only one oxygen species is found to incorporate into the Cs layer; in particular, O^{2-} , the species contained in cesium suboxides and Cs_2O , is not formed over the wide range of oxygen exposure studied ($0.5 - 1100$ L). With two to three monolayers of Cs present on the $GaAs$ surface, the oxidation property of the Cs atoms becomes similar to that of bulk Cs

such that all four oxygen species encountered in the oxidation of bulk Cs are formed; even at this stage the competition of the GaAs substrate for oxygen is not negligible.

p-GaAs(110) surfaces activated with (Cs,O) to NEA condition have also been studied. A typical activated GaAs surface is found to consist of a layer of oxygen bonded to GaAs and a (Cs^+, O^{2-}) layer. A GaAs-O-Cs dipole plus the polarization of a $Cs^+-O^{2-}-Cs^+$ sandwich layer is proposed to explain the NEA condition. The identification of the O-GaAs bonding layer explains the better yield achieved by the two-step activation process compared to that achieved by a single yo-yo process. Possible optimization of the activation process by forming the O-GaAs layer and the (Cs^+, O^{2-}) layer is also discussed. Adsorption of OH from the residual gas in an ultrahigh vacuum chamber is identified as one degradation mechanism of the GaAs photocathodes.

CONTENTS

ACKNOWLEDGEMENT	iii
ABSTRACT	v

<u>Chapter</u>	<u>page</u>
I. INTRODUCTION	1
II. INTERACTION OF OXYGEN WITH SI(111) SURFACES	4
Introduction	4
Experimental	4
The Nature of the 7x7 Reconstruction	6
Introduction	6
Results and Discussion	9
Possible Oxygen Chemisorption Configurations on the Si(111)	
2x1 Surface	17
Introduction	17
Results and discussion	17
Summary and Concluding Remarks	32
Appendix	33
REFERENCES	36
III. PHOTOEMISSION STUDIES OF THE INTERACTION OF OXYGEN WITH GAAS(110)	39
Introduction	39
Experimental	41
Results and Discussion - Room Temperature Adsorption on Cleaved GaAs(110)	42
Results from Core-level Spectra	43
Valence Band Spectra	49
Interpretation of the DOVS	57
The Low Coverage Adsorption State	65
Discussion of the Possible Adsorption Mechanisms	68
Results and discussion - Oxygen Adsorption on Disordered GaAs(110) Surfaces	73
The Sputtered Surface	75
The DOVS of Oxygen-adsorbed Sputter-disordered Surfaces	79
The Adsorption Process on Disordered Surfaces	87
Results and Discussion - Effects of Heat Treatments of Oxygen-covered Surfaces	90
Summary	106

REFERENCES	109
Appendix A: Photoemission Studies of the Electronic Structure of Ga ₂ O ₃	111
REFERENCES FOR APPENDIX A	122
Appendix B: Photoemission Studies of Room Temperature Oxidation of As	122
Introduction	122
Experimental	123
Results and Discussion	125
Summary	136
REFERENCES FOR APPENDIX B	137
Appendix C: Fermi Level Movement and Electron Affinity Change	138
REFERENCES FOR APPENDIX C	144
Appendix D: Calculation of the N-B Splittings	144
IV. PHOTOEMISSION STUDIES OF CLEAN AND OXIDIZED CS	146
Introduction	146
Experimental	148
Results and discussion-Clean Cs	150
Valence Band Spectra of Clean Cs	150
Core Levels and Auger Transitions	152
Results and Discussion - Oxidized Cs	157
Summary of 0-2p Related Features	158
Valence band region spectra	159
Core Levels and Auger Transitions	169
Results and Discussion - Identification of the Oxygen Species Adsorbed in Cs	186
Multiplet structure	188
The Binding Energies and the Ionization Energies	193
The oxidation process	204
Summary	207
REFERENCE	209
V. PHOTOEMISSION STUDIES OF THE INTERACTION OF (CS ₂ O) WITH THE GAAS(110) SURFACE	212
Introduction	212
Experimental	213
Photoemission Spectra of Oxidized Cs	215
Results and Discussion - Properties of the Cs overlayer	217
Results and Discussion - Adsorption of Oxygen on Monolayer- Cesium-Covered GaAs (110)	219
Identification of oxygen induced features	221
The Oxygen Adsorption Process on Cs-covered GaAs(110)	234

Results and Discussion - Effects of Additional Cs	
Treatments	239
The Photoelectron spectra	241
Adsorbate Induced Surface Electrostatic Potential Change and the Shift of Adsorbate Core Levels	251
The Interaction Mechanisms	257
Summary	258
Appendix	260
REFERENCES	262
VI. PHOTOELECTRON SPECTROSCOPIC DETERMINATION OF THE STRUCTURE OF (Cs,O) ACTIVATED GAAS(110) SURFACES	264
Introduction	264
Experimental	268
Summary of Some Fundamental Properties of the (Cs,O,GaAs) System	270
Results and Discussion - Model of the (Cs,O) Activated GaAs(110) Surface Prepared by the "Yo-yo" Technique	271
The Model	272
Other Implications of the Model	285
The Influence of OH ⁻ on Activated Surfaces	290
Conclusion	299
REFERENCES	301
VII. CONCLUSIONS: LOOKING AHEAD	304
Adsorption of oxygen on Si and GaAs surfaces	304
The (Cs,O) activated GaAs surfaces	306

LIST OF TABLES

<u>Table</u>	<u>page</u>
1. Summary of Measurements	6
2. Heats of formation, chemical shifts in Si-2p and the number of affected Si atoms of various Si-O bonding configurations . . .	22
3. Percent of shifted As-3d and Ga-3d at various exposures	49
4. Qualitative trends in the characteristics of the DOVS' of a few oxygen bonding configurations	60
5. Intensity changes in Ga, As, and oxygen levels induced by oxygen adsorption on a sputter-disordered GaAs surface	88
6. Summary of binding energies (BE) of photoelectron core lines and kinetic energies (KE) of Auger transitions of clean Cs. . .	157
7. Summary of binding energies of different oxygen states observed in the oxidation of Cs	158
8. Changes in the binding energy of the $4d_{5/2}$ level and the N00 transition at different oxygen exposures.	183
9. The nearest O-O distance in Cs-O compounds (a)	187
10. Comparison of calculated and measured BE of oxygen levels of various oxygen species in Cs	197
11. Heats of formation, standard entropies, and free energies of reaction of Cs, Ga, and As oxides	237
12. Heats of formation and free energies of reaction of adding Cs to various oxides	261
13. Heats of formation of OH compounds	299

LIST OF ILLUSTRATIONS

<u>Figure</u>	<u>page</u>
1. The surface reconstructions of the (111) surface of Si, viewed along a [112] direction.	8
2. Si-2p spectra of a Si(111) 7x7 surface subjected to a sequence of oxygen exposures at room temperature.	10
3. Valence band region spectra of three different oxygen-covered surfaces.	12
4. Si-2p spectra of corresponding surfaces in fig. 3.	14
5. Schematic illustration of how oxygen atoms move below the surface layer of the 7x7 structure described by "defect" models.	16
6. Spectra of the Si-2p level of a Si(111) 2x1 surface before and after exposure to 1000 L oxygen, and their difference. . . .	19
7. The Si-2p spectrum of the surface in fig. 7 after annealing at 350°C for 10 minutes	20
8. As-3d and Ga-3d levels of clean and oxygen-exposed n-GaAs(110) measured at $h\nu=100$ eV.	44
9. Difference curve between the As-3d and the Ga-3d spectra of clean and oxygen-exposed n-GaAs(110).	46
10. Photoemission spectra of clean and oxygen-exposed n-GaAs(110) obtained at $h\nu=21$ eV.	50
11. Photoemission spectra of clean and oxygen-exposed GaAs(110) obtained at $h\nu=30$ eV.	52
12. Photoemission spectra of clean and oxygen-exposed p-GaAs(110) obtained at $h\nu=21$ eV.	54
13. Removal of the coverage dependent features in the DOVS.	56
14. Comparison of the experimental DOVS of O/GaAs(110) to those of As_2O_3 and Ga_2O_3	62

15.	A proposed bonding model for room temperature adsorption of oxygen on GaAs(110).	65
16.	The photoemission spectra of a clean n:GaAs(110) (top and the difference curves	67
17.	A proposed mechanism of the dissociation of oxygen molecules on GaAs(110) surfaces	72
18.	He-I spectra of clean, sputtered, and oxygen-exposed p-GaAs(110).	74
19.	Ga-3d and As-3d levels of clean and oxygen-exposed sputter-disordered GaAs(110).	76
20.	The valence band spectra of clean and oxygen-exposed sputter-disordered GaAs(110) measured at $h\nu=100$ eV.	78
21.	Comparison of the Ga-3d and the valence band region of an oxygen-exposed sputtered-GaAs to those of Ga_2O_3	80
22.	He-II spectra of the surfaces of fig. 18.	83
23.	Comparison of the Ga-3d and the valence band region of oxygen-exposed sputtered-GaAs and cleaved-GaAs(110).	86
24.	The effect of annealing of a room temperature oxygen-exposed surface at 370°C for 30 min.	91
25.	The effect of annealing of a room temperature oxygen-exposed surface at 250°C for 30 min.	93
26.	Effects of annealing of a room temperature oxygen-exposed n-GaAs(110) in the temperature range of $50-200^\circ\text{C}$	95
27.	Effects of annealing of the surface of fig. 26 in the temperature range $250-450^\circ\text{C}$	97
28.	Difference curves between before and after heating	99
29.	Annealing of a low oxygen coverage surface to 350°C	101
30.	Re-exposure of the heat-cleaned surface of fig. 27 to oxygen. Spectra were taken at $h\nu=40.8$ eV.	102
31.	The effect of fast-heating of a room-temperature oxygen-exposed surface to $\sim 430^\circ\text{C}$	104
32.	Changes of the proposed O/GaAs(110) bonding under fast heating.	106
33.	Photoemission spectra of clean and oxygen-exposed Ga taken at $h\nu=32$ eV.	112

34.	Blow-ups of the valence band region of the $2 \times 10^6 \text{L}$ spectrum of fig. 33,	114
35.	Blow-ups of the Ga-3d level of clean and oxidized Ga.	118
36.	Photoemission spectra of clean As taken at $h\nu=30 \text{ eV}$ and $h\nu=21$ eV.	126
37.	Photoemission spectra of clean As with the backgrounds due to the secondary electrons being removed.	128
38.	Photoemission spectra of clean and oxygen-exposed As taken at $h\nu=30 \text{ eV}$	130
39.	Comparison of spectra of oxidized As film to the spectra of gas phase As_4O_6 and crystalline As_2O_3	132
40.	Summary of the changes of the surface Fermi level position with oxygen exposures on samples studied.	139
41.	Changes of the surface Fermi level positions after annealing of oxygen-exposed surfaces to elevated temperatures.	141
42.	Details in the low kinetic energy cutoff of the 21 eV spectra of clean and oxygen-exposed p-GaAs(110)	142
43.	Valence band region spectra of clean Cs obtained at, from bottom to top, $h\nu= 21, 28$, and 30 eV	151
44.	EDCs of the 5p and the 5s levels, and OVV Auger transitions of clean Cs	154
45.	EDCs of the Cs-4d levels and the NOO Auger transition at, from bottom to top, $h\nu= 110, 120$ and 150 eV	156
46.	The first 13 eV of the EDC's of clean and oxygen-exposed Cs taken at $h\nu= 30 \text{ eV}$	160
47.	The first 13 eV of the EDC's obtained on Cs film No.2 before and after a sequence of oxygen exposures.	163
48.	Changes in the photoelectron yield of Cs at $h\nu= 30 \text{ eV}$ when subjected to a sequence of oxygen exposures.	165
49.	The first 13 eV of the EDC's obtained on Cs film No.3 before and after oxygen exposures, spectra taken at $h\nu= 100 \text{ eV}$	168
50.	EDC's of the Cs-5p levels of the surfaces of fig. 46.	170
51.	EDC's of the Cs-5p levels of the surfaces of fig. 47.	172
52.	EDC's of the Cs-5p levels of the surfaces of fig. 49.	174
53.	EDC's of the Cs-5s level of the surfaces of fig. 49.	175

54.	EDC's of the Cs-4d levels of the surfaces of fig. 49 taken at $h\nu=120$ eV.	177
55.	EDC's of the Cs-4d levels of the same surfaces of fig. 54 taken at $h\nu=110$ eV.	178
56.	The N00 Auger transition of Cs film No.3 at various oxygen exposures.	180
57.	Changes in the 0VV Auger transitions at low oxygen exposures.	185
58.	Comparison of the multiplet structures of free (thin lines) and adsorbed (short bars) oxygen species:	189
59.	Spectra of various oxygen species in Cs, obtained from oxidizing thick Cs films.	216
60.	EDC's of As-3d, Ga-3d, Cs-5s and O-2s levels of clean, monolayer-Cs-covered and oxygen-exposed GaAs(110), $h\nu=120$ eV.	223
61.	EDC's of Cs-4d and the N00 Auger transition of clean and oxygen-exposed monolayer-Cs on a GaAs(110) surface, at $h\nu=120$ eV.	225
62.	Cs-5p levels and the valence band region of the EDC's of clean, Cs-covered and oxygen exposed GaAs(110), $h\nu=120$ eV.	226
63.	Comparison of oxygen induced feature in the spectra of oxygen adsorbed on a Cs-covered and a bare GaAs(110) surface.	229
64.	He-I spectra fo sample P1 covered with 0.6 monolayer Cs and subsequently subjected to a series of oxygen exposures.	231
65.	He-I spectra of sample P2 covered with one monolayer of Cs and subjected to a sequence of oxygen exposure.	232
66.	21 eV spectra of a bare p-GaAs(110) surface subjected to two heavy oxygen exposures.	233
67.	EDC's of the Cs-4d levels and the N00 Auger transition of sample N2 subjected to alternating Cs and oxygen treatments.	243
68.	EDC's of the Cs-5p levels and the valence band region of sample N2 subjected to alternating Cs-O treatment.	246
69.	EDC's of Ga-3d, As-3d, Cs-5s and O-2s of sample N2 subjected to alternating Cs-O treatment.	248
70.	EDC's of As-3d, Cs-5s, O-2s, and Ga-3d spectra of sample N2 subjected to alternating Cs and O treatments.	250
71.	Schematic illustration of the changes in the surface dipole potential induced by oxygen or Cs adsorption.	256

72.	The He-II spectrum of a typical activated p-GaAs surface . . .	274
73.	EDC's of an unsuccessfully activated p-GaAs(110) surface before and after heating at 385°C for 10 min.	276
74.	Structural model typical activated GaAs surfaces (a) and the corresponding potential profile (b)	277
75.	Comparison of the oxygen coverages using He-I spectra	282
76.	EDC's of three p-GaAs surfaces activated to different white light sensitivity, $h\nu=40.8$ eV (He-II).	293
77.	Evolution of a thick (Cs, O, OH) overlayer on sample P6 in ultra high vacuum as recorded in He-II photoemission spectra. . .	296
78.	Overnight degradation of an activated surface as recorded in He- II photoemission spectra.	298

Chapter I

INTRODUCTION

Oxides are abundant in nature and are important material for many technological applications. The process of oxidation is therefore interesting and important to study. This especially true for modern day technology where the use of oxides very often requires precise control of the oxidation process. The first step of an oxidation process is the interaction of oxygen with the surface of a solid. Our aim is to obtain understanding of such interaction on the atomic scale. We therefore pursue to study the adsorption of oxygen on well characterized solid surfaces under ultrahigh vacuum conditions. Such adsorption phenomena, however, encompass an enormously large branch of surface science which is certainly beyond the appropriate scope for a dissertation research. Particular choices of subjects of study are therefore necessary. Some perspective views of the subjects studied and the organization of this dissertation are given below, more specific reasons for studying each subject will be found in the Introduction section of the chapter covering that subject.

The adsorption systems studied can be roughly divided into two areas according to the two types of devices they are related to. One area currently of strong practical interest due to the importance of MOS devices is the understanding of oxide-semiconductor interfaces. For this area we have chosen to study oxygen adsorption on the surfaces of two technologically important semiconductors, Si and GaAs. These oxygen

adsorption studies are relevant for understanding of oxide-semiconductor interfaces not only because critical information can be gained about the oxidation processes, as mentioned above, but also because the bonding of oxygen to semiconductor surface in the chemisorption stage simulates the oxygen-semiconductor bonding environment at oxide-semiconductor interfaces. For example, at the Si-SiO₂ interface we have to consider oxygen atoms bonded to Si atoms which are bonded to other Si atoms, i.e., in considering the Si-O bonding at the interface we have to take into account the constraints of the Si lattice. Such constraints of the substrate lattice are also present in the chemisorption of oxygen on semiconductor surfaces.

The Si(111) surface and the GaAs(110) surface also form an interesting case of comparison in studying the oxygen adsorption process: Si is covalent whereas GaAs is ionic; Si(111) transforms from a 2x1 surface reconstruction to a 7x7 reconstruction when it is heated, whereas GaAs has only one surface structure at all temperature below the dissociation point. How these different properties between the Si(111) surfaces and the GaAs(110) surface influence the oxygen adsorption properties of the two semiconductor surfaces will be seen in Chapter II (for Si(111)) and Chapter III (for GaAs(110)).

Another area of studies is related to the negative electron affinity (NEA) GaAs photocathodes. The NEA condition is achieved by treating GaAs surfaces with Cs and oxygen. Clear understanding of the mechanism of achieving NEA conditions, however, has been lacking. Since the successful operation of a photocathode depends on the escape of photoelec-

trons through the surface, it can be considered as a "surface device" which naturally brings in a few interesting surface science problems. To attack this problem from a fundamental point of view, we have studied the oxidation of bulk Cs which will be presented in chapter IV, and the adsorption of Cs and oxygen on GaAs(110) surfaces which will be presented in chapter V. These two studies, together with the study of oxygen adsorption on GaAs(110) in chapter III, provide a solid basis for studying GaAs(110) surfaces activated with a less-well defined "yo-yo" process, which we will discuss in chapter V.

The study of the oxidation of Cs is also of fundamental interest on its own. The large ionicity difference between oxygen and Cs allows the opportunity to examine the electronic structure of a series of oxygen species (O^{-2} , O_2^{-2} , O_2^{-} , etc.) with photoemission. The interaction of oxygen with Cs also forms sharp contrast with the adsorption processes on semiconductor surfaces. The study of co-adsorption of Cs and oxygen on GaAs(110) surfaces brings two extreme types of adsorption together. As we will see in Chapter V, the oxygen adsorption process on GaAs surfaces is drastically modified by the presence of a monolayer of Cs. The oxidation property of a monolayer Cs is also altered by the presence of the strongly localized oxygen-GaAs bonding. Such co-adsorption studies thus shed light on both the adsorption of oxygen on GaAs and the oxidation of Cs. The fundamental understanding of the O/GaAs, the O/Cs and the co-adsorption of Cs and oxygen on GaAs(110) finally lead to a new model of the (Cs,O) activated GaAs surfaces in Chapter VI.

Chapter II

INTERACTION OF OXYGEN WITH Si(111) SURFACES

2.1 INTRODUCTION

In this chapter we will report new experimental results of the interaction of oxygen with the (111) surfaces of Si. In particular, the difference between the 2x1 and the 7x7 reconstructions will be considered. Implications to both the understanding of the clean surfaces (section 3) and the oxygen adsorption properties (section 4) will be discussed.

2.2 EXPERIMENTAL

Experiments are performed in a standard stainless steel ultra high vacuum chamber with base pressure about $3\sim 5 \times 10^{-11}$ torr. The samples studied were single crystals of n-type Si (As doped, $N \sim 10^{16} \text{ cm}^{-3}$). These crystals were cut into bars oriented in the [111] direction, with a cross section of 5x5 mm. The 2x1 surfaces were prepared by cleaving in situ, and the 7x7 surfaces were prepared by thermal conversion of cleaved surfaces ($530^\circ \text{ C} \sim 560^\circ \text{ C}$, for >20 min.). Sharp 7x7 LEED patterns were observed after such treatment. Heating of the samples was achieved by either passing a current through the sample or by using a well outgassed and enclosed filament behind the samples.

Oxygen exposures were made by leaking oxygen gas (research grade, obtained in glass flasks) through a bakable leak valve (Varian Associates). Sizes of exposures are measured in Langmuirs (L) where $1 \text{ L} = 10^{-6}$ torr-sec. To avoid complications arising from dependence of the oxygen

adsorption process, as reported by Garner et al [10], the lowest oxygen pressure used was 10^{-6} torr. Care had been taken to avoid any source of excited oxygen. The gauges used include a Redhead coldcathode gauge (maximum pressure 10^{-5} torr) and a Varian cold cathode gauge (Model 860, 10^{-7} torr $< p < 10^{-2}$ torr).

The photoemission experiments were performed on the 4 degree line at the Stanford Synchrotron Radiation Laboratory (SSRL). Some experiments were performed with a 600 lines/mm grating in the monochromator and some with a 1200 lines/mm grating. Photoelectron energy analyses were performed using a double pass cylindrical mirror analyzer (Physical Electronics) and pulse counting techniques. The combined analyzer-monochromator energy resolution is set at ~ 0.35 eV for obtaining Si-2p level spectra. (This was measured by the FWHM of Au-4f_{7/2} line.), and at ~ 0.4 eV for obtaining the valance band region spectra (as measured by the Au Fermi edge). A Mg-K α X-ray source is used to measure the O-1s level. The combined resolution in this case is about 1.3 eV as measured by the FWHM of the Au-4f_{7/2} line. The photoemission measurements are listed in table 1.

TABLE 1
Summary of Measurements

Measurements	Information Gained
valence structure at $h\nu = 130$ eV	1. energy positions of the O-2p levels 2. amount of oxygen
Si-2p core level at $h\nu = 130$ eV	1. oxygen induced chemical shifts 2. number of Si atoms bonded to oxygen
O-1s at $h\nu = 1253$ eV	1. amount of oxygen 2. binding energy of O-1s

2.3 THE NATURE OF THE 7X7 RECONSTRUCTION

2.3.1 Introduction

Surface reconstructions are important phenomena observed on covalent semiconductor surfaces. When a surface is created by terminating the bulk structure of a covalent solid, a large number of unsatisfied bonds are present on the surface. The surface therefore has a tendency to adjust itself in order to lower the total energy of the system. Thus, understanding of how the surface reconstruct is an important step in advancing our knowledge of covalent bonds in semiconductors in general.

It is well known that (111) surface of Si exhibits a 2x1 structure after cleaving at room temperature, and transforms to a 7x7 structure after annealing at elevated temperature ($\geq 200^\circ\text{C}$). As schematically

depicted in fig. 1, the generally accepted description of the 2×1 reconstruction is that rows of surface atoms are alternately raised and lowered [1]. While various models for the 2×1 surface differ only quantitatively in the structural parameters describing the "buckling", two qualitatively distinct groups of models have been proposed: the "weak perturbation" [2] and the "defect" [3] models. Although we realize the use of "weak perturbation" and "defect" here may raise objections, we hope that the conceptual contrast between the two groups of models are well brought out. As are also illustrated in fig. 1, the first group of models describe the tendency of the surface to reconstruct within the constraints of the crystal structure, so the final structure is obtained by applying a "perturbation" to the smooth plane. The second group describes the tendency of the surface to break away from the constraints of the crystal structure through "defect creation" in the smooth plane.

Clearly, experimental inputs are required to distinguish the two rivary theories of surface reconstruction. In the past, gas adsorption experiments involving hydrogen [4] and chlorine [5] have provided a simple test to distinguish the two types of models. There the relative stability of the 7×7 structure (as compared with the 2×1 structure) against hydrogen [4] and chlorine [5] adsorption strongly supports the "defect" type models. Employing gas adsorption experiments to distinguish reconstruction models is a particularly viable approach here because the 2×1 structure can be taken as a "known reference" for the "weak perturbation" type 7×7 surfaces in considering the adsorption behavior. In the present case, we have adopted the same general approach with oxygen as the particular adsorbate. The advantage of

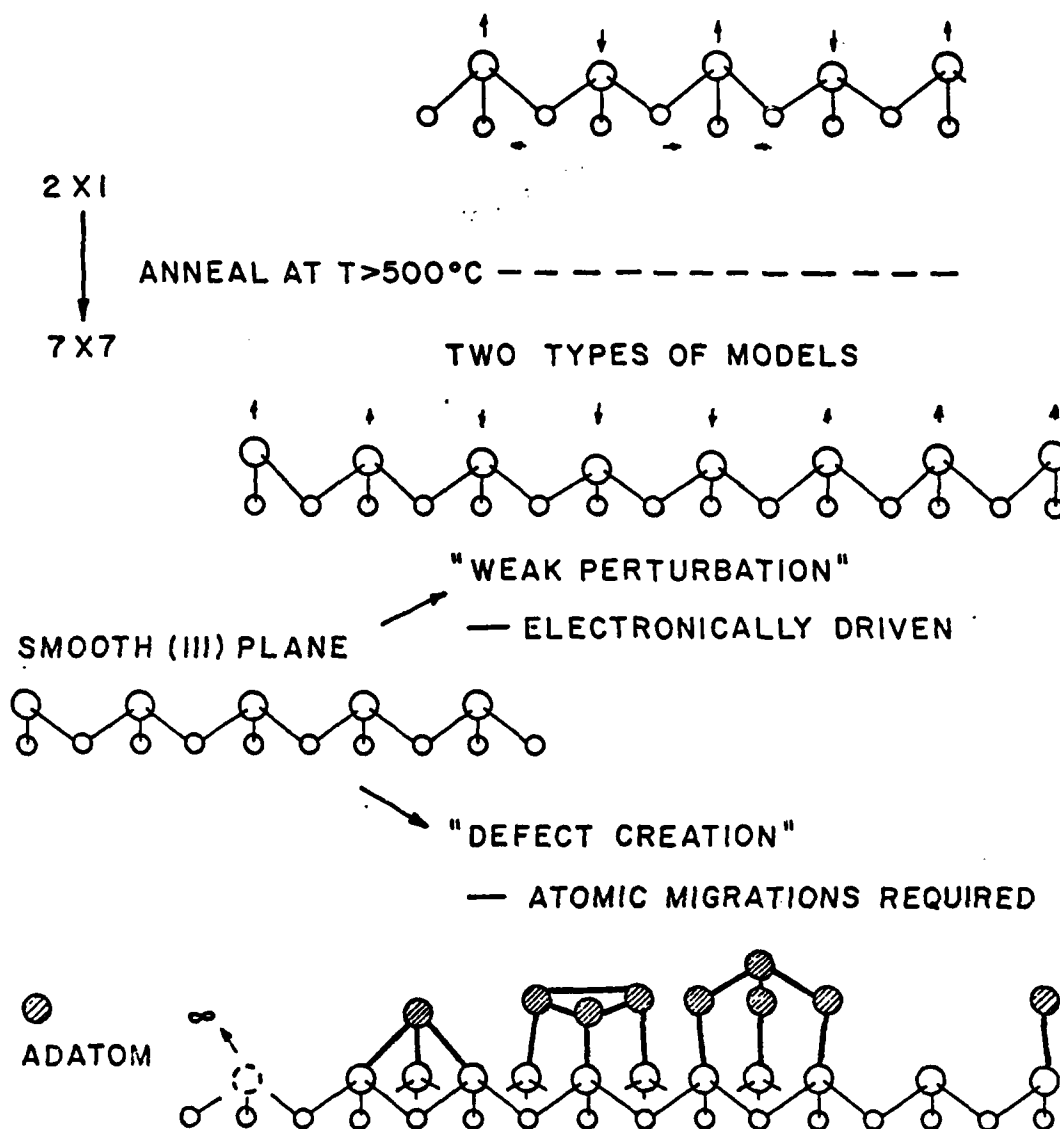


Figure 1: The surface reconstructions of the (111) surface of Si, viewed along a [112] direction. Buckling of alternate rows of surface atoms is the generally accepted description of the 2x1 reconstruction (top). The two competing types of models for the 7x7 structure are constrained by their relations to a smooth plane. Specific models in the "defect" group mentioned in Ref. 3 are depicted in the bottom schematics.

using oxygen is that Si-O bonding is known to induce large chemical shifts in the Si core levels, which, in turn, may facilitate more definite comparison between the adsorption properties of the 2x1 and 7x7 surfaces.

2.3.2 Results and Discussion

We will compare the 2x1 and the 7x7 surface at the saturation point of the fast chemisorption stage. This point represents the completion of the interaction of oxygen with surface, and hence is useful in revealing the surface structure. Our long experience with the cleaved surfaces has shown that the 2x1 surface can be saturated with $\sim 10^3$ L oxygen exposure. This has found close agreement with the recent systematics studies of Kasupke and Henzler [6], which have also clarified the early finding [7] of a large variation of oxygen sticking coefficient on the 2x1 surfaces. The saturation point for the 7x7 structure was not as well established in the literature. Hence we show in fig. 2 a set of spectra of a 7x7 surface subjected to increasing oxygen exposures. Both the O-1s and the Si-2p clearly established that the saturation exposure is equal to or less than 100 L. Thus the 7x7 surface is at least 10 times more reactive to oxygen than the 2x1 surface. This difference between the 2x1 and the 7x7 surfaces favors the "defect" models to some extent, because we do not expect such a large difference in chemical reactivity if the two structures are very similar.

Fig. 3 gives the valence band region spectra of a 7x7 (curve a) and a 2x1 (curve b) surface saturated with oxygen. Curve c is the spectrum of a 2x1 surface (curve b) oxidized at room temperature and then annealed

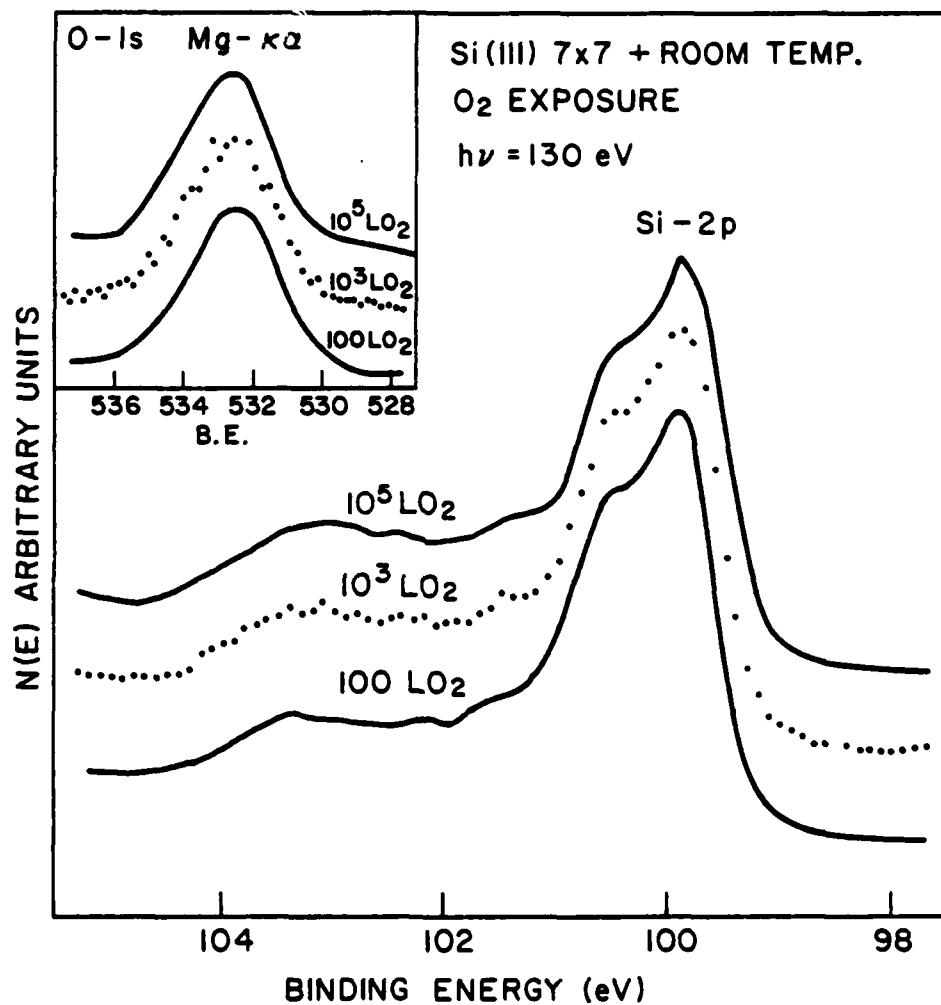


Figure 2: Si-2p spectra of a Si(111) 7x7 surface subjected to a sequence of oxygen exposures at room temperature. The inset displays the corresponding O-1s spectra. Saturation of oxygen adsorption is seen to take place at or below 100 L exposure.

at 350°C for 10 min.. A spectrum of the clean surface is also shown to indicate that the peak at ~ 3 eV binding energy (BE) is due to the Si substrate emission. The peak at 7.3 eV BE is the oxygen nonbonding orbital. We observe the following: (i) The amount of oxygen on the two surfaces are about equal, as measured by the relative peak height of the 7.3 eV BE peak and the 3 eV BE peak. (ii) The valence band region spectra do not reveal significant difference between the two surfaces. This is consistent with the early UPS result [8,9]. The lack of difference in valence band spectra, however, does not imply same oxidation state for the 2x1 and the 7x7 surfaces, as was concluded in early UPS work [8]. On the contrary, the oxidation states on the two surfaces are distinctly different as found in the Si-2p spectra (fig. 4, to be discussed below).

Fig. 4 shows the Si-2p core level spectra of the corresponding surfaces of fig. 3. A spectrum of the corresponding clean surface (dashed) is also included in each case for reference. In fig. 4a we see the presence of several chemical shifts on the 7x7 surface, with the highest value of shift being 3.4 eV. This suggests the existence of strongly inequivalent groups of surface atoms in the clean 7x7 structure. In the models within the "defect" group we can easily identify such distinctly inequivalent groups, hence this finding is taken as strongly supporting the "defect" type model. This finding is against the "weak perturbation" model, because in a structure close to the smooth plane no such inequivalent groups of atoms can be unambiguously identified; in particular, we cannot identify a special group of Si atoms that can easily achieve, at room temperature, high oxygen coordination number, which is required by the presence of the 3.4 eV shift. The above conclusions can find further support from comparison with the 2x1 surface (which we

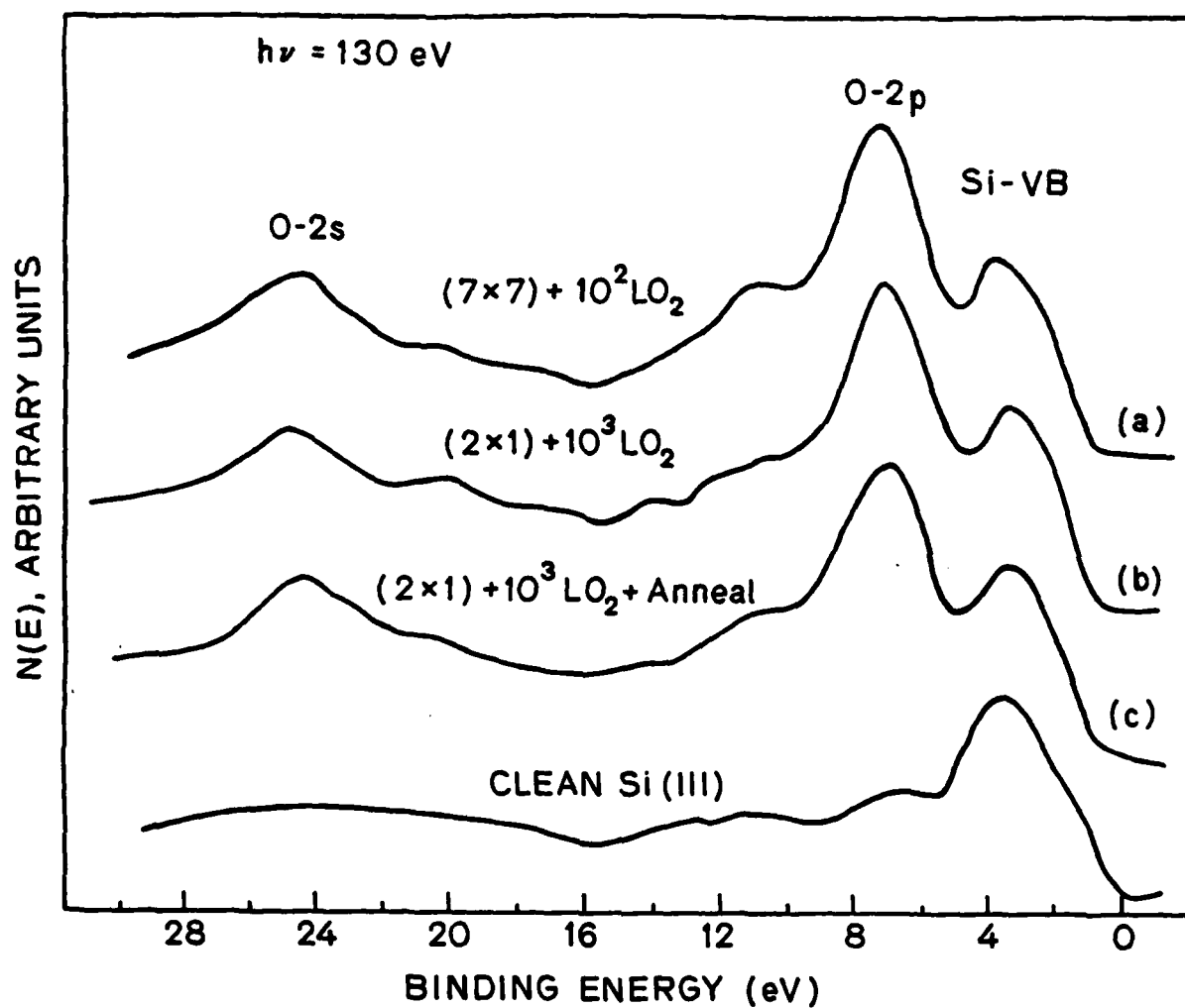


Figure 3: Valence band region spectra of three different oxygen-covered surfaces. (a) A Si(111) 7×7 surface exposed to 100 L oxygen at room temperature. (b) A Si(111) 2×1 surface exposed to 1000 L oxygen at room temperature. (c) The surface of (b) annealed at 350°C for ~ 10 min.. The bottom curve is the spectrum of a clean surface.

have taken as the known reference for the "weak perturbation" model). Fig. 4b shows that the chemical shift developed on the 2x1 surface after room temperature oxygen adsorption is small (0.9~1.4 eV). Even after annealing this 2x1 surface to an elevated temperature, the chemical shift (1.8~2.5 eV, fig 4c) is still distinctly smaller than what is expected for SiO₂ (3.8 eV [10]). The transformation of chemical shifts in fig. 4b to those in fig. 4c is rather intriguing for understanding the oxidation of the 2x1 surface per se, and this will be discussed in the next section. The important conclusion to draw here is the integrity of the 2x1 surface against oxygen attack at room temperature. A similar integrity should be found on the 7x7 surface if it were similar to the 2x1 surface with nearly identical vertical displacements of the surface atoms [Chadi, reference 2].

Another difference between the 2x1 and the 7x7 surfaces is the number of Si atoms bonded to oxygen. These numbers can be obtained by measuring the intensity of the chemically shifted components and by using a reasonable value of the photoelectron escape depth. The percent of shifted Si-2p is about ~23% for the 2x1 surface both before and after annealing, and is about 35% for the 7x7 surface. If we assume that on the 2x1 surface there are one monolayer of Si atoms bonded to oxygen, an escape depth of 6.5 Å is obtained [11]. On the other hand, unusual escape depth of 2.5 Å and 12 Å are obtained, respectively, for assuming $\frac{1}{2}$ and $1\frac{1}{2}$ monolayer of Si bonded to oxygen. Thus it is reasonable to postulate that only the top surface monolayer of Si atoms are bonded to oxygen for 2x1 surface saturated with oxygen. In contrast to the case of the 2x1 surface, the same postulate leads to ~1.6 monolayer of Si bonded to oxygen for the 7x7 surface. This number of ~1.6 monolayer

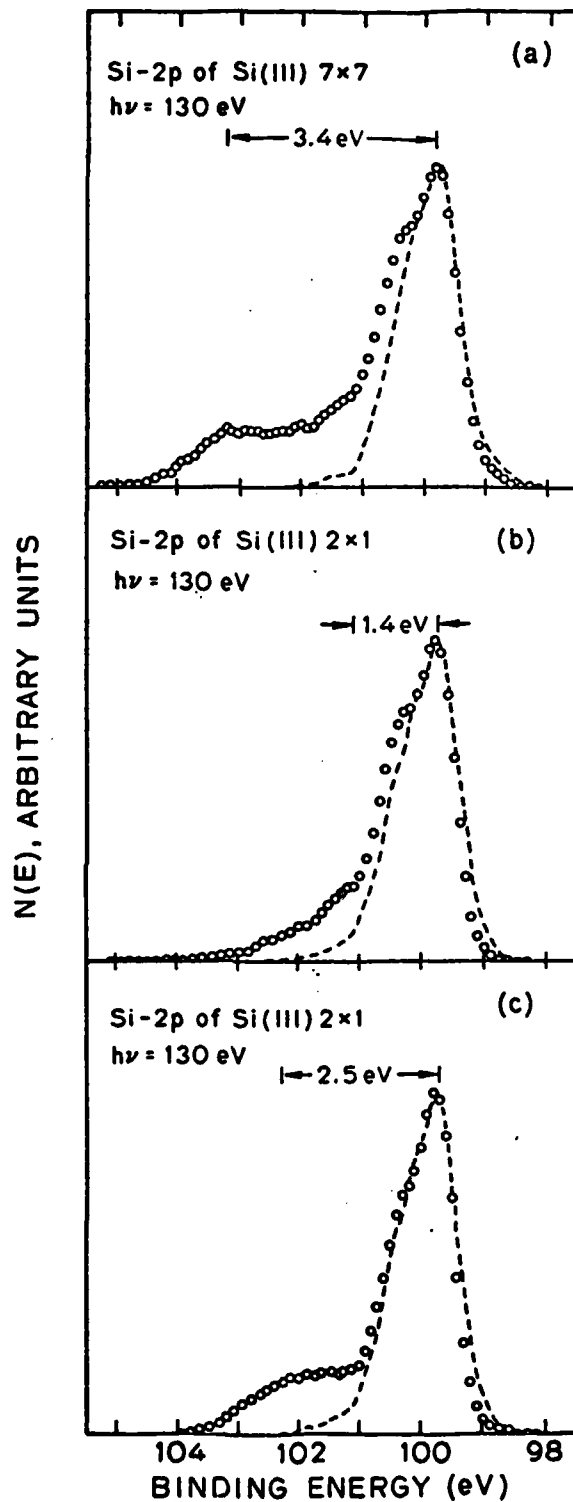


Figure 4: Si-2p spectra of corresponding surfaces in fig. 3. The spectrum of the clean surface of each case is shown by the dashed curve.

unambiguously suggests that oxygen has moved beneath the top layer of the 7x7 structure. This is another evidence strongly supporting the "defect" model for the 7x7 structure. In general, models within the "defect" group offer an open structure in which oxygen atoms can easily be incorporated into the second layer. In particular, oxygen atoms can access the second layer atoms through vacancies in Lander's vacancy model, or oxygen can attack the relatively exposed backbonds in the adatom structure of either Harrison's adatom model or the Milk-Stool model. These ideas are schematically illustrated in fig. 5. Again, the "weak perturbation" model is disfavored because no special passage for oxygen to reach the second layer can be found in this type structure.

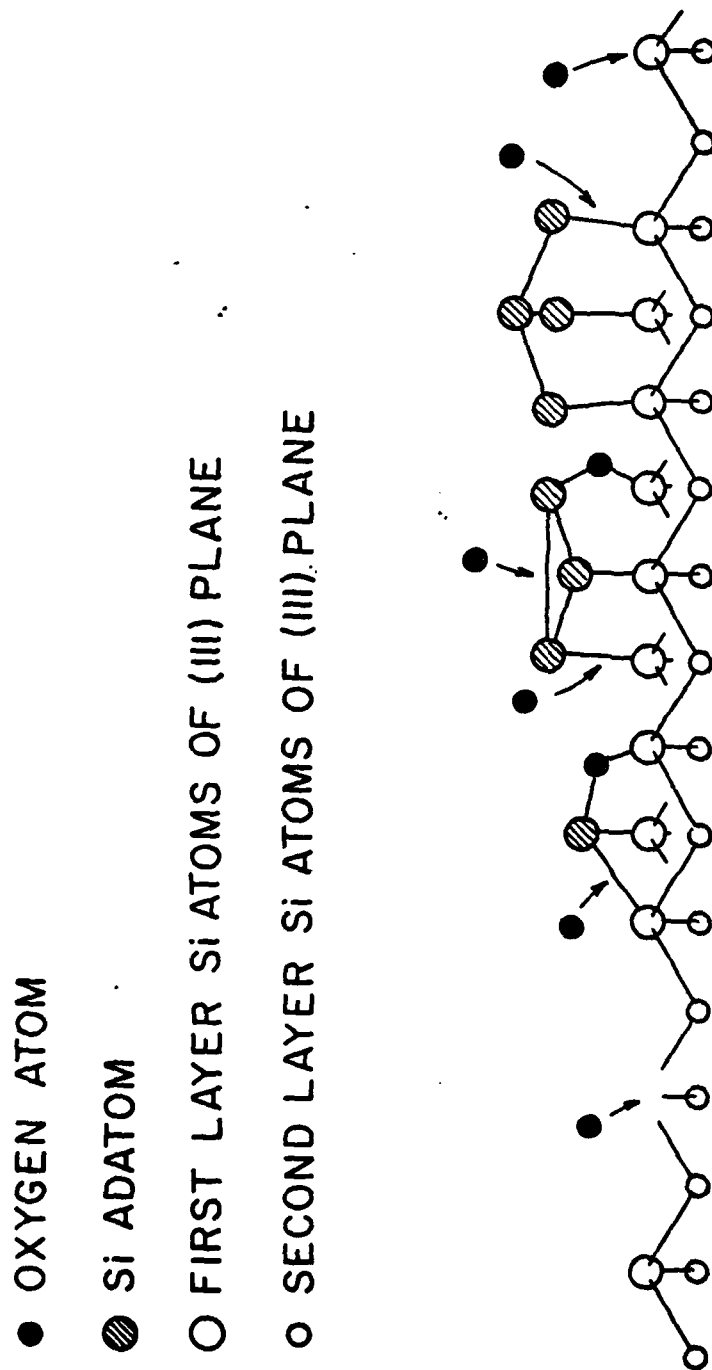


Figure 5: Schematic illustration of how oxygen atoms move below the surface layer of the 7x7 structure described by "defect" models. The particular 7x7 models depicted here are, from left to right, Lander's vacancy model, the milk-stool model and the epitaxial-bilayer model.

2.4 POSSIBLE OXYGEN CHEMISORPTION CONFIGURATIONS ON THE Si(111) 2x1 SURFACE

2.4.1 Introduction

The initial stage of oxygen adsorption at room temperature (RT) on the Si(111) surface has been a controversial question over the past two decades[7,10,12-18]. One position shared by these past discussions is the lack of distinguishing between the 2x1 and 7x7 surfaces. This has been invalidated by the findings in section 3, where distinctly different oxygen-induced chemical shifts in the Si-2p are found on the two surfaces. The discussion here will be concentrated on the 2x1 surface. More work is required to understand the oxygen adsorption on the 7x7 surface.

We report elevated-temperature annealing effects on the room-temperature(RT) chemisorption phase. By examining the specific way the RT adsorption phase transforms under heat-treatment, we have obtained new information concerning the possible Si-O bonding configurations for RT adsorption on the 2x1 surface. Although no definitive answer can be offered by the present study, we hope to show the importance of the annealing experiments.

2.4.2 Results and discussion

Fig 1 gives the energy distribution curve (EDC) of the Si-2p core level of a 2x1 surface before (dashed) and after (dotted) exposure to 1000L oxygen, and their difference (bottom). The oxygen coverage is near

saturation of the fast-chemisorption process [10]. This surface was then annealed at 350°C for 10 minutes, and the resultant spectrum is shown by the dotted curve in fig 2. The spectrum of the clean surface is also plotted in fig 2 (dashed) for reference; the difference between the two EDCs in fig 2 is shown at the bottom.

The difference curve in fig.1 indicates more than one chemical shift. Two pieces of structure are marked with arrows: one with $\Delta E = 0.9$ eV and the other with $\Delta E = 1.4$ eV [19]. The existence of a 0.9 eV or smaller shift is also confirmed by its disappearance after annealing, as seen by comparing fig. 6 and fig. 7. The 1.4 eV shift is also absent after annealing. A broad peak shifted by ~ 2 eV is now apparant. The 1.8 eV FWHM of the difference curve in fig. 7 is still suggestive of more than one chemically shifted component, although the components are more closely spaced in energy. The range of possible shifts is from $\Delta E = 1.8$ eV to $\Delta E = 2.5$ eV. The strength of the shifted peaks is $\sim 23\%$ of the total Si-2p intensity both before and after annealing. Hence the number of chemically affected Si atoms remains unchanged (within experimental error) after annealing. The number of oxygen atoms is also conserved after annealing, as measured by the O-2p and O-2s intensities.

Interpretation of chemical shifts of the Si-2p core level of silicon oxides is complicated and a controversial matter [21]. We will not rely heavily on absolute values of chemical shift for identifying bonding configurations, but will use the relative magnitude of the chemical shifts to complement other results. Ab initio calculations of chemical shifts of a limited number of chemisorption configurations became avail-

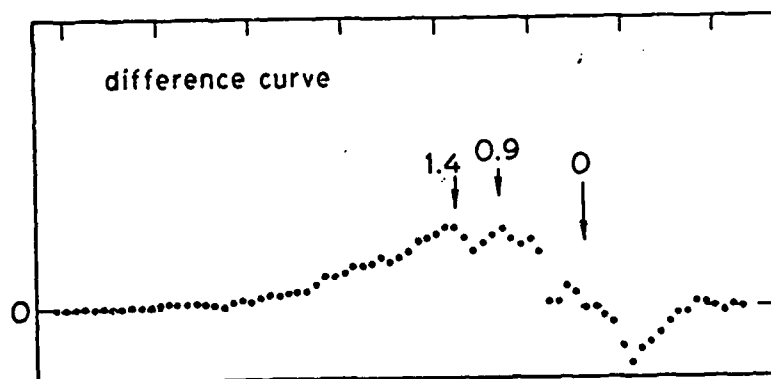
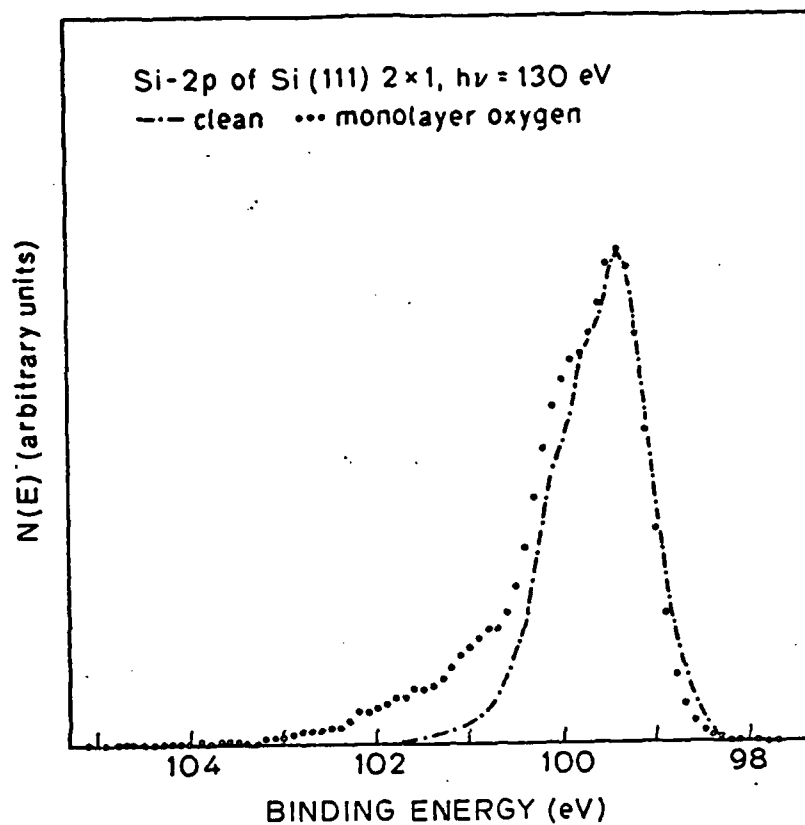


Figure 6: Spectra of the Si-2p level of a Si(111) 2×1 surface before and after exposure to 1000 L oxygen, and their difference.

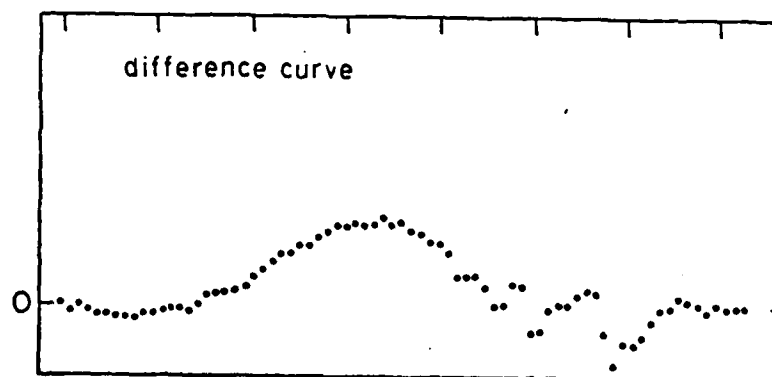
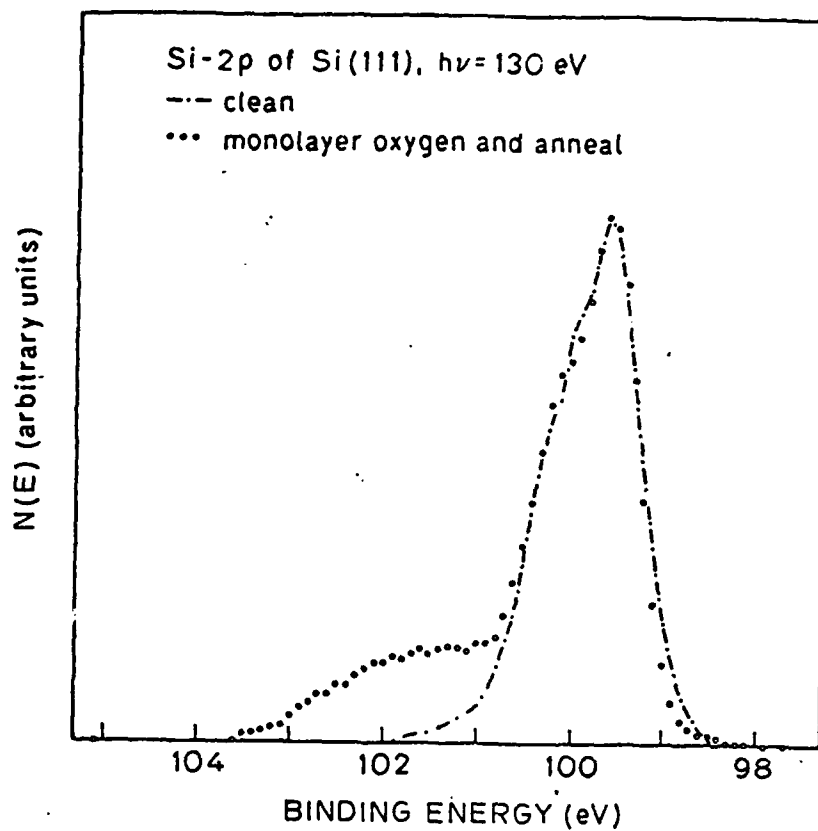


Figure 7: The Si-2p spectrum of the surface in fig. 7 after annealing at 350°C for 10 minutes and the spectrum of the clean surface (dashed), and their difference (the lower panel).

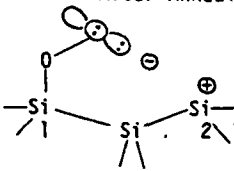
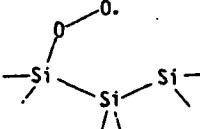
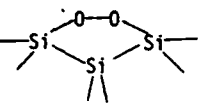
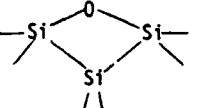
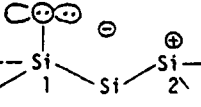
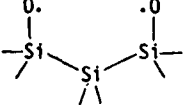
able only very recently [20]. These available values are entered in table 2. For other bonding configurations in table 2, estimates are made based on ligands of chemical shifts [10] and a shift of 2.8 eV for SiO_2 [20]. The 2.8 eV shift for SiO_2 is calculated in the same way the chemical shifts for configurations II and VI are calculated. It is more appropriate for a SiO_4 unit in a Si matrix than for bulk SiO_2 . This calculated value is used, rather than the normally quoted value of 3.8 eV [10,21], to provide a consistent scale for comparing the relative magnitude of chemical shifts of various chemisorption configurations. Caution must be exercised when attempting to directly compare the experimentally measured chemical shifts with the calculated shifts listed in table 2. Although we feel that the chemical shift for the SiO_4 unit is more appropriate than that of bulk SiO_2 in applying the ligand shifts to other surface chemisorption configurations, the reliability of such a calculation has not been tested.

Instead of trying to identify the RT and after-annealing chemisorption configurations individually, we will first select possible pairs of configurations that can properly account for the before- and after-annealing transformation properties observed. The requirements for a proper pair of before- and after-annealing configurations are listed below. A number of examples applying these conditions are given in the Appendix.

- i) The annealing transforms a bonding config. with lower heat of formation to one with higher heat of formation. (This is not the result of photoemission measurements, but is expected based

TABLE 2

Heats of formation, chemical shifts in Si-2p and the number of affected Si atoms of various Si-O bonding configurations

No.	Bonding Configurations	Heat of Formation (eV/mole O ₂)	Calculated Chemical Shift (eV)	Number of Si atoms affected per adsorbed O
Experimental Results	Before Annealing After Annealing	- -	0.9, 1.4 ~2.0	1 1
I.		0.6 ^b	1. 0.5 ^{e,9} 2. >1.0	1.0
II.		2.3 ^a	0.8 ^b	0.5
III.		3.7 ^c	<1.1	1.0
IV.		3.82 ^c	0.9	2.0
V.		4.7	1. <1.1 ^{f,9} 2. >1.0	2.0
VI.		4.7 ^{a,d}	1.1 ^b	1.0

VII.		5.0 ^d	0.7	2.0
VIII.		5.86 ^c	1. 1.49 2. 0.9	1.5
IX.		6.3	1. 1.1 2. 0.7	1.5
X.		>6.3	1. 1.89 2. 0.7	1.0
XI.		6.9 ^c	1.1 2.2	1.0
XII.	SiO ₂	9.1	2.8 ^b	0.5

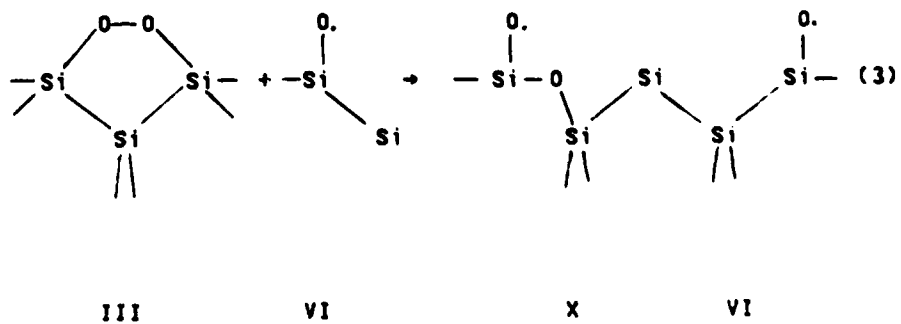
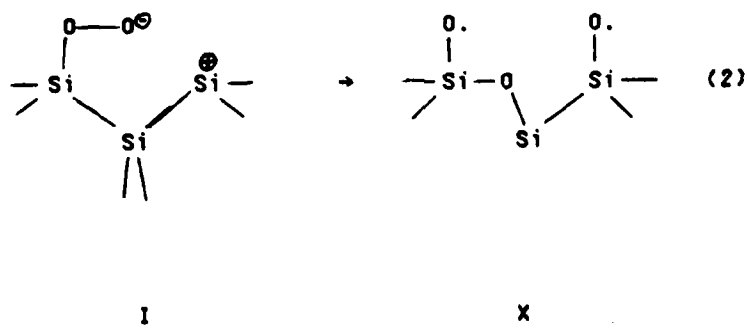
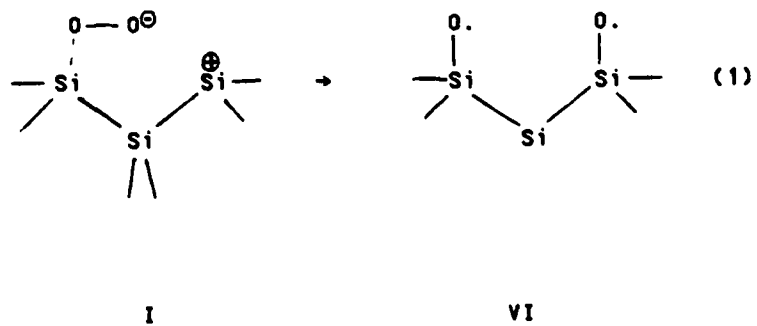
- a. Reference [6]. b. Reference [11]. c. Reference [4]
d. Estimate based on Si-O bond energy (in quartz)=4.8eV, (O=O) dissociation energy=2.5eV and Si-Si bond energy=2.0eV.
e. The extra charge on the oxygen molecule makes the oxygen atom bonded to Si less electronegative than the corresponding oxygen atom in configuration I, hence a smaller shift is expected.
f. The upper limit is assigned for reason similar to that stated in 5.
g. Notice that there are two inequivalent Si atoms in this configuration. They are numbered 1 and 2 in the configuration representation.

on thermodynamical considerations.) Heats of formation of various bonding configurations are included in table 2, and bonding configs. in table 1 are arranged with ascending stability (heats of formation) from the beginning to the end of the table.

- ii) The after annealing config. has a higher value chemical shift in Si-2p level.
- iii) The number of chemically affected Si atoms is the same for both configs. in the pair, with a conservation of the number of oxygen atoms before and after annealing. The absolute number of Si atoms chemically affected by oxygen adsorption, both before and after annealing, is one monolayer (see discussions in section 3).

Other possible pairs having the double-bond configuration (config. XI) as the end product of annealing are not included. A stable silicon-oxygen double bond is only known to occur in gas phase SiO [22]. It is doubtful if stable silicon-oxygen double bonds can be formed where two Si-Si backbonds are retained.

Applying the above conditions, we are left with the following possible pairs: (The Roman numerals indicated under each configuration representation are the corresponding configuration numbers given in table 2)



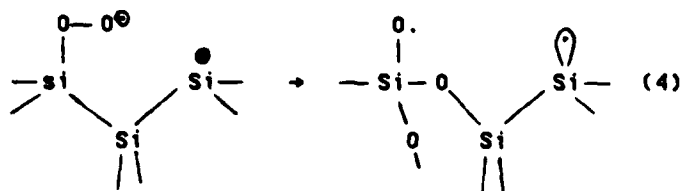
•

No definitive choice of the above possible pairs can be offered in this paper. Below, we will discuss some interesting features of these pairs and the uncertainties associated with the present results. We hope to illustrate the usefulness of annealing studies in advancing our knowledge of the oxygen adsorption processes.

In pair (3) above, a mixture of peroxide bridge (config. III) and chemisorbed O atoms (config. VI) is assigned as the possible RT chemisorption phase, because neither config. alone produces the different chemical shifts observed. The peroxide bridge is expected to be symmetric because the distortion energy changes quadratically with bond angles. The peroxide bridge is also highly strained (strain energy 50 kcal/mole [14]) so that the activation barrier separating it from the config. of chemisorbed atoms is expected to be low. The population of each of the two configs., if they exist, may therefore be comparable. The chemical shifts expected for these two configurations (table 2) are not inconsistent with the observed values.

Both (1) and (2) have the peroxy-zwitterion (config. I) as the initial RT chemisorption configuration. Since the O-O bond in the peroxy-zwitterion is weak due to the presence of the extra charge, the effect of annealing can be pictured as causing release of one oxygen atom from the peroxy. In (1) the released oxygen atom bonds to another surface atom, whereas in (2) the released oxygen atom attacks one backbonds and occupies a bridge-bonding position. The end product of transformation (5) (config. X) is more stable than the end product of transformation (1) (config. VI). The question is whether the activation barrier for

transformation (2) is low enough so it can occur instead of (1). We notice that the backbonds to the Si atom chemisorbed with oxygen atom may be considerably weakened by the Si-O bonding and are thus more exposed to attack. The released oxygen atom may also be energetic enough [23] to break one backbond. Transformation (2) thus appears to be more favorable than transformation (1) in describing our experimental results. The possibility of having a mixture of transformations (1) and (2) certainly cannot be ruled out. We call attention to the arbitrariness of the annealing condition. By no means do we expect a single bonding configuration to result from this annealing condition. We also recognize that more than one backbond to the same surface Si atom may be broken



I

so that islands of high-oxygen coordinated SiO_x units start to grow. This brings the value of the chemical shift closer to that which is observed after annealing than (5). Another difference between (1) and

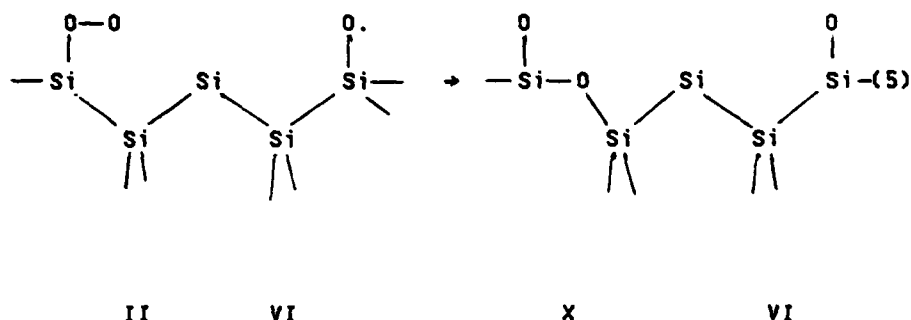
(2) is that in (2) a singly occupied dangling bond is left unsatisfied after annealing. Such a dangling bond has been found by Pointdexter [24] to be stable at the Si/SiO₂ interface. It is interesting to notice the similarity between these two cases: when a deficiency of oxygen (for forming SiO₂) exists, more bridge-bonding oxygen is formed at the price of leaving more dangling bonds on Si.

An interesting speculation may be made about the role of the 2x1 reconstruction in relation to having the peroxy zwitterion as the initial RT chemisorption configuration. On a 2x1 reconstructed surface, there is, roughly speaking, a doubly occupied orbital localized on the raised surface atom, and there is an empty orbital on the lowered atom. Since the formation of silicon-oxygen-molecule bonding requires the presence of a singly occupied Si orbital, the extra electron in the doubly occupied Si orbital has to be removed before bonding to adsorbed oxygen molecules. This electron can be either promoted into the empty dangling orbital or transferred to the 1 π_g orbital of oxygen. A smaller energy barrier probably is encountered initially in transferring the electron to oxygen, because the 1 π_g orbital of oxygen initially lies below the Si dangling orbital in energy, and the formation of O₂⁻ is exothermic by 0.43 eV [25]. It is thus possible to form the peroxy-zwitterion, if that electron remains on the oxygen molecule during the bonding process. 1.7 eV, however, can be gained by transferring the electron to the empty Si orbital and forming the peroxy radical configuration. The question is then if an activation barrier exists to stabilize the peroxy-zwitterion. Theoretical investigation of this question may be important.

It should be emphasized at this point that the above selection of possible pairs was done without appealing to the specifics of the annealing condition. The conditions of annealing were chosen rather arbitrarily. The particular approach used here is to exploit the specific properties relating the before- and after-annealing configurations. An attractive choice for the RT chemisorption configuration and an attractive choice for the after annealing configuration, based on the measured results of a single configuration alone, may not be consistent with conditions (i) and (ii) stated above.

We also recognize that the above selection of possible pairs has assumed high accuracy in the measurement of the numbers of chemically affected Si atoms (condition iii above). If that condition is relaxed to some extent, a mixture of chemisorbed oxygen atoms and peroxy radicals becomes one attractive choice for the RT chemisorption configuration, because a good match is found in the values of chemical shifts: the 1.1 eV shift expected for the chemisorbed atom (config. VI, table 2) corresponds to the measured 0.9 eV shift, and the 1.5 eV shift of the peroxy radical (config. II, table 2) corresponds to the measured 1.4 eV

shift. Annealing causes the transformation



which gives an increase in the number of chemically affected Si atoms after annealing. The higher the number of peroxy radicals adsorbed at RT, the larger is the deviation of (5) from condition (iii) stated above, and hence will be less favored by the present result. Adsorption of the peroxy radical at RT also has difficulty to meet simultaneously the following two observations: (a) one monolayer of Si atoms are affected by oxygen adsorption (this work), and (b) one monolayer of oxygen atoms (one oxygen atom/surface Si atom) are adsorbed at saturation [7,12,13,15]. For the peroxy radical to be the dominate chemisorption configuration, it is necessary to have two monolayers of oxygen atoms (one monolayer of peroxy radical) adsorbed if (a) is rigorously met, and to have only half monolayer of Si atoms affected if (b) is rigorously met. A more definite experimental verification or refutation of conditions (a) and (b) in the future would therefore greatly clarify the role

of peroxy radical in the initial RT chemisorption on the Si(111) 2x1 surface.

In general, the picture of mixed bonding configuration suggested by the finding of more than one chemical shift in the Si-2p level, may reflect the imperfection rather than the perfection of the 2x1 surface. For example, steps are known to play a role in the oxygen adsorption process, although the effect may not be as pronounced as it was thought to be (see discussions in section 3, and references 6 and 7). Such imperfection cannot be well controlled or characterized in our experiments, and it may therefore be a source of uncertainty for the interpretation of the present experimental results. We have found that, however, for all cleaved surfaces with visually equally good quality (i.e., cleaves that are flat and smooth but normally show more than one domain when examined with LEED), there is little variation in the line shape of the Si-2p level. This suggests that there is no significant variation in the relative magnitude of the different chemically shifted components. Another possibility for explaining the presence of more than one chemical shift is the occurrence of a 'flip-over' condition at the transition from the fast chemisorption to the slow chemisorption process, namely, a single chemisorption configuration is responsible for the fast (initial) chemisorption process and conversion of this configuration to a second configuration begins at the onset of the slow adsorption process. A future high energy-resolution study of the evolution of the chemical shift with oxygen coverage can certainly resolve this issue. We notice that, however, conditions (i) and (ii) holds true even with the above-mentioned complications in interpretation.

The existence of non-dissociated oxygen in the initial RT chemisorption process has been a major concern in the past [13,14,16-18]. For the three possible configurations of non-dissociative chemisorption (I,II,III in table 1), our results here point to more difficulties with the peroxy radical configuration. Angle-resolved and polarization-dependent photoemission studies of Bauer et. al. [18], which have identified features due to O-O bonding, are not against the possibility of having the peroxy-zwitterion and the peroxide bridge as initial chemisorption configurations. Thus at the present the peroxy zwitterion should be considered a strong contender for the non-dissociative chemisorption configuration on the 2x1 surface. Future experiments should be designed to distinguish between the peroxy zwitterion and the peroxy radical. Our results do not show any evidence against the existence of peroxide bridges in the initial adsorption stage. In fact it is interesting to make the following speculation about the peroxide bridge. If the formation of the peroxy zwitterion--the least stable configuration in table 2-- is indeed the first step of the adsorption process, the energy barrier in closing the peroxy zwitterion to form the peroxide bridge-- the most stable non-dissociative chemisorption configuration-- may be smaller than or comparable to that in transferring one electron away from the peroxy zwitterion to form the peroxy radical. Such a possibility may be important for future theoretical investigation.

2.5 SUMMARY AND CONCLUDING REMARKS

In conclusion, the photoemission results presented in this chapter (section 3) strongly support a "defect" model for the 7x7 structure of

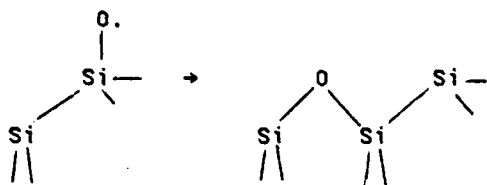
the Si(111) surface. We have also demonstrated that,, for the same crystalline plane of Si, the two different surface reconstructions can give rise to drastically different oxygen adsorption properties.

We have also analyzed in detail the chemical shift in the Si-2p level of both the Si(111) 2x1 surface with a monolayer of oxygen adsorbed at room temperature and such a surface subjected to annealing at elevated temperature. The annealing is seen to reveal new chemical shifts in Si-2p. Comparison of both the values and the intensities of the chemical shift before and after annealing has provided new information about the room temperature chemisorption configuration. We have eliminated many possibilities and have narrowed the choice to a few possible Si-O bonding configurations. More systematic studies of the annealing effects in the future may lead to the determination of the room temperature chemisorption configuration.

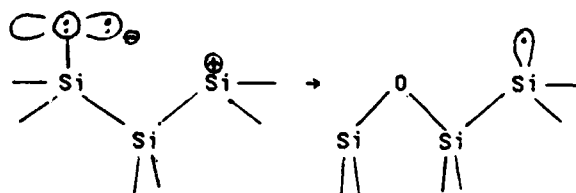
2.6 APPENDIX

We give here examples of pairs of configurations that are inappropriate for the before and after annealing transformation.

We first consider condition (ii) in the text. For example, the transformation

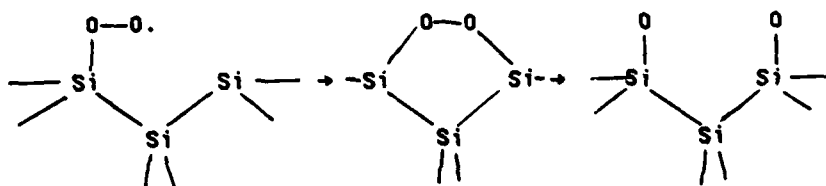


proceeds to increased heat of formation; however, the chemical shift in Si-2p moves toward lower value [16], and hence it is not a proper pair. For the same reason, the pair



is not favored. The first example given above also violates condition (iii) of the text.

Another example violating condition (iii) is the closing of peroxy radical to peroxide bridge or dissociation of it into oxygen radical:



REFERENCES

1. R. Feder, W. Monch, and P. P. Auer, J. Phys. C: Solid State Phys. 12, L179(1979) and references therein
2. This group includes the buckling model of Haneman, D. Haneman, Phys. Rev. 121, 1093(1961), D. J. Miller and D. Haneman, J. Vac. Sci. Technol. 16, 1270(1979); the long range rippling model of Mark et al, P. Mark, J.D. Levine and H. McFarlane, Phys. Rev. Lett. 38, 1408(1977); and the ring-like arrangement buckling model of Chadi et al (ref. 5).
3. This group includes the point vacancy model of Lander, J.J. Lander and J. Morrison, J. Chem. Phys. 37, 729(1962), J. Appl. Phys. 34, 1403(1963); the ad-atom model of Harrison, W. A. Harrison, Surf. Sci. 55, 1(1976); the milk-stool model of Snyder et al, L. C. Snyder, Z. Wasserman, and J. W. Moskowitz, J. Vac. Sci. Technol. 16, 166(1979); and the epitaxial microdomain model of Phillips, J. C. Philips, Phys. Rev. Lett. 45, 905(1980)
4. H. Ibach and J. E. Rowe, Surf. Sci. 43, 481(1974); T. Sakurai and H. D. Hagstrum, Phys. Rev. B 12, 15349(1975)
5. K. C. Pandey, T. Sakurai, and H. D. Hagstrum, Phys. Rev. B 16, 3648(1977) and references therein.
6. N. Kasupke and M. Henzler, Surf. Sci. 92, 407(1980)
7. H. Ibach, K. Horn, R. Dorn and H. Luth, Surf. Sci. 38, 433(1973)
8. H. Ibach and J.E. Row, Phys. Rev. B 9, 1951(1974); Phys. Rev. B 10, 710(1974)
9. Guichar et. al., by differentiating high energy resolution photoelectron yield, have found some difference between the two oxidized surfaces near the valence band maximum. Such minor difference can escape our detection due to the insufficient resolution used here. G. M. Guichar, C. A. Sebenne, G. A. Garry, and M. Balkansky, Surf. Sci. 58, 374(1976)
10. C.M. Garner, I. Lindau, C.Y. Su, P. Pianetta and W.E. Spicer, Phys. Rev. B 19, 3944(1979); C.M. Garner, I. Lindau, C.Y. Su, J.N. Miller, P. Pianetta and W.E. Spicer, Phys. Rev. Lett 40, 403(1978)

11. This value of escape depth is typical of semiconductors. For example, a minimum escape depth of $\sim 6 \text{ \AA}$ is found for GaAs: P. Pianetta, I. Lindau, C. M. Garner, and W. E. Spicer, Phys. Rev. B 18, 2792(1978)
12. M. Green and K.H. Maxwell, J. Phys. Chem. Solids 13, 145(1960)
13. J.E. Rowe, G. Margaritondo, H. Ibach and H. Froitzheim, Solid State Comm. 20, 277(1976)
14. R. Ludeke and A. Koma, Phys. Rev. Lett. 34, 1170(1975)
15. F. Meyer and J.J. Vrakking, Surf. Sci. 38, 275(1973)
16. W.A. Goddard III, A. Redondo and T.C. McGill, Solid State Comm. 18, 981(1978); W.A. Goddard III, J.J. Barton, A. Redondo and T.C. McGill, J Vac. Sci. Technol. 15, 1274(1978)
17. M. Chen, Inder P. Batra and C.R. Brundle, J. Vac. Sci. Technol. 16, 1 (1979)
18. R. S. Bauer, R. Z. Bachrach, G. V. Hansson, and W. Gopel, J. Vac. Sci. Technol. 18, NO. 2, 1981
19. A higher shift with small intensity is also discernable in fig. 6. We believe this corresponds to the commencement of the slow sorption process and is not important in the present consideration. The negative peak on the low binding energy side appears in the difference curves in both fig. 6 and fig. 7 and probably is a manifest of the surface shift reported by Himpsel et. al.. F. J. Himpsel, P. Heimann, T. C. Chiang, and D. E. Eastman, Phys. Rev. Lett. 45, 1112(1980)
20. A. Redondo, C. A. Swarts, W. A. Goddard III, and T. C. McGill, J. Vac. Sci. Technol. 18, Mar/Apr 1981
21. G. Hollinger, Y. Jugnet, P. Pertosa and Tran Minh Duc, Chem. Phys. Lett. 36, 441(1975)
22. This does include the case of dative bonds involving Si d-orbitals. R. T. Sanderson, Chemical bonds and bond energy, Academic, N. Y., 1971
23. It carries $\sim 1 \text{ eV}$. The difference in energy between config. I and config. II is 4.1 eV , and the dissociation energy of the O-O bond in the peroxy-zwitterion is $\sim 3 \text{ eV}$. The dissociation energy of the O-O bond in H_2O_2 is $\sim 2 \text{ eV}$, and the dissociation energy $\text{O}_2^-(^2\Pi_g) \rightarrow \text{O}(^3P) + \text{O}^-(^2P^0)$ is $\sim 3.6 \text{ eV}$ (Kruperne, ref. 18 below). Since the O-O bond in the peroxy zwitterion is weakened by the Si-O bonding compared to free O_2^- , an estimate of the dissociation energy is therefore chosen to be $\sim 3 \text{ eV}$.

24. P. J. Caplan and E. H. Pointdexter, The physics of MOS insulators
ed. G. Lucovsky, S. T. Pantelides and F. L. Galeener, Pergmon, N.
Y., 1980
25. P. H. Kruperne, J. Phys. Chem. Ref. Data. 1, 423(1972)

Chapter III

PHOTOEMISSION STUDIES OF THE INTERACTION OF OXYGEN WITH GAAS(110)

3.1 INTRODUCTION

The interaction of oxygen with GaAs(110) surfaces has attracted much attention in the past few years [1-9]. In particular, these studies have addressed the question of adsorption sites and the question of whether oxygen adsorbs nondissociatively or dissociatively.

Several different experimental techniques have been applied to this problem. Among them, the studies of chemical shifts in the Ga-3d and in the As-3d were often used in the past to address the question of chemisorption sites [2,3,5]. The involvement of surface As atoms in bonding to oxygen has been firmly established by the observation of a well resolved chemical shift in the As-3d level following oxygen adsorption [2,3,5]. The involvement of surface Ga atoms, however, is unclear because only a broadening in the Ga-3d level is observed following oxygen adsorption. The interpretation of the broadening in the Ga-3d is not straight forward. Brundle and Seybold [3] have proposed the direct growth of Ga_2O_3 and As_2O_3 , as the magnitude of chemical shifts are close to those expected for the two bulk oxides. Pianetta et al [5] have suggested that As-O bonding could induce broadening in the Ga-3d level. For oxygen bonding only to the surface As, Barton and Goddard [4] have calculated an As-O bonding induced shift of 0.8 eV in the Ga-3d level in addition to a 2.6 eV shift in the As-3d level; these shifts agree well

with experiments [2,3,5]. Such divergence of interpretations illustrates the difficulty in attaining an unambiguous answer from the magnitude of the shifts in core level alone.

In this work, we turn our attention to the density of valence states (DOVS) of the GaAs(110) surface adsorbed with oxygen (that produced by exposure to unexcited oxygen [5], hereinafter referred to as the DOVS of O/GaAs. We will also compare DOVS' obtained from oxygen adsorption on a variety of surfaces. It will be seen that careful examination of the DOVS can often resolve the ambiguities associated with the core-level spectra. After describing the experimental details in section 2, the results of oxygen adsorption on cleaved GaAs(110) will be given in section 3. Particular emphases are given to the 30 eV spectra which are better representation of the DOVS than spectra obtained with lower photon energies. Coverage dependent features and the substrate features in the 30 eV spectra are carefully separated out in order to obtain a representation of the DOVS of O/GaAs(110). An interpretation of the DOVS obtained this way will be offered based on comparisons made with the experimental DOVS' of Ga_2O_3 and As_2O_3 . In section 4, we will present results of oxygen adsorption on sputter-disordered GaAs surfaces. The understanding of the adsorption process on the disordered surfaces provides great insights into the adsorption process on ordered surfaces. The photoemission spectra obtained for oxygen adsorption on disordered surfaces also serve as useful references for interpreting photoemission spectra obtained under other conditions. In section 5, studies are made on surfaces which were first covered with oxygen and then annealed to elevated temperatures. Such annealing studies reveal the stability of

the bondings formed by room temperature adsorption. The oxidation of Ga and As metals have also been studied and the results are given in Appendices A and B. Other than the bonding properties, there is also the aspect of oxygen-induced changes in the electronic structure of GaAs. Such changes, as reflected in the positions of the surface Fermi level in the band gap, are summarized in Appendix C.

3.2 EXPERIMENTAL

Experiments were performed in a stainless steel ultrahigh vacuum chamber with base pressure $\sim 10^{-10}$ Torr.

The light sources used include synchrotron radiations from the 8° and the 4° beam lines of the Stanford Synchrotron Radiation Laboratory (SSRL) [10], and monochromatized He-I(21.2 eV), He-II(40.8 eV) radiations from a He discharge. The O-1s spectra were obtained with Mg-K α emission ($h\nu=1253.6$ eV). Energy analyses of photoelectrons were performed with a double-pass cylindrical mirror analyzer (Physical Electronics). Combined monochromator-analyzer energy resolutions are 0.2 eV for 21 eV spectra, 0.3 eV for 30 eV spectra, 0.35 eV for 100 eV spectra, 0.3 eV for He-I spectra, and 0.4 eV for He-II spectra.

Research grade oxygen were used in making the oxygen exposures. Unless otherwise stated, oxygen exposures were made with all the precautions necessary to avoid generating excited oxygen which could lead to different oxygen adsorption process [5].

The heatings were achieved by a tungsten filament which was enclosed in the molybdenum sample holder positioned at the back end of the crystal.

To avoid contamination during heating the heaters had been thoroughly outgassed to temperature 2500°C prior to the heating experiments. Temperatures were monitored with a thermocouple mounted near the back end of the crystals and an infrared pyrometers focused near the crystal surfaces. A consistent temperature scale for different experiment runs was obtained from the pyrometer reading. The discrepancies in the thermocouple readings from different experiment runs, however, place the accuracy of the quoted temperature to $\pm 30^\circ\text{C}$.

Samples used in this work are assigned identification such as N1, N2, P1 etc., with the characters N and P indicating n-type and p-type samples, respectively. The crystal suppliers and the doping concentrations are: samples P1-P4, $1.8 \times 10^{18} \text{cm}^{-3}$ Zn doped, Laser Diode; samples N1-N5, $4 \times 10^{17} \text{cm}^{-3}$ Sn doped, Varian Associates; samples N6-N8, $5 \times 10^{17} \text{cm}^{-3}$ Te doped, Crystal Specialty; samples N9-N12, $5 \times 10^{18} \text{cm}^{-3}$ Si doped, Laser Diode.

3.3 RESULTS AND DISCUSSION - ROOM TEMPERATURE ADSORPTION ON CLEAVED GAAS(110)

In this section, we present results of room temperature adsorption on cleaved GaAs(110) surfaces. Emphasis is given to the valence band spectra, but a summary of the results from the core-level spectra will be given in 3.1. Experimental valence band spectra of O/GaAs(110) are presented in 3.2. The different coverage dependence of the various features in the spectra are carefully analyzed in 3.2. Contributions to the valence band spectra from two different forms of adsorbed oxygen are separated from each other by such analyses. The interpretation of the

spectrum of the major chemisorption form - oxygen which adsorb on normal surface sites and produce chemical shifts in the core levels - is attempted in 3.3. The nature of other form of oxygen is discussed in 3.4. Some speculations about the mechanism of adsorption, particularly the role of defects in the initial steps of adsorption, are given in 3.5.

3.3.1 Results from Core-level Spectra

The basic facts available in the core-level spectra have been reported by Pianetta et al [5]. We have repeated the measurements of Pianetta et al with improved energy resolution and signal-to-noise ratio. An overview of the Ga-3d and the As-3d levels of GaAs(110) surfaces subjected to a sequence of oxygen exposures is given in fig. 1. All important features reported by Pianetta et al are reproduced: (1) no chemical shift in either the As-3d or the Ga-3d can be observed for oxygen exposures smaller than 10^7 L ($1 \text{ L} = 10^{-6} \text{ Torr} \times 1 \text{ sec}$), (2) a well resolved chemical shift ($\Delta E = 3.0 \pm 0.1 \text{ eV}$) in the As-3d is observed for oxygen exposures higher than 10^7 L, and (3) the full width at half maximum (FWHM) of the Ga-3d level increases with increasing exposure, but no resolvable shift can be observed throughout the whole exposure range we have studied.

The broadening of the Ga-3d level is further examined in fig. 2, where the Ga-3d and the As-3d spectra of the clean surface are subtracted from those of the oxidized surface (10^{10} L exposure). The subtraction was done by aligning the unshifted As-3d in the two spectra in energy and by adjusting intensities of the two spectra to have equal areas under the unshifted As-3d. The difference curve (the bottom

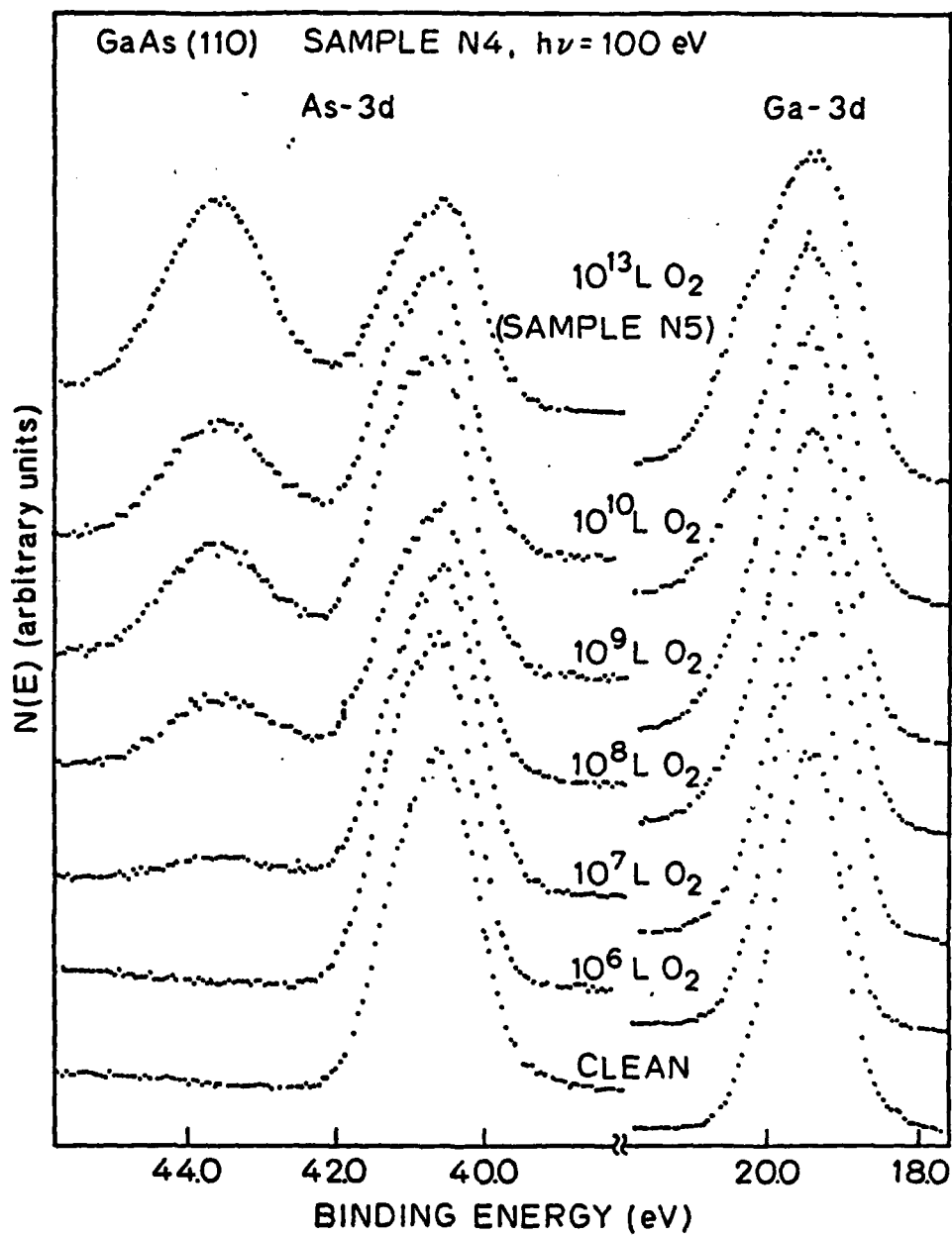


Figure 8: As-3d and Ga-3d levels of clean and oxygen-exposed n-GaAs(110) measured at $h\nu = 100$ eV. The 10^{13} L spectrum was obtained on a different surface.

curve, fig. 2) shows two peaks in the Ga-3d region, whereas the intensity in the energy region of the unshifted As-3d is zero. One of the two peaks in the Ga-3d region has binding energy higher than that of the unshifted Ga-3d while the other has lower BE. Because oxygen adsorption induced both a high BE component and a low BE component in the Ga-3d, Pianetta et al [5] have described it as 'homogeneous' broadening. The difference curve in fig. 2, however, clearly indicates that the broadening is asymmetrically toward the high BE side.

There are two possible explanations for the appearance of a component shifted to the low BE side as well as a component shifted to the high BE side.

The first is that the assumption that $BE(As-3d) - BE(Ga-3d)$ of the unshifted levels remains constant with oxygen adsorption is invalid. In the spectrum of a clean GaAs(110) surface, there are contributions from both atoms in the surface layer and atoms in the bulk. Eastman et al [11] have found that the BE's of the As-3d and the Ga-3d of the surface atoms are different from those of the atoms in the bulk. Thus the value of $BE(As-3d) - BE(Ga-3d)$ observed on a clean relaxed GaAs(110) surface is different from that expected in the absence of surface shifts. Assuming the surface atoms contribute 50% intensity to the observed spectrum and using the values of surface shifts of Eastman et al [11], the observed $BE(As-3d) - BE(Ga-3d)$ is estimated to be 0.33 eV smaller than that in the absence of surface shifts. If the oxygen adsorption removes the surface shifts, the value of $BE(As-3d) - BE(Ga-3d)$ would be changed following oxygen adsorption. We have indeed found it possible to eliminate the low BE

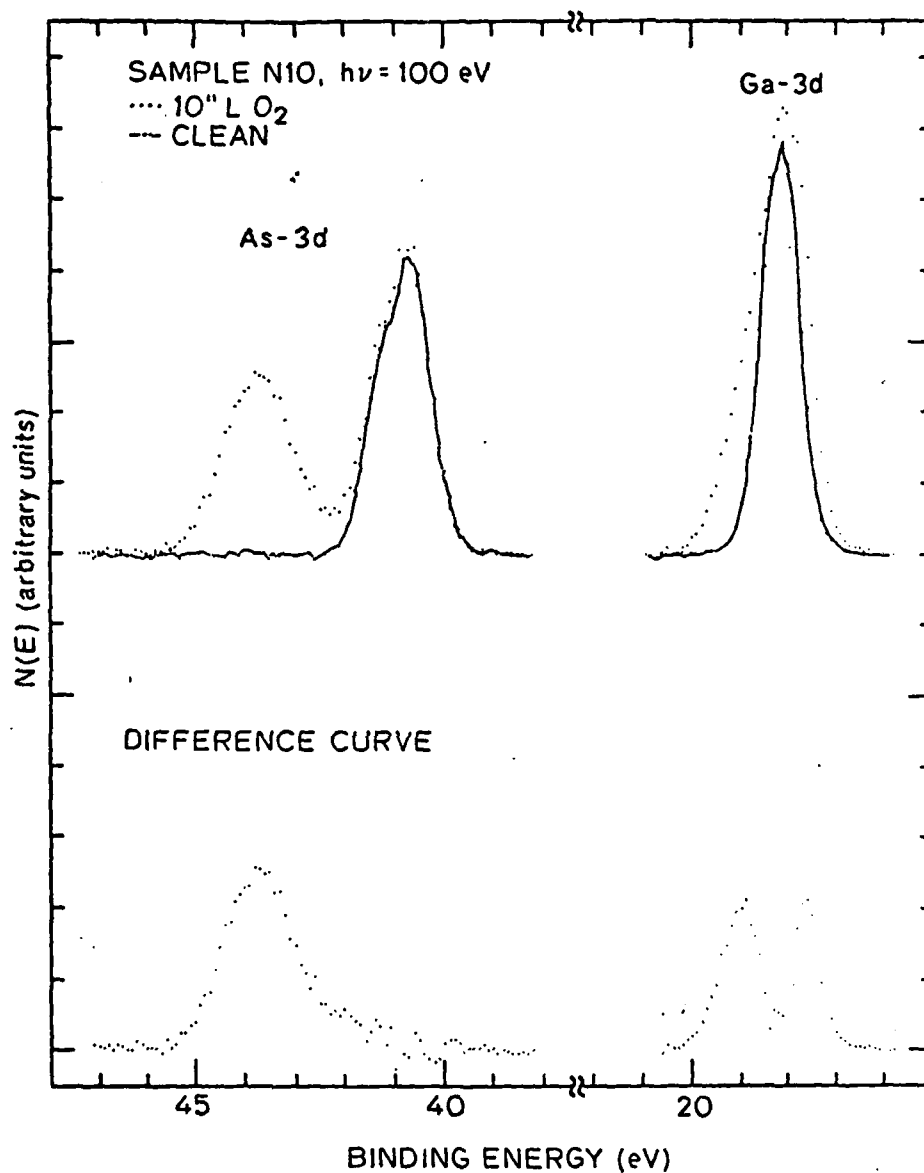


Figure 9: Difference curve between the As-3d and the Ga-3d spectra of clean and oxygen-exposed n-GaAs(110). Notice that oxygen exposure induced broadening in the Ga-3d toward both the low energy side and the high energy side.

component of the shifted Ga-3d in the difference curve by increasing the value of $BE(As-3d) - BE(Ga-3d)$ by 0.4 eV after oxygen adsorption. We should also notice that for this explanation to hold the removal of the surface shifts has to occur at an oxygen coverage significantly below monolayer. This is because the low BE component of the shifted Ga-3d appears following exposure as low as 10^8 L ($\theta \approx 0.4$ monolayer). In LEED I-V studies [6], the I-V structure characteristic of an ideally relaxed GaAs(110) surface was found to be drastically modified after an exposure of 10^8 L. It is thus conceivable that the surface shifts, which are directly related to the long range relaxation of the GaAs(110) surface [11], are lost after an exposure of 10^8 L.

Another possible explanation is simply that the adsorption of oxygen induces a broad shifted Ga-3d peak which extends to both the high BE and the low BE side of the unshifted Ga-3d. This explanation is reasonable especially in view of findings to be reported in Appendix A. There the Ga-3d of clean Ga metal is found to show well resolved spin-orbit splitting. Such resolvable splitting is absent for either the Ga-3d of clean GaAs or the Ga-3d of GaAs adsorbed with oxygen or the Ga-3d of Ga_2O_3 . The FWHM of the Ga-3d of Ga_2O_3 is also significantly larger than that of clean Ga (Appendix A).

At the present, we do not have experimental data to distinguish the two possibilities. The complex oxygen induced change in the Ga-3d as revealed in fig. 2, however, illustrates the difficulty in interpreting the core level spectra of surfaces.

The amount of shifted As-3d and shifted Ga-3d at various oxygen exposures, expressed respectively as a percentage of the total As-3d emission and the total Ga-3d emission, are listed in table 1. The amount of shifted Ga-3d were estimated using three methodes: (1) measure the area under the shifted Ga-3d in the difference curve, (2) fit the Ga-3d peak with three skewed Gaussians, one unshifted (which remains the same BE relative to the As-3d as on the clean surface) and two shifted (toward higher BE and lower BE), and (3) fit the Ga-3d with two components, one 'unshifted' and one shifted toward higher BE (the position of the 'unshifted' component was also permitted to vary in the fitting procedure). All three methodes agree within 10%. We notice that for all exposures, the percentage of shifted As-3d is roughly the same as the Ga-3d.

It is also interesting to notice that the percentage of shifted As-3d at 10^{13} L exposure is about the same as that reported by Pianetta et al [5] at 10^{12} L exposure. Since only two data points are available, it is not clear if a saturation of the adsorption process is reached between 10^{12} L and 10^{13} L, although the data are suggestive of this. The escape depth analyses of Pianetta et al, however, have indicated that it is reasonable to assume the 52% shifted As-3d corresponds to the adsorption of one monolayer oxygen. This assumption is adopted here and is used in estimating the oxygen coverages at various exposures; these estimates are listed in table 1. The intensity of the O-2p normalized to the intensity of the Ga-3d at each exposure is also entered in table 1 for later comparisons.

TABLE 3

Percent of shifted As-3d and Ga-3d at various exposures

Treatment	Percent shifted As-3d	Percent shifted Ga-3d	Intensity O-2p	Coverage (monolayer)
10^7 L O ₂	9	12	0.09	0.17
10^8 L O ₂	23	22	0.16	0.35
10^9 L O ₂	27	26	0.26	0.5
10^{10} L O ₂	34	28	0.33	0.65
10^{13} L O ₂	52	47	0.49	1.0

The fact that the shift in the As-3d is constant at any coverage below one monolayer (fig. 1) is worth emphasizing: it indicates that the oxygen coordination number of As in the O/GaAs(110) bonding is constant with increasing oxygen coverage.

3.3.2 Valence Band Spectra

Overviews of the valence band spectra of a n-GaAs(110) surface subjected to a sequence of oxygen exposures, taken at 21 eV and 30 eV photon energies, are displayed in figs. 10 and 11, respectively.

The major oxygen induced feature seen in the 21 eV spectra is a relatively sharp peak at $4.6 \text{ eV} \pm 0.1 \text{ eV}$ below VBM. Because of the relatively long escape depth of the photoelectrons excited by this photon energy from the peak (6.9 eV BE) due to the s-p hybrid band of bulk GaAs, it is seen in all spectra. Knowledge of the energy position of this peak relative to the Fermi level is useful in determining the band bending in GaAs induced by oxygen adsorption (to be discussed in Appendix C). The

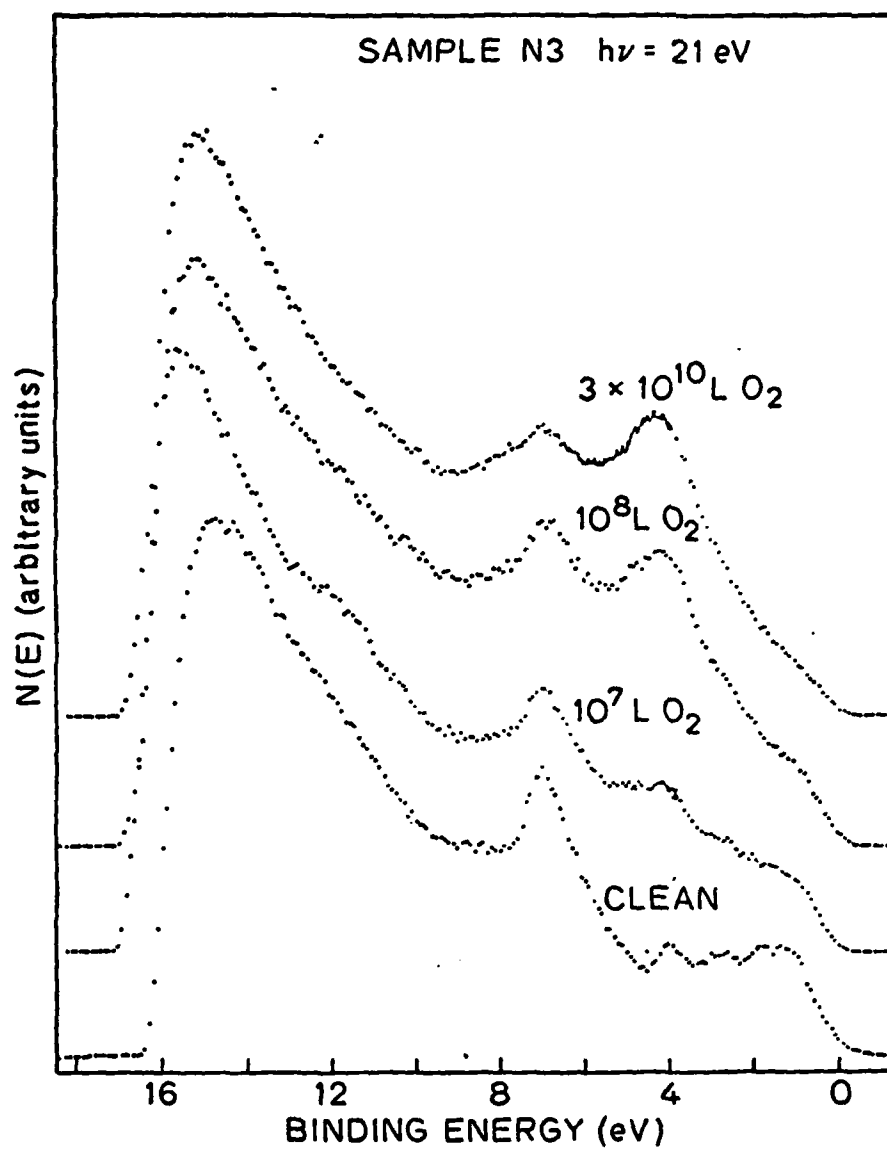


Figure 10: Photoemission spectra of clean and oxygen-exposed n-GaAs(110) obtained at $h\nu=21 \text{ eV}$.

energy separation between the oxygen peak (4.6 eV BE) and the substrate peak (6.9 eV BE) is constant with increasing oxygen exposures. This reflects the same fact that is given by the constant energy separation between shifted and unshifted As-3d peaks, namely, the oxygen substrate bonding is probably coverage independent. In addition, this separation is same for a n-type sample and a p-type sample whose surface Fermi level positions in the band gap are significantly apart (~0.4 eV) from each other at low oxygen coverages (<0.6 monolayer). This is seen in fig 12 where we have displayed the 21 eV spectra obtained on a p-type sample, with the Fermi level position indicated in each spectrum. Therefore the binding energy of the oxygen peak is a constant when referenced to the valence band maximum of the GaAs substrate, but not a constant when referenced to the surface Fermi level. If room temperature adsorption of oxygen on GaAs(110) resulted in the direct formation of islands of bulk oxides (As_2O_3 , Ga_2O_3) that are chemically separated from the substrate, the change in band bending within the GaAs substrate is not expected to affect the binding energy of oxygen levels referenced to the Fermi level. An oxygen-substrate bonding configuration with oxygen atom "continuing" or "inserted into" the lattice conforms better to the above observation than the formation of oxide islands.

In the 21 eV spectra, some oxygen induced features at higher binding energy may be shadowed by the secondary electron emission. The secondary background in the region of interest is greatly reduced in the 30 eV spectra. As an example, the As-4s-like band of clean GaAs(110), which cannot be unambiguously identified in the 21 eV spectrum, is clearly discernable in the 30 eV spectrum (~11 eV BE). The 30 eV spectra also

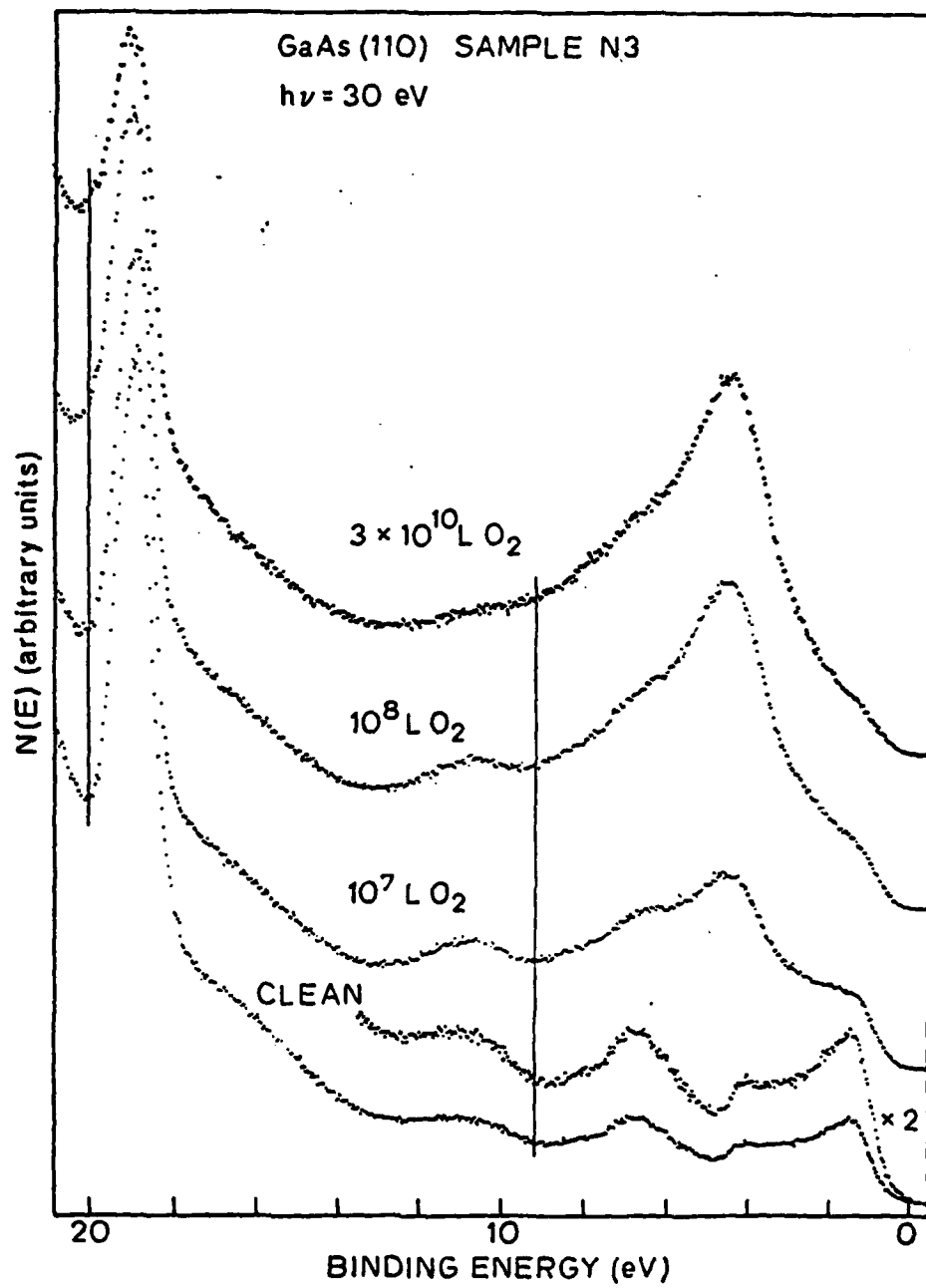


Figure 11: Photoemission spectra of clean and oxygen-exposed GaAs(110) obtained at $h\nu=30$ eV.

give increased cross section for oxygen levels and decreased cross section for substrate features, when compared to the 21 eV spectra. the s-p mixed band (6.9 eV BE) in the $10^7\text{L} \sim 3 \times 10^{10}\text{L}$ spectra in fig.11. The density of valence states of O/GaAs(110) is therefore better represented by the 30 eV spectra.

To further reveal details in the DOVS of O/GaAs(110), we have obtained a few difference curves which are shown in fig 13. Pannel (a) gives the difference curve between the 10^7L spectrum and the clean spectrum of sample N3 (the bottom curve). The original spectra with smooth and featureless backgrounds removed are also shown in th top part of panel (a). The subtraction necessary for obtaining the difference curve is done in such a way that (i) zero intensity is reached in the difference curve at the energy position corresponding to the clean component of the Ga-3d level (not shown in fig. 13), and (ii) the intensity of the leading peak of the clean spectrum and the intensity of the shoulder near VBM in the 10^7L spectrum are adjusted to be about equal before the subtraction. The difference curve between the $3 \times 10^{10}\text{L}$ spectrum and the clean spectrum is obtained in a similar way and is shown in panel (b). The two difference curves in panels (a) and (b) are compared in panel (c). Overall resemblance can be seen between the two difference curves in the BE region 0-10 eV. The relative heights of the major oxygen peak and the feature in the 10-12 eV BE region (labeled S in panel (c)), however, are quite different in the two difference curves. An examination of fig. 11 shows that feature S does not grow with increasing oxygen exposure as the 4.6 eV peak does. This is verified by the difference curve taken between th $3 \times 10^{10}\text{L}$ spectrum and the 10^7L spectrum, which is shown in panel (d). In that difference curve, little

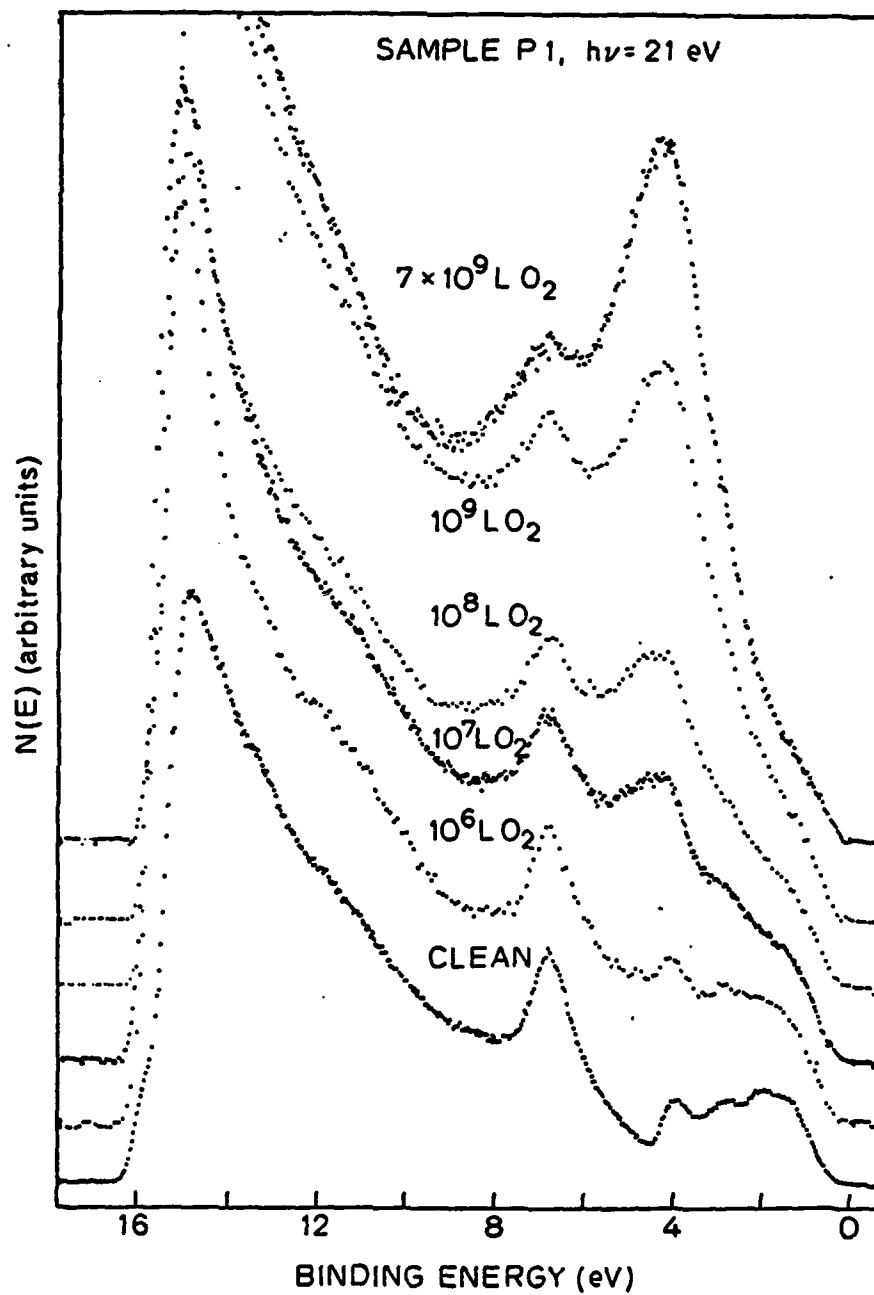


Figure 12: Photoemission spectra of clean and oxygen-exposed p-GaAs(110) obtained at $h\nu = 21$ eV. The 10^9 L and the 10^{10} L exposures were made with excited oxygen.

intensity is seen in the region between 10 and 12 eV BE, where feature S appears in the 10^7 L-clean difference curve. Feature S is attributed to a different form of oxygen which saturates at low exposure and low coverage. More detailed discussion of this low coverage state will be postponed until section 3.4. Sufficient to point out here that the difference curve given in panel (d) is a true representation of the DOVS of the major form of adsorbed oxygen, i.e., the adsorbed oxygen that produce the chemical shifts in As-3d and Ga-3d discussed in the last subsection. The DOVS in panel (d) consists of a prominent peak at 4.6 eV BE and a broad shoulder in the region of 6.5-10 eV BE. Interpretations of these features will be given in the next subsection.

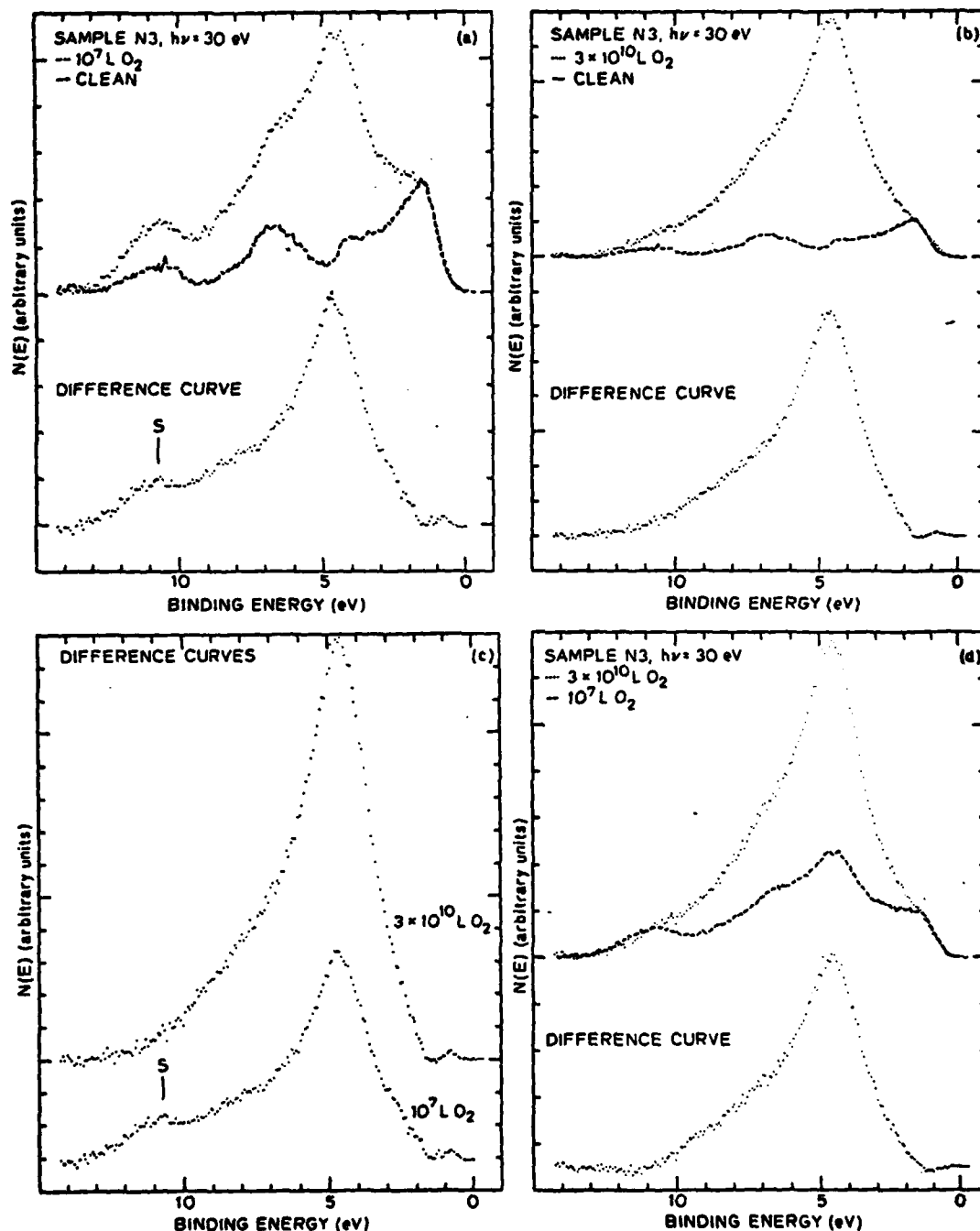


Figure 13: Removal of the coverage dependent features in the DOVS. The difference curves between the spectra of clean and oxygen-exposed surfaces at two different exposures are obtained in (a) and (b). When these two difference curves are compared in (c), coverage dependent variations in the spectra are revealed. The coverage dependent features can be removed by taking difference between the high coverage and the low coverage spectra (d).

3.3.3 Interpretation of the DOVS

The first piece of information to be drawn from the DOVS shown in fig 13-(d) is that oxygen adsorb dissociatively on the GaAs(110) surface. Molecular species such as O_2^- , O_2^{2-} , are expected to give multiplets with comparable strength in the photoemission spectrum [12]. Mele and Joannopoulos [1] in their tight binding calculations have found three molecular levels of comparable strength, with binding energies of 4, 8, and 10 eV for peroxy radicals chemisorbed on either Ga or As sites, and with binding energies of 4, 8, and 12 eV for peroxide bridge bridging over second nearest Ga and As atoms. The DOVS in fig 13-(d), showing a single dominant peak at 4.6 eV BE, gives no reminiscence of the multiplets characteristic of the O-O bonding. We therefore conclude that non-dissociative chemisorption, either in the form of peroxy radical or in the form of peroxide bridge, does not occur for room temperature adsorption of oxygen on GaAs(110) surfaces. The same conclusion has been reached by Brundle and Seybold [3] based on the binding energy of the O-1s level.

Having established that the adsorption is dissociative, the DOVS can be described in general terms of the bonding properties of the oxygen atom. There are four electrons in the p-shell of an oxygen atom leading to one doubly-occupied and two singly-occupied p-orbitals. Only the two singly-occupied p-orbitals participate in the bonding of oxygen atom to other atoms, and the doubly occupied p-orbital remains non-bonding. The essential feature of the DOVS of any oxide therefore consists of a non-

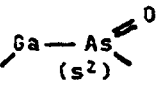
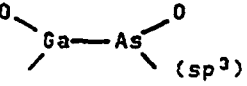
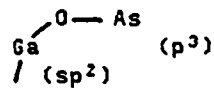
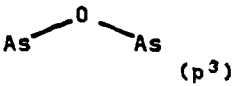
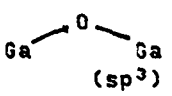
bonding band and a bonding band. A simple characterization of such DOVS can be made in terms of two parameters: the energy splitting between the nonbonding and the bonding bands (hereinafter referred as N-B splitting), and the ratio of the density of the nonbonding and bonding states (hereinafter referred to as the N-B ratio). For example, when the oxygen atom is in a bridge bonding position, the N-B ratio is 1:2 based on simple counting of the nonbonding and the bonding electrons. In practice, however, both the N-B splitting and the N-B ratio may be difficult to extract from the experimental DOVS. For example, the different matrix elements for the photoionization of the nonbonding and the bonding orbitals may make the density ratio ambiguous; the broadening in the bonding band due to the disorder the oxides may cause difficulty in determining the energy splitting between the nonbonding and the bonding bands.

To avoid the difficulties in extracting absolute numbers for the N-B splitting and the N-B ratio from the experimental DOVS', the approach to be used below is to qualitatively compare the N-B splitting and the N-B ratio between the DOVS' of several possible oxygen bonding configurations. In particular, we will compare the DOVS of O/GaAs(110) to the DOVS' of As_2O_3 and Ga_2O_3 .

As a first step of comparing the experimental DOVS', we have theoretically projected the two-parameters (the N-B splitting and the N-B intensity ratio) of a few possible oxygen bonding configurations and have listed the results in table 4. Configurations As-O-As (IV) and Ga-O-Ga (V) are included to simulate the known oxides, As_2O_3 and Ga_2O_3 , respectively, in calculating the N-B splittings. Configurations I-III

are candidates to be considered for the O/GaAs(110) bonding. In configuration I of tabel 4, the oxygen atom terminates a doubly-occupied surface As dangling orbital; the As=O bonding involves π - as well as σ -interactions, as discussed by Lucovsky and Bauer [13] and Barton et. al. [4]. In configuration II, the oxygen terminates a singly occupied sp^3 hybrid of As or Ga or both; this configuration has been examined in detail by Mele and Joannopoulos [1] with tight binding calculations. In configuration III, the oxygen atom breaks a surface bond and bridges over a pair of nearest-neighbor Ga and As.

The N-B ratios given in table 4 are based on simple counting of bonding and nonbonding electrons. No distinction is made between s-electrons (contributed by the Ga or the As to the bonding band) and p-electrons, although in our condition ($h\nu=30$ eV) p-electrons may be preferentially emphasized over s-electrons in the measured DOVS'. Such error, however, is expected to be the same for all bonding configurations considered in table 4. As mentioned above, in configuration I the two doubly-occupied O-2p orbitals have π -interaction with the empty 4d orbitals of As [4,13]. The π -interaction, however, is weaker than the σ -bonding, hence we expect a splitting between the π and σ bondings. We will therefore count electrons in the donor-like π bonding as 'nonbonding'. The nonbonding to bonding electrons ratio for configuration I is the highest in table 4. For oxygen in bridge position, the N-B ratio is 1:2 in all cases (configurations III through V). In bulk Ga_2O_3 , complication arises because some oxygen lone pairs can interact with nearby empty Ga orbitals and form donor-like bonds (see Appendix A for more details). This complication has been ignored in table 4, but it is discussed below when making comparisons of the experimental DOVS.

TABLE 4			
Qualitative trends in the characteristics of the DOVS' of a few oxygen bonding configurations			
No.	Bonding Configuration	N-B Splitting (eV)	N-B Ratio
I		3.36	2:1
II		O-Ga 5.75 [2.5*] O-As 7.04 [6.0*]	3:2
III		5.19 $\left(\begin{matrix} \pi: 2.86 \\ \sigma: 7.52 \end{matrix} \right)$	1:2
IV		4.85 $\left(\begin{matrix} \pi: 2.76 \\ \sigma: 6.94 \end{matrix} \right)$	1:2
V		5.62 $\left(\begin{matrix} \pi: 4.10 \\ \sigma: 7.15 \end{matrix} \right)$	1:2
	As ₂ O ₃	(exp) 3.3 $\left(\begin{matrix} \pi: 2.41 \\ \sigma: 4.13 \end{matrix} \right)$	
	Ga ₂ O ₃	(exp) ~4.5	
*Calculated values of Mele and Joannopoulos [1].			

Simple LCAO calculations, similar to that done for Si-O-Si by Harrison [14], have been performed to obtain the N-B splittings in table 4. These calculations were done only to reveal the trend in the N-B splitting among the various configurations considered. No absolute

correspondence between these numbers and the experimental DOVS should be sought. Some of the details of the calculation can be found in Appendix D. We notice here that for configurations containing bridge oxygen (III-V) the bonding band further splits into a σ component and a π component. Broader bonding bands are therefore expected for configurations III through V when compared to configuration I. In tabel 4, we have listed the centers of gravity of σ and π components as the N-B splittings for configurations III through V; splittings between the nonbonding oxygen orbital and the individual σ and π components are enclosed in parenthesis. The following trends in the theoretical N-B splittings are observed:

- i) configuration I has the smallest N-B splitting and the narrowest bonding band among all the bonding configurations considered in table 4
- ii) single As-(sp^3) hybrid bonded to oxygen gives an N-B splitting even bigger than those expected for As_2O_3 and Ga_2O_3 .
- iii) the N-B splitting for the Ga-O-As bridge is intermediate between that of As-O-As and that of Ga-O-Ga, or it is intermediate between the N-B splittings of As_2O_3 and Ga_2O_3 .

In fig 14, we compare the experimental DOVS of As_2O_3 (top) and Ga_2O_3 (bottom) to that of oxygen adsorbed on GaAs(110) (center, reproduced from fig 13-(d)). All the three spectra are displayed with the Fermi level as the energy zero. More detailed discussion of the DOVS' of

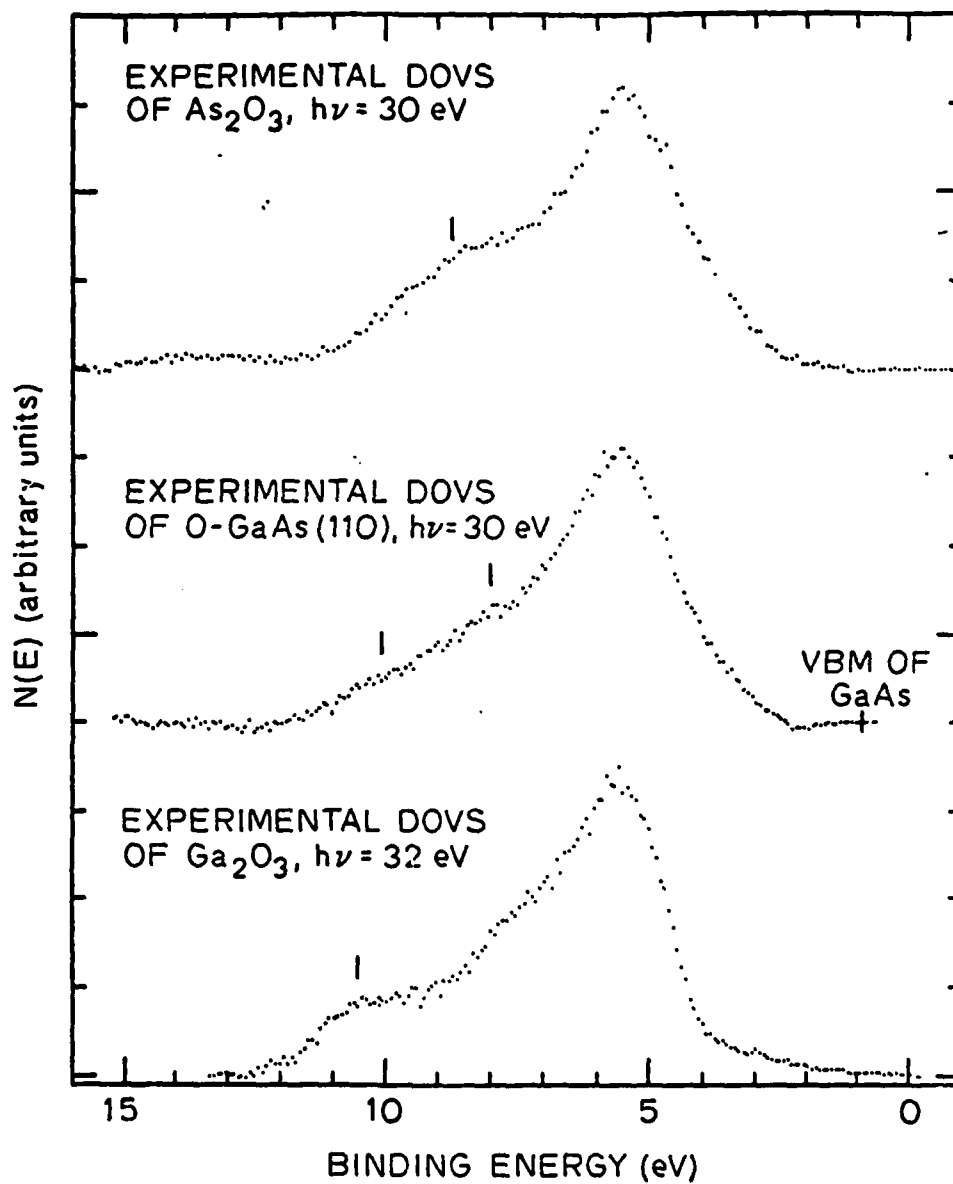


Figure 14: Comparison of the experimental DOVS of O/GaAs(110) to those of As_2O_3 and Ga_2O_3 . The DOVS of O/GaAs(110) and As_2O_3 were obtained at $h\nu = 30$ eV, whereas that of Ga_2O_3 was obtained at $h\nu = 32$ eV.

As_2O_3 and Ga_2O_3 will be given in Appendices A and B. Here we can make the following qualitative observations:

- i) The bonding band of the DOVS of oxygen adsorbed on $\text{GaAs}(110)$ is not as pronounced as those of the DOVS' of As_2O_3 and Ga_2O_3 . The comparison made with the DOVS of Ga_2O_3 is somewhat ambiguous due to the presence of the donor-like bonding band (see Appendix B). The comparison made with the DOVS of As_2O_3 , however, is clear. This suggests the importance of nonbridging oxygen (configurations I or II) bonding for oxygen chemisorbed on $\text{GaAs}(110)$.
- ii) There is no component of the bonding band of the DOVS of $\text{O}/\text{GaAs}(110)$ that has a N-B splitting bigger than that of Ga_2O_3 . This, according to table 4, disfavors configuration II. The same conclusion is reached by comparing the more accurate tight-binding values [1] to experimental DOVS. We therefore suggest that, in conjunction with (i), $\text{As}=\text{O}$ provides the important nonbridging oxygen bonding.
- iii) The bonding band in the DOVS of $\text{O}/\text{GaAs}(110)$ is broad and its high binding energy edge lies at a binding energy higher than that in the DOVS of As_2O_3 but comparable to that in the DOVS of Ga_2O_3 . This suggests other types of bonding besides $\text{As}=\text{O}$. In section 4 below we will give evidence showing that $\text{Ga}-\text{O}-\text{Ga}$, and hence $\text{As}-\text{O}-\text{As}$, bonds are unlikely to result from room temperature adsorption of oxygen on $\text{GaAs}(110)$. The $\text{Ga}-\text{O}-\text{As}$ bridge is therefore important to consider in addition to the $\text{As}=\text{O}$ bond-

ing. The specific way the As=O and the Ga-O-As bondings is mixed, however, cannot be deduced from the DOVS of O/GaAs(110).

In fig 15, we suggest an adsorption configuration consisting of an oxygen atom datively bonded (i.e., the As=O bond [13]) to an surface As and an oxygen atom inserted into one of the backbonds to the same surface As. Further explanations of the motivations for this suggestion will be pointed out in section 3.5 where we discuss the adsorption mechanism. Here we only notice that the model is not inconsistent with the chemical shifts in core levels: a surface As atom is bonded to two oxygen atoms but with three electrons participated in bonding, hence the chemical shift is comparable to that found for As₂O₃ (Appendix A); a surface Ga atom is bonded to only one oxygen atom, hence a small and unresolved chemical shift in the Ga-3d level.

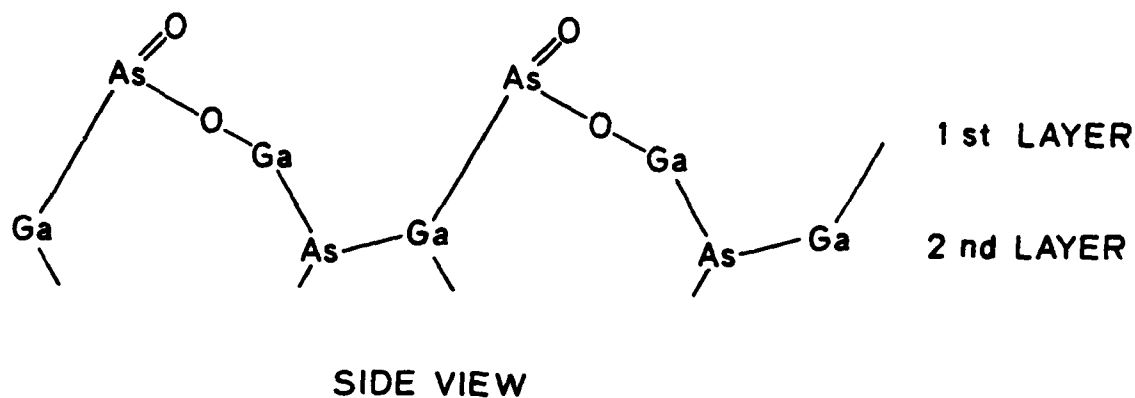


Figure 15: A proposed bonding model for room temperature adsorption of oxygen on GaAs(110). A side view of the (110) surface is shown here.

3.3.4 The Low Coverage Adsorption State

We now return to discuss the feature between 10-12 eV BE in fig. 13. In fig. 16, we show the spectrum of a clean GaAs(110) (top curve) and the difference spectra (the oxygen-exposed minus the clean) of this sur-

face subjected to three different oxygen exposures. The same feature between 10-12 eV BE (labeled 4 in fig 16) is seen in the 10^5 L difference spectrum. This feature probably is shadowed by the 4.6 eV BE nonbonding oxygen peak in high exposure spectra shown in fig 13. Feature 1 is weak and feature 3 appears nearly in the noise level in the 10^5 L difference spectrum, but they are clearly the dominant features in the 10^7 L spectrum. Features 1 and 3 are, then, the key features of the major chemisorbed species, as discussed in the last subsection. Features 2 and 4 are therefore associated with a different oxygen state which, according fig 16, saturates at 10^5 L exposure. The saturation coverage of this state can be estimated in the following way: the intensity of emission from features 2 and 4 in the 10^7 L spectrum is less than 10% of that due to features 1 and 3 (features of the chemisorption state). The oxygen coverage of the major chemisorption state is approximately 0.1 monolayer for a surface exposed to 10^7 L oxygen (table 1, section 3.1). Thus the saturation coverage of the low exposure state is less than 0.01 monolayer.

The low saturation coverage reaches with low exposure suggests that the adsorption of this state of oxygen may be at surface defect sites. Some clues to the nature of this state and the nature of the defect sites are given below.

The binding energies of features 2 and 4, 5.3 eV and ~10.3 eV, respectively, are the same as those found for Ga-O-Ga bridge bonds (to be discussed in the next section, where a large number of such bonds are found on a sputter-disordered Ga-rich GaAs surface). Heating experiments

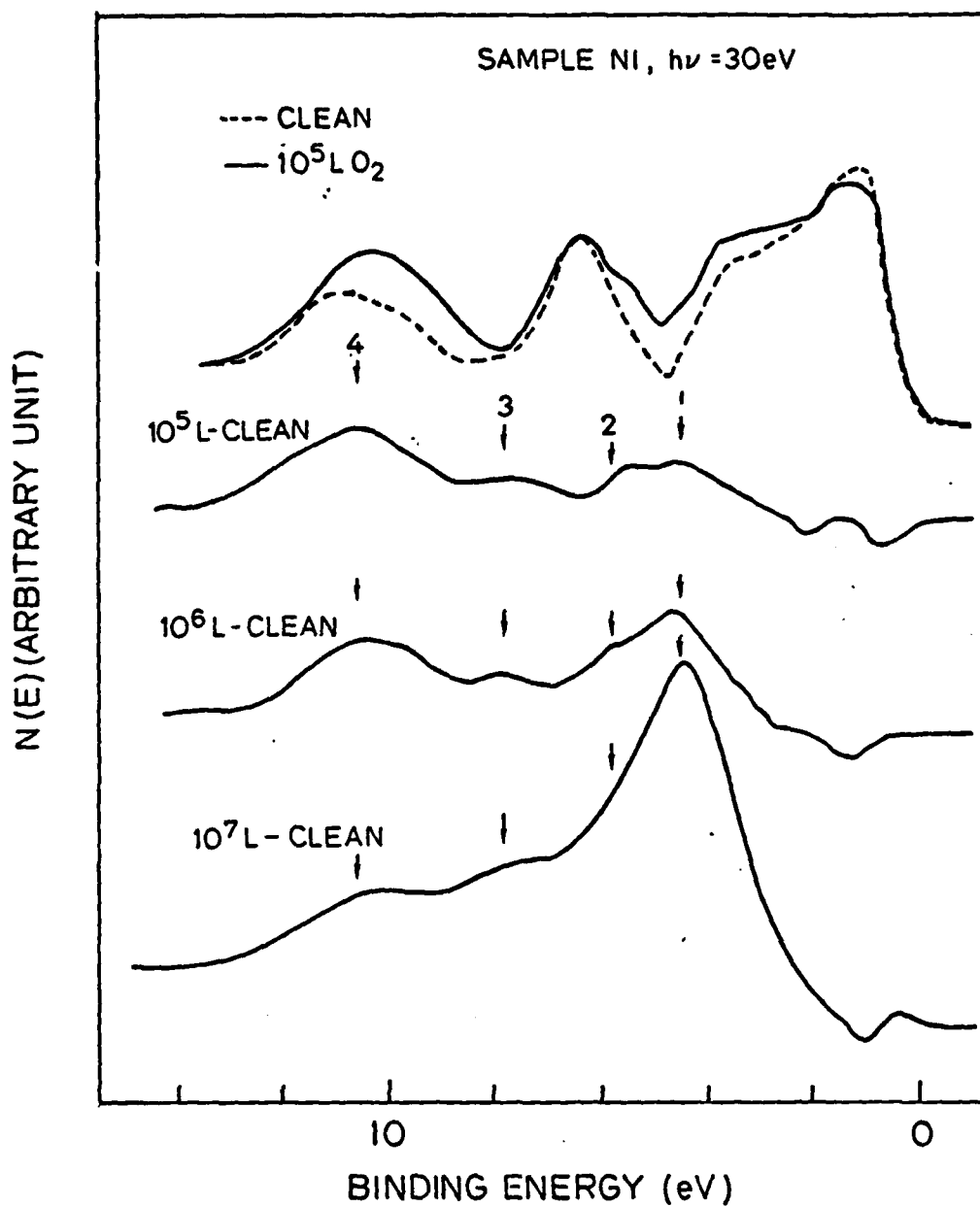


Figure 16: The photoemission spectra of a clean n:GaAs(110) (top and the difference curves between spectra of clean and oxygen-exposed surfaces at a sequence of oxygen exposures. The spectra were obtained at $h\nu=30\text{ eV}$. Feature 1, 3 are associated with one form of oxygen, and 2, 4 with another.

(to be discussed in section 4) also revealed that this low coverage state of oxygen desorbs at $\sim 150^\circ\text{C}$, which is consistent the high volatility of Ga_2O_3 . This low coverage state of oxygen is therefore interpreted as oxygen bridge-bonded over two closely positioned Ga atoms. This interpretation is consistent with the results of Thuault et al [15]. They have found, using photoemission yield spectroscopy, that a partially filled band of Ga-derived defect states present on cleaved GaAs(110) can be removed by oxygen exposure as low as 1L.

The types of surface defects that can give the partially filled Ga-derived states observed by Thuault et al [15] and that can easily form the Ga-O-Ga bonding are, for example, surface As vacancies or Ga terminated steps or As vacancies at steps. (This suggestion is supported by the following interatomic distance: the shortest Ga-Ga distance in Ga-As is 3.99 Å, and the Ga-Ga distance in the Ga-O-Ga unit of Ga_2O_3 is 3.45 Å.) The detailed nature of the defects on cleaved GaAs(110) surfaces remains to be determined by other methods. However, it is important to point out that we have obtained a signature of an important class of defects on cleaved GaAs(110).

3.3.5 Discussion of the Possible Adsorption Mechanisms

Suggestions have been made in the past that the dissociation of molecular oxygen on GaAs(110) occurs at defect sites [3]. The identification of the low coverage state of oxygen indicates that one important (possibly the most important) class of defects on GaAs(110) are passivated by oxygen before the major chemisorption state emerges. This observation suggests that the role of defects in the dissociative adsorption of oxygen (the high coverage state) on GaAs(110) may be

insignificant. Dissociation of molecular oxygen at defect sites has been proposed to control the kinetics of gas adsorption on many metal surfaces [16]. In that picture oxygen molecules are dissociated at defect sites and the dissociated oxygen atoms migrate away to bond at normal surface sites (i.e., surface sites defined by the ideal surface lattice, including reconstruction or relaxation if that occurs). On semiconductor surfaces, a picture with much more localized reactions may apply. That is, oxygen molecules dissociated at defect sites also react with atoms surrounding the defect sites, and thus leading to the passivation of the defect sites in the rest of the adsorption process. This picture of localized reaction clearly applies to the low-coverage-adsorption state (section 3.4) which we have observed on GaAs(110). Although other types of defects capable of nonlocalized dissociation reaction may exist on GaAs(110) without being detected, the present finding at least suggests that localized reaction of oxygen at defect sites is important to consider.

Defect sites on semiconductor surfaces may enter the oxygen adsorption process in another way. Mark et al [17] have proposed that defect sites on GaAs surfaces serves as the nucleation centers for the the oxidation process. In that picture, oxygen molecules dissociate and react locally at defect sites, but the heat of adsorption induces more defect sites around these defect sites and the oxidation process continues on. In section 4 below we will show that on sputter-disordered GaAs(110) surfaces, where gross disorder is introduced such that there are more defect sites than normal sites, the adsorption of oxygen is separated in two distinct steps: oxygen first adsorb on defect (Ga-rich) regions to

saturation, and then adsorb on normal sites with a rate comparable to that found on ordered GaAs(110). As explained in the last subsection, the same two-site oxygen adsorption occurs on cleaved, ordered GaAs(110), only that the amount of oxygen adsorbed on defect sites is much smaller. Since the numbers of oxygen atoms adsorbed in the first step on ordered and disordered surfaces are proportional to the numbers of defect sites that are present on the two surfaces before oxygen adsorption, it is reasonable to assume that adsorption on the two types of sites are independent of each other. This suggests that the picture of Mark et al [17] may be inappropriate for the adsorption of oxygen on GaAs(110).

The above discussion was meant to point out that the dissociation of oxygen molecules does not necessarily occur through interactions with defect sites. In fig. 17-(a), a possible mechanism of dissociating oxygen molecules at normal surface sites of GaAs(110) is suggested. On perfect, relaxed GaAs(110) the most easily accessible electrons for impinging oxygen molecules are those in the As lone pairs, hence an impinging oxygen molecule is forced to interact with an As lone pair. That interaction is then assumed to lead to the formation of a peroxy zwitterion, as shown on the left of fig 17-(a). The peroxy zwitterion is highly unstable because the O-O antibonding π orbitals are filled. The O-O bond thus breaks as the released O atom simultaneously bridge over the As atom under consideration and a nearest-neighbor surface Ga; the other O atom at the same time strengthens its bonding with the As atom, forming the As=O dative bond [13]. This leads to the oxygen bonding configuration we proposed in section 3.3, which is shown on the right of fig 17-(a). In fig 17-(b), we show the top view of the proposed oxygen

bonding configuration. In the top view, we recognize that there are two equivalent surface bonds for which the released O atom from the peroxy zwitterion can attack. This ambivalent position of the released O atom from the peroxy zwitterion may lead to a random variation between 1 and 2 in the oxygen coordination number of surface Ga atoms. Since the chemical shift in Ga-3d induced by oxygen adsorption is not resolved, the randomness of the oxygen coordination of surface Ga is not inconsistent with the experimental results. The oxygen coordination number for surface As, however, is fixed in this proposed adsorption mechanism, which is consistent with the constant value of chemical shift in As-3d at various oxygen coverages.

In contrast to the above-proposed dissociation mechanism, if oxygen molecules dissociate at defect sites and then react at normal sites, the dissociated O atoms would be very reactive and would favor the formation of the Ga-O-As bond over the As=O bond [4]; in forming the Ga-O-As bonds, surface Ga-As bonds may be randomly attacked to cause random oxygen coordination of surface As at different oxygen coverages, which is inconsistent with the constant value of chemical shift in As-3d.

In summary, we have proposed that oxygen molecules dissociate on GaAs(110) through interacting with the As lone pairs of surface As. This proposal is motivated by

- i) one class (perhaps the most important class) of defects on GaAs(110) are found to be passivated before oxygen begins to adsorb on normal surface sites.

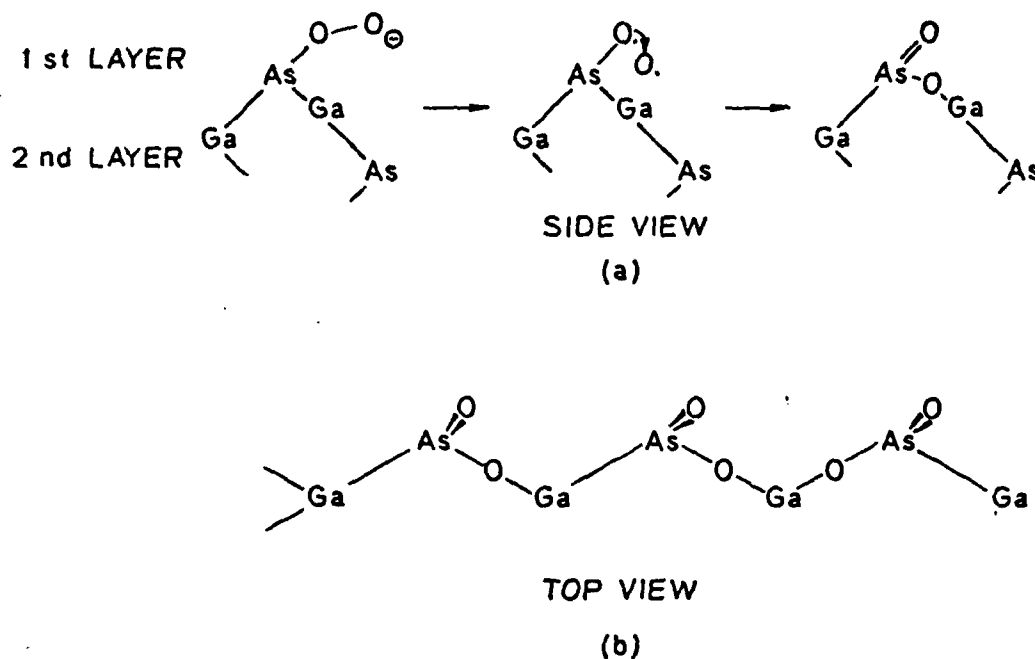


Figure 17: A proposed mechanism of the dissociation of oxygen molecules on GaAs(110) surfaces (a) and the top view of the proposed bonding model, showing that the oxygen coordination number of surface Ga may vary between 1 and 2 (b).

ii)

the constant oxygen coordination number of surface As at different oxygen coverages.

3.4 RESULTS AND DISCUSSION - OXYGEN ADSORPTION ON DISORDERED GAAS(110) SURFACES

In this section we present results of room temperature oxygen adsorption on GaAs(110) surfaces disordered by inert ion (Ar^+) sputtering. Sputtering introduces both structural disorders (loss of LEED pattern) and compositional imperfection (loss of stoichiometry) to GaAs(110) surfaces. Oxygen adsorption on disordered surfaces tests the importance of the long range order of the surface structure in the oxygen adsorption processes, when compared to adsorption on cleaved surfaces.

Two samples have been studied: one p-type sample (sample P3, figures 18,22) studied with He-I and He-II radiation, and one n-type sample (sample N6, figures 19,20) studied with 100 eV synchrotron radiation. We will first describe the properties of the sputter-disordered surfaces, as deduced from the photoemission spectra of these surfaces (section 4.1). Oxygen induced features in the photoemission spectra are analyzed in section 4.2. The oxygen adsorption process on disordered GaAs(110) will be discussed in section 4.3.

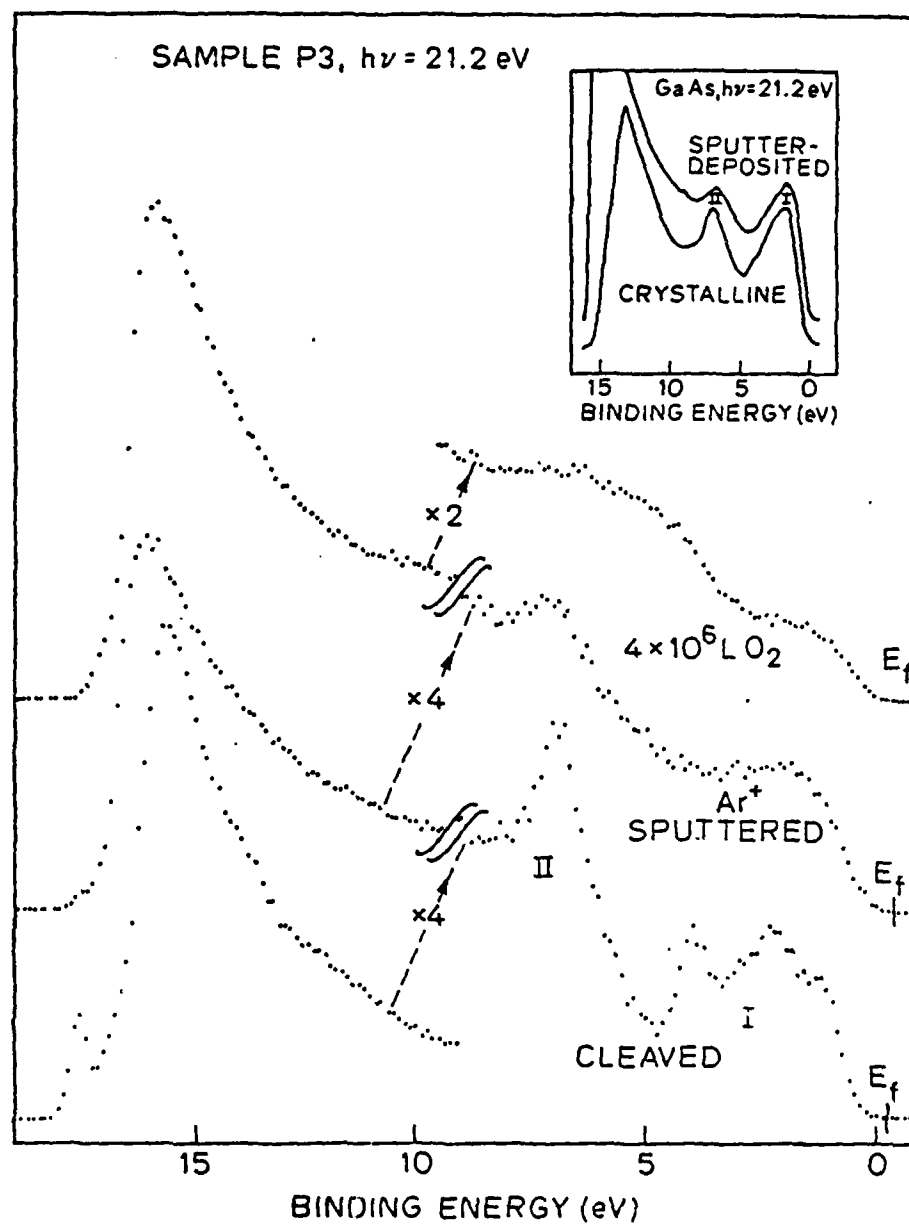


Figure 18: He-I spectra of clean, sputtered, and oxygen-exposed p-GaAs(110). The inset shows the He-I spectra of crystalline and amorphous GaAs obtained by Shevchik et. al. [18].

3.4.1 The Sputtered Surface

The He-I spectra obtained on sample P3 are shown in figure 18. The sputtering (500 eV Ar^+ , 15 minutes) had produced layers of well disordered GaAs, as can be seen by comparing the smearing of the 'fine' structures in the upper p-like band (in the 0-5 eV BE region, labeled I in fig. 18) and the broadening of the s-p mixed band (peak II in fig. 18, 6.9 eV BE). Similar, but to less degree, smearing of the valence band features were observed in the He-I spectrum of sputter-deposited GaAs (the upper curve in the inset of figure 18) obtained by Shevchik et. al. [18]. The different degree of smearing could be due to real difference in the properties of the sputter-disordered surface in our work and the sputter-deposited film studied by Shevchik et. al.. A high stoichiometry of the sputter-deposited film was reported by Shevchik et. al., whereas As deficiency is expected for the sputter-disordered surface (figure 19, to be discussed below).

The bottom curve fig. 19 shows the Ga-3d and the As-3d levels of a n-type sample cleaved in vacuum and then sputtered with 1 KeV Ar^+ ion for 10 min.. (The spectra for the cleaved surface was not obtained.) A comparison of the ratio of the areas under Ga-3d and As-3d of the sputtered surface to that of a cleaved surface (that of fig. 1, for example) reveals that about ~22% As in a region near the surface were lost during (see table 5 below for more discussion). However strong the As-deficiency may be, no coagulation of Ga atoms into droplets occurs under the sputtering conditions used here. This is evidenced by (1) the lack of

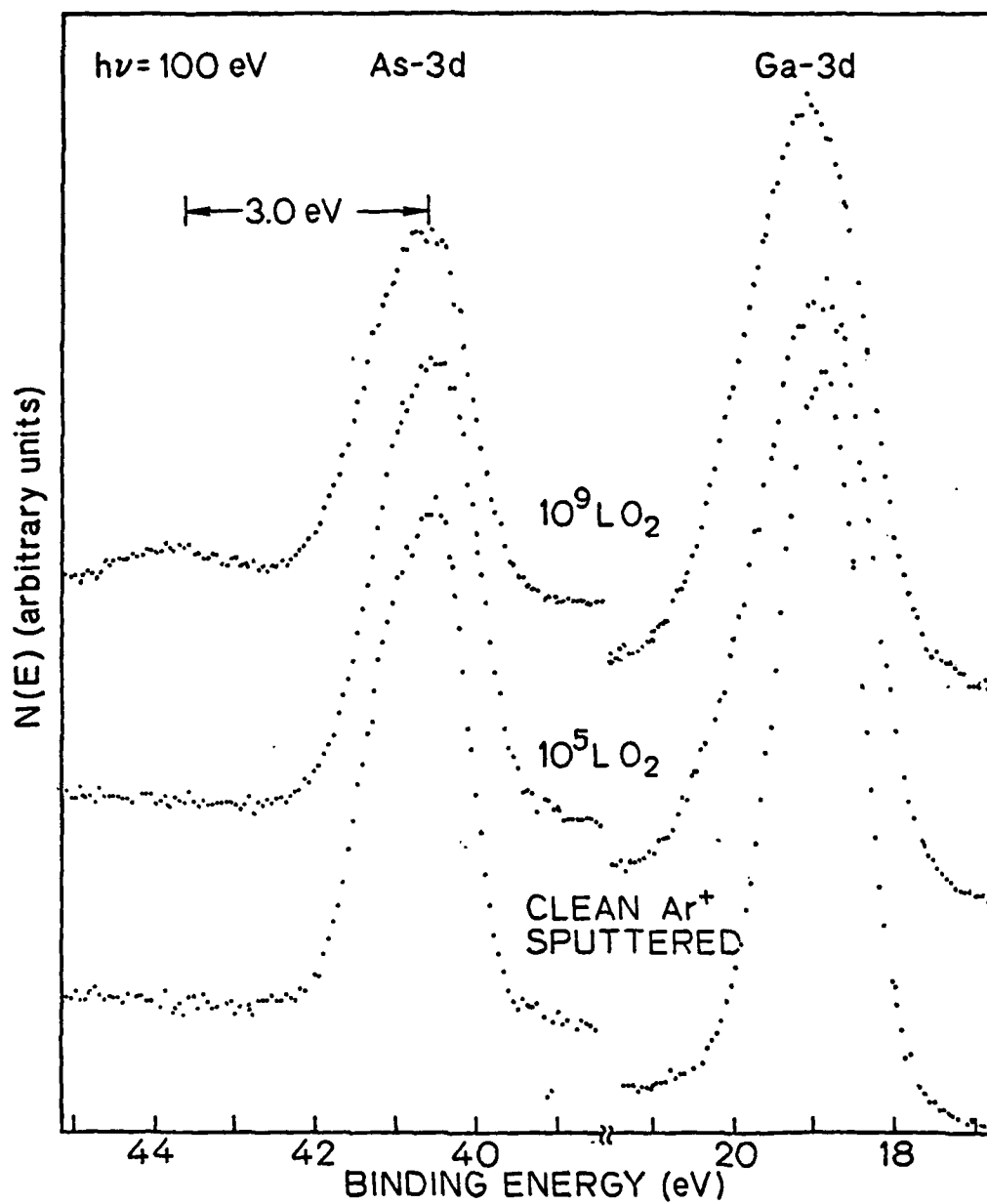


Figure 19: Ga-3d and As-3d levels of clean and oxygen-exposed sputter-disordered GaAs(110). At the 10^5 L exposure oxygen atoms are bonded to Ga only.

emission in the energy region above the valence band maximum and below the Fermi level in the valence band spectra of sputtered surfaces (figs. 18, 20, and 22), and (2) the lack of chemical shift in the Ga-3d level toward the lower BE side (fig. 19, and fig. 22 to be discussed below). Thus the majority of Ga atoms occupies tightly bonded tetrahedral sites even at the presence of a larger number of As deficiency. The As deficiency leaves behind simple As vacancies or sites with a few of the four Ga-As bonds to a Ga atom being replaced by Ga-Ga wrong bonds [18] or both, since a substantial amount of Ga atoms in the surface region are seeing other Ga atoms as nearest neighbors. This picture of the sputtered surfaces is important in understanding the oxygen adsorption process on disordered GaAs(110).

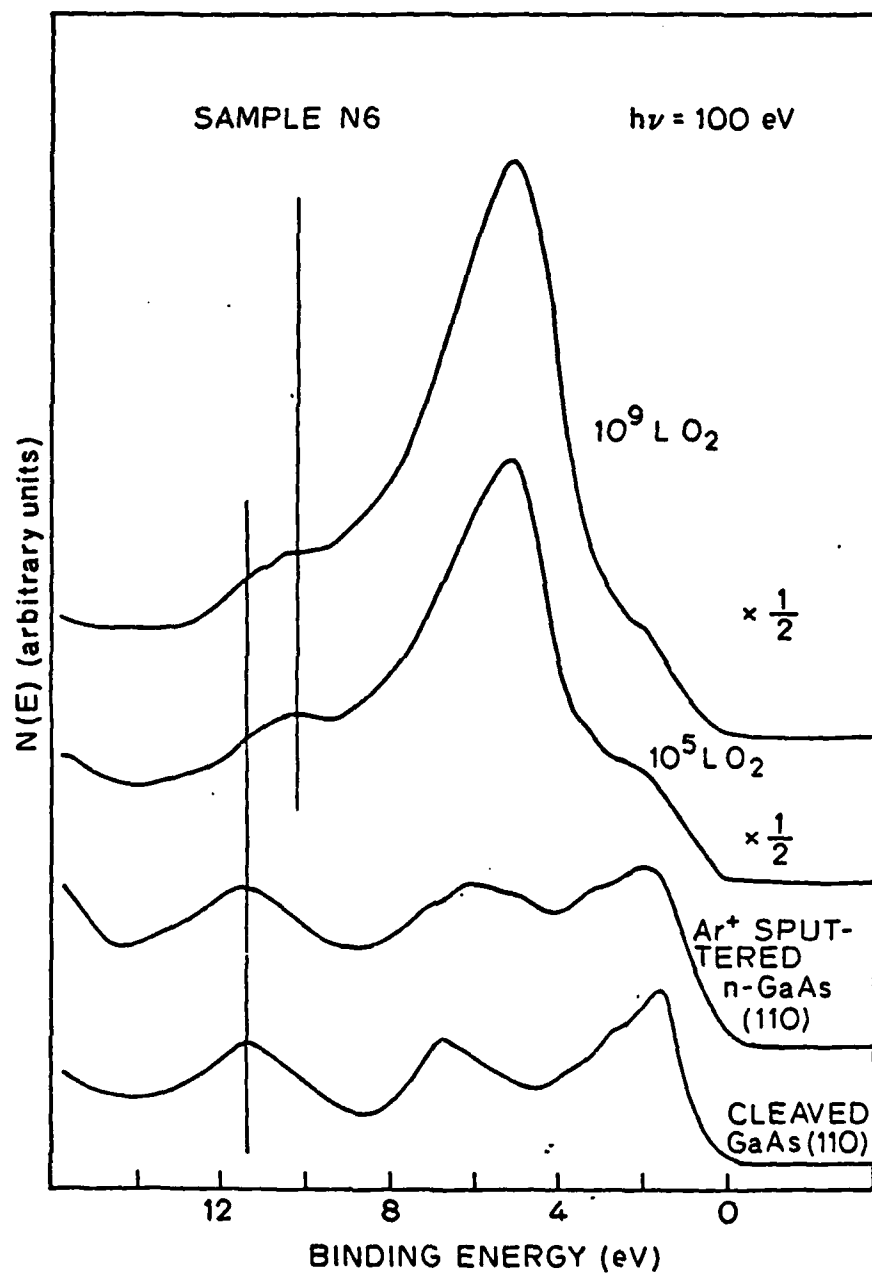


Figure 20: The valence band spectra of clean and oxygen-exposed sputter-disordered GaAs(110) measured at $h\nu=100$ eV.

3.4.2 The DOYS of Oxygen-adsorbed Sputter-disordered Surfaces

Figure 19 shows the effect of oxygen adsorption on the Ga-3d and the As-3d levels of a sputter-disordered surface; the spectra were taken with 100 eV synchrotron radiation. Exposing the disordered surface to 10^5 L oxygen produced a significant amount asymmetric broadening of the Ga-3d level toward the high binding energy side (~36%, table 5, to be discussed below), whereas no change was induced in the As-3d level (center curve, figure 19). We therefore have a clear-cut case in which oxygen is bonded to Ga but not to As. Spectra of the O-2p level are presented in figure 20. With the 10^5 L exposure, the spectrum represents oxygen bonded to Ga only. The oxygen induced features in this spectrum are the broad peak at 5.3 eV and the shoulder at ~10.3 eV peak.

As oxygen exposure is increased to 10^9 L, a small amount of shifted As-3d characteristic of oxygen bonding to As also appeared (top curve, figure 19), while the broadening in the Ga-3d level is furthered increased. Oxygen induced features do not change significantly. We conclude that the 10^9 L valence band spectrum in fig. 20 is dominated by that due to oxygen bonded to Ga.

The oxygen bonded to Ga atoms on disordered GaAs surfaces is in a form distinctly different from Ga_2O_3 . In figure 21 we compare the Ga-3d level and the O-2p level of the disordered surface exposed to 10^5 L oxygen and those of a GaAs surface oxidized by oxygen plasma to Ga_2O_3 . The two spectra are plotted with the major oxygen peak aligned. The three features associated with Ga_2O_3 at 5.5, 7.3, and 9.7 eV BE (Appendix A)

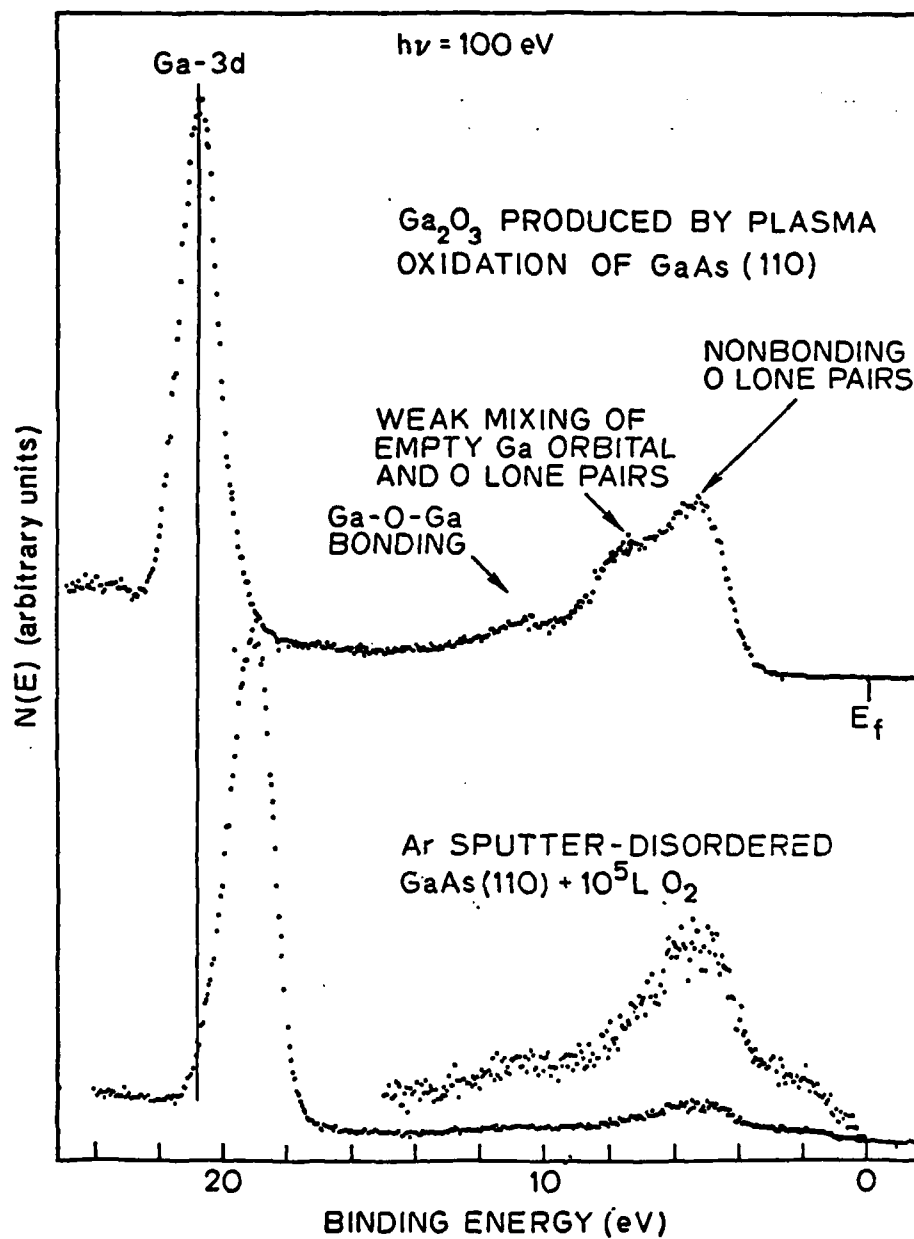


Figure 21: Comparison of the Ga-3d and the valence band region of an oxygen-exposed sputtered-GaAs to those of Ga_2O_3 . Both spectra were obtained at $h\nu=100 \text{ eV}$.

are clearly seen in the top curve of figure 21. The 7.3 eV feature is missing in the spectrum of the disordered surface. Another distinction between the spectrum of oxygen adsorbed on disordered GaAs(110) and that of Ga₂O₃ is in the energy positions of the Ga-3d level. When the major oxygen peaks are aligned the Ga-3d levels in the two cases are separated by 1.7 eV. As indicated in figure 21, the vertical line drawn through the Ga-3d peak of the Ga₂O₃ spectrum intercepts little of the Ga-3d peak in the spectrum of oxygen adsorbed on disordered GaAs. Chemical shift in core levels, when applied to the adsorption problem, is ambiguous in distinguishing between the binding energy references of the adsorbate and the In making the comparison in figure 21 we have suggested the use of an internal reference, namely, the separation between the nonbonding O-2p peak and the Ga-3d peak, to identify different oxygen bonding states. The separation between the Ga-3d peak and the oxygen peak in the lower curve of figure 21 is 13.6 ± 0.2 eV. The apparent peak position of the Ga-3d peak in the spectrum of the sputtered surface, however, is determined by the Ga-3d emission from Ga atoms not bonded to oxygen, because the surface is only partially covered with oxygen. The Ga-3d from Ga atoms bonded to oxygen is shifted to the high BE side of the substrate Ga-3d. The shift was not resolved in either figure 22 or figure 19. Curve fitting the broadened Ga-3d peak after oxygen adsorption with two clean Ga-3d components or taking difference between the before and after adsorption Ga-3d spectra suggests the shift to be at most 0.8 eV. The separation between the Ga-3d peak and the oxygen peak for oxygen adsorbed on disordered GaAs is therefore 14.4 ± 0.2 eV. The corresponding separation of Ga₂O₃ is 15.3 ± 0.2 eV. The 0.9 eV difference unambiguously

distinguish the two forms of O-Ga bonding. A parallel situation has been reported for O-Al bonding: the separation between the Al-2p peak and the oxygen peak is 1.3 eV smaller for a well-defined chemisorption phase than that for Al₂O₃ [20]. This parallel with the better studied Al-O system seems to support the appropriateness of assigning one form of O-Ga bonding as a chemisorption phase and the other form as bulk oxide.

An interpretation of the spectrum of oxygen adsorbed on disordered GaAs surfaces, on the other hand, can be offered by noticing both its similarity to and its differences with the spectrum of Ga₂O₃. As discussed in detail in Appendix A, the three features in the spectrum of Ga₂O₃ have their origins as the nonbonding oxygen lone pair (5.5 eV BE), the donor-like bonding between an oxygen lone pair and an empty Ga orbital (7.3 eV BE), and the Ga-O-Ga bonding band (~9.7 eV BE). The spectrum of O-Ga on disordered GaAs(110) is essentially the same Ga₂O₃ spectrum with the donor-like bonding band missing. As pointed out in Appendix A, the donor-like bonding between oxygen lone pairs and empty Ga orbitals can be viewed either as the result or as the cause of the high coordination number in Ga₂O₃. We therefore simply interpret the spectrum the O-Ga bonding on sputter-disordered GaAs(110) as due to isolated Ga-O-Ga units.

A similar spectrum has been observed on Ga metal at 70°K by Schmeisser et. al. [19]. This is seen in fig. 22, where we have displayed the He-II spectra of the surfaces of fig. 18 and the spectrum of oxygen adsorbed on Ga metal at 70°K (the top curve, reproduced from the work of Schmeisser et. al. [19]). The peak at 5.3 eV BE and the shoulder centered at ~10.3 eV BE developed after the 4x10⁶ L exposure on this sput-

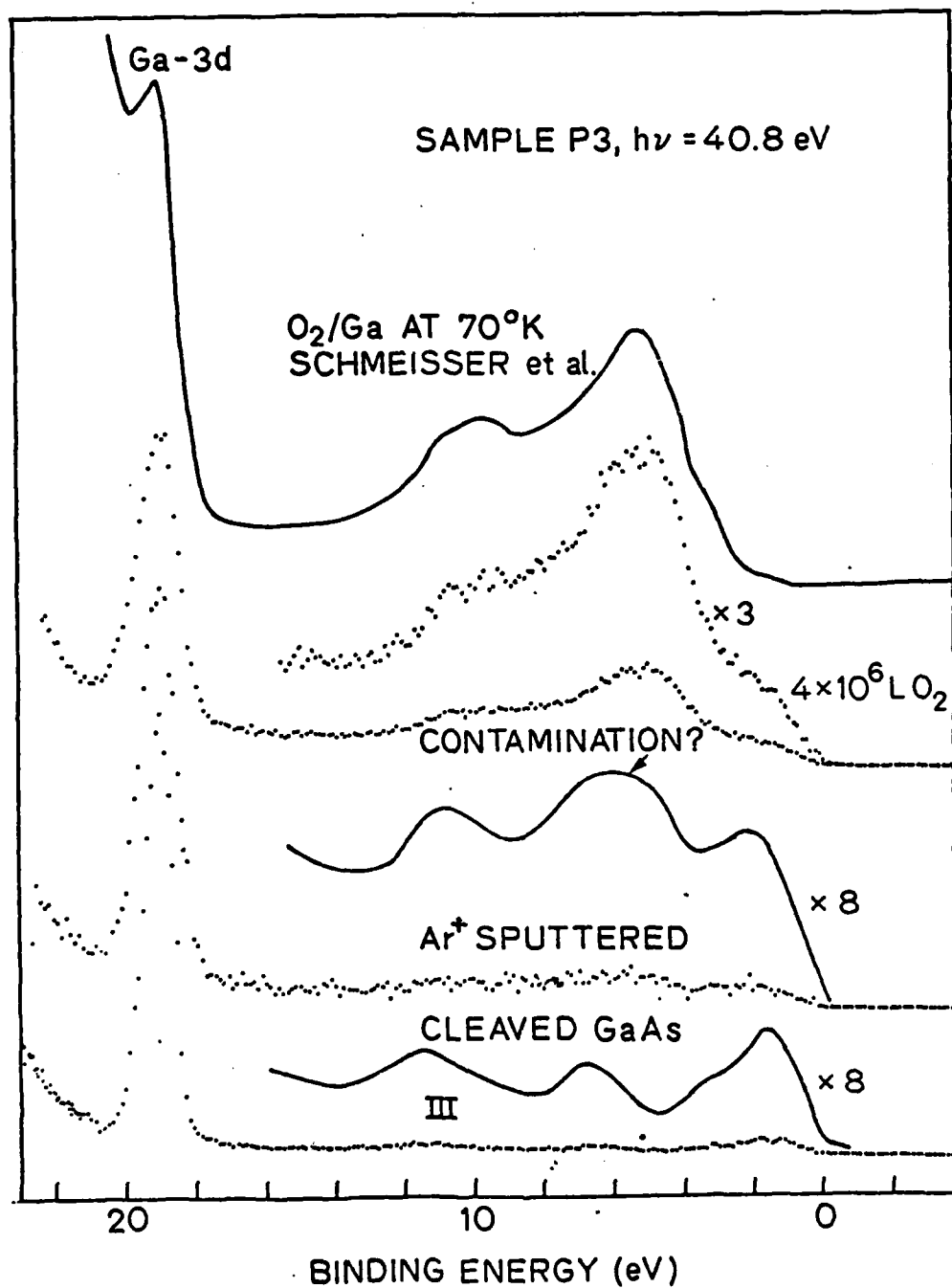


Figure 22: He-II spectra of the surfaces of Fig. 18. The top spectrum is due to oxygen chemisorbed on Ga metal at 70°K [19]. Notice the similarity between the two spectra.

ter-disordered GaAs(110) are the same as those shown in fig. 20, and they also appear in the spectrum of oxygen adsorbed on Ga metal at 70°K (top curve, fig. 22). The spectrum of the chemisorbed oxygen, however, does not show strong reminescence to the multiple splittings characteristic of the O-O bonding. Therefore we believe the spectrum observed by Schmeisser et. al. can also be explained by dissociated oxygen in the Ga-O-Ga bonding. The observation of the same Ga-O-Ga chemisorption form on both the crystalline Ga surface and the sputter-disordered GaAs(110) surface is rather intriguing. Exposure of Ga to oxygen at room temperature always results in the formation of Ga₂O₃ [Appendix A]. This is expected because Ga is a liquid at room temperature; the condition is comparable to high temperature oxidation of Al where Al₂O₃ is always formed [20]. The high mobility of Ga at room temperature does not allow any intermediate state but the most stable Ga₂O₃ to form. At low temperature Ga metal is in crystalline form, the low mobility and the close packing of Ga may stabilize the chemisorption phase. As discussed in section 4.1 above, the majority of Ga atoms occupies tightly bonded tetrahedral sites even at the presence of a large As deficiency, rather than forming Ga clusters. The tight binding of the Ga atoms may present an activation barrier against the direct formation of Ga₂O₃.

Since the sputter-disordered surface is deficient of As, the preferential bonding of oxygen to Ga is not surprising as it is expected from elemental thermodynamics. The absence of the formation of Ga₂O₃, however, is rather intriguing. Since even on a disordered GaAs surface with a large number of Ga atoms seeing Ga atoms as next nearest neighbors the formation of Ga₂O₃ is prohibited, it is very unlikely that room

temperature adsorption of oxygen on an cleaved, ordered GaAs(110) surface can result Ga_2O_3 at the initial stage.

The chemisorbed oxygen on the disordered surface is also different from the oxygen adsorbed at the normal sites on cleaved, ordered GaAs at room temperature (section 3.2, 3.3). In figure 23, we compare the He-II spectra of a cleaved, ordered GaAs(110) surface exposed to 10^8 L oxygen and a disordered surface exposed to 4×10^6 L oxygen (sample P3, figure 22). The Ga-3d peaks of the two cases are aligned. The major oxygen peak of the ordered surface is 4.5 ± 0.2 eV below VBM, whereas that for the disordered surface is 5.3 ± 0.2 eV below VBM. The relatively pronounced 10.3 eV shoulder appeared in the spectrum of the disordered surface is insignificant in the spectrum of the ordered surface. The intensity which exists in the region near 10.3 eV BE in the spectrum of the ordered surface is due to the small amount of Ga-O-Ga bonding at defect sites of the GaAs(110) surface (see section 3.4 above). We thus conclude that the oxygen adsorbed at the normal sites on cleaved, ordered GaAs(110) surfaces does not occur in the form of Ga-O-Ga bonding.

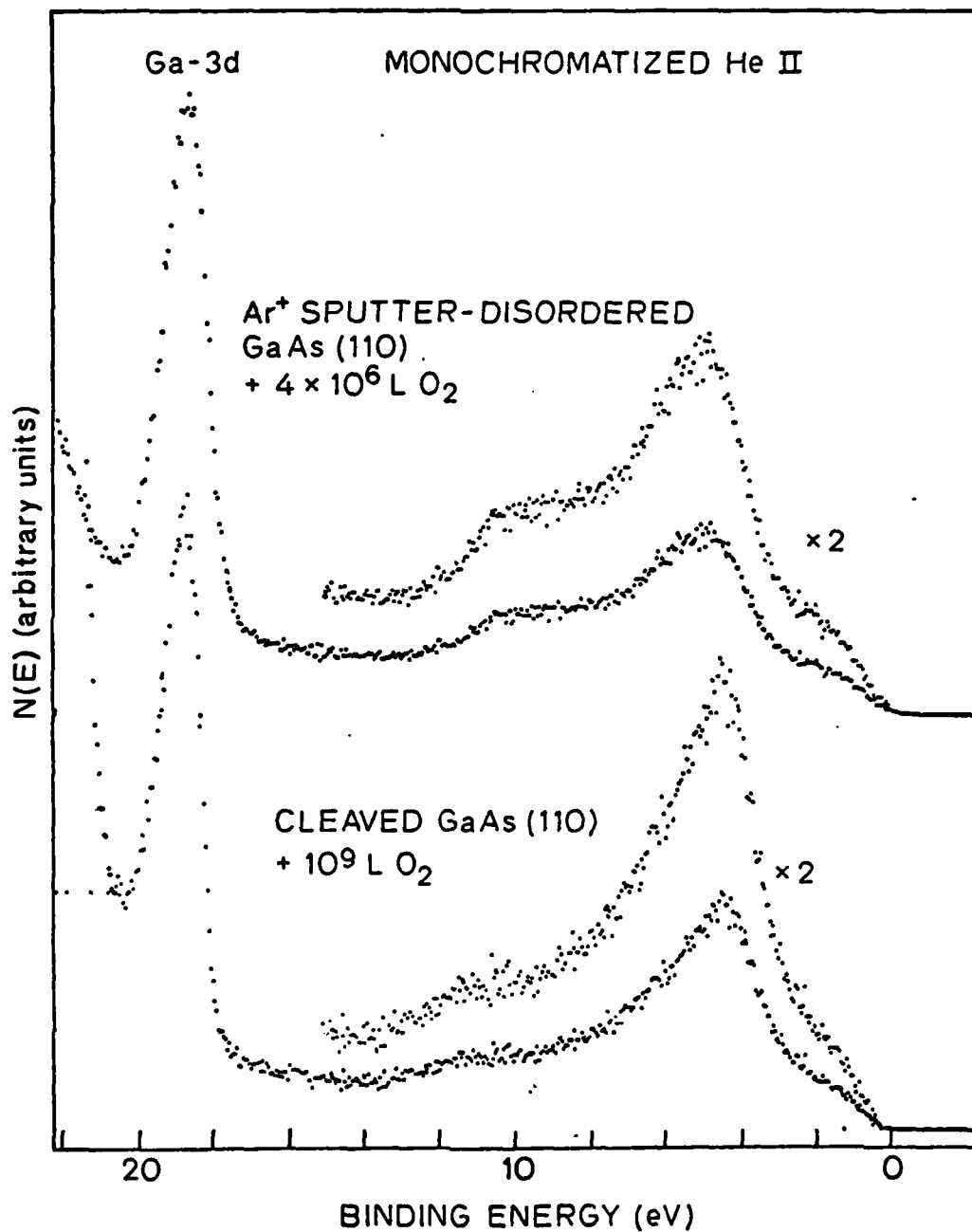


Figure 23: Comparison of the Ga-3d and the valence band region of oxygen-exposed sputtered-GaAs and cleaved-GaAs(110). Both spectra were taken at $h\nu=40.8$ eV (He-II).

3.4.3 The Adsorption Process on Disordered Surfaces

Information revealing a different adsorption process on disordered GaAs surfaces, based on the results obtained on sample N6, are summarized in table 5. Again, intensities of different peaks of each treatment are normalized to the total intensity of Ga-3d level. As atoms in the surface layer contribute about 50% of the total emission of the As-3d level when excited by 100 eV photon (table 1, section 3.2). The 22% loss of As created by sputtering is equivalent to 1/2 of the surface layer. This deficiency of As, however, is more likely to be distributed over a few layers below the surface, because the 1 KeV ion is capable of producing damages a few lattice layers deep [21]. The value of 1/2 can be taken as an upper limit of the deficiency of As in the surface layer. Perhaps the most interesting number in table 5 is the decrease in the As-3d intensity after the 10^5 L oxygen exposure. The decrease of 0.13 corresponds to ~1/4 of the As in the surface layer of a stoichiometric GaAs(110) surface. If the surface layer was 1/2 As deficient before the oxygen adsorption, the decrease is even more significant. Several possibilities can account for this decrease:

- i) shift of the photoelectron escape depth minimum to lower kinetic energy by oxygen adsorption, so more Ga atoms are sampled after oxygen adsorption.
- ii) preferential attenuation of the As-3d signal by the oxygen overlayer.

iii) depletion of As atoms from the surface layer during the adsorption process.

TABLE 5					
Intensity changes in Ga, As, and oxygen levels induced by oxygen adsorption on a sputter-disordered GaAs surface					
Treatment	Ga-3d (total)	Ga-3d (shifted)	As-3d (total)	As-3d (shifted)	O-2p
cleaved	1.0	0	1.0	0	0
sputtered (Ar ⁺ , 1 KeV, 10 min.)	1.0	0	0.78	0	0
10 ⁵ L O ₂	1.0	0.36	0.65	0	0.20
10 ⁹ L O ₂	1.0	0.48	0.64	0.07	0.28

Possibility (i) is not favored, because we did not observe an increase in the absolute intensity of the Ga-3d level after oxygen adsorption; instead, we observed an ~12% decrease in the absolute intensity of the Ga-3d level after oxygen exposure, which is reasonable with the attenuation by the 0.3 monolayer oxygen. Possibility (ii) is unlikely because oxygen is bonded to Ga only. Two possible channels exist for depleting As (possibility (iii) above) during the oxygen adsorption process:

- i) formation of As₂O₃ with loosely bonded As in the disordered surface layer, and the subsequent desorption of As₂O₃ by the exothermic oxidation energy.

ii) formation of the Ga-O-Ga bonding requires Ga-Ga nearest neighbors, hence some As in Ga-rich regions (i. e., regions containing substantial amount of Ga-Ga nearest neighbors because of As vacancies or Ga-Ga wrong bonds or both, see section 4.1 above for more rigorous description) are removed (as As_2 or As_4) before O-Ga bonding commences; the energy needed for the removal of As can be supplied by the exothermic adsorption energy from initial O-Ga bondings in the surrounding Ga-rich region.

We could not distinguish between the two possibilities from the results discussed so far. The important thing to point out here is that the depletion of As in the adsorption process on disordered surfaces forms a striking contrast to the adsorption on ordered surfaces. The oxygen uptake on the disordered surface is faster compared to that on ordered surfaces only initially, when all adsorbed oxygen are bonded to Ga. At 10^9 L exposure, the total amount of oxygen adsorbed is comparable to that adsorbed on ordered surfaces using the same oxygen exposure (compare with Table 1). We also notice the increasing oxygen exposure from 10^5 L to 10^9 L did not introduce further loss of As. It appears that after the 10^9 L exposure some oxygen were adsorbed on a number of 'normal' surface sites (sites retaining the local bonding structure of the ordered GaAs(110)), because chemical shift in the As-3d level characteristic of oxygen chemisorbed on ordered surfaces had emerged. We can tentatively separate the oxygen adsorption process on disordered GaAs surfaces into two steps. Oxygen are first adsorbed at sites with Ga-Ga nearest neighbors on the disordered surface and this adsorption

quickly slows down as the available sites for such adsorption decreases. Oxygen atoms are then adsorbed on patches of normal GaAs sites at a rate no faster than that on ordered GaAs(110) surfaces. We see no evidence here that the gross disorders introduced by sputtering speed up the formation of bulk oxides (Ga_2O_3 , As_2O_3).

As mentioned in section 3.5, Mark et. al. [17] have suggested that the oxidation of GaAs(110) commences on residual defect sites and produces additional disorder owing to the release of exothermic adsorption energy, so that, as the oxidation progresses, the entire surface becomes disordered. If oxygen adsorbs only on defect sites, one would expect to observe the same state of oxygen, possibly Ga_2O_3 and As_2O_3 , being formed on ordered and disordered surfaces.

3.5 RESULTS AND DISCUSSION - EFFECTS OF HEAT TREATMENTS OF OXYGEN-COVERED SURFACES

In this section we present results of thermal annealing experiments. The annealing was carried out on surfaces which were adsorbed with oxygen to various coverages at room temperature. Knowledge of the effects of annealing reveals the stability of the room-temperature O/GaAs(110) bonding and thus provides additional insights into the room temperature interaction of oxygen with GaAs(110).

A basic effect of annealing is the transfer of oxygen from As to Ga and the loss of those As atoms which are released from the arsenic-oxygen bonding from the surface. In panels (a) and (b) of fig 24, we show, respectively, the As-3d and Ga-3d core levels of GaAs(110) surface exposed to 10^{10} L O_2 ($\theta \approx 0.6$) at room temperature and then annealed to 370°C for approximately 30 min.. The spectra are normalized to have equal

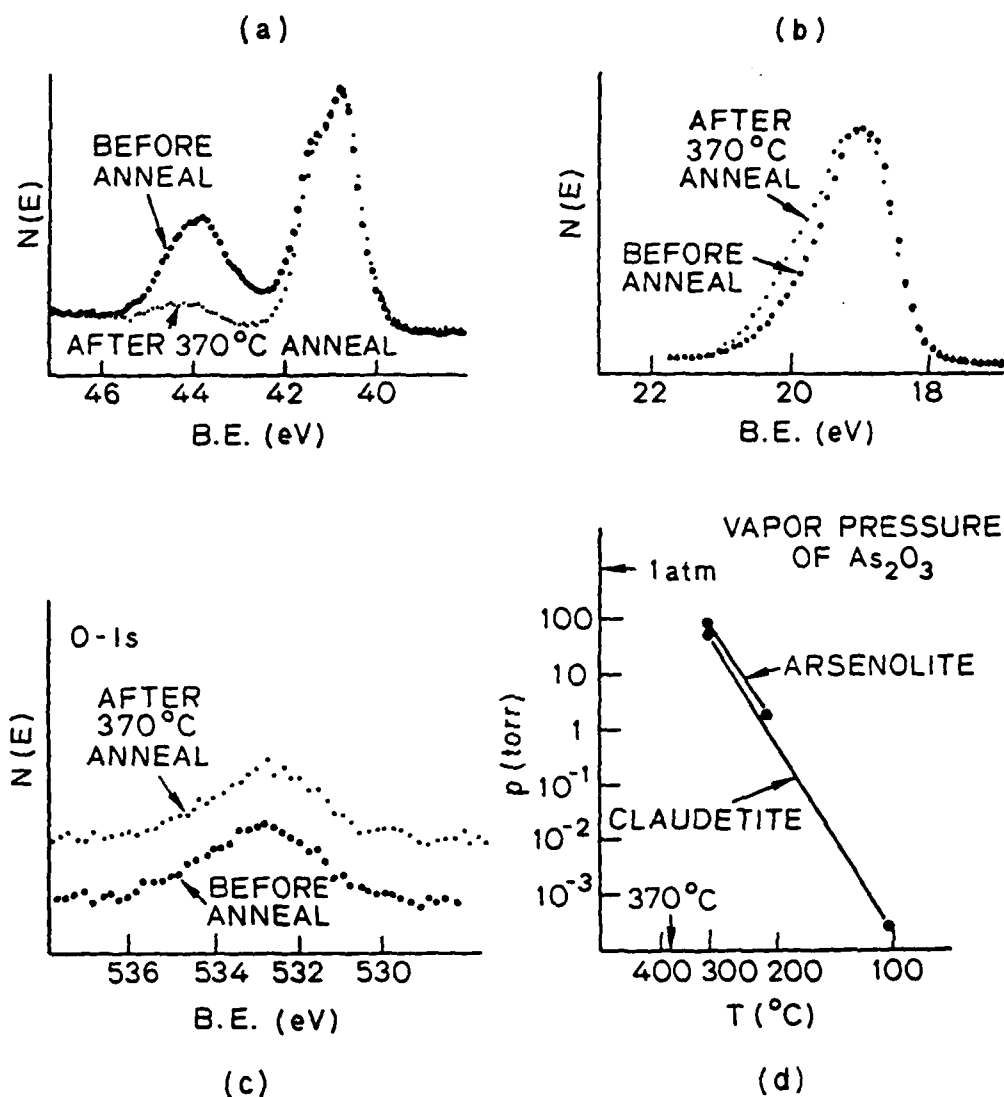


Figure 24: The effect of annealing of a room temperature oxygen-exposed surface at 370°C for 30 min. Transfer of oxygen from As to (panel a) to Ga (panel b) without losing oxygen (panel c) has been observed. However, As originally bonded to oxygen leaves the surface after releasing its oxygen to Ga. For reference, panel d shows the temperature dependence of the vapor pressure of the two forms of As_2O_3 .

height for the unshifted As-3d peaks. The sharp decrease (by a factor ~6) in the intensity of the shifted As-3d (fig 24-(a)) and the increase in the broadening toward high BE of the Ga-3d (fig 24-(b)) are clear. Also apparent is the increase in the ratio of total intensity of Ga-3d to As-3d. (This ratio is not affected by the normalization.) The decrease in the intensity of the shifted As-3d approximately equals the decrease in the total intensity of As-3d. Thus only those surface As atoms bonded to oxygen after room temperature adsorption are lost from the surface during annealing. On the other hand, the O-1s intensity is seen in fig 24-(c) to show no detectable change after annealing, indicating that no desorption of oxygen has occurred during annealing.

In fig 25, we show the effects of annealing to 250°C for 30 min. on another surface exposed to $\sim 10^{11}$ L O₂ ($\theta=0.75$). The decrease in the intensity of the shifted As-3d and the increase in the broadening toward high BE side of the Ga-3d after annealing is much less pronounced than that caused by the 350°C anneal (fig 24). This suggests that the arsenic-oxygen bonding formed by room temperature adsorption of oxygen on GaAs(110) is rather stable at 250°C. This is consistent with the presence of As=O bond (section 3.3), because the As=O bond in As₂O₃ becomes unstable only at temperatures above 315°C [22].

On the other hand, the results in figs. 24 and 25 are inconsistent with the presence of As₂O₃ after room temperature adsorption. If the chemically shifted As-3d were to be interpreted as due to As₂O₃, there would be two competing channels to remove As₂O₃ at elevated temperatures: one is the evaporation of As₂O₃, and the other is the reaction

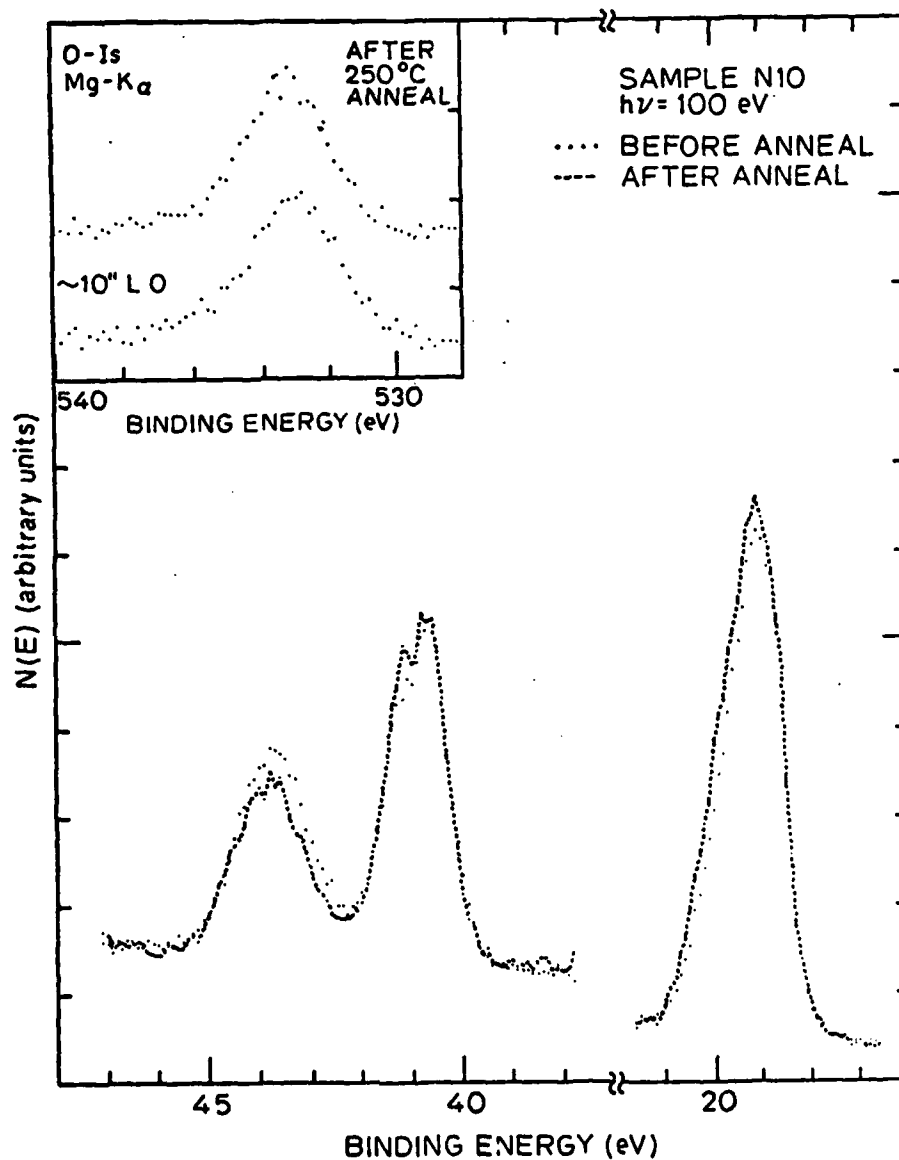


Figure 25: The effect of annealing of a room temperature oxygen-exposed surface at 250°C for 30 min. The changes in the As-3d and the Ga-3d are much less pronounced than that observed in fig. 24.

of As_2O_3 with substrate GaAs to form Ga_2O_3 . In fig 24-(d) we show the variation of vapor pressure with temperature of the two crystalline forms of As_2O_3 [23]. These curves indicate high volatility of As_2O_3 at room temperature and above. In particular, by using the extrapolated values of vapor pressure at 250°C and 370°C, and by using an unusually low evaporation coefficient of $\sim 10^{-7}$ [24], evaporation rates of $\sim 1 \times 10^{14}$ molecules/cm²-sec and 7.5×10^{15} molecules/cm²-sec are found at 250°C and 370°C, respectively. With these evaporation rates, it requires only 0.1 sec to evaporate a monolayer (10^{15} molecules/cm²) of As_2O_3 at 370°C and 10 sec at 250°C. The absence of desorption of oxygen is possible only if the reaction of As_2O_3 with GaAs to form Ga_2O_3 is much faster than the evaporation of As_2O_3 and the shifted As-3d disappears completely in 0.1 ~ 10 sec after anneal. However, the chemically shifted As-3d did not disappear completely (figs 24 and 25) after holding the sample at either 250°C or 370°C for 30 min.. The shifted As-3d remained after the 250°C anneal is about 90% of the original intensity and that remained after the 370°C anneal is about one-sixth of the original intensity. It is hard to explain why such significant amount of As_2O_3 which escaped transforming into Ga_2O_3 by heating could stay on the surface without being evaporated away. The interpretation of the chemical shift in As-3d as due to As_2O_3 is thus considered highly improbable.

The end product of the annealing process can be determined by combining results from the valence band spectra and the results from the core level spectra described above. In fig 26 and 27, we show He-II spectra of a GaAs(110) surface subjected to programmed temperature treatments (in which the sample was raised to successively high temperatures) after the

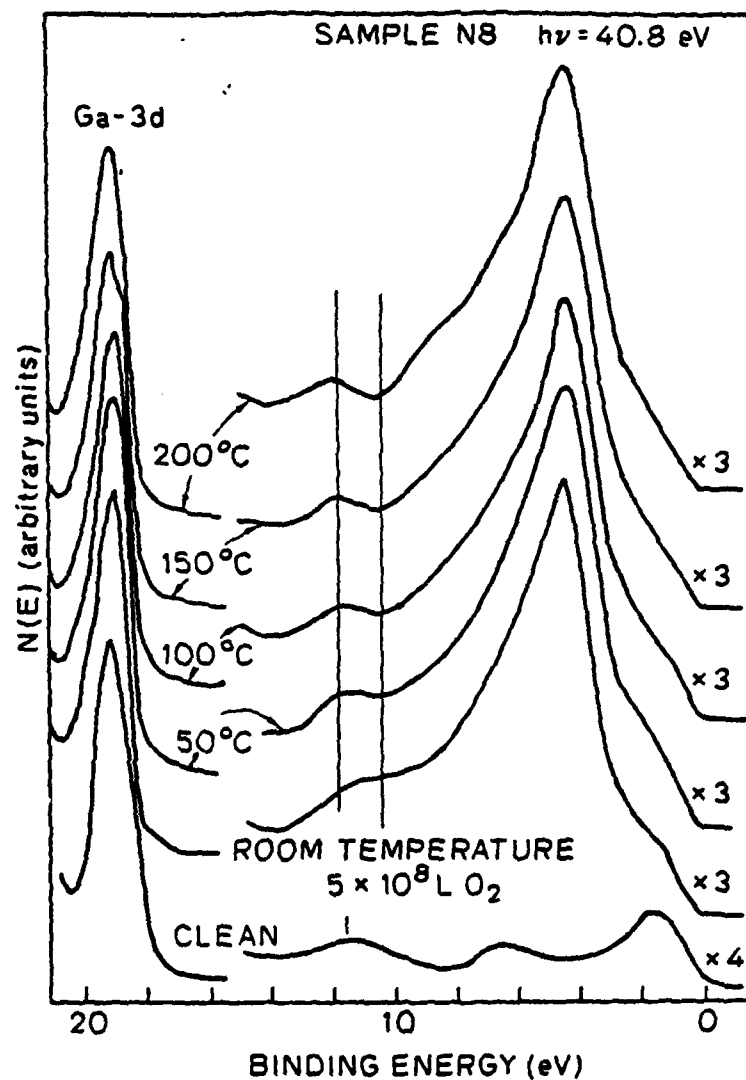


Figure 26: Effects of annealing of a room temperature oxygen-exposed n-GaAs(110) in the temperature range of 50-200 °C. The sample was held at each temperature for 10 minutes. Spectra were taken at $h\nu = 40.8$ eV (He-II). The bottom curve is the spectrum of the clean surface.

room temperature exposure. The temperature increment is 50°C and the annealing time at each temperature was ~10 min.. Different changes induced by annealing in the valence spectra are seen in the low temperature range (50°C - 200°C) and the high temperature range (250°C - 450°C), hence they are separately displayed in figs. 26 and 27. The major change produced by annealing in Fig 26 is the removal of intensity from the region at ~10.3 eV BE. This effect is noticable at 50°C and is about complete at 200°C. The major effect of annealing at higher temperatures, as seen in fig. 27, is the development of a new feature in the 8-10 eV BE region. This effect is noticable at 250°C and becomes very pronounced at 450°C. At 480°C, all oxygen desorb and the surface is heat-cleaned.

The annealing effects in the DOVS' are more closely examined in fig. 28. In panel (a), the 200°C spectrum is subtracted from the room temperature spectrum, and the difference is displayed at the bottom. The difference is noisy, but two features at ~5.5 eV and 10.5 eV BE are discernable. These binding energies are the same as those found for the low coverage state oxygen in section 3.4. Thus oxygen adsorbed at the defect sites of GaAs(110) desorb at temperatures between 150°C and 200°C. The binding energies of the two features in the difference curve of fig. 28-(a) are also the same as those of the Ga-O-Ga bonding complexes found on the sputter-disordered GaAs surfaces (section 4). We therefore propose the low coverage state of oxygen to be in the Ga-O-Ga bonding form. This proposal is consistent with its low desorption temperature, because Ga₂O, which is essentially an isolated Ga-O-Ga bonding unit, is known to be highly volatile.

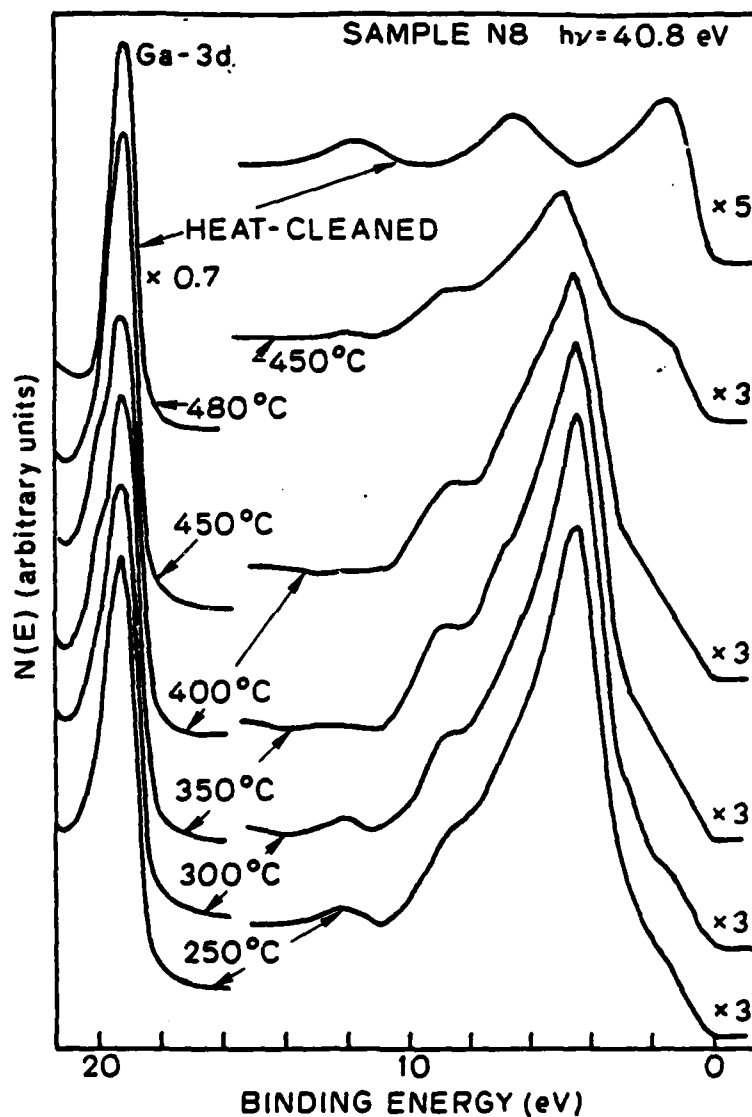


Figure 27: Effects of annealing of the surface of fig. 26 in the temperature range 250-450 °C. The sample was held at each temperature for 10 minutes. The top spectrum shows the surface being heat-cleaned after heating at 480°C.

In panel (b) of fig 28, we have obtained the difference curve between the 350°C spectrum and the clean spectrum. The difference curve bears clear resemblance to the DOVS of Ga₂O₃ (fig. 13, section 3.2). Hence the new feature developed in the 8-10 eV BE region observed in fig. 27 is due to the formation of Ga₂O₃. Fig. 27 also indicates that the formation of Ga₂O₃ is significant only at temperatures above 300°C, which is consistent with the conclusion drawn from comparing figs. 24 and 25.

It is also interesting to notice the difference in binding energies of the features in panel (a) and those of the difference curve in panel (b). The difference is consistent with the comparison made in fig 21 between Ga-O-Ga and Ga₂O₃.

In fig. 27, an additional change in the DOVS is seen to have occurred at 450°C: the nonbonding oxygen peak shifted to higher binding energy. We also notice that a considerable amount of oxygen desorb at 450°C such that the oxygen coverage after the 450°C anneal is low. The same shift in oxygen nonbonding peak is also produced by going directly to an annealing temperature on a low oxygen coverage surface. In fig. 29, we show sample P2 exposed to 10⁷ L O₂ (θ≈0.15) at room temperature and then annealed at 350°C for 30 min.. Since low oxygen coverage is a common factor in the two cases, we suggest that the 450°C spectrum in fig. 27 or the after-anneal spectrum in fig. 29 represents DOVS of oxygen-deficient gallium oxide, i.e., Ga₂O_{3-x}, with the value of x between 1 and 2. At high temperature (450°C - 480°C), the desorption is likely to occur through the reduction reaction

$$\text{Ga}_2\text{O}_3 + 4 \text{Ga} \rightarrow 3 \text{Ga}_2\text{O} \uparrow$$

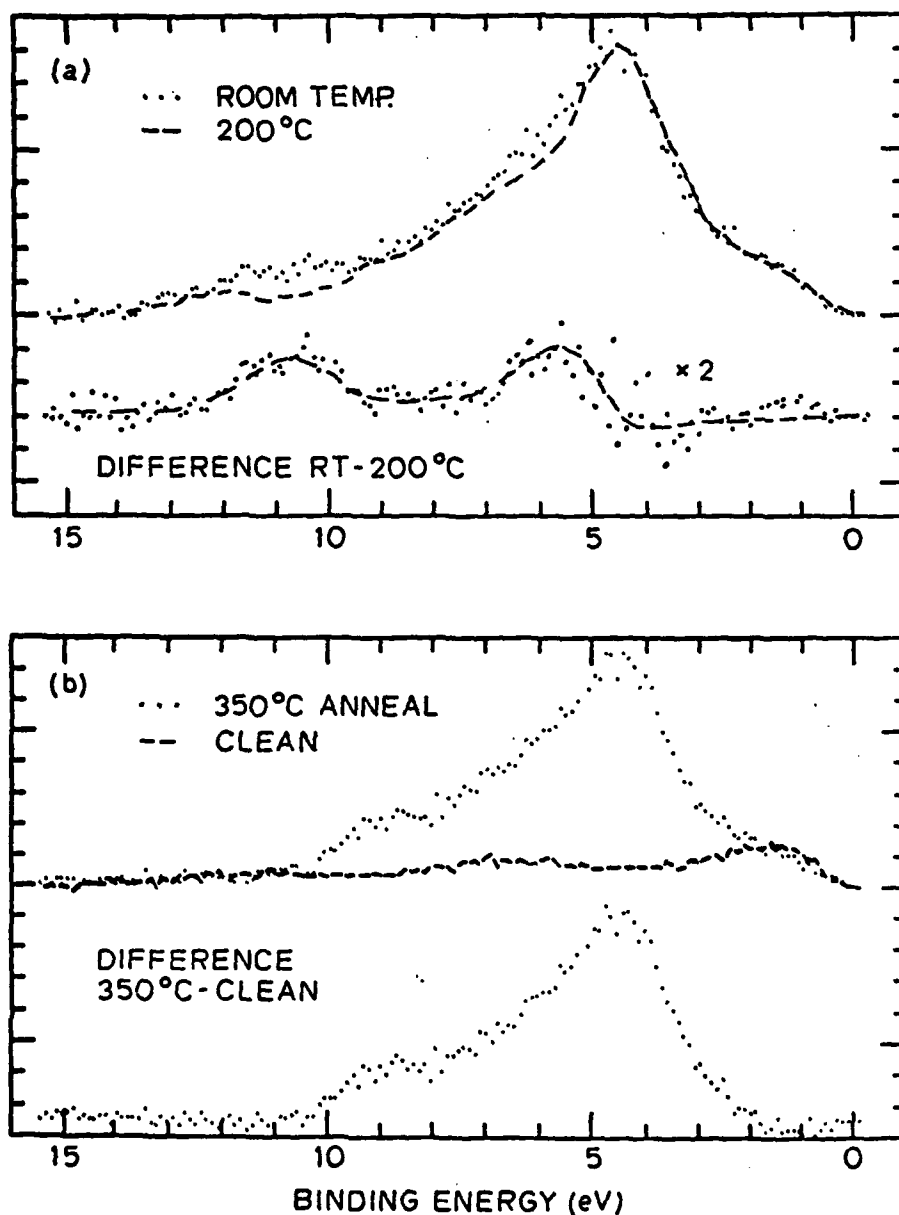


Figure 28: Difference curves between before and after heating (a) Difference curve (the bottom curve) obtained by subtracting the 200°C (dashed) from the room-temperature spectrum (dotted). It shows that the oxygen adsorbed at defect sites of GaAs(110) desorbs at ~200°C. (b) Difference curve (the bottom curve) between the 350°C spectrum (dotted) and the clean-surface spectrum (dashed). The resemblance of the difference curve to the spectrum of Ga_2O_3 indicates the formation of Ga_2O_3 by annealing to temperature $\geq 300^\circ\text{C}$.

Before complete desorption of oxygen occurs, it is possible that some oxide intermediate between Ga_2O_3 and Ga_2O may be on the surface which is less volatile than Ga_2O . For surfaces initially covered with small amount of oxygen, annealing brings nearby oxygen to form $\text{Ga}_2\text{O}_{3-x}$, but Ga_2O_3 cannot be formed because of the deficiency of oxygen at a particular site on the surface. This result of annealing of low oxygen coverage surface is in fact an evidence against the picture that oxygen adsorb in patches or islands on $\text{GaAs}(110)$.

When the heat-cleaned surface of sample N8 is re-exposed to oxygen, the same Ga-O-Ga state as that observed on sputter-disordered surface is found. This is shown in fig. 30, where two oxygen features at 5.3 eV and at 10.3 eV BE are clearly seen. The amount of oxygen adsorbed in the Ga-O-Ga form on heat-cleaned surface is smaller than that found on sputter-disordered surfaces but is far higher than that found on cleaved surfaces. Since heating is expected produce As deficiency in the surface region, the results shown in fig. 30 again reinforce the importance of removing As before forming the Ga-O-Ga bonding units.

In all the above annealing experiments, temperature was slowly ($15^\circ\text{C}/\text{min}$) brought up to the annealing temperature and then kept at that temperature for the indicated time. Only slight increases in the background pressure were detected during annealing. On two other surfaces, where we have attempted to heat to higher temperatures with faster rates ($220^\circ\text{C}/\text{min}$ for $T \geq 300^\circ\text{C}$), heatings were terminated immediately after sharp pressure rises were detected. Although no mass-spectrometric measurement was done, the photoelectron spectroscopic measurements of

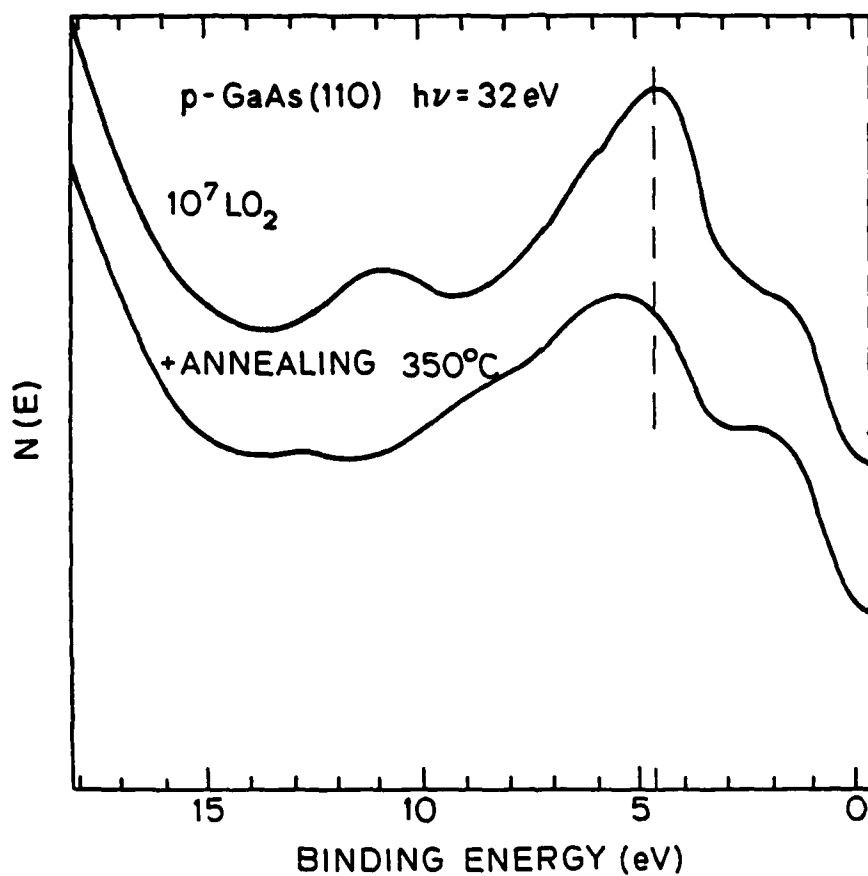


Figure 29: Annealing of a low oxygen coverage surface to 350°C . The changes seen here are the same as that observed between annealing at 400°C and at 450°C of a high oxygen coverage surface (fig. 27). Spectra were taken at $h\nu = 30 \text{ eV}$.

the resulting surfaces indicate that, as will be discussed below, the sharp pressure rises could well be correlated to desorption of As and oxygen from the sample surfaces, and did not correspond to any outgass-

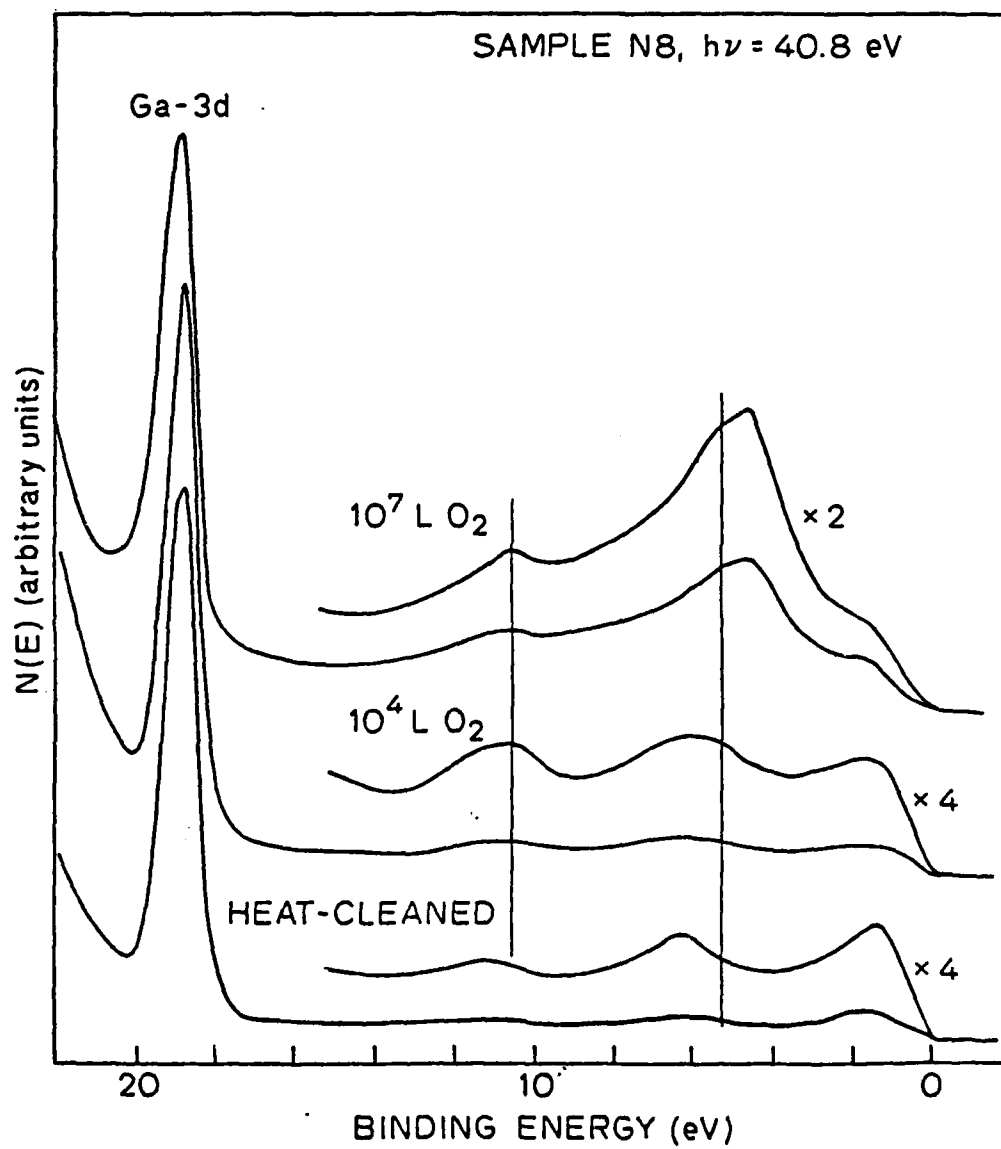


Figure 30: Re-exposure of the heat-cleaned surface of fig. 27 to oxygen. Spectra were taken at $h\nu=40.8$ eV.

ing of other surfaces in the vacuum chamber. In one case, substantial transformation of oxygen from As to Ga was also observed in addition to the desorption of As and oxygen. Such complication reflects the lack of accurate control in the heating rate in our experiments. Better control of the heating rate and systematic search for effects due to different heating rates should be of great interest in the future. However, in the other case, little transformation of oxygen from As to Ga was observed to accompany the desorption. Results from this latter case clearly contrast the results from the annealing experiment we just discussed, hence they will be presented below.

In fig. 31, we show core level spectra of a GaAs(110) surface exposed to 10^9 L O_2 ($\theta \approx 0.5$) at room temperature and then heated at a relatively rapid rate to 430°C . The curve with heavy dots in fig. 31 shows the normally observed chemically shifted As-3d and the broadening in the Ga-3d after room temperature adsorption. The spectrum taken after heating to 430°C shows complete disappearance of the shifted As-3d. But in contrast to the results shown in fig. 24, there is only a barely detectable increase in the broadening in the Ga-3d. The O-1s intensity, as shown in the inset of fig. 31, decreased by a factor close to two. The total intensity of As-3d decreased by approximately 25% which is equal to the percent shifted As-3d before heating. The decrease in intensity of O-1s and As-3d in conjunction with the pressure burst detected immediately prior to the termination of heating are strong indications of desorption of both oxygen and As from the sample surface. The slight increase in the broadening in Ga-3d and the small deviation of the oxygen intensity ratio from two is attributed to a small amount of oxygen transformed from As to Ga before the termination of the heating.

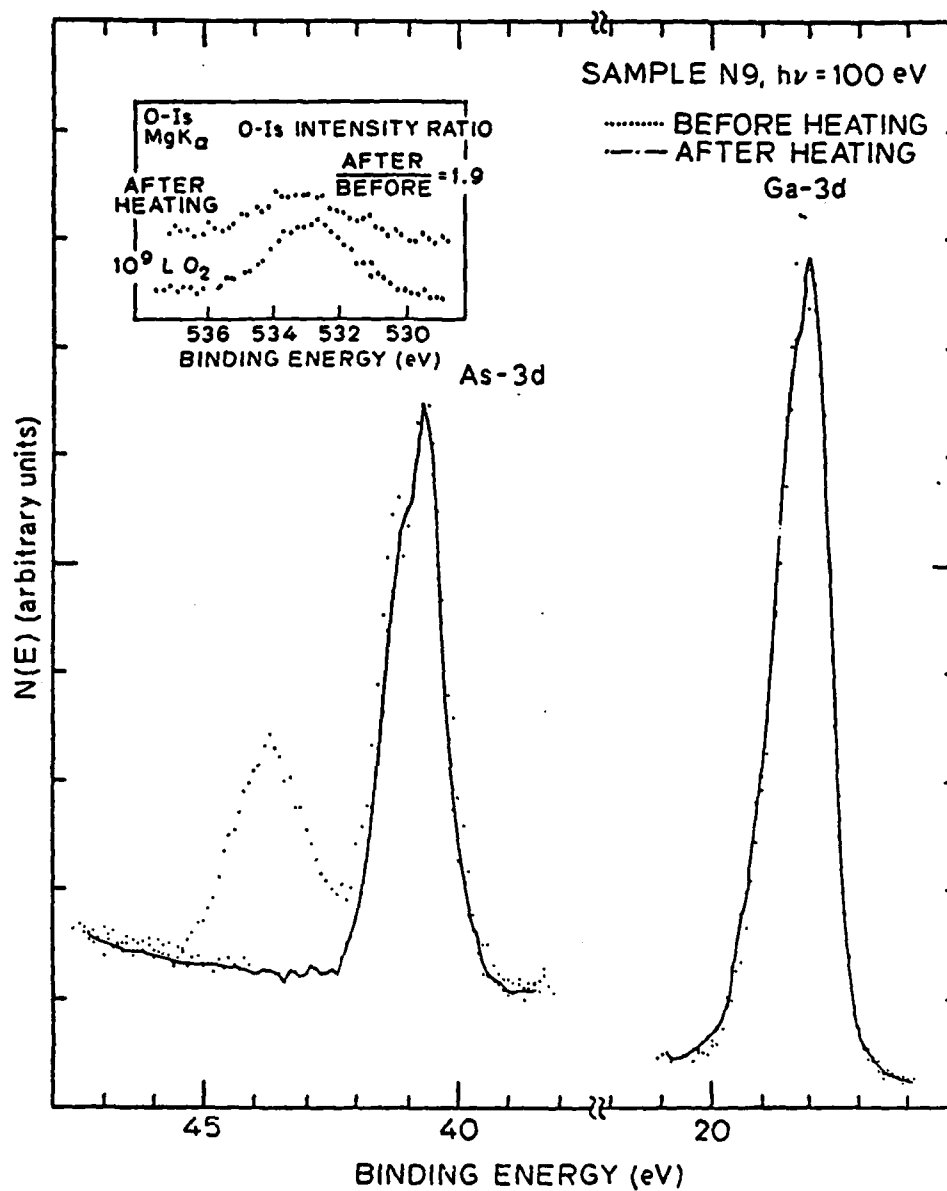


Figure 31: The effect of fast-heating of a room-temperature oxygen-exposed surface to $\sim 430^\circ\text{C}$. In contrast to the effect of annealing at 370°C and at 250°C (figs. 24 and 25), a decrease of about a factor of two is seen in the O-1s intensity (inset) and the shifted As-3d disappeared without appreciable change in either the unshifted As-3d or the Ga-3d.

The result of fig. 31 is not inconsistent with the oxygen bonding model we proposed in section 3.3. In fig. 32, we show on the left the proposed oxygen bonding in a zig-zag chain in the (110) surface. After fast heating to 430°C, the As=O units desorb from the surface as AsO molecules, and oxygen atoms originally bridged over Ga and As now bridge over two neighboring Ga, as displayed on the right of fig. 32. The transformation shown in fig. 32 makes the number of chemically affected Ga atoms unchanged after heating, and hence gives little change in the amount of broadening in Ga-3d after heating. The value of chemical shift in Ga-3d, however, should increase after heating, because each Ga bonds to one oxygen before heating and bonds to two after heating. This increase in the value of chemical shift may be small, because Ga atoms are required to supply more charges to O in Ga-O-As bridges than in Ga-O-Ga bridges. The increased oxygen coordination number and the decreased charge-transfer-per-oxygen-atom compensate each other to give a small net increase in the shift in Ga-3d, which may well escape our detection. Inclusion of valence band spectra in future studies of heating-rate-dependent-effects may give more unambiguous informations.

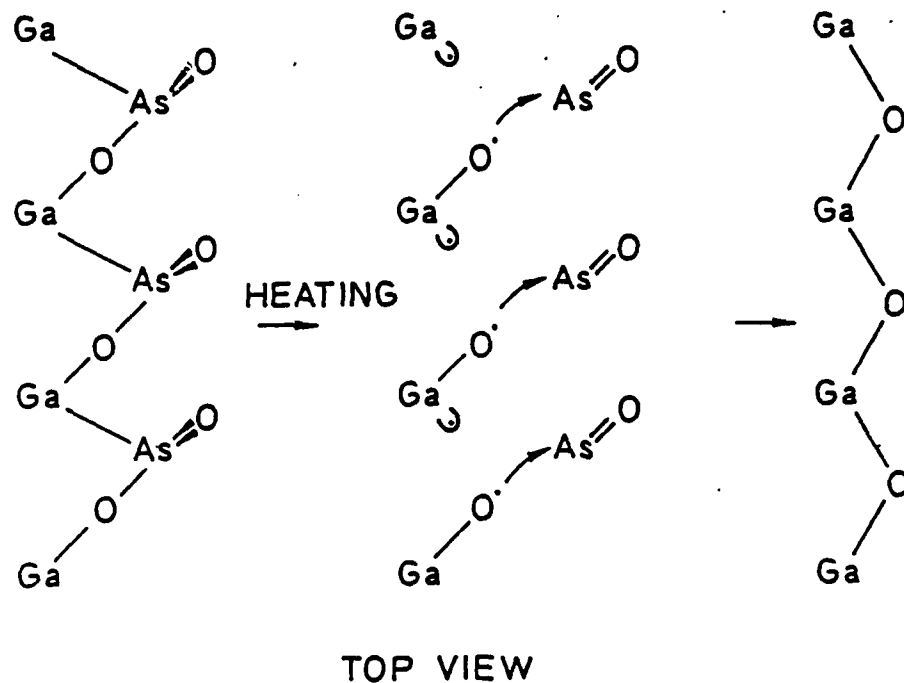


Figure 32: Changes of the proposed O/GaAs(110) bonding under fast heating.

3.6 SUMMARY

In summary, we have made detailed analyses of the DOVS of O/GaAs(110). Through the coverage dependence of the DOVS, two different forms of oxygen have been identified.

Adsorption in the first form saturates at a low coverage (~ 0.01 monolayer), and is suggested to occur at defect sites with As deficiency in the form of Ga-O-Ga. The first form of oxygen desorb at $\sim 150^\circ\text{C}$, which is further support for the proposal that this form is in a bonding configuration closely resembles the highly volatile species Ga_2O .

Adsorption in the second form emerges after the saturation of the first form, and produces well resolved shift in the As-3d ($\Delta E = 3.0$ eV) and broadening in the Ga-3d. The second form contains both nonbridging oxygen ($\text{As}=\text{O}$) and bridging oxygen ($\text{Ga}-\text{O}-\text{As}$) and is suggested to be in a $\text{Ga}-\text{O}-\text{As}=\text{O}$ unit (fig. 15). This suggested model is based on

- i) the detailed interpretation of the DOVS of O/GaAs(110); in particular, the interpretation has been substantiated by the comparison with the experimental DOVS' of As_2O_3 and Ga_2O_3 (section 3.3),
 - ii) the stability of the arsenic-oxygen bonding under thermal annealing, which has been found to be consistent with the known stability of the $\text{As}=\text{O}$ bond (section 5),
 - iii) the constant chemical shift in the As-3d at oxygen coverages below one monolayer, which is consistent with the fixed oxygen coordination of As in this model,
 - iv) the small shift in the Ga-3d at oxygen coverages below one monolayer, which is consistent with the low oxygen coordination number of Ga in this model,
- and

- v) its successful explanation of the dissociation of oxygen molecules without invoking the dissociation at defect sites (section 3.5).

Adsorption of oxygen on sputter-disordered Ga-rich GaAs(110) surfaces has been found to proceed in the same two-stage process as that found on ordered GaAs(110), only the relative concentration of the two forms of oxygen are reversed in the two cases according to the relative concentration of defect sites and normal sites on the two surfaces. This suggests that the adsorption on defect sites and the adsorption on normal sites are independent of each other. The picture that adsorption nucleates at defect sites and propagates through adsorption-induced defect sites may not be appropriate for the room temperature adsorption of oxygen on GaAs(110).

On either ordered or disordered surface, direct formation of Ga_2O_3 is not possible due to the activation barrier to bring Ga atoms together. The possibility of the formation of As_2O_3 by room temperature adsorption of oxygen on GaAs(110) has also been definitively ruled out by the annealing experiments. The picture that room temperature adsorption of oxygen on GaAs(110) produces islands of Ga_2O_3 and As_2O_3 is therefore considered inappropriate.

This work has demonstrated that many critical informations can be obtained from careful examination of the DOVS'. It is therefore hoped that further theoretical calculations will be carried to allow more definitive interpretations of the DOVS'.

REFERENCES

1. E. J. Mele and J. D. Joannopoulos, Phys. Rev. B 19, 6999(1978); Phys. Rev. Lett. 40, 341(1978); J. Vac. Sci. Technol. 15, 1287(1978)
2. P. W. Chye, C. Y. Su, I. Lindau, P. R. Skeath, and W. E. Spicer, J. Vac. Sci. Technol. 16, 1191(1979)
3. C. R. Brundle and D. Seybold, J. Vac. Sci. Technol. 16, 1186(1979)
4. J. J. Barton, W. A. Goddard III, and T. C. McGill, J. Vac. Sci. Technol. 16, 1178(1979)
5. P. Pianetta, I. Lindau, C. M. Garner, and W. E. Spicer, Phys. Rev. B 18, 2792(1978); Phys. Rev. Lett. 35, 780(1975); Phys. Rev. Lett. 37, 1166(1976)
6. A. Kahn, D. Kanani, P. Mark, P. W. Chye, C. Y. Su, I. Lindau, and W. E. Spicer, Surf. Sci. 87, 325(1979)
7. P. Pianetta, I. Lindau, P. E. Gregory, C. M. Garner, and W. E. Spicer, Surf. Sci. 72, 298(1978)
8. R. Ludeke, Solid State Commun. 21, 815(1977)
9. W. Ranke and J. Jacobi, Surf. Sci. 81, 504(1979)
10. S. Doniach, I. Lindau, W. E. Spicer, and H. Winick, J. Vac. Sci. Technol. 12, 1123(1975)
11. D. E. Eastman, T.-C. Chiang, P. Heiman, and F. J. Himpsel, Phys. Rev. Lett. 45, 656(1980)
12. Chapter IV, this dissertation
13. G. Lucovsky and R. S. Bauer, Solid State Commun. 31, 931(1979)
14. W. A. Harrison, the Solid State Table and Chapter 11, Electronic Structure and the Properties of Solids, Freeman, San Francisco, 1980
15. C. D. Thualt, G. M. Guichar, and C. A. Sebenne, Surf. Sci. 80, 273(1979)
16. see, for example, S. P. Singh-Boparai, M. Bowker, and D. A. King, Surf. Sci. 53, 55(1975)

17. P. Mark and W. F. Creighton, Thin Solid Film, 56, 19(1979); P. Mark, S. C. Chang, W. F. Creighton and B. W. Lee, Crit. Rev. Solid State Sci. 5, 189(1975)
18. N. J. Shevchik, J. Tejada, and M. Cardona, Phys. Rev. B 9, 2627(1974)
19. D. Schmeisser and K. Jacobi, Surf. Sci., in press
20. S. A. Flodstrom, C. W. B. Martinsson, R. Z. Bachrach, S. B. M. Hagstrom, and R. S. Bauer, Phys. Rev. Lett. 40, 907(1978) and references cited
21. C. M. Garner, C. Y. Su W. E. Spicer, P. D. Elwood, D. Miller, and J. S. Harris, Appl. Phys. Lett. 34, 934(1979)
22. G. Lucovsky and R. S. Bauer, J. Vac. Sci. Technol. Sept/Oct, 1981, in press
23. O. Kubaschewski, Metallurgical Thermochemistry, 5th edition (Oxford, New York, 1979)
24. Here we use the Knudsen-Hertz equation to calculate the evaporation rate, $R_{ev} = \alpha_v(p^* - p)/(2\pi mkT)^{1/2}$. In this equation α_v , the evaporation coefficient, is the fraction of evaporant flux that makes the transition from condensed to vapor phase; p^* is the vapor pressure of the evaporant; p is the hydrostatic pressure of the return flux. With $\alpha_v = 10^{-7}$, $p^* = 1$ atm at $T = 643^\circ K$, $p^* - p \approx p^*$, we obtain $R_{ev} = 7.5 \times 10^{15}$ molecules/cm²-sec. As stated in the text, 1 monolayer As₂O₃ can be evaporated in 0.1 sec. For the ~0.065 monolayer of chemically affected As atom to survive heating at 370°C for 30 min, as is the case show in fig. 24, α_v has to be smaller than 3×10^{-11} . Such a small evaporation coefficient is not found to our knowledge. [L. I. Maissel and R. Glang, Handbook of Thin Films (McGraw Hill, New York, 1970) Chap. 1] In general, the evaporation coefficient is smaller when polymerization is involved in the vaporization process. For example, the evaporation coefficient of As has been measured to be 8.3×10^{-5} [M. B. Dowell, J. Chem. Phys. 66, 1875(1977)], where 'polymerization' to As₂ and As₄ are required. For As₂O₃ in either the arsenolite or the claudetite form, units of As₄O₆ are clearly distinguishable, hence no polymerization is necessary when vaporized into As₄O₆ molecules. Therefore we have no reason to expect the evaporation coefficient of As₂O₃ to be much lower than 10^{-4}

3.7 APPENDIX A: PHOTOEMISSION STUDIES OF THE ELECTROIC STRUCTURE OF Ga_2O_3

We present here UPS spectra of Ga_2O_3 , which was formed by room temperature oxidation of in situ evaporated Ga thin film.

Experiments were performed in a stainless steel ultra high vacuum chamber with base pressure $\sim 10^{-10}$ torr. Ga metal was deposited on an in situ cleaved GaAs(110) surface. The thickness of the Ga film was about 100 Å, as determined by a quartz crystal thickness monitor. Oxygen exposures were made by leaking in research grade oxygen through a bakable leak valve. Oxygen pressure was monitored by a Redhead cold cathode gauge and a Varian 860 cold cathode gauge. The light source used was synchrotron radiation from the 8° line of the Stanford Synchrotron Radiation Laboratory (SSRL). Photoelectrons were energy analyzed with a double pass cylindrical mirror analyzer. The combined monochromator-analyzer resolution for 30 eV photon energy is 0.3 eV.

Fig. 33 gives an overview of the spectra, displayed vertically with oxygen exposures indicated with each spectrum. The spectrum of clean Ga shows a featureless valence band and spin-orbit splitted Ga-3d levels. With 100 L oxygen exposure, only a weak oxygen induced feature is seen in the valence band region and little change occurred to the Ga-3d levels. With 10^4 L exposure, a chemically shifted Ga-3d appeared and strong oxygen induced features appeared in the valence band region. The adsorption of oxygen appears to have saturated at 10^4 L exposure, because no significant change is seen in the spectra of higher exposures (10^5 L and 10^6 L).

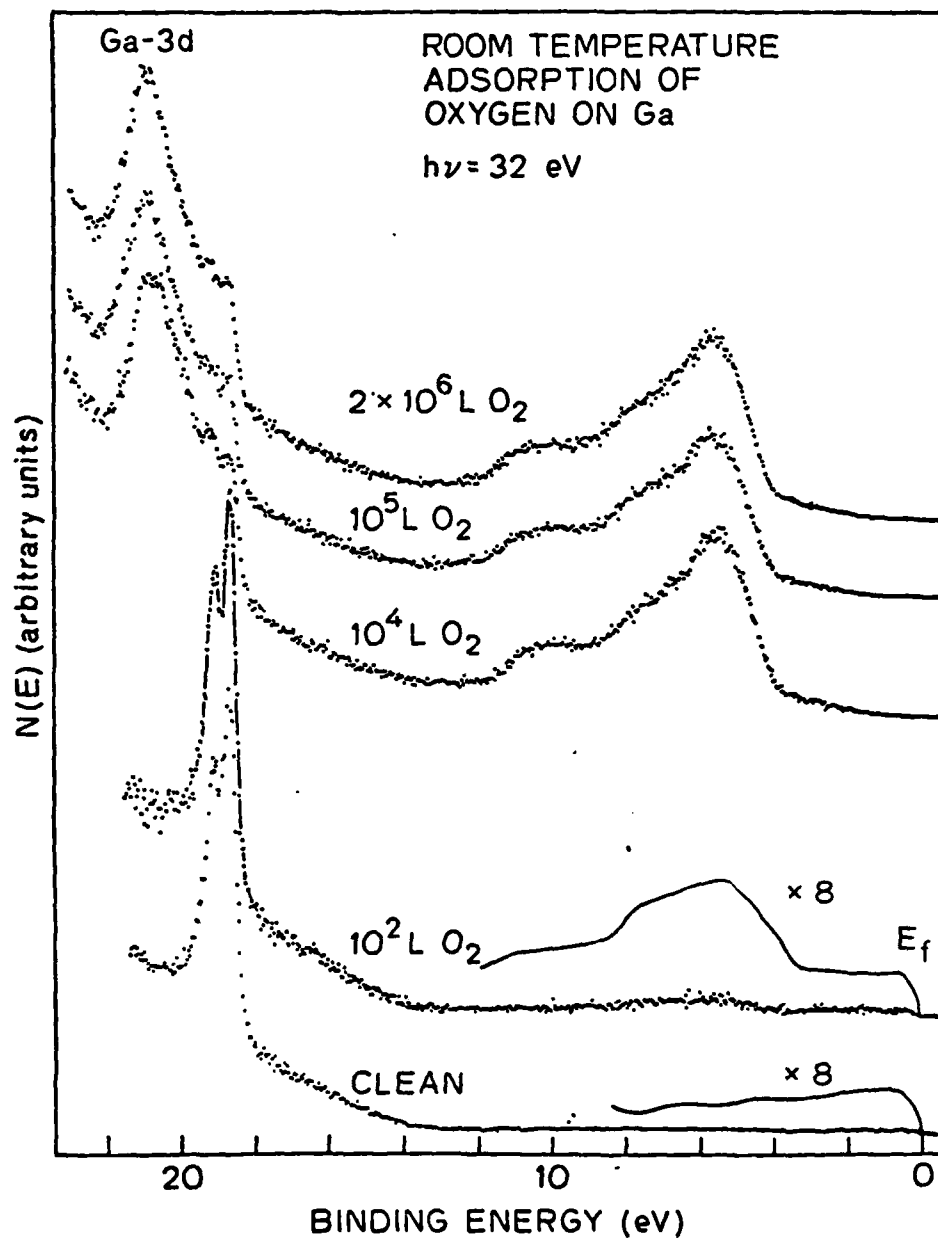


Figure 33: Photoemission spectra of clean and oxygen-exposed Ga taken at $h\nu=32$ eV.

Details of the density of valence states (DOVS) of oxidized Ga are shown in fig. 34. The upper curve is a blow-up of the valence band region of the 2×10^6 L spectrum of fig. 33, with the smooth, featureless secondary electron background indicated. The lower curve shows the DOVS after removing the background. There are three features in the DOVS at 5.6, 7.7, and 10.5 eV below the Fermi level of the underlying Ga, in good agreement with the results obtained by Bachrach at 130 eV photon energy [1]. These features are labeled I, II, III, and IV in fig. 2 in the order of increasing binding energy.

Since the oxidation of Ga was carried out near the melting point of Ga, we can consider it being an equivalent-high-temperature oxidation process, and can expect the direct formation of Ga_2O_3 . With this assumption, the three features in the DOVS of oxidized Ga can be understood by following the tight binding analysis of the electronic structure of Al_2O_3 by Reilly [2]. The α -form (corundum) crystalline Al_2O_3 and Ga_2O_3 are isomorphic. In such a structure [3] each Ga atom is at the center of a distorted octahedron of oxygen atoms, with three oxygen closer to the Ga atom than the other three. Each Ga atom is thus expected to bond strongly with three O's and weakly with three other. Each oxygen atom is surrounded by four Ga's, bonding strongly to two and interacting weakly with the other two. The three oxygen atoms that are strongly bonded to a center Ga can be considered approximately at three corners of a tetrahedron enclosing that Ga. We can thus form sp^3 hybrids on each Ga, with three hybrids participating in bonding to three O's and one hybrid left empty. For an oxygen atom in a Ga-O-Ga bridge-bonding position, only two of the three p-orbitals participate in Ga-O bonding; the third p-orbital which is perpendicular to the plane

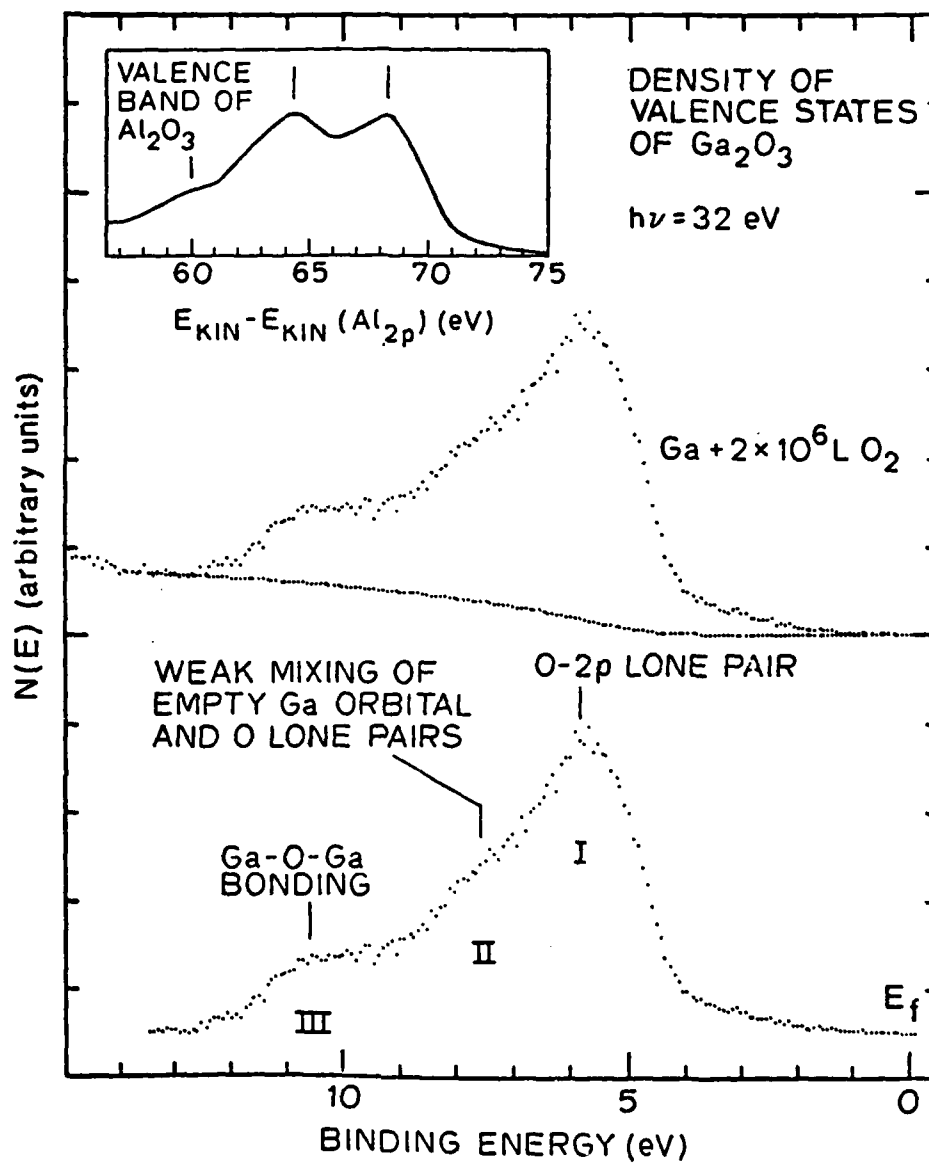


Figure 34: Blow-ups of the valence band region of the $2 \times 10^6 \text{ L}$ spectrum of fig. 33, with the featureless background due to secondary electrons indicated (the center curve). The bottom curve shows the spectrum with the background removed; origins of the features in the spectrum are also indicated. The inset shows the valence band spectrum of Al_2O_3 [5] for comparison.

containing the Ga-O-Ga angle remains non-bonding and forms a doubly-occupied lone pair. The oxygen lone pair interacts with the empty sp^3 orbital on a nearby Ga atom and lowers its energy. Because the oxygen lone pair and the Ga empty orbital point to each other at an angle, the interaction is expected to be weak. In addition, not all oxygen lone pairs can find available Ga empty orbital; only two of the three oxygen atoms in the Ga_2O_3 unit can have such interaction, an oxygen lone pair remains intact on the third oxygen atom. Origins of the three features in the DOVS can now be assigned: feature I, the one with the lowest binding energy, is due to non-bonding oxygen lone pairs, feature II is due to the weak interaction between the oxygen lone pair and the empty Ga orbital, and feature III is due to bonding electrons in the Ga-O-Ga bonding unit.

There is one aspect of the DOVS in discordance with the above simplified picture. In that picture, the ratio of non-bonding:weak-bonding:bonding electrons is expected to be 1:2:6. Such a ratio is certainly not indicated by the DOVS in fig. 34. Part of this deviation can be explained by the matrix elements of the photoionization process. Band I is purely p in character, whereas band II and III have considerable s character, it is thus possible to have band I preferentially enhanced at this photon energy. Another possible explanation is the deviation from the corundum structure. In the β -form of the gallium sesquioxide [4], Ga atoms occupy two sets of crystallographic nonequivalent sites: half of the Ga atoms occupy octahedral sites and the other half occupies tetrahedral sites. Thus the average coordination of Ga atoms in β - Ga_2O_3 are reduced compared to α - Ga_2O_3 . This tends to reduce

the interactions between oxygen lone pair and empty Ga orbital. In fact, detailed structural studies of β -Ga₂O₃ have shown three nonequivalent oxygen atoms in the Ga₂O₃ unit, and careful examination of the different Ga-O bond lengths has led to the conclusion that only one of the three O's has a bond order greater than two. Namely, only one of the three oxygen lone pairs interacts with empty Ga orbitals and lowers its energy. This brings the ratio of non-bonding, weak-bonding, and bonding electrons to 2:1:6. This ratio is closer to that can be deduced from the experimental DOVS in fig. 34. Thermodynamic measurements show the β -Ga₂O₃ to be more stable at room temperature [4]. It is thus likely that β -form-like structure was produced by the room temperature oxidation of Ga. It is also possible that we have obtained disordered oxide layer which contains both β -like and α -like local order. The broad bonding band (band III) in the experimental DOVS also suggests the formation of either β -like or a disordered layer. This is because the bonding band should be splitted into a σ -band and a π -band if only a single value of Ga-O-Ga angle exists, as is the case for α -form Ga₂O₃; there are, however, three different Ga-O-Ga angles in the β -form Ga₂O₃, and a random variation of the Ga-O-Ga angle may occur in noncrystalline Ga₂O₃, which tend to smear the splitting.

In the inset of fig. 34, we show the experimental DOVS of Al₂O₃ for comparison [5]. The spectrum was obtained by Balzarotti and Bianconi [5] using Al-K α radiation. There are also three bands in the DOVS. The energy positions of the bands agree semiquantitatively with the tight binding calculation of Reilly [2]. This gives indirect support to the assignments of the origins of the bands in the DOVS of Ga₂O₃. The fact

that the strength of the weak-bonding band is comparable to that of the non-bonding band is consistent with higher cross-section for the s-electrons at Al-K α radiation. The larger splitting between the non-bonding band and bonding bands in the Al₂O₃ DOVS merely reflects the fact that the cohesive energy of Al₂O₃ is higher than that of Ga₂O₃.

The existence of a weak bonding band in addition to a non-bonding band and a bonding band is a unique feature of the oxides of column III metals. This is a direct manifest of the existence of oxygen atoms with bonding order greater than two. It is possible because

- i) empty orbitals in the right energy range are available on metal atoms; In contrast, in oxides of column V elements such as As₂O₃, this does not happen because no empty orbitals are available from As. The doubly occupied lone pairs on As in fact interact repulsively with oxygen lone pairs in As₂O₃.
- ii) high ionicity of the metal-oxygen bond; Once the electronegativity of oxygen is fulfilled through the charge transfer in metal-oxygen bonds, the tendency of oxygen lone pairs to form donor bonds increases. In other words, the splitting between the non-bonding band and the weak-bonding band should scale with the splitting between the non-bonding band and the strong-bonding band. For example, Al-O bond is more ionic than Ga-O bond, hence the splitting between the non-bonding and the metal-O-metal bonding band is bigger in Al₂O₃ (~8.5 eV) than in Ga₂O₃ (~4.9 eV), and the splitting between the non-bonding band and the O-metal dative bonding is also in the same order (4.2 eV in Al₂O₃, 2.1 eV in Ga₂O₃).

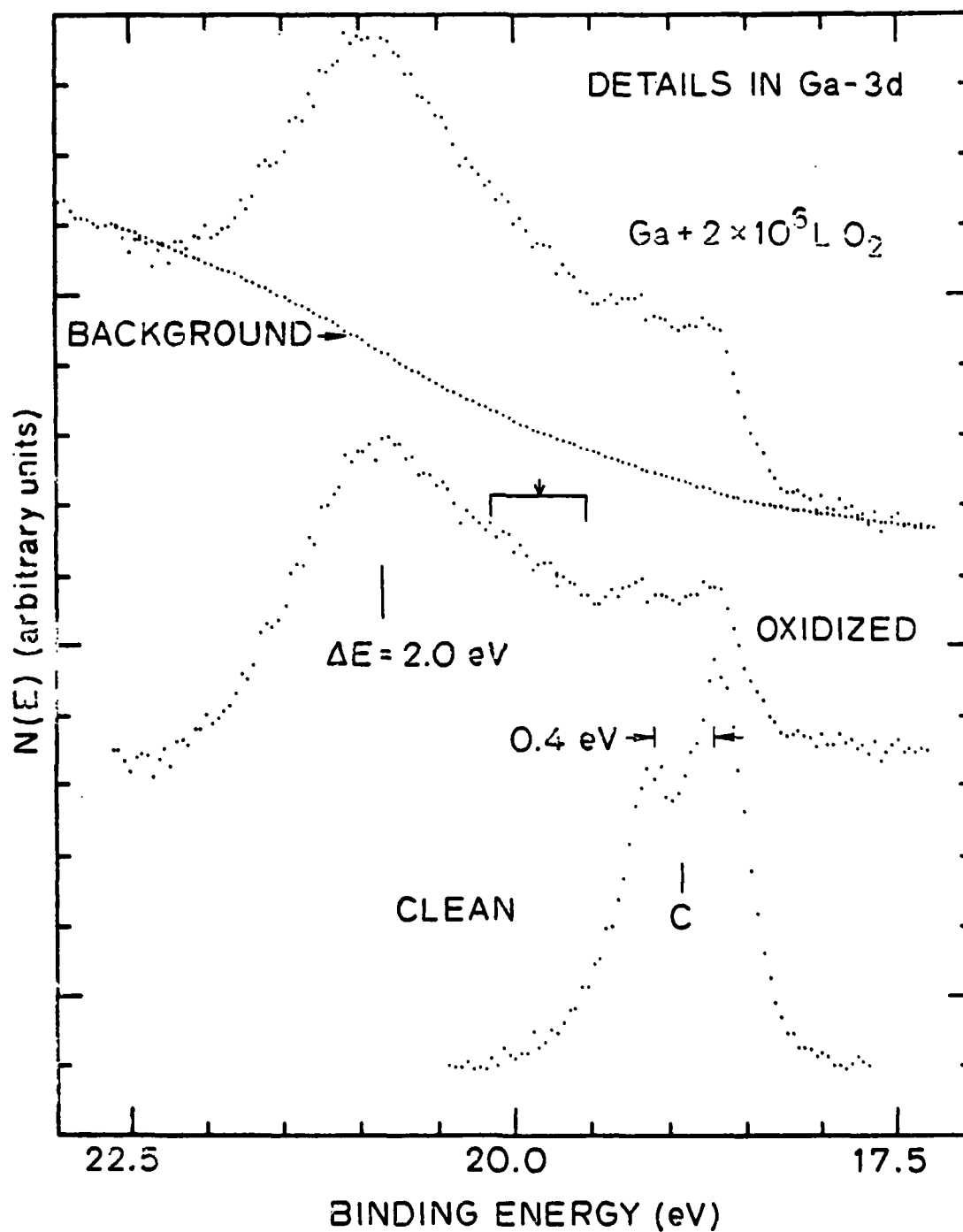


Figure 35: Blow-ups of the Ga-3d level of clean and oxidized Ga. The arrows in the center spectrum point to unresolved chemical shifts in the Ga-3d.

Fig. 35 details the Ga-3d level. The upper curve is a blow-up of the Ga-3d part of the 2×10^6 L spectrum in fig. 33, with the smooth, featureless secondary background indicated. The center curve shows the spectrum with background removed. The lower curve is the Ga-3d spectrum of the clean Ga-3d film, with the secondary background removed. The Ga-3d levels of clean Ga-film show a well-resolved spin-orbit splitting of 0.39 ± 0.08 eV, and the binding energy of the Ga-3d_{5/2} is 18.7 ± 0.15 eV below Fermi level. The spin-orbit splitting is lost in the chemically shifted Ga-3d levels of the oxidized Ga. The separation between the apparent peak position of the chemically shifted Ga-3d and the center of gravity of the Ga-3d of the clean surface is 2.0 ± 0.2 eV, in good agreement with the result of Schon [6]. A more careful examination of the center curve of fig. 35, however, suggests the presence of other intermediate chemical shifts. These smaller shifts probably arise from incompletely oxidized Ga, i.e., Ga atoms bond to less than three oxygen atoms. This can occur when the oxidation process becomes diffusion-limited and a deficiency of oxygen atoms for oxidizing subsurface Ga atoms sets in. A question immediately arises is the influence of these oxygen-deficient bonding complexes on the DOVS which we have just analyzed in terms of complete Ga₂O₃ order. We expect oxygen in these oxygen deficient bonding complexes to assume the same bridge bonding configuration, GA-O-Ga, and hence the approximately same non-bonding-bonding splitting. The weak-bonding or the O-Ga dative bonding band, however, is expected to be missing, due to two possible reasons:

- i) an empty Ga orbital, if exists, cannot find a nearby oxygen lone pair because of the reduced oxygen coordination.
- ii) no empty Ga orbitals are available in the region of intermediately oxidized Ga. In such regions, Ga atoms bonded to oxygen are also bonded to other Ga atoms. Because the Ga-Ga bond is not as directional as the Ga-O bond, the hybridization of the orbitals of Ga atoms may change in such a way to eliminate any empty Ga orbital with the favorable energy position to form donor-like bond with the oxygen lone pairs.

Oxygen adsorption phases with the donor-like bonding band missing in the DOVS have indeed been observed by Schmeisser et. al. [7] on Ga metal surface at low temperature (70°K), and by the present authors on disordered, Ga rich GaAs surfaces at room temperature [8]. The postulate of Schmeisser et. al. [7] that such DOVS is due to chemisorbed molecules appears to be entirely unnecessary. In their case, the low mobility of Ga atoms at low temperature prohibits the formation of Ga_2O_3 , and oxygen lone pair in the surface Ga-O-Ga bonding units point to no Ga empty orbitals so that the donor-like bonding band is suppressed. Returning now to the effect of these oxygen-deficient bonding complexes on the experimental DOVS of fig. 34, we believe that the major effect is to make the donor-like bonding band (band II) less prominent than that expected for the true DOVS of Ga_2O_3 [9], by contributing intensities only to the non-bonding band and the bonding band.

In summary, we have performed high energy resolution photoemission studies of room temperature adsorption of oxygen on Ga metal. At saturation of the adsorption process, both Ga_2O_3 and regions of Ga bonded to less than three oxygen atoms are present. The chemical shift in the Ga-3d level characteristic of Ga_2O_3 has been measured to be 2.0 ± 0.2 eV. Three features in the DOVS at 5.6, 7.7, and 10.5 eV binding energy have been identified as the oxygen non-bonding, the O-Ga donor-like bonding, and the Ga-O-Ga bonding band of Ga_2O_3 .

REFERENCES FOR APPENDIX A

1. R. Z. Bachrach, J. Vac. Sci. Technol. 15, 1340(1978)
2. M. H. Reilly, J. Phys. Chem. Solids 31, 1041(1970)
3. R. W. G. Wyckoff, Crystal Structures, 2nd ed., vol. 2 (Wiley, New York, 1964)
4. S. Geller, J. Chem. Phys. 33, 676 (1961)
5. A. Balzarotti and A. Bianconi, Phys. Stat. Sol. 76, 689(1976)
6. G. Schon, J. Electron Spectr. Related Phenom. 2, 75(1973)
7. D. Schmeisser, K. Jacobi, and D. M. Kolb, Proc. ECOSS 3, Cannes 1980
8. see section 4 of the text
9. In one case (reference 7) where we have obtained the spectrum of a thicker Ga_2O_3 film by heavy plasma oxidation of GaAs, the dative-bonding band indeed appeared to be more pronounced than that is shown in fig. 34. The experimental DOVS in that case, however, was taken at 100 eV photon energy, so it is not clear if direct comparison can be made with the present results.

3.8 APPENDIX B: PHOTOEMISSION STUDIES OF ROOM TEMPERATURE OXIDATION OF AS

3.8.1 Introduction

Two arsenic chalcogenides, As_2S_3 and As_2Se_3 , are known to form stable semiconducting glasses of considerable technological significance as infrared transmitting window materials and as visible-sensitive large photoconductors. Because of this, the optical properties and transport properties of these glasses, including their crystalline counterparts,

have been well studied; efforts to describe the underlying electronic structure with theoretical calculations and photoelectron spectroscopic measurements of the density of valence states (DOVS) have also emerged [2-7]. Similar studies have also been extended to include As_2O_3 [5-7]. There are a few reasons to study As_2O_3 . As_2O_3 forms layer-lattice compound (claudetite) similar to As_2S_3 and As_2Se_3 . However, the intralayer bonding in As_2S_3 and As_2Se_3 is highly covalent, whereas that in As_2O_3 is more ionic. Another property makes arsenic oxide unique among arsenic calcogenides is that molecular compound can be formed with the composition As_2O_3 (arsenolite), whereas molecular compounds with S or Se are formed only with As rich compositions (As_4S_3 , As_4S_4 , etc.). Measurements of the DOVS of As_2O_3 is also of interest for the extensively investigated problem of oxygen adsorption on GaAs surfaces [8].

Previous photoemission measurements of DOVS of As_2O_3 have been performed on vacuum deposited As_2O_3 film [5-7]. We report here results obtained from exposing clean As film, prepared in ultra high vacuum, to controlled amount of oxygen.

3.8.2 Experimental

The As film was obtained by flashing As from a GaAs crystal onto an in situ cleaved Si(111) surface in an ultra-high-vacuum preparation chamber connected to the measurement chamber. The GaAs crystal was contained in a quartz crucible held by the heater filament. The crucible and the heater was surrounded by a ~4 inch long stainless steel collimating shield. The open end of the crucible was not in line with the direction of the collimating shield such that the ratio of As flux to Ga

flux at the exit of the shield can be maximized. The GaAs crystal was well outgassed before deposition, and mass spectral analyses were carried out to determine the heater current that delivers negligible amount of Ga. The Si-2p emission from the Si substrate was measured before deposition by a Mg-K α mounted in the measurement chamber. This emission was completely attenuated after deposition, hence the thickness of the As film should be at least 100 Å. No oxygen contamination was found by checking the O-1s signal. Some Ga incorporation, however, had occurred. The Ga-3d signal was detectable only in the spectrum taken with 30 eV photon (fig. 36 below); in the Mg-K α spectrum, the Ga-3d intensity was below the noise level. Assuming approximately equal photoionization cross section for the As valence band and the GaAs valence band, the amount of Ga was estimated to be at most 1% of a monolayer.

Oxygen exposures were made in the measurement chamber (base pressure $\sim 7 \times 10^{-11}$ torr) by leaking research grade oxygen through a bakable leak valve. Oxygen pressure was monitored by a cold cathode gauge. A hot filament ion gauge operating at 0.4 mA emission current was also present during one exposure in hope to speed up the oxygen uptake.

Photoelectrons were energy analyzed with a double pass cylindrical mirror analyzer (CMA) operated in the pre-retarding mode. Light sources used were synchrotron radiation from the 8 $^{\circ}$ line of the Stanford Synchrotron Radiation Laboratory (SSRL). The combined monochromator-analyzer resolution was 0.25 eV for 21 eV spectra and 0.3 eV for 30 eV spectra.

3.8.3 Results and Discussion

Clean As

Before discussing the DOVS of oxidized As, we briefly examine the spectra of clean As.

In fig. 36 we show the valence spectra taken with 21 eV and 30 eV photons. The leading edge of the DOVS of As extends up to the Fermi level. The density of states near Fermi level is quite low, as can be seen by comparing with the spectrum of the substrate Si (the second from top curve, fig. 36), upon which the As was deposited, and by comparing with the Fermi edge of the spectrum of an in situ evaporated Ag film (the top curve, fig. 36). The peaked feature superposed on the leading edge of the Si spectrum, indicated by an arrow in fig. 36, is due to the now well known surface states of the Si(111) surface [9]. The coincidence of the valence band maximum (VBM) and the Fermi level and the low density of states near Fermi level are characteristics expected for semimetals. The contrast provided by the surface states of Si also clearly suggests that no 'extra' states near or above the VBM have to be considered for As, even though the As film studied here are likely to be amorphous. (The conditions for preparing this film is similar to that used by Ley et. al. [10] to prepare amorphous As.)

Other features in the DOVS of As are the two peaks in the 0-6 eV binding energy region, which are primarily bonding p electrons in character. Features expected for the s electrons of As are barely seen in the secondary electron background of the 30 eV spectrum. In fig. 37 we have fitted the 21 eV and the 30 eV spectrum with smooth, featureless

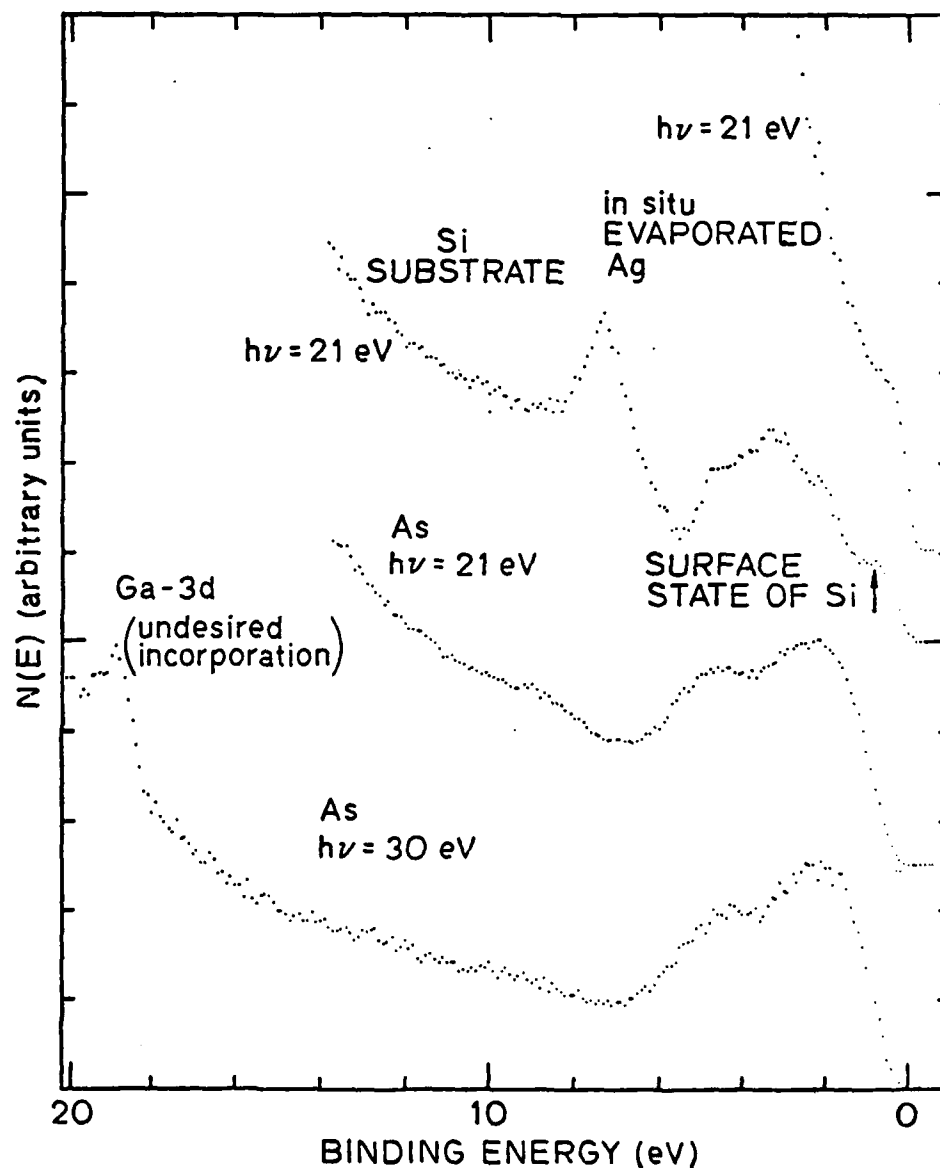


Figure 36: Photoemission spectra of clean As taken at $h\nu=30$ eV and $h\nu=21$ eV. The spectrum of the Si substrate taken at $h\nu=21$ eV prior to the deposition of As is also shown for comparison (the second from top curve); we notice particularly the feature indicated by an arrow which is attributed to the surface states of Si(111). The top curve is the Fermi edge in the spectrum of an in situ evaporated Ag film.

backgrounds. The corrected spectra can be compared to the XPS spectra of crystalline and amorphous As (the inset) obtained by Bishop and Schevichik [2]. Good agreement can be found in the p-band: the binding energy of the first peak in the p-band is 2.3 ± 0.2 eV, and the splitting in the p-band is 2.2 ± 0.2 eV. The s-band cannot be truthfully uncovered from the 21 eV spectrum, because part of the band is close to the work function cutoff. The 30 eV spectrum fully covers the s-band; however, the intensity of the s-band is drastically suppressed compared to that in the XPS spectra, due to a matrix element effect. The major change in going from crystalline to amorphous As in XPS spectra, as shown in the inset, is the flattening of the splitted s-band. Owing to the low intensity of the s-band in the 30 eV spectrum, no clear assessment of the splitting of the s-band can be made. Nevertheless, we have indicated above the region of the s-band in the 30 eV spectrum the 3.5 eV splitting deduced from the XPS spectrum of crystalline As. It appears that two features with the right splitting are discernable. It can therefore at least be said that the case of replacement of the doublet with a single peak in amorphous As, as stated by Ley et. al. [10], is not observed here.

Oxidized As

An overview of the DOVS of As subjected to two oxygen exposures, taken with 30 eV synchrotron radiation, is shown in fig. 38. The changes in the As-3d level, measured with Mg-K α source, with oxygen exposures are also shown in the inset of fig. 38. There is no measurable oxygen uptake after exposing to 10^5 L molecule oxygen (i.e., an exposure made without the presence of a hot filament ion gauge or any other source of excitation of the oxygen molecules), as evidenced by the lack of change

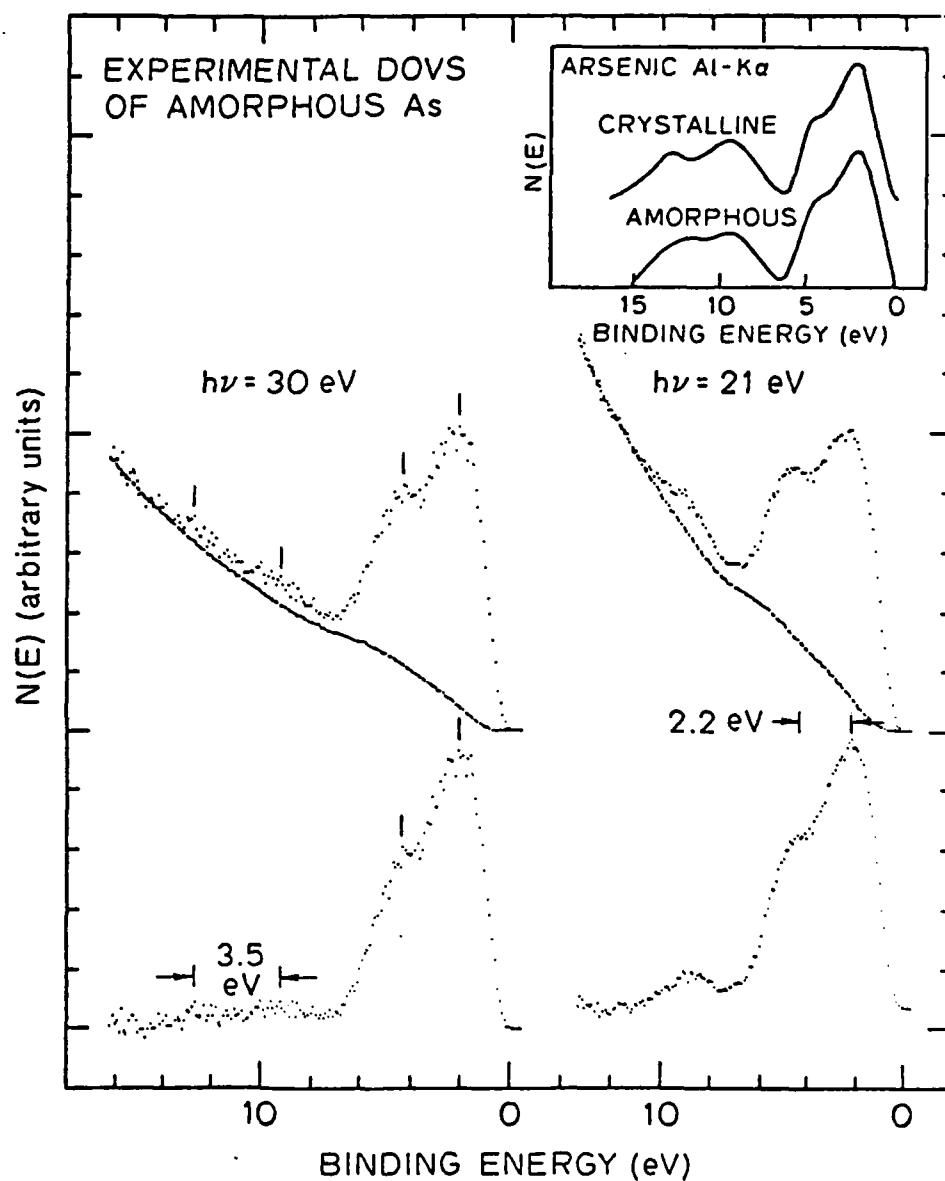


Figure 37: Photoemission spectra of clean As with the backgrounds due to the secondary electrons being removed. When compared to the XPS spectra (the inset) of Bishop and Schevichik [2], the s-band in the 30 eV and the 21 eV spectra appear to be drastically suppressed.

in either the valence band or the As-3d level. Further exposure to 10^7 L oxygen with the presence of a hot filament ion gauge (emission current = 0.4 mA) produced a 3.4 ± 0.2 eV chemical shift in the As-3d level and drastic changes in the valence band region characteristic of oxidized surfaces. Assuming an escape depth of ~ 30 Å for photoelectrons excited from the As-3d level, the strength of the shifted peak indicates an oxide coverage only ~ 0.8 monolayer. The valence band spectra, which are more surface sensitive, however, are dominated by oxygen induced features.

The 3.4 eV shift in the As-3d level is close to the usually quoted binding energy difference between elemental As and As_2O_3 , although ambiguity still exists in the literature on how such value should be obtained. We mention only the result of Holm and Storp [11], who have measured the As level due to elemental As and that due to As_2O_3 simultaneously on one sample, and found the separation between the two levels to be 3.5 eV. The agreement with the present result is satisfactory.

A more definite signature of the formation of As_2O_3 is found in the DOVS. In the center panels of fig. 39, we present the 21 eV and the 30 eV spectrum of oxidized As, with smooth backgrounds of secondary electrons removed. In the lower panel of fig. 39, we have reproduced the He-I spectrum of gas phase As_4O_6 obtained by Canning and Whitfield [12]. The As_4O_6 molecules was produced by vacuum sublimation of powdered As_2O_3 at 190°C . A comparison of the lower panel and the second lower panel suggests that the spectrum of the oxidized As fits as an envelope over the fine structures of the spectrum of gas phase As_4O_6 , or that homoge-

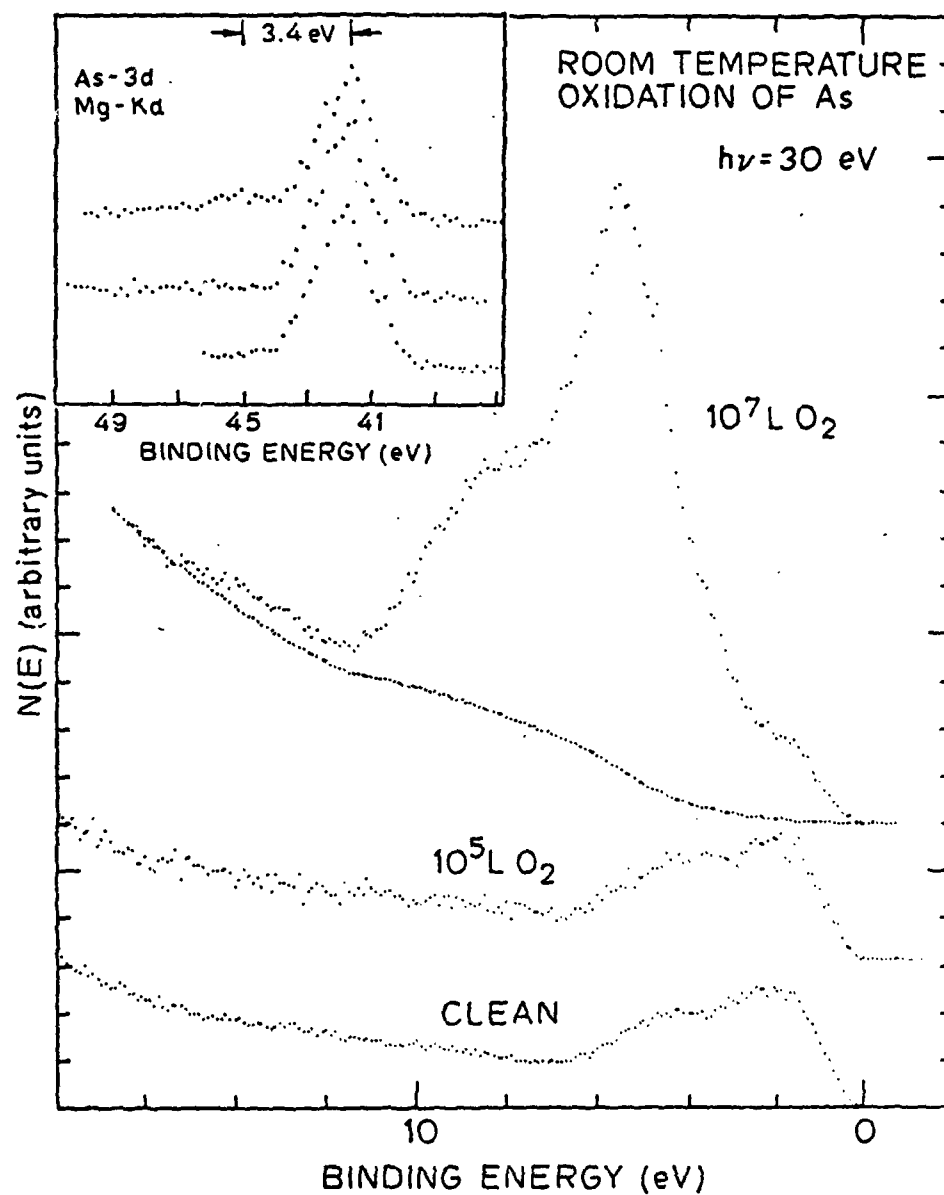


Figure 38: Photoemission spectra of clean and oxygen-exposed As taken at $h\nu = 30 \text{ eV}$. The 10^7 L exposure was made with excited oxygen (see text). The inset gives the As-3d levels of clean and oxygen-exposed As, obtained with Mg-K α excitation.

neous broadening of all fine structures in the spectrum of gas phase As_4O_6 leads to the spectrum of oxidized As. Part of the broadening is instrumental. The energy resolution in the gas phase spectrum is not constant through the spectrum and ranges from 30 meV to 60 meV, whereas the energy resolutions used in this work is constant through the whole spectrum and is 250 meV for the 21 eV spectrum and 300 meV for the 30 eV spectrum. Part of the broadening has to come from solid state effects, if there is a true correspondence between the solid spectrum and the gas phase spectrum, because there are features in the gas phase spectrum separated by more than 1 eV and yet are not resolved in the spectrum of oxidized As. This point will later be further elucidated by comparing with spectra of crystalline As_2O_3 films.

The correspondence between the gas phase spectrum and the spectrum of oxidized As can be put on an absolute energy scale. The gas phase spectrum is presented in fig. 39 by aligning the most prominent non-bonding oxygen peak with the peak at 5.4 eV binding energy (referenced to the Fermi level of the underlying As) in the spectrum of oxidized As. The ionization energy of that peak is 11.52 eV (table 1 of reference 12). The work function of As is about 5.1 eV [13]. Hence peak N in the spectrum of oxidized As has a binding energy of 10.5 eV referenced to the vacuum level. This binding energy is ~1 eV lower than the ionization energy of the corresponding peak in the gas phase spectrum, which can be easily accounted for by the additional extra-atomic relaxation energy in solids.

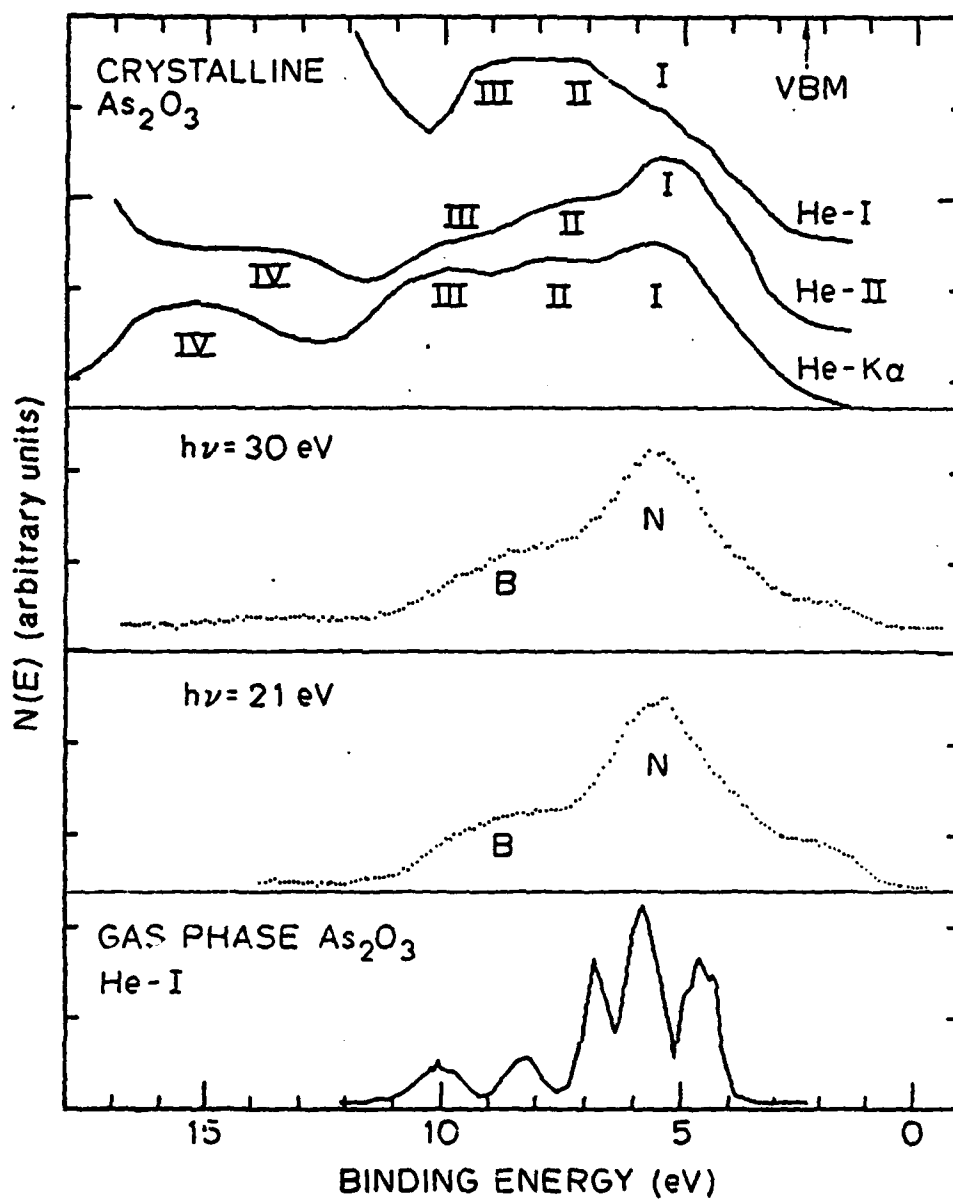


Figure 39: Comparison of spectra of oxidized As film to the spectra of gas phase As_2O_3 and crystalline As_2O_3

The structural order of the oxide layer can be examined by comparing with the spectra of crystalline As_2O_3 . The He-I, He-II, and Al-K α spectra of crystalline As_2O_3 obtained by Wimmer et al. [5-7] are reproduced in the top panel of fig. 39. In the work of Wimmer et al., the As_2O_3 film was prepared by high vacuum (10^{-8} torr) in situ evaporation of powdered As_2O_3 onto stainless steel substrate, and the film was checked by RHEED to be crystalline. There are more features in the crystalline spectra than in the spectra of oxidized As; they are labeled I, II, III, and IV from low binding energy to high binding energy in fig. 39. The binding energies given by Wimmer et al. were referred to the VBM of the As_2O_3 film. Here we have presented these spectra with feature II lined up with peak N in the spectra of oxidized As. This corresponds to a VBM-Fermi level separation of ~ 2.3 eV in the case of oxidized As. This separation is roughly confirmed by extrapolating the low binding edge of peak N in the second-lower panel. After such alignment, good overall correspondence can be seen between the crystalline spectra and the monolayer-oxide spectra. A few differences in details are explained below. In the He-I spectrum of the crystalline form, feature I has an apparent height above feature II due to the steeply rising background. The prominent feature IV in the He-II and the Al-K α spectrum of the crystalline form originate mainly from the 4s level of As. This feature is again suppressed in the 21 and 30 eV spectra of the monolayer-oxide because of matrix element effect. One last difference between the spectra of the crystalline form and the monolayer-oxide, however, can be explained only in terms of differences in structural orders. In the 7-11 eV binding energy region, the crystalline spectra show two resolved features, II

and III, in good correspondence to the gas phase spectrum, whereas the monolayer-oxide spectra show only one broad feature (band B). This difference cannot be explained by different energy resolutions used, because the energy resolution used to obtain the Al-K α spectrum was far poorer (21.2 eV [5]) than the resolutions used in this work. The splitting in the 7-11 eV binding energy region in the gas phase spectrum and the crystalline spectra arises from As-O bonding orbitals with opposite symmetries with respect to the plane bisecting the As-O-As angle (i.e., the splitting between the σ and the π component of the As-O-As bonding). A random variation and/or a distortion of the As-O-As angles tend to flatten out the splitting. This suggests that room temperature adsorption of oxygen on As results in disordered oxide layer.

It is not clear if the structural arrangement of the disordered monolayer oxide is similar to that of vitreous As₂O₃. There is little direct structural information available for vitreous As₂O₃. Lucovsky and Galeener [14], through detailed interpretation of both Raman spectra and ir reflectance, have proposed that v-As₂O₃ contains local regions characterized by either a layer-like local order or an As₄O₆-like local order. Since the standard free energies of reaction for forming arsenolite ($\Delta G = -137.6$ Kcal/mole) and claudetite ($\Delta G = -135.9$ Kcal/mole) at room temperature are close, the picture described by Lucovsky and Galeener [14] is likely to be also applicable to the monolayer oxide resulted from room temperature oxidation of As. If this is indeed the case, the similarities observed between all spectra in fig. 39 then suggests that the influence of the difference between layer-like and As₄O₆-like order on electronic structures is not important. The essential feature of the

electronic structure of As_2O_3 consists of a non-bonding band and a bonding band, whose centers of gravity are separated by ~ 3.3 eV. This essential feature is largely determined by the $\text{AsO}_{3/2}$ pyramids, which are the building units in either layer-like or As_4O_6 structural arrangement.

Another point of interest in studying the electronic structure of A_2B_3 compounds is that whether the non-bonding band is purely B-atom derived [1,3]. For powdered crystalline arsenolite, Wimmer et. al. [5-7] have shown by soft x-ray emission spectra that As lone pair has significant contribution to the non-bonding band. Question can be asked if in different long range structural arrangements (i.e., different ways of connecting $\text{AsO}_{3/2}$ pyramids) the relative contribution from As and O lone pairs to the non-bonding band would change. Two extreme pictures can be considered: In one As participates in bonding with three oxygen atoms in p^3 configuration so that all p-like electrons from As are in the bonding band and the lone pair on As has an s^2 configuration [3]. In the other, As assumes sp^3 bonding configuration, and the bonding to three oxygen leaves one sp^3 lone pair [1]. The two pictures predict different non-bonding to bonding p-electrons ratio. Such ratio of p-electrons should be rather uniquely reflected in our spectra of the monolayer As_2O_3 , because s-electrons are preferentially suppressed due to a weak matrix element for the photoionization transition. The formal picture predicts a non-bonding to bonding p-electron ratio of 3:6, while the latter predicts 4.5:4.5. The spectra of the oxidized As shown in the center two panels of fig. 39 are suggestive of the latter picture, (i.e., s-p hybridization to some extent is important even for a disordered layer of As_2O_3 ,) although no quantitative assesment of the ration of the

strengths of the bonding and nonbonding bands can be extracted from the spectra. This result should be contrasted to the case of amorphous As_2S_3 , where soft x-ray emission experiments do not show significant contribution from the S lone pair to the non-bonding band. This difference can be explained by the higher ionicity of the As-O bond: The repulsion between the ionic charges on oxygen atoms prevents the O-As-O angle in any $\text{AsO}_{3/2}$ pyramid from closing to 90° , and hence prohibits the p^3 configuration.

3.8.4 Summary

In summary, we have shown that room temperature adsorption of oxygen on amorphous As results in direct oxide formation. The electronic structure of oxidized As has been shown to be similar to either that of isolated As_4O_6 molecules, or that of crystalline As_2O_3 . The photoemission spectra of the oxidized As film also suggest that As_2O_3 formed in such a way is noncrystalline. The essential features of the electronic structure of As_2O_3 are a non-bonding band and a bonding band separated by ~ 3.3 eV. The contribution of As lone pairs to the non-bonding band was found to be important in the case of disordered monolayer As_2O_3 .

REFERENCES FOR APPENDIX B

1. R. Zallen and D. F. Blossey, The Optical and Electrical Properties of Compounds with Layered Structures, ed. P. A. Lee (Reidel, Netherlands, 1975)
2. S. G. Bishop and N. J. Shevchik, Phys. Rev. B 12, 1567(1975)
3. N. J. Schevchik and S. G. Bishop, Solid State Comm. 17, 269(1975)
4. W. R. Salaneck and R. Zallen, Solid State Commun. 20, 793(1976)
5. E. Wimmer, P. Weinberger, A. Kosakov, and G. Leonhardt, Phys. Stat. Sol (b) 89, 619(1978) and references cited
6. A. Kosakov, H. Neumann, and G. Leonhardt, Phys. Lett. 62A, 95(1977)
7. G. Leonhardt, H. Neumann, A. Kosakov, T. Gotze, and M. Petke, Physica Scripta 16, 448(1977)
8. C. Y. Su, I. Lindau, P. W. Chye, P. R. Skeath, and W. E. Spicer, J. Vac. Sci. Technol. 17, (1980) and references cited
9. L. F. Wagner and W. E. Spicer, Phys. Rev. Lett. 28, 1381(1972)
10. L. Ley, R. A. Pollak, S. P. Kowalczyk, R. McFeely, and D. A. Shirley, Phys. Rev. B 8, 641(1973)
11. L. D. Hulett and T. A. Carlson, Appl. Spectroscopy, 25, 33(1971); W. J. Stec, W. E. Morgan, R. G. Albridge, J. R. van Walzer, Inorg. Chem. 11, 219(1972); R. Holm and S. Storp, Appl. Phys. 9, 217(1976); C. D. Wagner and Biloen, Surf. Sci. 35, 82(1973)
12. P. H. Cannington and H. J. Whitfield, J. Electr. Spectr. Related Phenom. 10, 35(1977)
13. V. S. Formenko, Handbook of Thermionic Properties, ed. G. V. Samsonov (Plenum, New York, 1966)
14. G. Lukovsky and F. L. Galeener, J. Non-cryst. Solids 37, 53(1980)

3.9 APPENDIX C: FERMI LEVEL MOVEMENT AND ELECTRON AFFINITY CHANGE

In this section we summarize the results of the movement of surface Fermi level with oxygen adsorption obtained on many samples we have studied. Changes in the electron affinity induced by the adsorption of oxygen, which can be measured on p-type samples only, will also be examined.

In figure 40, the energy positions of the surface Fermi level in the band gap is displaced vertically; The lower horizontal scale in fig. 40 indicates oxygen exposures in L, and the upper horizontal scale indicates estimated oxygen coverages (based on table 1, section 3.1). Results obtained from different samples are divided into a few groups, either because different oxygen exposure conditions were used or because different methods of determining the Fermi level position were adopted. Surface Fermi level positions in the top three panels were obtained from valence band spectra using a technique mentioned in section 3.2 and previously described in detail [26]. Those in the bottom panel were obtained from core level spectra, based on the energy position of unshifted As-3d relative to the Fermi level. The 10^{13} L data point on sample N5 (the bottom panel) was obtained without checking the Fermi level position of a freshly evaporated Au film. A big error bar covering the uncertainty due to typical variation in the analyzer work function after heavy gas exposures is therefore attached to this point. Sample N11 and sample P4 (top panel) were exposed to oxygen simultaneously. Data on these two samples thus give a most reliable comparison of the Fermi level movement on n- and p-type samples. The 10^9 L and the 10^{10} L exposures made on samples N1 and P1 (the second from top panel) were excited by a 300 V voltage source.

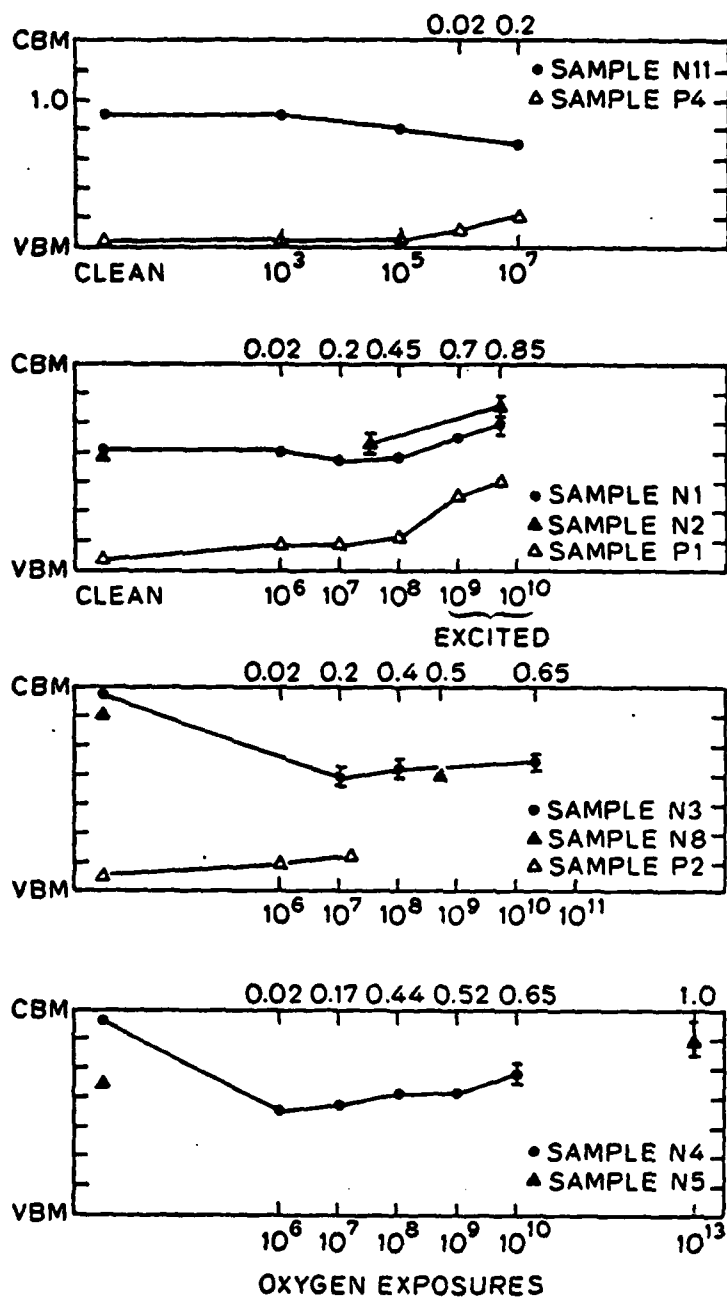


Figure 40: Summary of the changes of the surface Fermi level position with oxygen exposures on samples studied. The lower scale of each panel indicates the oxygen exposures in L, and the upper scale indicates the estimated oxygen coverages in monolayer.

It is seen in fig. 40 that the surface Fermi level positions are less sensitive to oxygen exposures for p-type samples than for n-type samples. The Fermi level positions of n-type and p-type samples are well separated at all oxygen coverages studied. For n-type samples the lowest energy position of the surface Fermi level in the band gap is 0.7 eV above VBM. For p-type samples the highest energy position of the surface Fermi level in the band gap is 0.55 eV above VBM.

Annealing of room-temperature oxygen-covered surfaces to elevated temperatures also causes changes in the surface Fermi level positions. The results obtained on samples N8, N9, N10, and P2 are shown in fig. 41. The surface Fermi level of all n-type samples tend to move deeper into the band gap after annealing. Annealing experiment on p-type sample has so far been carried out only on a low coverage surface, where the Fermi level stays close to the VBM (~ 0.2 eV above VBM). Such annealing leaves the Fermi level of the p-type sample unchanged.

Changes in electron affinity induced by the adsorption of oxygen are shown in fig. 42. In panel (a), details near the low kinetic energy cutoff of the 21 eV spectra of a p-type sample subjected to various oxygen exposures are shown. The low kinetic energy cutoff of every spectrum shown in fig 42 contains a sharply dropping edge and small shoulder extending to the low kinetic energy side of the sharply dropping edge. The small shoulder is due to the secondary electrons generated on the first retarding grid of the analyzer. The energy position of the sharply-dropping edge is determined by the sample work function. On n-type samples the small shoulder is not observed and the observed sharply-

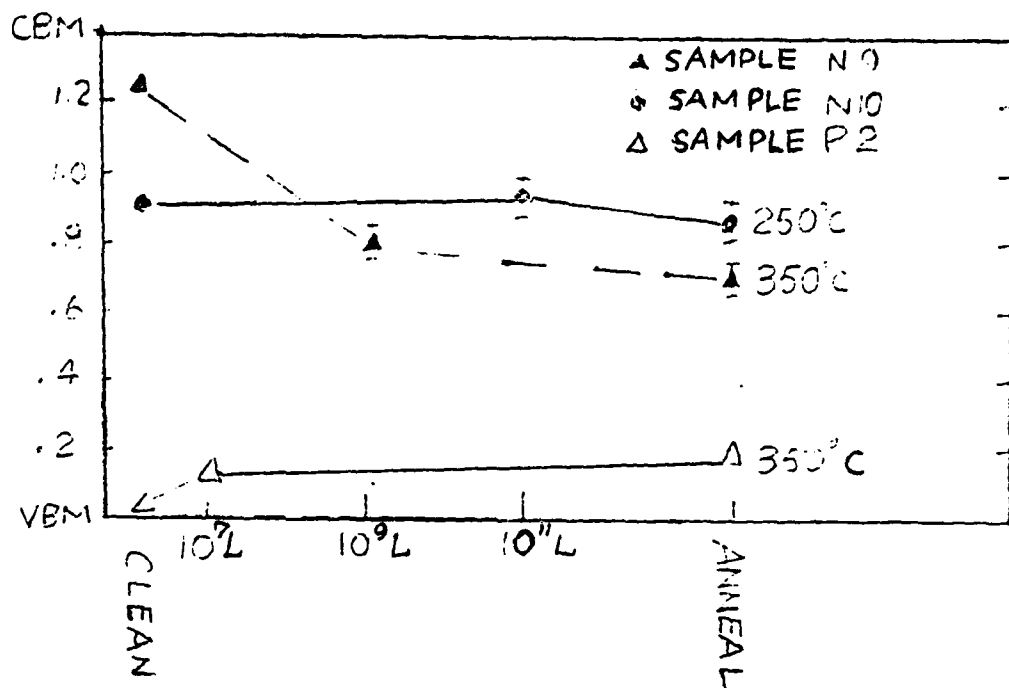


Figure 41: Changes of the surface Fermi level positions after annealing of oxygen-exposed surfaces to elevated temperatures.

dropping edge is determined by the analyzer work function, hence no electron affinity change can be measured for n-type samples in our experimental setup where no voltage bias was applied between the sample and the analyzer. The spectra shown in fig. 42 were also shifted to have the VBM's aligned. Changes in the electron affinity are thus directly reflected in the shifts of the sharply-dropping edges. The results are summarized in panel (b). The electron affinity is seen to first decrease and then increase with increasing oxygen exposures. The two highest

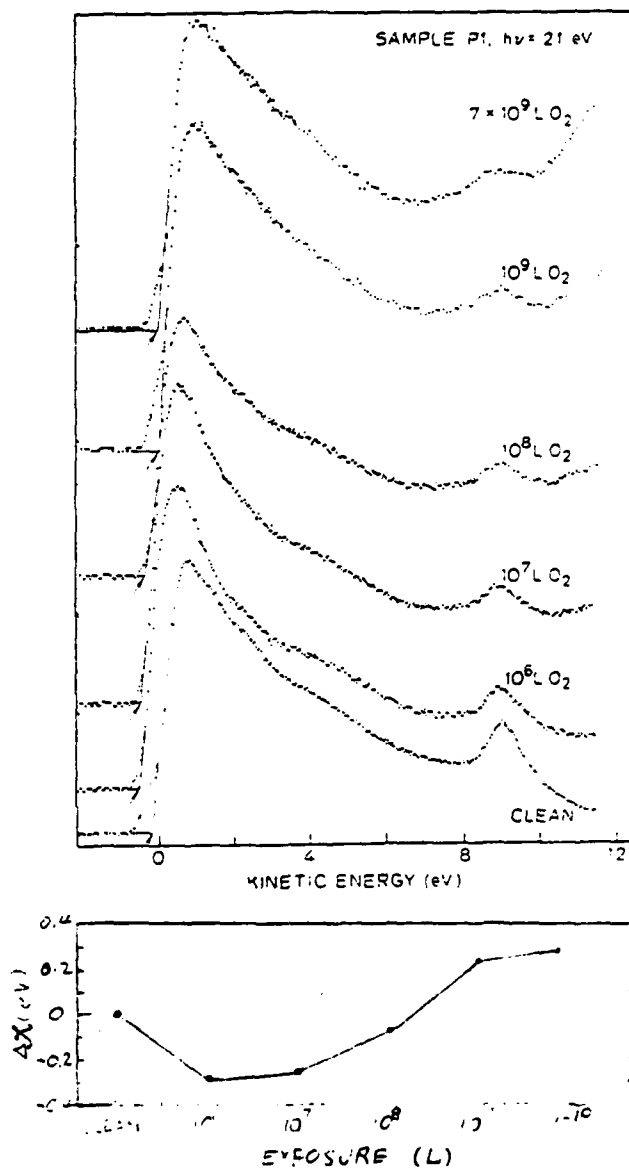


Figure 42: Details in the low kinetic energy cutoff of the 21 eV spectra of clean and oxygen-exposed p-GaAs(110) (a). The arrows point to the extrapolated low energy cutoffs which are used to determine the electron affinity change. (b) Changes in the electron affinity of two p-GaAs(110) surfaces at various oxygen exposures.

exposures, 10^9L and $7 \times 10^9\text{L}$, were made with excited oxygen. The oxygen bonding configuration at these two points may therefore be different from that of other points. The increase in electron affinity produced by exposures to excited oxygen is consistent with the findings of Monch and Enninghorst on n-type samples [1]. Monch and Enninghorst have explained the increase in electron affinity as due to charge transfer from GaAs to oxygen. No explanation, however, can be given to the decrease in electron affinity at low oxygen exposures observed here.

REFERENCES FOR APPENDIX C

1. W. Monch and R. Enninghorst, J. Vac. Sci. Technol. 17, 942(1980)

3.10 APPENDIX D: CALCULATION OF THE N-B SPLITTINGS

In this Appendix we give some details of the simple LCAO calculations which were used to obtain the N-B splittings of section 3.3.

The values of atomic levels used are $E(\text{As-4s}) = -17.33$ eV, $E(\text{As-4p}) = -7.91$ eV, $E(\text{Ga-4s}) = -11.37$ eV, $E(\text{Ga-4p}) = -4.90$ eV, $E(\text{O-2p}) = -14.13$ eV. The values of matrix elements used are $V_{sp} = 14.02/d^2$ eV for that between s and p orbitals, and $V_{pp} = 24.69/d^2$ eV for that between p orbitals, where d is the bond length in Å. The bond lengths used are, $d = 1.62$ Å for the As=O bond, and $d = 1.8$ Å for As-O and Ga-O bonds.

For configuration I, we have considered the As-lone pair on the As atom to be purely s-like. Bonding of oxygen to this lone pair gives an N-B splitting of 3.91 eV. The donor-like bonding between oxygen lone pair and the empty As-4d orbital lowers the oxygen lone pair in energy by -0.55 eV [13]. Hence the net N-B splitting entered for configuration I is 3.36 eV. For onfiguration II, we have considered the interactions between O-2p and the Ga-sp³ and the As-sp³ hybrids.

For simplicity in making comparisons, we have chosen the X-O-X' angle to be 125° for configurations III, IV, and V. Small variations around

this angle change the splitting between the σ and the π components rapidly but not the center of gravity of these two components. In considering the As-O-As bonding we have assumed the p^3 configuration for As, whereas we have assumed sp^3 configuration for Ga in considering the Ga-O-Ga bonding. Such assumptions are justified by the bonding angles found in As_2O_3 and Ga_2O_3 . For similar reasons, we have retained the p^3 configuration of the backbonds of an As atom in a relaxed GaAs(110) surface when considering the Ga-O-As bridge (config. IV).

There are many variations of bond angles and hybridizations that can be considered, but those variations do not change the qualitative trend in the N-B splittings stated in the text (section 3.3).

Chapter IV

PHOTOEMISSION STUDIES OF CLEAN AND OXIDIZED CS

4.1 INTRODUCTION

There are two major reasons for investigating the oxidation properties of Cs.

Firstly, the oxidation of Cs is a subject of fundamental scientific interest. This is because the oxidation of, and/or the oxygen-adsorption on free-electron-like metals constitute simple systems which provide insights into understanding the oxygen-metal interaction in general. Such interest has been exemplified by previous photoelectron spectroscopic measurements of oxidation of Sr [1], Ba [1,2], Al [3,4], Na [5], K [6,7], Rb [7,8], Cs [7-10], Ag [11], Mg [12], and theoretical calculations of oxygen adsorption on Al [13]. As pointed out by Wijers et al [7], Al (the most studied substrate metal in both theoretical and experimental investigation of oxygen adsorption) has a wide valence band (~13.5 eV) degenerate with the oxygen valence states and thus strong intermixing with oxygen states is expected. Cs, on the other hand, has a valence band only 1.6 eV wide and is separated by ~10 eV from the next lower inner shell (5p). The oxygen valence states thus fall in a band gap of Cs and minimum mixing of Cs and O states is expected. Minimum intermixing of substrate-adsorbate states is also expected from the large electronegativity difference between Cs and O; formation of ionic oxygen species, such as O^{2-} , O_2^{2-} , O_2^- , can be anticipated in oxidizing

Cs. The O/Cs system thus provides a unique opportunity for exploring the electronic structure of a series of ionic oxygen species.

Secondly, cesium oxides are technologically important materials to study. Cesium oxide in thin layers is known to be perhaps the lowest-work-function material. The low-work-function property of cesium oxide has been exploited in fabricating the early generation photocathodes (S-1, the Ag-Cs-O system [14]) and the more recent negative electron affinity photocathodes (III-V compound semiconductor-Cs-O systems [15]). However, no definite identification of the forms of the optimum cesium oxides in these cathodes has been obtained yet, due to the complex phase diagram of the Cs-O system [9]. The strong interaction of the substrate materials with the (Cs,O) layers on various cathodes further complicates the understanding of such system (see ref.16 for GaAs-Cs-O, and ref.17 for Ag-Cs-O). It is therefore useful to obtain sufficient understanding of the oxidation properties of thick Cs films before going to the more complicated photocathode systems. In particular, photoelectron spectroscopic data obtained for the Cs-O system can provide reference information for similar studies made on photocathodes.

Some early UPS measurements of the oxidation of Cs have been made at low photon energy [7] and 21.2 eV and 40.8 eV [8,9]. Particularly interesting in these results are the sharp, multiple oxygen-induced structure in the valence band region and the negative shifts (lowering of binding energy) of the Cs-5p electrons upon oxidation. Ambiguities existed in earlier work as to whether some features should be assigned to plasmon loss features or to multiple splittings of different oxygen species. Cs core level shifts for higher oxidation states have not been well stud-

ied. In this work, we have performed photoemission measurements of the oxidation of Cs using synchrotron radiation in two ranges of photon energies (21-30 eV, and 100-150 eV) to include both the valence band region and several deeper lying Cs core levels (5p, 5s, and 4d). More definite identification of spectrum features belonging to different oxidation states can be arrived by correlating spectra obtained at different photon energies.

After giving the experimental details in section 2, we will first present photoemission spectra of clean Cs in section 3. The rather complex photoemission spectra (both the valence band and the core level spectra) of Cs films exposed to oxygen are examined in detail in section 4. In the analyses of section 4, four different forms of oxygen adsorbed in Cs are identified over an oxygen exposure range of 0.1-200 L. These four forms of oxygen are identified with four different ionic oxygen species in section 5. After identifying the oxygen species, a brief discussion of the oxidation process is given in section 6.

4.2 EXPERIMENTAL

The experiment was carried out in a stainless-steel ultra-high-vacuum chamber with base pressure $\sim 7 \times 10^{-11}$ torr.

The Cs source was contained in vacuum sealed glass ampoules. An ampoule contained $\sim 1/2$ g of Cs which had been vacuum ($\sim 10^{-7}$ torr) re-distilled through one liquid nitrogen trap[†] from a 5-g, 99.95 pure Cs ampoule. The re-distilled Cs ampoule was placed in a copper side arm

[†]Heating of the big 5-g ampoule with torch flame was necessary to drive the Cs through the liquid nitrogen trap.

which was separated from the main chamber by a all-metal straight-through valve. A copper dosing needle (1/8 " I.D.) pointed to the substrates was used on the other side of the straight-through valve. The dosing needle is necessary to restrict the Cs vapor to a limited volume inside the measurement chamber. Both the copper side arm and the copper dosing needle were baked to ~240°C for a prolonged duration (~12 hrs.) before breaking the Cs ampoule for experiments. The Cs ampoule was broken by carefully squeezing the copper side arm from outside. Evaporation of Cs was achieved by heating the copper side arm from outside. Evaporation time required for preparing thick Cs films (≥ 100 Å) ranges from 30-90 minutes with pressure during evaporation not exceeding 3×10^{-9} torr.

Substrates used for evaporation were in situ cleaved GaAs crystals and evaporated Cu thick film. Substrates temperatures range from 140°K (Cu film) to 160°K (one of the two GaAs cleaves). During measurements and oxygen exposures, substrate could either warm up or cool down, but the variation in temperature was no more than 15°K.

Oxygen exposures were made with research grade oxygen through a bakable leak valve.

Light source used was synchrotron radiation from the Stanford Synchrotron Radiation Laboratory (SSRL). Photoelectron energy analyses were performed with a double-pass cylindrical-mirror-analyzer (Physical Electronics) and pulse counting electronics. Combined monochromator and analyzer resolution (as determined by the Fermi edge width of Cu or Au) were 0.45-0.7 eV for photon energies 100-150 eV and 0.2-0.3 eV for photon energies 16-32 eV. Binding energies are referenced to the Fermi level.

4.3 RESULTS AND DISCUSSION-CLEAN CS

As a basis for discussion of the various features in the photoemission spectra of oxidized Cs, in this section we present photoemission spectra obtained on clean Cs films. Photoelectron spectroscopic studies of clean Cs are of interest because of its reported short photoelectron escape depth [18]. Several photoemission studies of clean Cs have been made in the past with low photon energies (≤ 11.8 eV [18] and Ne-I and He-I [8,19]). We will see below that new information is available from the present high photon energy studies.

4.3.1 Valence Band Spectra of Clean Cs

Fig.1 shows the first 5 eV below the Fermi level in the EDCs (energy distribution curves) obtained at several photon energies. The width of the valence band is 1.50 eV, as measured from Fermi level to the minimum in the valley just below the leading peak. This is close to the calculated value of 1.58 eV. The shape of the valence band emission appears to resemble a free electron distribution better at 21 eV, whereas it becomes more triangular at higher photon energies (28 eV and 30 eV). Such effect has been discussed in terms of surface effects such as surface band narrowing [20], and breakdown of direct transition model [21]. Strong surface effects are expected because of the unusually short photoelectron escape depth of ~ 1 Å [20]. This minimum escape depth occurs in a kinetic energy region of 10-20 eV [18]. Increasing photon energy from 21 eV to 30 eV therefore moves the spectrum out of the escape depth minimum rather than moving into it. Hence the surface-effect explanations do not apply here. It is more likely that the relative cross sec-

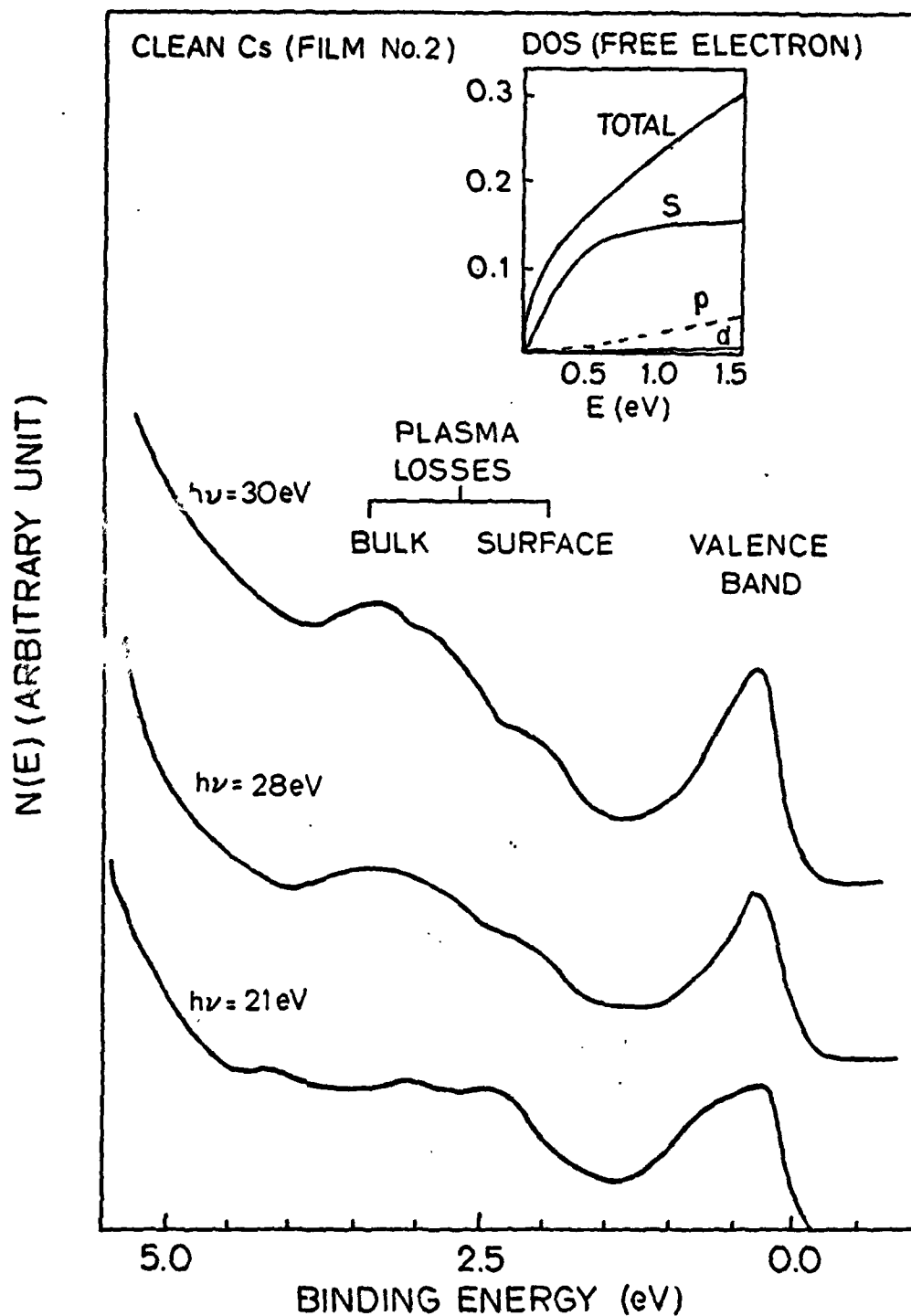


Figure 43: Valence band region spectra of clean Cs obtained at, from bottom to top, $h\nu = 21$, 28 , and 30 eV. The inset is the approximate total DOS of Cs and its s decompositions (see text).

tion of electrons with different angular momentum has changed in going from 21 eV to higher photon energies. In the inset of fig. 43 we show the l decomposition (i.e., into s, p and d components) of the free electron total density of states (DOS). This DOS is only approximate and has been obtained by rescaling the free electron DOS calculated by Gupta and Freeman [22] for Na. It appears that in the 21 eV spectrum the s-DOS dominates, and in 28-30 eV spectra the p-DOS becomes important.

Below the valence band structure in fig. 43, two plasmon loss features can be identified. A surface plasmon is located approximately 2.2 eV below the leading peak. This same value of surface plasmon energy is also found in the core level spectra (fig. 44,3). The fainter structure at approximately 3.2 eV below the leading peak is associated with bulk plasmon excitation. Bulk plasmon loss feature is not pronounced in any spectrum obtained in this study, hence we can not assess its energy position with great accuracy. The best estimate of 3.2 eV is intermediate to the free electron value of 3.54 eV [23] and the value corrected for ion core polarization of 3.0 eV [24]. Using the value of 3.2 eV, the $\sqrt{2}$ ideal ratio of the bulk plasmon energy to surface plasmon energy, however, is approximately observed.

4.3.2 Core Levels and Auger Transitions

Fig.2 shows EDCs covering the region of 5p levels. EDCs of photon energies below 32 eV were obtained on one Cs film, and the 100 eV EDC was obtained on another different Cs film. The sharp, well resolved $5p_{3/2}$ and $5p_{1/2}$ pair are immediately recognized in fig. 44. The spin-orbit splitting of the 5ps is 1.90 ± 0.05 eV. The FWHMs (without correc-

tions to the instrumental broadening) in the 30 eV spectrum are estimated to be 0.45 eV and 0.70 eV for $5p_{3/2}$ and $5p_{1/2}$ peaks, respectively. Considering that the broadening of the $5p_{1/2}$ peak relative to the $5p_{3/2}$ is partly caused by the surface and bulk plasmon loss from the $5p_{3/2}$ peak, the difference in the intrinsic line width between the two 5p levels may not be as drastic as suggested by Simon [8], and may be well be accounted for by a Coster-Kronig process that is only moderately strong.

The O_{3VV} Auger transition appears at a fixed kinetic energy of 6.5 eV relative to the vacuum level of the analyzer, or 11.15 eV above the Fermi level. (In the 21 eV EDC of Au standards, the Fermi level appeared at a kinetic energy of 16.35 eV, hence the work function of the analyzer is 4.65 eV.) The high energy edge can be approximately located at 12.35 eV, in reasonable agreement with other results (11.8 eV by Oswald et al [19], and 12.3 eV by Simon [8]). The width of this Auger transition is about 2.8 eV (measured from the high energy edge to the valley right below the peak), which is comparable with twice the width of the valence band and is in agreement with the simple picture of Auger transition.

Another peak that stayed at fixed kinetic energy with varying photon energy is 1.9 eV below the O_{3VV} transition. This peak can be interpreted as either due to the surface plasmon from O_{3VV} peak or the O_{2VV} transition. There is no doubt that the O_{3VV} Auger electron has sufficient energy to excite surface plasmon, as has been demonstrated in previous work [9]. The O_{2VV} transition, however, has been suggested to be completely suppressed by the strong Coster-Kronig process ($5p_{3/2} \rightarrow 5p_{1/2}$).

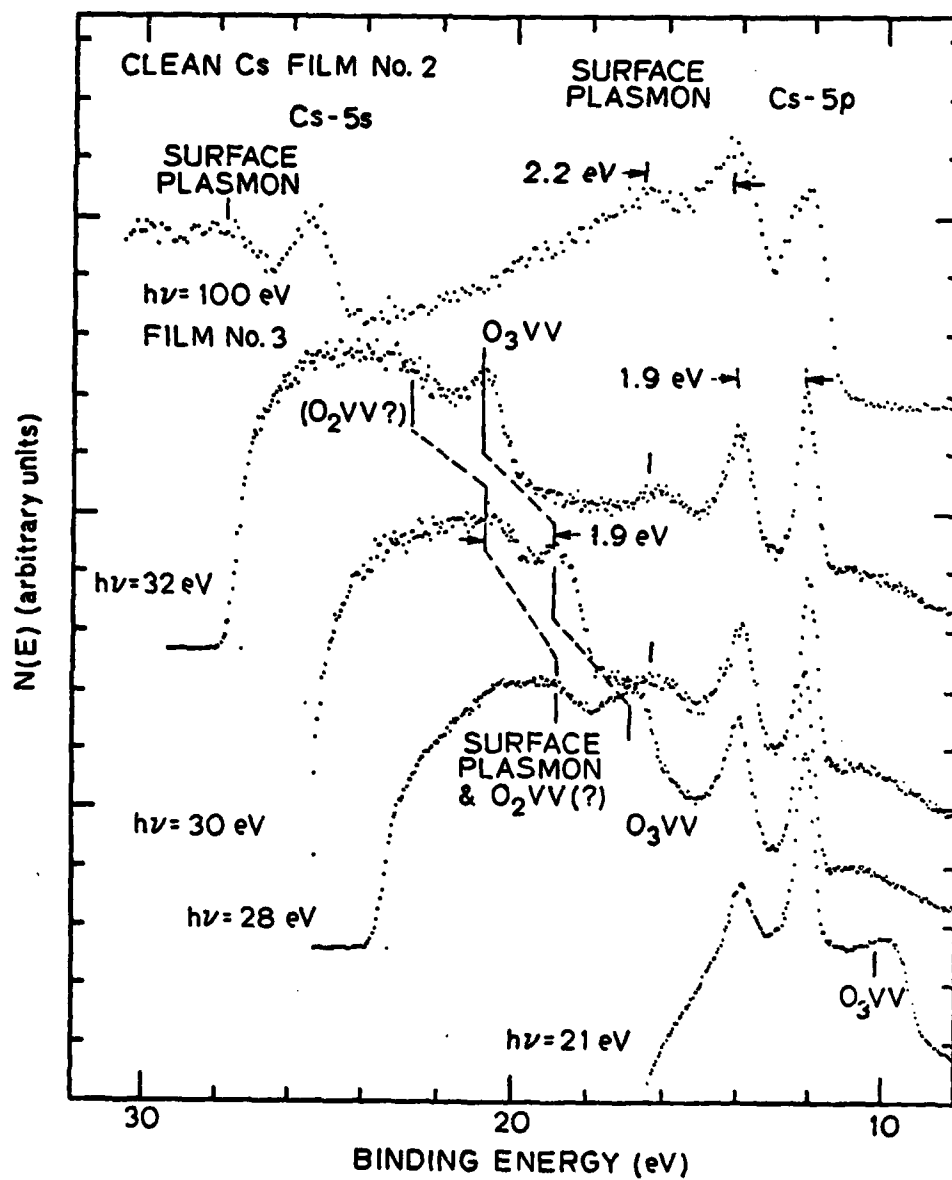


Figure 44: EDCs of the 5p and the 5s levels, and OVV Auger transitions of clean Cs obtained at, from bottom to top, $h\nu=21$, 28, 30, 32 and 100 eV.

In our measurement the separation of this peak from the O_3VV peak, 1.9 eV, is identical to the spin-orbit splitting of the 5p levels, and thus it favors a significant contribution from the O_2VV transition. Accurate determination of the energy position of this peak may be difficult because it rides on the secondary tail; in that case, however, the apparent separation from the O_3VV peak should be even larger than the true separation. We therefore take the measured 1.9 eV as meaningfully different from the 2.2 eV surface plasmon energy. (We have used 0.05 eV/channel accuracy in obtaining the spectra.) The fact that the O_2VV transition is not completely suppressed is consistent with our suggestion of a moderate $5p_{3/2}$ to $5p_{1/2}$ Coster-Kronig process made in relation to the relative width of the two 5p levels.

One additional feature included in the 100 eV EDC in fig. 44 (the top curve) is the Cs-5s level at 25.4 eV BE. The plasma loss features associated with this peak are also clearly seen. The expected configurational splitting of the 5s level is not observed here, indicating perhaps a suppressed (5s,6s) interaction in Cs metal.

Fig. 45 shows EDCs of Cs-4d levels at several photon energies. The $N_{4,5}O_{2,3}O_{2,3}$ Auger transition is also included in the 110 eV EDC. The spin-orbit splitting of the 4d levels is 2.2 ± 0.1 eV.

Table 6 summarizes the energy positions of core levels and Auger transitions observed in the photoemission spectra of clean Cs.

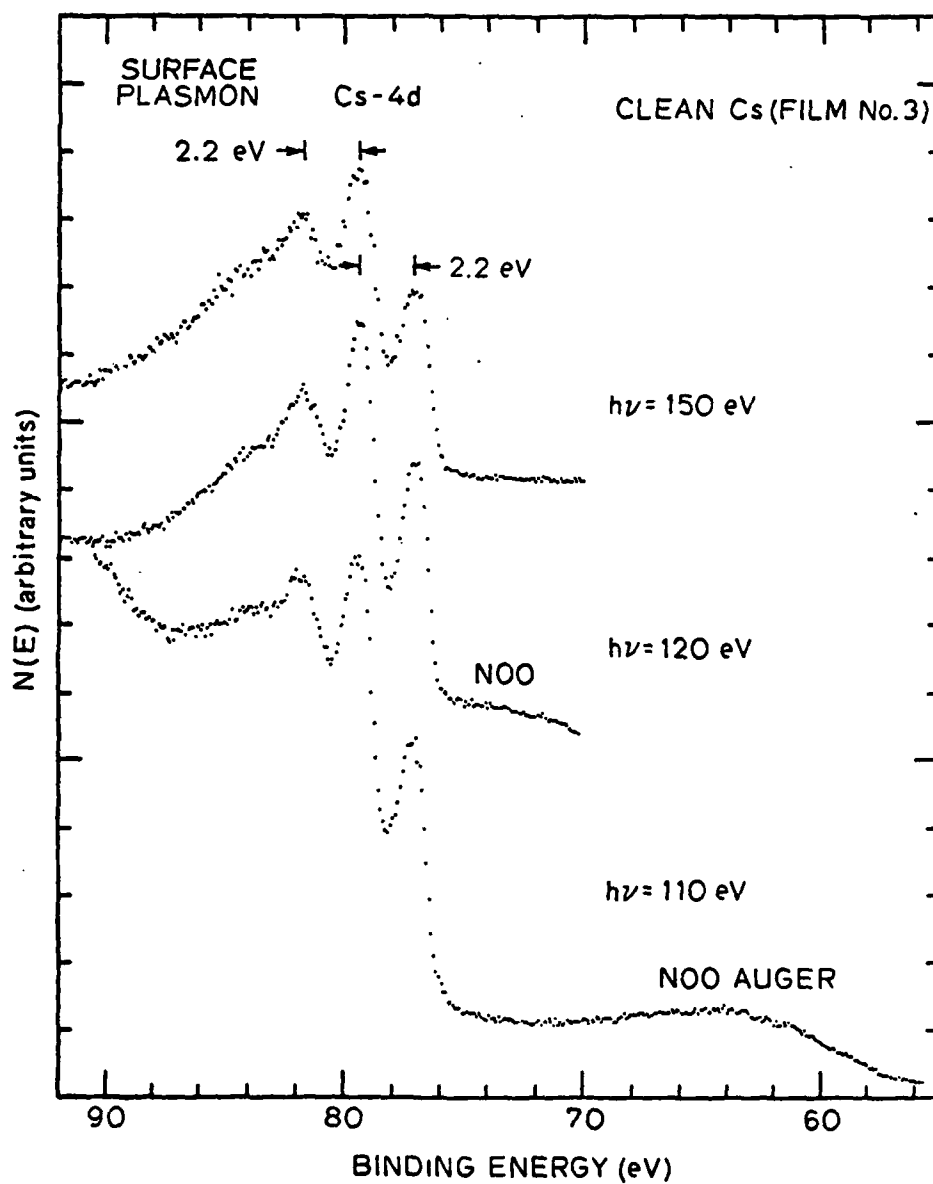


Figure 45: EDCs of the Cs-4d levels and the NOO Auger transition at, from bottom to top, $h\nu = 110, 120$ and 150 eV.

TABLE 6

Summary of binding energies (BE) of photoelectron core lines and kinetic energies (KE) of Auger transitions of clean Cs.

Levels	BE (or KE) in eV referenced to the Fermi level
5p _{3/2}	12.1
5p _{1/2}	14.0
5s	25.5
4d _{5/2}	77.3
4d _{3/2}	79.5
O ₃ VV (O ₂ VV?)	11.15 (9.25?)
NOO	46.3

4.4 RESULTS AND DISCUSSION - OXIDIZED CS

Different ranges of oxygen exposures were made on the three Cs films prepared: 0.1 - 2 L for one film, 1 - 100 L for a second film, and 1 - 200 L for a third film. The first two films were studied with 21-32 eV photons, the third film was studied with 100-120 eV photons.

The photoemission spectra obtained on these surfaces are very complex, especially the spectra containing features derived from ionizing the O-2p subshell. We will first give a summary of the different forms of oxygen adsorbed in Cs and the corresponding O-2p related features in the photoemission spectra (4.1). Detailed examination of the photoemission spectra will be given in sections 4.2 and 4.3. 4.2 covers the

valence band region spectra and 4.3 covers the spectra of core levels and Auger transitions.

4.4.1 Summary of O-2p Related Features

The evolution of O-2p related features in the photoemission spectra with increasing oxygen exposure is complex. Previously, Wijers et. al. [7], studying a limited range of oxygen exposures and showing difference curves only, have concluded the existence of only two different states of oxygen adsorbed in Cs. We have compared photoemission spectra with oxygen exposure ranging from 0.1 L to 200 L, at which point the oxidation appears to have reached saturation, and we have identified four different states of oxygen. Detailed examination of the photoemission spectra of these four states of oxygen will be given in 4.2. Here we summarize the binding energies of O-2p related features of the four states of oxygen in table 7.

TABLE 7

Summary of binding energies of different oxygen states observed in the oxidation of Cs

State Label	BE's of features (eV)
A	2.7, (4.4) ⁺ , (5.4) ⁺
B	3.3, 6.4, 7.8
C	5.5, 8.3, 10.4
D	4.7, 5.8, 6.2, 8.5, 10.7
⁺ Plasmon losses from the 2.7 eV peak, see text.	

4.4.2 Valence band region spectra

The first 13 eV of EDCs taken at $h\nu=30$ eV for the first film subjected to increasing oxygen exposures are shown in fig. 46. A small amount of oxygen was incorporated into the Cs film prior to the intended oxygen exposure, as can be seen from the bottom curve in fig. 46. The "contaminant" feature (at 2.7 eV below the Fermi level) grows in intensity with subsequent oxygen exposures. By comparing the intensity of the 2.7 eV BE peak before and after the 0.1 L exposure, the amount of the oxygen incorporated into the Cs film prior to the intended oxygen exposure is estimated to be equivalent to that due to 0.1 L of controlled exposure.

The 2.7 eV BE peak (labeled A1 in fig. 46) is the dominant feature in the spectra shown in fig. 46. The conspicuous growth of it after the 2 L exposure is especially clear. This feature is associated with state A oxygen (table 7 in section 4.1). The 2.7 eV peak has been observed by Gregory [9] on similarly prepared Cs film with low photon energy, and by Simon [8] for bulk suboxides (Cs_{11}O_3 , Cs_7O) and mono-oxide (Cs_2O).

Other weaker features are seen in the region of 3.2 eV, 4.4 eV, 5.4 eV, 6.1 eV and 7.8 eV BE. The feature at 3.3 eV BE (labeled B1 in fig. 46) obviously is not associated with the same oxygen state responsible for the 2.7 eV peak, because its intensity does not increase in proportion to that of the 2.7 eV peak in going from 0.5 L to 2 L exposure. It is the first feature which we have entered for state B oxygen in table 7. This feature, which is discernable in the 0.5 L spectrum, becomes completely smeared in the 2 L spectrum due to its overlap with the

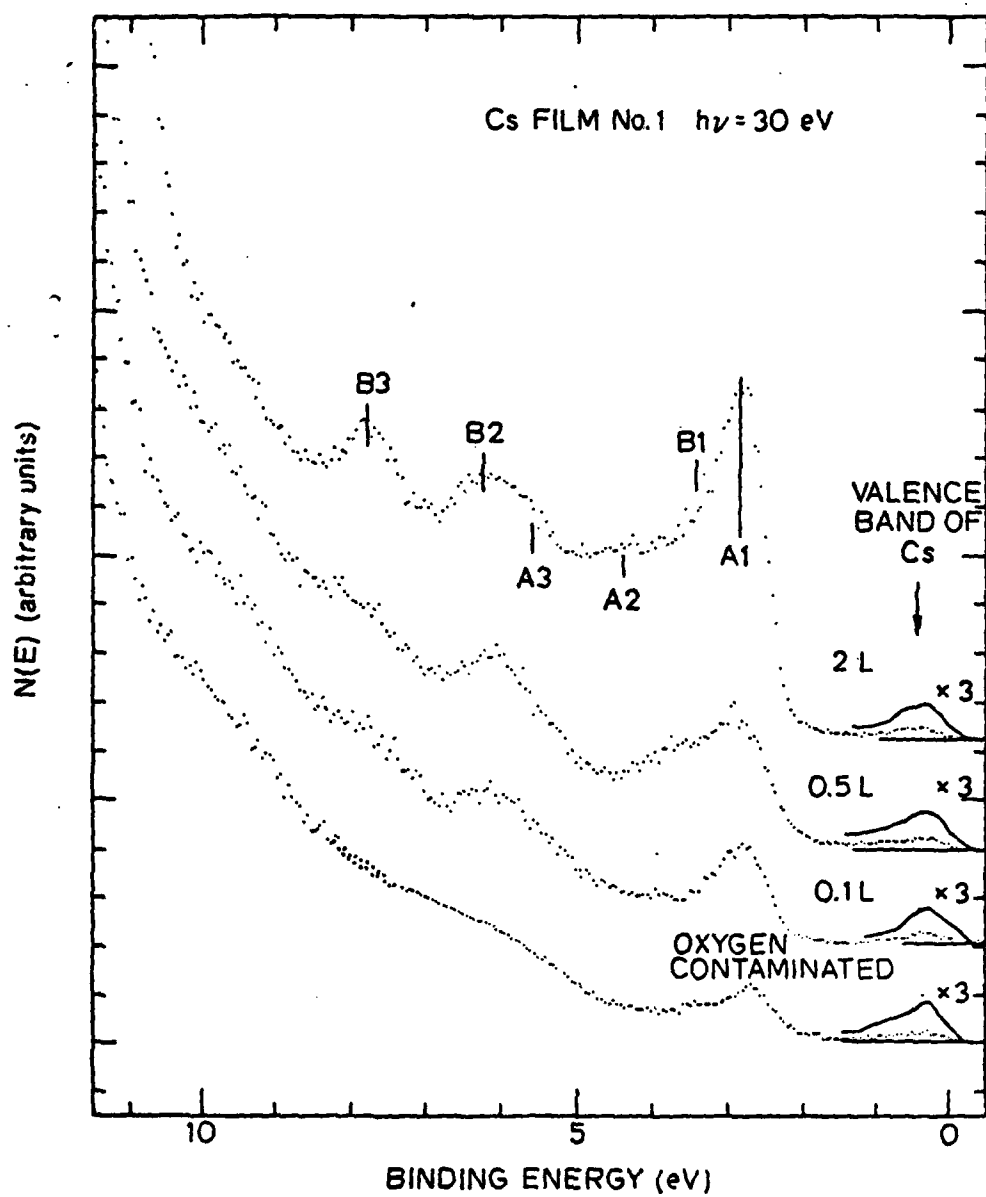


Figure 46: The first 13 eV of the EDC's of clean and oxygen-exposed Cs taken at $h\nu = 30$ eV. Some oxygen was incorporated into the Cs film prior to the intended exposure (the bottom curve). Notice that emission from the valence band of Cs is visible in all spectra.

strong 2.7 eV peak and a new feature (A2) appeared at ~4.4 eV below the Fermi level (labeled A2 in fig. 46). Both feature A2 and feature A3 (which is further discussed below) become significantly only after the 2 L exposure at which point the 2.7 eV peak dominates the spectrum. The energy position of feature A2 is appropriate for a surface plasmon loss from the 2.7 eV peak if the surface plasmon energy of the oxygen-exposed Cs film is reduced to ~1.7 eV from the 2.2 eV value of clean Cs. Such reduction in the surface plasmon energy is also observed in core level spectra to be discussed below. Surface plasmon energy of ~1.7 eV has also been observed by Simon [8] in bulk Cs suboxides (Cs_{11}O_3 , Cs_7O). Feature A3 is at an energy position appropriate for a bulk plasmon loss from the 2.7 eV peak. Thus features A2 and A3 are also entered in the first row of table 7 in parenthesis, as has been explained in section 4.1.

Developments of the peaks in the regions of 6.1 eV and 7.8 eV with increasing exposure are less clear in their relation to the state A oxygen and the state B oxygen. The intensity in the 6.1 eV region increased more than that in the 7.8 eV region from 0.1 to 0.5 L exposure. The shape of the 6.1 eV feature also changed slightly in going from 0.1 L to 0.5 L, indicating the possible existence of two peaks under this feature. In the 2 L spectrum, a shoulder at 5.7 eV BE (labeled A3 in fig. 46) indeed becomes distinguishable. It is therefore possible that in the low exposure (0.1 L and 0.5 L) spectra the 6.1 eV feature has contribution from both the state associated with the 2.7 eV (state A) peak and the state associated with the 3.3 eV peak (state B). The 7.8 eV feature grew significantly only at 2 L exposure. It is thus tempting to associate it with the 2.7 eV peak, but the simultaneous

growth of the 3.3 eV peak at 2 L exposure makes such association completely ambiguous. A definite separation of the oxygen induced features into two states will be seen below in the results obtained on another Cs surface.

Studies of higher oxygen exposures (than that made on film No. 1) were made on a second Cs film, and the results are shown in fig. 47. Same oxygen induced features as those found on film No.1 (fig. 46), are present on this surface after the first oxygen exposure. The difference is that, at 1 L exposure, the 3.3 peak (B1) showed intensity comparable with that of the 2.7 eV peak (A1, fig. 47). Thus, this film exposed to 1 L oxygen appears to be in a even more advanced oxidation stage than film No.1 exposed to 2 L oxygen. Such difference is likely to be explained by the difference in substrate temperature and/or texture, therefore no special significance will be given to the absolute values of exposures. (Film No.3, to be discussed below, appeared to be in the most advanced oxidation stage among the three films after 1 L exposure; the temperature of film No. 3 happened to be the lowest of the three.) We also notice that (in fig. 51) with most of the strength of the 5p levels shifted to lower BE, the spin-orbit splittin of the 5p's becomes 1.55 ± 0.05 eV, which is narrower than that found for clean Cs.

With 10 L exposure on film No.2, the 2.7 eV peak disappeared completely. The 3.3 eV peak revealed its full shape and shows a FWHM of ~ 1 eV. It therefore appears that we observed a single state of oxygen at this stage, whereas in earlier stages of oxidation we observed a mixture of states. Since the relative height of the 3.3 eV, 6.1 eV, and 7.8 eV peak remains about the same in going from 1 L spectrum to the 10 L spec-

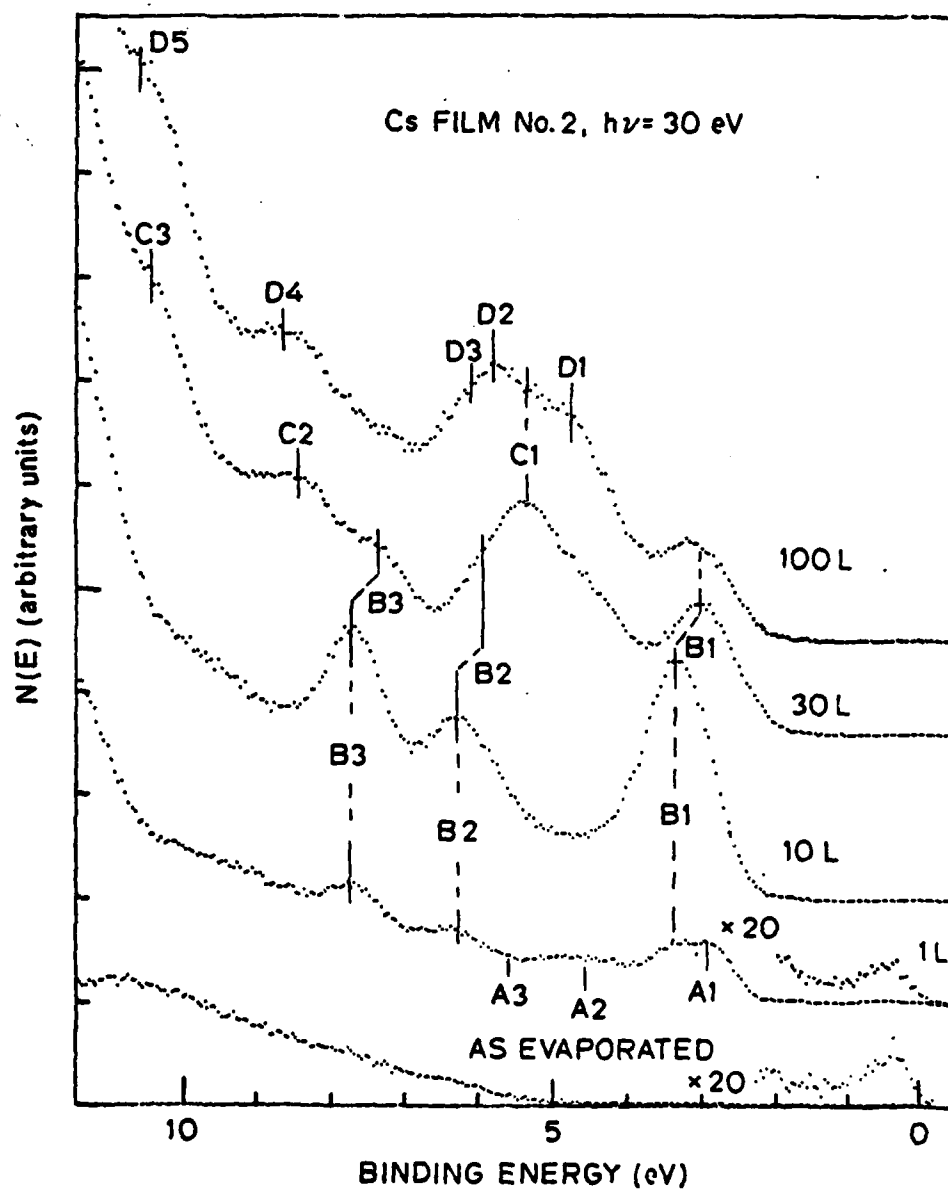


Figure 47: The first 13 eV of the EDC's obtained on Cs film No.2 before and after a sequence of oxygen exposures. Emission from the valence band of Cs is visible after the 1 L exposure, but it disappeared completely after 10 L and higher exposures.

trum, the oxygen state associated with the 2.7 eV peak is likely to have little contribution to intensities near 6.1 eV and 7.8 eV BE regions. We therefore make the assignments of the features to the first two oxygen states as that were entered in the first two rows in table 7.

The transition from state A to state B is also characterized by the disappearance of emission near the Fermi level. As can be seen in fig. 46, when adsorption of oxygen in state A dominates at low exposures, emission near the Fermi level can be clearly seen. When adsorption of oxygen in state B becomes dominant, as is the case of the 10 L spectrum in fig. 47, the emission near the Fermi level disappears completely. This observation suggests that when oxygen adsorption in state A occurs, the surface region of Cs remains metallic. This justifies the association of state A oxygen with Cs suboxides of O^{-2} ions dissolved in Cs, which will be discussed in section 5.

Another even more drastic change characterizing the transition from state A to state B is a sharp increase in the photoelectron yield. (Notice that all spectra in figs. 46 - 57 are normalized such that comparison of intensities between spectra is possible.) As shown in fig. 48, the secondary electron tails were flat in the clean and the 1 L spectra, but become sharply peaked in spectra of oxygen exposures above 10 L. The yield in the primary photoelectrons also increases significantly in going from 1 L to 10 L exposure, as evidenced by the increase in the area under the Cs-5p levels shown in fig. 48. The low yield of the clean and the 1 L-exposed Cs films is characteristic of metallic surfaces with short photoelectron escape depth, whereas the high yield

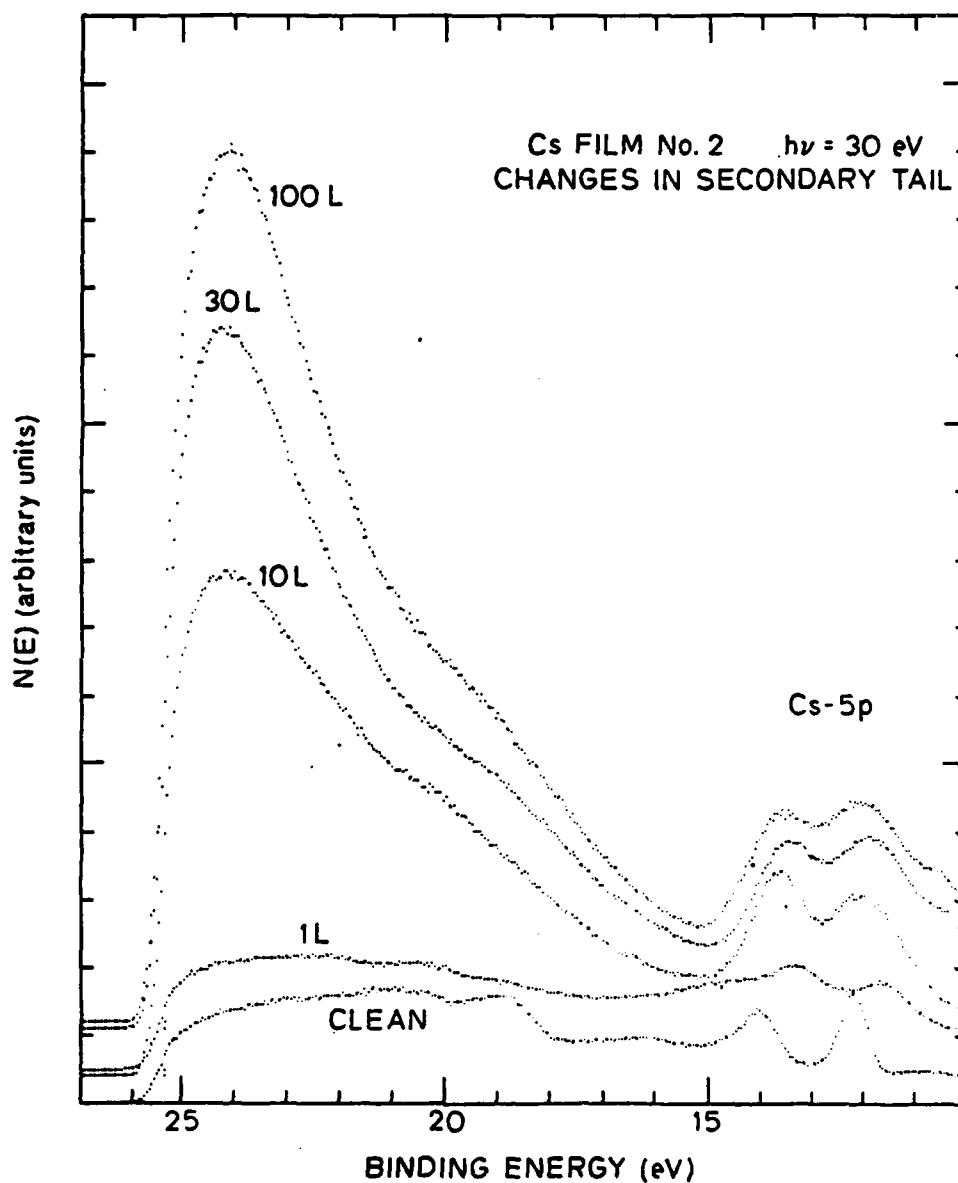


Figure 48: Changes in the photoelectron yield of Cs at $h\nu = 30$ eV when subjected to a sequence of oxygen exposures.

of the Cs films subjected to 10 L and higher exposures is typical of semiconducting or insulating surfaces with moderate photoelectron escape depth.

A third distinction between state A oxygen and state B oxygen is the difference in chemical shifts induced in the 5p levels; discussion of this point will be deferred until section 4.3.

More oxygen induced states were observed at higher oxygen exposures. In fig. 47, new peaks appear in the 30 L spectrum at 5.5 eV, 8.5 eV and 10.4 eV BE. The 10.4 eV BE feature appears as a shoulder on the high BE side of the 5p levels (fig. 51, labeled C3 and D5). The possibility of this peak being a shifted 5p level must be explored, although it would imply an unusually large negative shift -- 1.7 eV toward lower BE. Negative shift of this order had indeed been suggested by Feubacher in his study of the oxidation of Cs [10]. This possibility, however, is ruled out in this work by examining changes in other Cs core levels upon oxidation (to be discussed below in 4.3). Reminiscence of the three peaks associated with state B can be easily recognized in the 30 L spectrum, although these peaks appeared to have shifted to lower BE by about 0.2 eV. Thus the new oxygen features introduced by the 30 L exposure are at 5.5 eV (C1), 8.3 eV (C2), and 10.4 eV (C3) below the Fermi level; these features correspond to the emergence of a new state of oxygen, state C, as given in the third row of table 7.

In the 100 L spectrum, the intensity of the 3.3 eV peak is further reduced, and the 6.4 eV and the 7.8 eV peaks are barely recognizable in the background distribution. Two new features (D1 and D2) clearly appear at 4.7 and 5.8 eV BE in the 100 L spectrum; shoulders at 6.2 eV

BE (D3) and 10.7 eV BE (D5) are also discernable. The intensity filling the region between 4.7 and 5.8 eV BE is due to the remains of the 5.5 eV peak in the 30 L spectrum. The remains of the 10.4 eV feature is also visible in the 100 L spectrum (fig. 47). The strength of the feature at ~8.4 eV BE (D4), when compared to that of the remains of the 5.5 eV peak (C1), is too strong to be considered simply from feature C2 of the state C oxygen. Thus five features are introduced by the 100 L exposure, and they correspond the fourth state of oxygen - state D in table 7 - adsorbed in Cs. The 5p levels moved to lower BE in going from 10 L to 30 L exposure (fig. 51), but moved back to higher BE (12.0 eV for $5p_{3/2}$) with 100 L exposure. Apparent changes in the relative height of the $5p_{3/2}$ and $5p_{1/2}$ peaks are also observed in going from 10 L to 30 L and 100 L spectra. This change in the relative height of the 5p levels cannot be completely explained by the overlap with the 10.4 eV and/or the 10.7 eV oxygen peak, unless an unusually broad peak is assigned to the 10.4 eV and/or the 10.7 eV peak.

The 100 L spectrum in fig. 47 is representative of a "saturation" stage of the oxidation of a Cs film in our experimental conditions. This saturation is established by comparing the 100 L and 200 L spectra of a third Cs film studied with 100 eV photon. The top two curves in fig. 49 are those two spectra. Only small changes can be seen by increasing oxygen exposure from 100 L to 200 L. On the other hand, a one to one correspondence is found between the features in the 100 L spectrum of fig. 47 and the 200 L spectrum of fig. 49. We can therefore complete the list of oxygen states as shown in table 7.

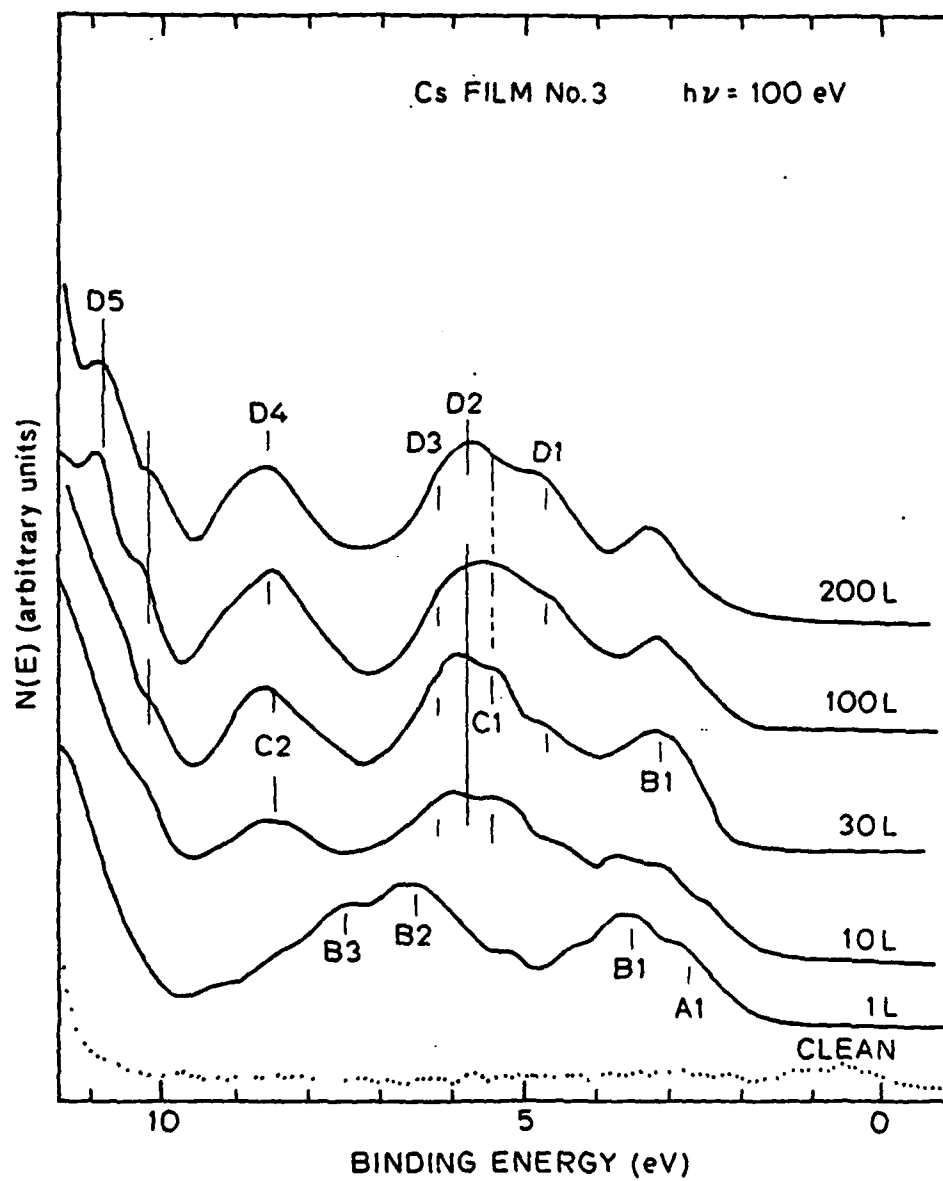


Figure 49: The first 13 eV of the EDC's obtained on Cs film No.3 before and after oxygen exposures, spectra taken at $h\nu = 100$ eV.

4.4.3 Core Levels and Auger Transitions

In this subsection, we discuss the changes induced by oxygen adsorption in Cs core levels and Auger transitions. The 5p levels of two Cs films (figs. 50 and 51) have been studied with high energy resolution (0.25 eV) using photon energies between 21 and 32 eV. Due to the low counting rate at high photon energies (≥ 100 eV), the Cs-5p levels of a third Cs film (fig. 52) were studied with far poorer energy resolution (~ 0.7 eV); the results from this film, however, are included here because (1) we are interested in comparing the oxygen induced changes in the 5p's to those in the 5s and the 4d levels; the latter levels were measured only on this film, and (2) different sampling depth is given by the high photon energy spectra of the 5p levels.

Fig. 50 shows the clean and oxygen exposed Cs film No.1, and fig. 51 gives the 5p levels of film No.2. Although changes in the 5p levels up to 0.5 L oxygen exposure are not pronounced, noticable broadening in the low BE side of the $5p_{3/2}$ level and the filling of the valley between the two 5p's can be seen in fig. 50. At 2 L exposure, a peak shifted to low BE by 0.6 eV has definitely developed. On film No.2, however, most strength of the Cs-5p is seen to have moved by 0.6 eV toward lower BE (fig. 51) after the 1 L exposure. As mentioned earlier, such difference is likely to be due to difference in the temperature and/or the texture of the Cs films. The extra intensity near 15.3 eV BE is due to surface plasmon associated with the shifted peak. Although the surface plasmon loss feature appears to be smeared in either the 2 L spectrum of fig. 50

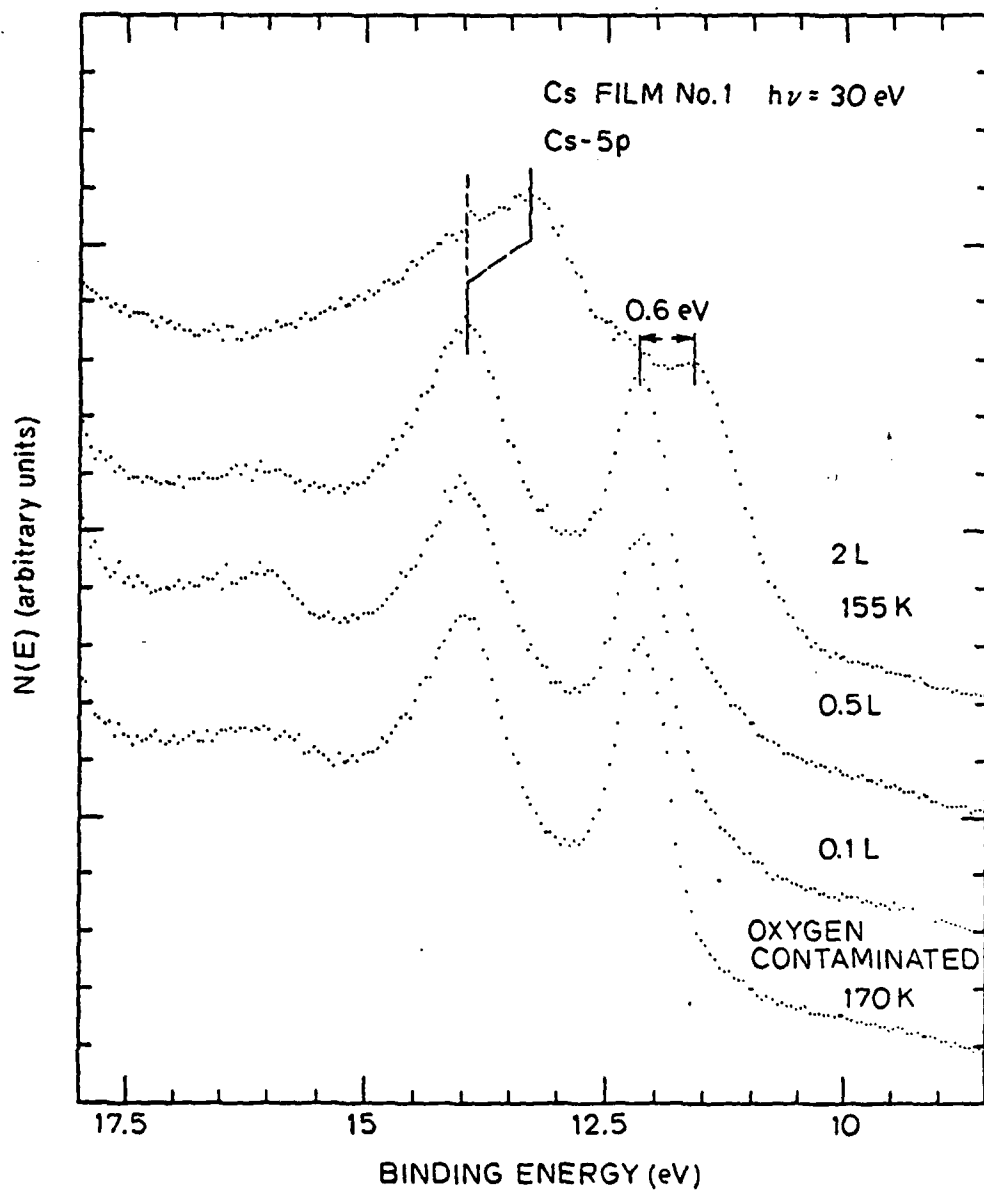


Figure 50: EDC's of the Cs-5p levels of the surfaces of fig. 46.

or in the 1 L spectrum of fig. 51, it can roughly be located at 1.7 eV below the Cs-5p_{3/2} peak, as indicated in figs. 50 and 51. Another change in the Cs-5p levels after ~1 L oxygen exposure, as can be seen in fig. 51, is the decrease in the spin-orbit splitting from the 1.9 eV of clean Cs to 1.5 eV.

The shift of the 5p levels to lower BE by 0.6 eV and the retention of the surface plasmon loss feature associated with the 5p are additional signatures of the state A oxygen. The surface plasmon loss associated with the 5p's disappeared when Cs film No. 2 was further exposed to 10 L oxygen, at which point the state B oxygen dominates. As can be seen in fig. 51, the 5p levels at 10 L exposure shifted to higher BE relative to the 5p levels at 1 L exposure, although they are still 0.1 eV above the 5p levels of the clean surface. The binding energy of the 5p's were little affected after the oxygen exposure was further accumulated to 30 L and 100 L. The spin-orbit splitting remains to be 1.5 eV - a value 0.4 eV smaller than that of clean Cs - throughout the whole range of oxygen exposures studied on Cs film No.2.

In section 4.2 above, we have found consistent changes in the valence band region spectra of film No.2 and film No.3 after exposing them to oxygen, we point out below that consistent changes in the 5p levels upon oxidation can also be found. The 1 L spectrum in fig. 49 contains more intensity from state B than the 1 L spectrum in fig. 47, but it still contains substantial emission from state A. In the spectrum of the 5p levels, the existence of state A after the 1 L exposure is also verified by the residual plasmon loss features seen in the 1 L spectrum in fig.

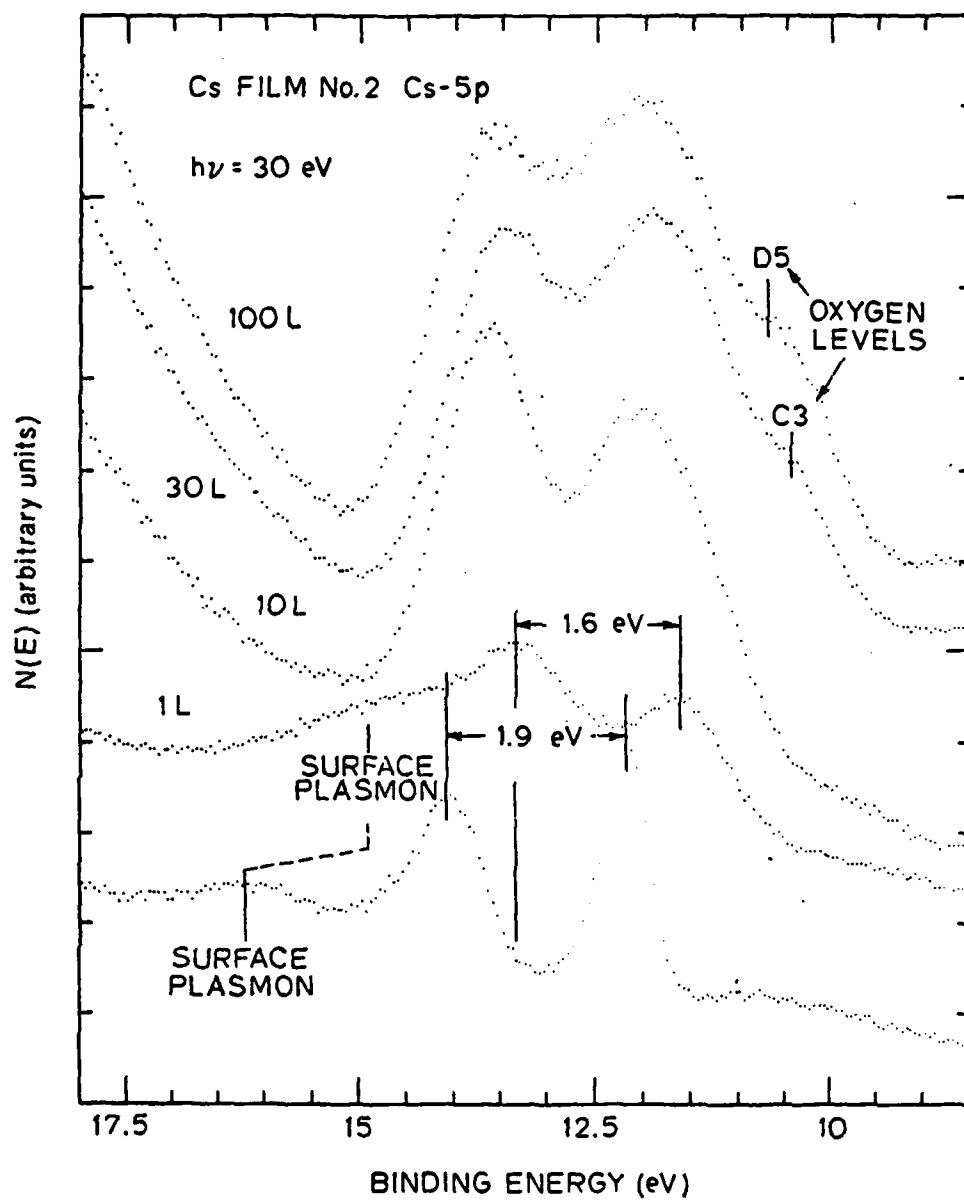


Figure 51: EDC's of the Cs-5p levels of the surfaces of fig. 47.

52. We also recall that, in fig. 51, the 0.6 eV negative shift and the narrowing of the spin-orbit splitting brings the $5p_{3/2}$ peak right above the valley between the two 5p peaks of clean Cs. This same indication of the existence of the 0.6 eV negative shift can be seen in fig. 52. This negative shift is also seen in the 1 L spectrum of 5s level in fig. 53. Oxidation at 10 L exposure is also more advanced on film No.3 than on film No.2, in the sense that features from state C are present in the 10 L spectrum in fig. 49. Shoulders at 0.6 eV on the low BE side of the 5p and the 5s levels (which indicate the presence of the state A oxygen), however, are still visible in the 10 L spectra in fig. 52 and fig. 53, respectively. We realize that the photoelectrons detected in the spectra of figs. 49, 52, and 53, have much less surface sensitivity than those detected in the spectra of figs. 47 and 51 [20]. This suggests that state A oxygen does not disappear with the appearance of state B and C, but is moved farther away from the surface. The characteristic rise of the $5p_{3/2}$ above the $5p_{1/2}$ peak at high oxygen exposures (≥ 30 L) is also seen in fig. 52. Although the 5p spin-orbit splitting is smeared in most of the after-oxidation spectra in fig. 52, a value smaller than that of clean Cs is discernable in the 100 L spectrum.

The Cs-4d

Having established the consistency of the oxidation of film No.3 and film No.2, we can point out some interesting difference between the changes in 4d and 5p levels upon oxidation:

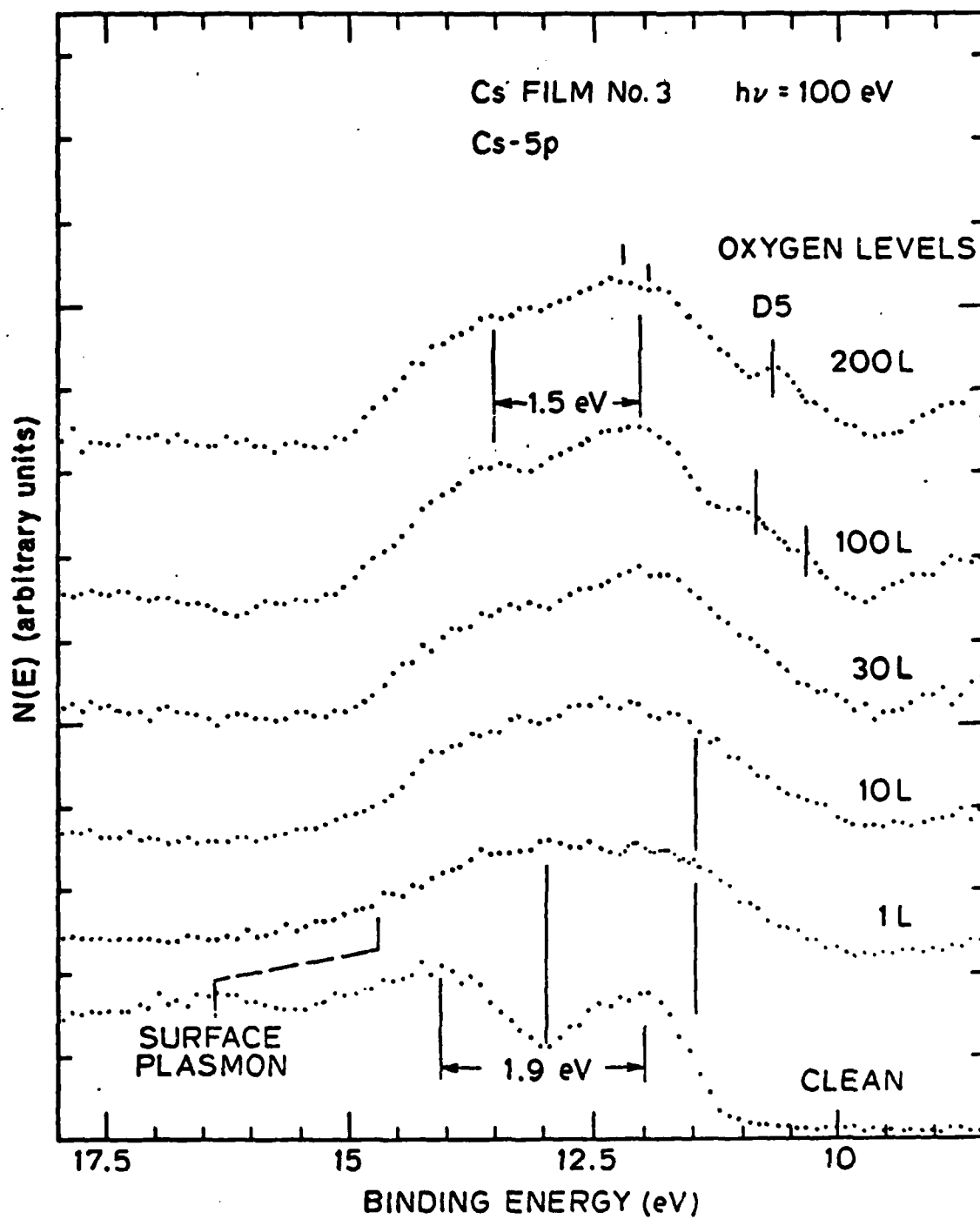


Figure 52: EDC's of the Cs-5p levels of the surfaces of fig. 49.

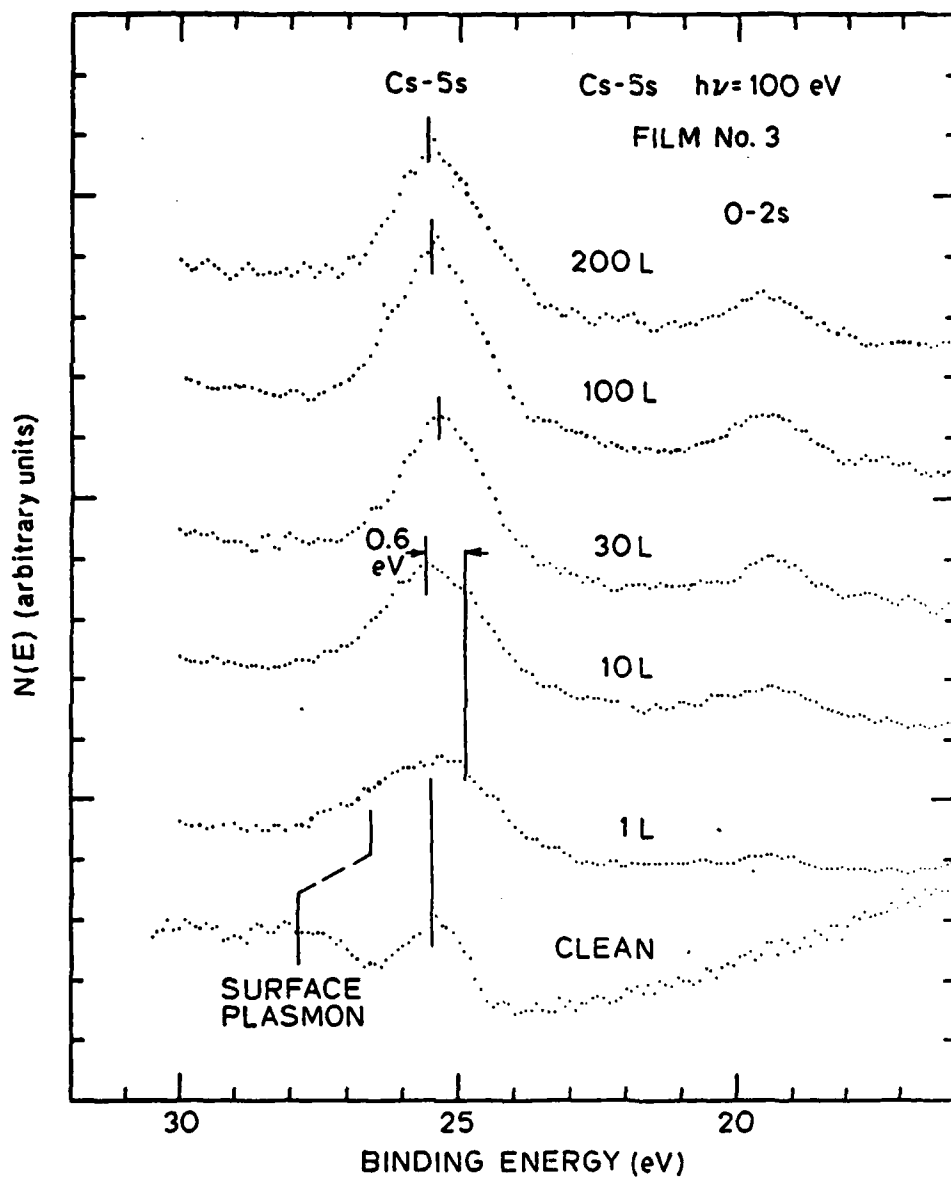


Figure 53: EDC's of the Cs-5s level of the surfaces of fig. 49.

- i) A smaller shift in the 4d levels is observed at 1 L exposure than that is observed in the 5p levels.
- ii) The spin-orbit splitting of the 4d levels remains constant and is equal to the value of clean Cs throughout the whole range of exposures, whereas that of the 5p's is reduced with oxygen exposure.

One possible explanation of the first point is the different surface sensitivity between photoelectrons originated from the 5p's and the 4d's.. The kinetic energy of the 4d electrons excited by the 120 eV radiation is closer to the escape depth minimum than the 5s and the 5p electrons excited by the 100 eV radiation. Further support for this comes from 4d spectra taken with 110 eV radiation (fig. 55). Photoelectrons detected in these spectra have kinetic energy even closer to the escape depth minimum than those in the corresponding 120 eV spectra. The 4d levels at 1 L exposure in fig. 55 shows noticeably less shift toward lower BE (~ 0.2 eV) than the corresponding 4d peaks in fig. 54 does. Another possible contributing factor to this result may simply be that the same state of oxygen can indeed induce different shifts in 4d and 5p levels. Further consideration of this latter idea and point (ii) noted above, will be given below together with discussion of the shifts in the N00 Auger transition.

The N00 Auger Transition

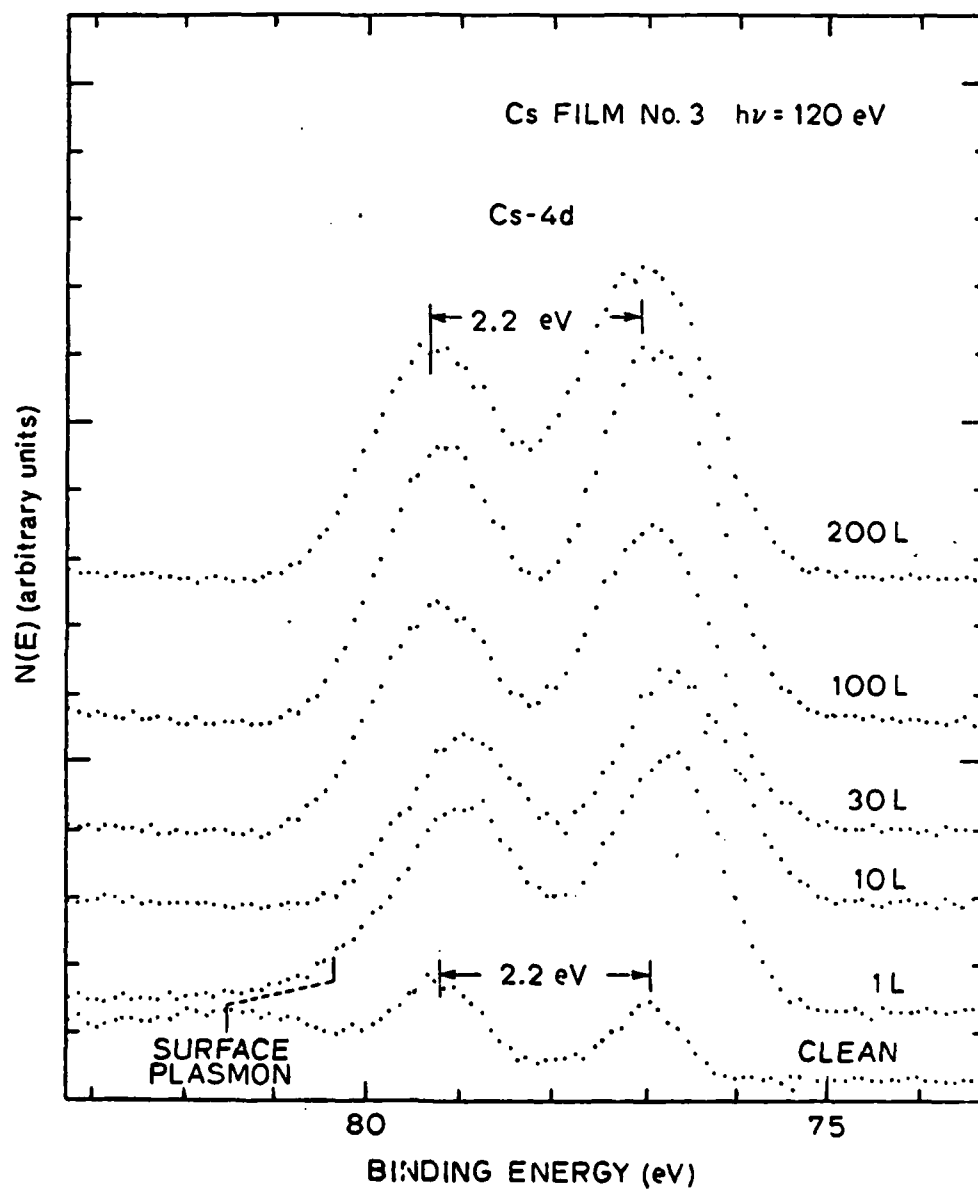


Figure 54: EDC's of the Cs-4d levels of the surfaces of fig. 49 taken at $h\nu=120$ eV. Notice that the spin-orbit splitting in the 4d's is constant through whole range of oxygen exposures studied.

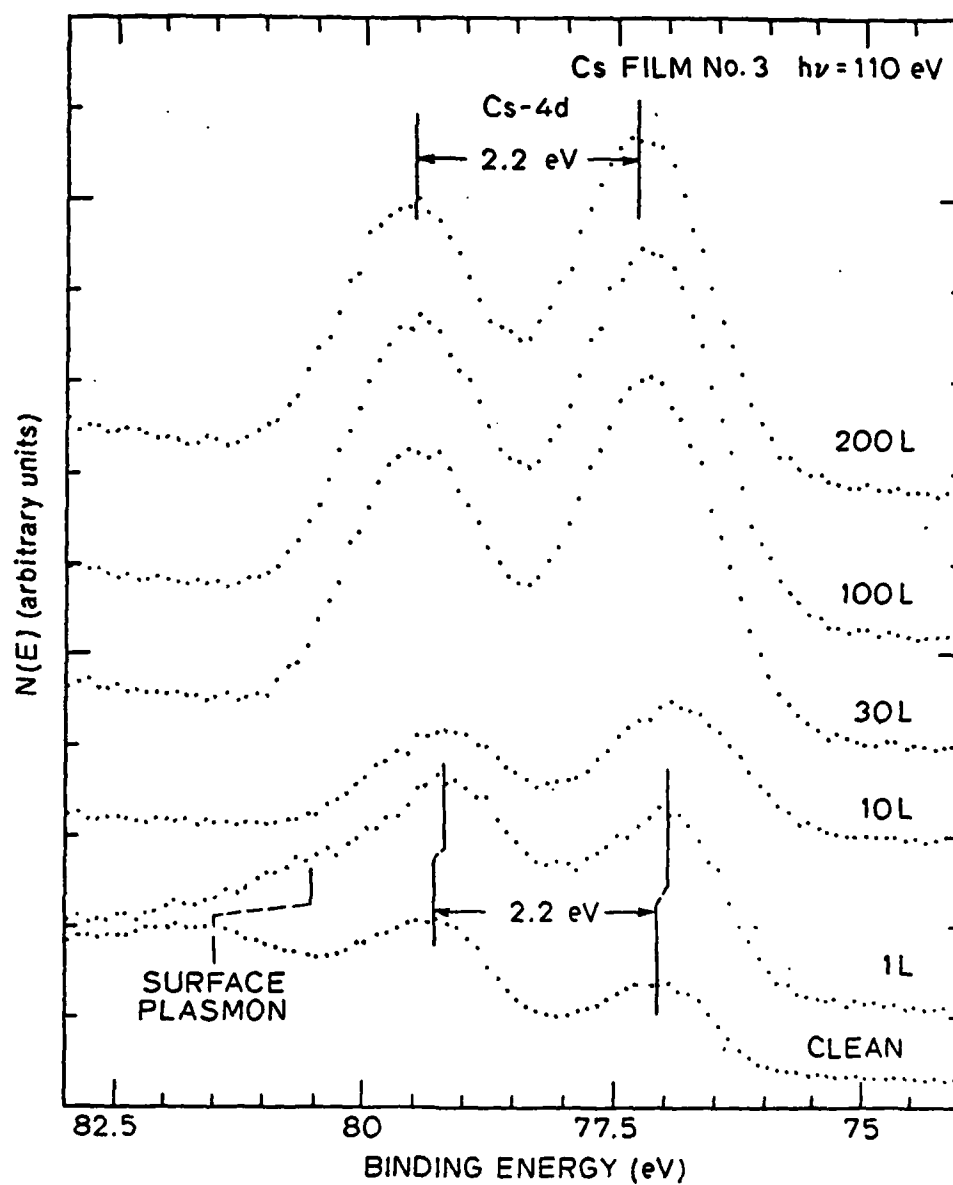


Figure 55: EDC's of the Cs-4d levels of the same surfaces of fig. 54 taken at $h\nu = 110$ eV.

The $N_{4.5}O_{2.5}O_{2.5}$ Auger transition gives a broad, featureless hump in the kinetic energy region of 35-47 eV. It does, however, exhibit some interesting shifts upon oxidation. We therefore display this transition at various oxygen exposures in fig. 56. The vertical bar under each curve indicates the energy position of the center of gravity of that curve. Positions of these bars are also entered in table 8. The N00 transition is seen to shift to 0.4 eV higher KE after 1 L exposure. We also observe the noticeable narrowing of this transition with increasing oxygen exposure up to 30 L, beyond which the width of the transition remains fixed. This narrowing is consistent with the decrease of spin-orbit splitting of the 5p levels upon oxidation.

An Auger parameter, defined as the difference between the binding energy of the initial core hole and the kinetic energy of the outgoing Auger electrons, can be obtained here despite the inaccuracy imposed by the broad width of the N00 transition. In this work, this is done by directly taking the kinetic energy difference between the $4d_{5/2}$ level excited with 120 eV photon and the N00 transition excited with 110 eV photon. The $4d_{5/2}$ electron excited with 120 eV photon is preferred because its kinetic energy is close to that of the N00 Auger electron excited by 110 eV, which, in turn, assures the same probing depth below the surface. The kinetic energy of $4d_{5/2}$ electrons excited by 110 eV photon and by 120 eV photon actually track each other very well, as shown in table 8. Despite the inaccuracy expected for the Auger parameters listed in table 8, a trend of change with oxidation can be seen: The Auger parameter at 1 L exposure is higher than the value of clean Cs, and those at higher exposures are lower than the value of clean Cs.

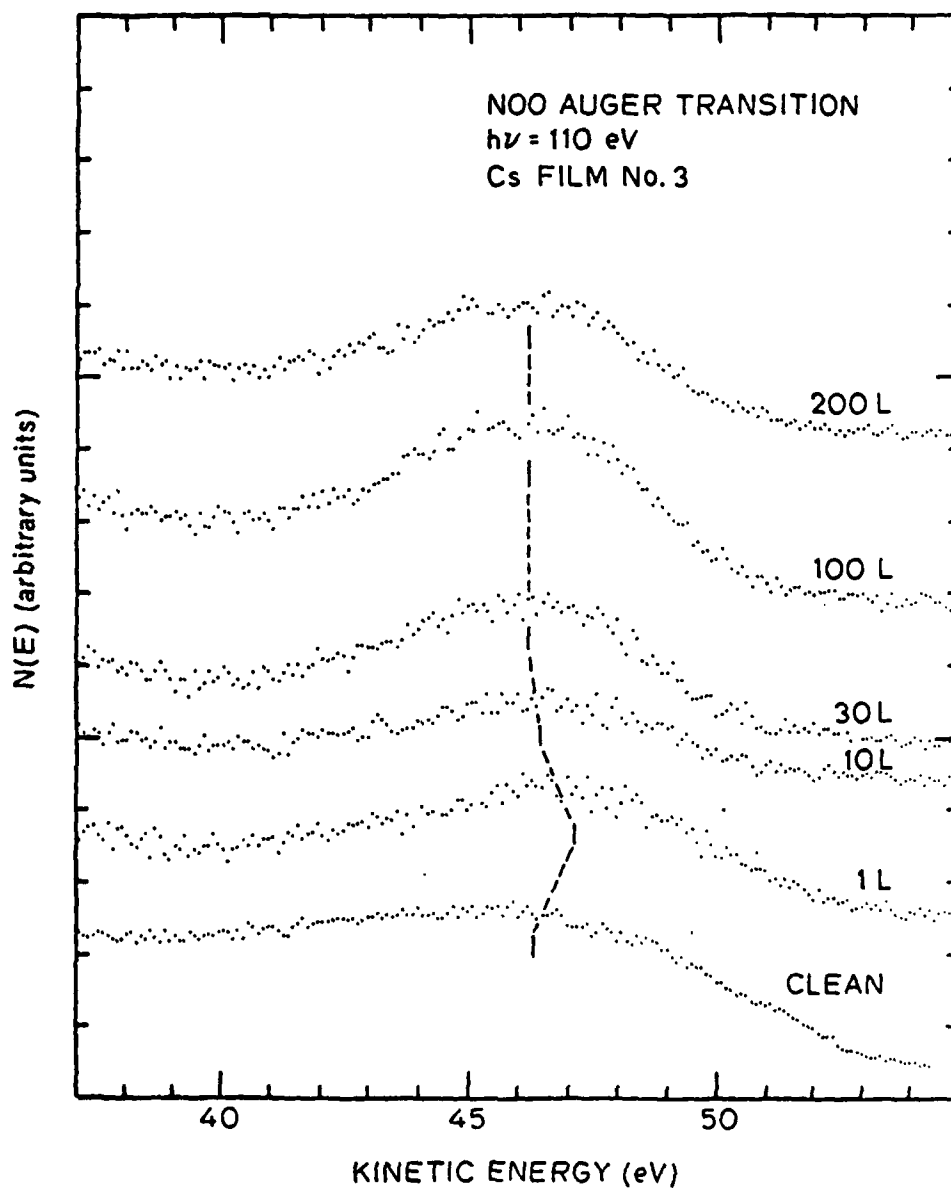


Figure 56: The NOO Auger transition of Cs film No.3 at various oxygen exposures. The vertical bar in each spectrum indicates the positions of the center of gravity of this peak.

The kinetic energy of the N00 Auger electrons is given by [25]

$$E_k(N00) = E_b(4d) - E_r(4d) - 2E_b(5p) + 4E_r(5p)$$

where $E_b(4d)$ and $E_b(5p)$ are the binding energies of the 4d and the 5p levels, respectively, and $E_r(4d)$ and $E_r(5p)$ are the core-hole relaxation energy of the 4d and the 5p levels, respectively. Assuming equal core-hole relaxation energies for the 4d and the 5p levels, the above equation becomes

$$E_k(N00) = E_b(4d) - E_b(5p) + 3E_r$$

and the change in the kinetic energy of the N00 electrons due to changes in the chemical environment is

$$\Delta E_k(N00) = \Delta E_b(4d) - \Delta E_b(5p) + 3\Delta E_r$$

The change in the kinetic energy of the 4d photoelectrons due changes in the chemical environment is given by

$$\Delta E_k(4d) = h\nu - \Delta E_b(4d) + \Delta E_r$$

The change in the Auger parameter can thus be expressed as

$$\Delta E(\text{Auger}) = \Delta E_k(4d) - \Delta E_k(N00) = 2(\Delta E_b(5p) - \Delta E_b(4d)) - 2\Delta E_r$$

Under the assumption of equal initial energy shifts for 4d and 5p levels upon changing of chemical environment, i.e., $\Delta E_b(4d) = \Delta E_b(5p)$, changes in the Auger parameter ($\Delta E(\text{Auger}) = -2\Delta E_r$) reflect changes in the extra-atomic relaxation energy for the core holes [25]. One would then tempt to conclude, based on table 8, that the extra-atomic relaxation energy increases (or at least it does not decrease) with 1 L oxygen exposure, at which point a mixture of state A oxygen and state B oxygen is present. Since state A brings reduction in the free electron density and state B shows insulating behavior (see discussion in 4.2 above), the free electron contribution to the extra-atomic relaxation energy has to

be replaced by a stronger ion core polarizability [25] to account for the increase in extra-atomic relaxation energy. Although such possibility cannot be ruled out, a simpler explanation in connection with our observation of unequal shifts in 4d and 5p levels is the breakdown of the assumption of equal initial state shifts in the two core levels. This latter proposal is reasonable if we recognize that the 5p electrons are in the outer shell of Cs^+ ion and may be subjected to a potential different from that felt by the 4d electrons. For example, Tsai et al [26], in their X-ray studies of the structure of Cs_2O , have found that the outer shell electrons of Cs^+ are highly polarized by the field produced by the O^{2-} ions toward the region between Cs^+ layers. The most intriguing clue in the present data leading to the suggestion of different potential felt by the 5p and the 4d electrons is that the 5p spin-orbit splitting decreases upon oxidation whereas the 4d splitting remains fixed at all oxygen exposures (fig. 54 and fig. 55). Since the spin-orbit splitting is determined by the intra-atomic interaction between the spin and the orbital angular momentum, a distortion of the spatial orbital causes changes in the orbital angular momentum which then change the spin-orbit splitting [27].

The OVV Auger Transition.

Another Auger transition, OVV, which involves the Cs-5p levels and the valence band of Cs, changes quite differently upon oxidation, when compared with the NDD transition. In fig. 57 we show changes in the OVV transition on both film No.1 and film No.2 when substantial amount of

TABLE 8

Changes in the binding energy of the $4d_{5/2}$ level and the N00 transition at different oxygen exposures.

Oxygen Exposure (L)	KE of $4d_{5/2}$ (eV)		KE of N00 (eV)	Auger Parameter
	$h\nu=110$ eV	$h\nu=120$ eV		
0 (clean)	32.8	42.8	46.3	3.5
1	33.0	43.2	47.1	3.9
10	33.0	43.0	46.4	3.4
30	32.9	42.9	46.2	3.3
100	32.9	42.9	46.2	3.3
200	32.9	42.9	46.2	3.3

state A oxygen is observed. At higher exposures when state A is no longer observed in the valence band region spectra, the OVV transition disappears completely (fig. 50), as would be expected from the disappearance of the metallic valence band. The 5p levels are also included in fig. 57 for reference. On film No.1 the 5p levels are smeared at 2 L exposure, so are the shifted OVV transitions. Shift of the OVV transitions to lower kinetic energy, however, is discernable. On film No.2 the major strength of the 5p levels have shifted to lower BE at 1 L exposure, hence two shifted OVV can clearly be identified. The shift is 1.4 eV to lower kinetic energy.

The change in the kinetic energy of the OVV Auger electrons upon changing of chemical environment of the Cs atoms, in analogy to the analyses given above for the N00 transition, can be expressed as

$$\Delta E_k(0VV) = \Delta E_b(5p) - \Delta E_r(5p) - 2\Delta E_b(6s) + 4\Delta E_r(6s)$$

Since the initial state energy of the valence electrons of Cs (Cs-6s) does not change upon adsorption of state A oxygen (figs. 46 and 47), i.e., $\Delta E_b(6s)=0$, the above equation becomes*

$$\Delta E_k(0VV) = \Delta E_b(5p) - \Delta E_r(5p) + 4\Delta E_r(6s)$$

We have measured $\Delta E_k(0VV) = -1.4$ eV and $\Delta E_b(5p) - \Delta E_r(5p) = -0.6$ eV, therefore we have $\Delta E_r(6s) = -0.2$ eV, i.e., the relaxation energy for an valence hole is reduced by 0.2 eV after ~1 L oxygen exposure. Since the relaxation energy for valence holes comes mainly from free electrons in Cs, its reduction is expected to accompany the reduction of free-electron density upon oxidation.

As mentioned earlier, the proper identities of the 10.4 eV (C3) and the 10.7 eV (D5) BE peaks on the low BE side of the Cs-5p levels are arrived at through comparison of 5p and 5s spectra taken with high energy photons. As can be seen in fig. 52, a shoulder appears on the low BE side of the $5p_{3/2}$ level at an energy position of ~10.5 eV BE in the 30 L spectrum, and a more pronounced feature at 10.7 eV BE also appears in the spectra of 100 L and 200 L exposures. No such shoulder, however, can be found in the corresponding spectra of the 5s level (fig. 53). This suggests that the 10.5 eV and the 10.7 eV BE features are oxygen levels rather than shifted Cs-5p levels.

*We did not consider interatomic Auger transition between Cs and O, the kinetic energy of such Auger transition is estimated to be at least 4 eV lower than that of the 0VV and hence would be too close to the low energy cutoff to be observed.

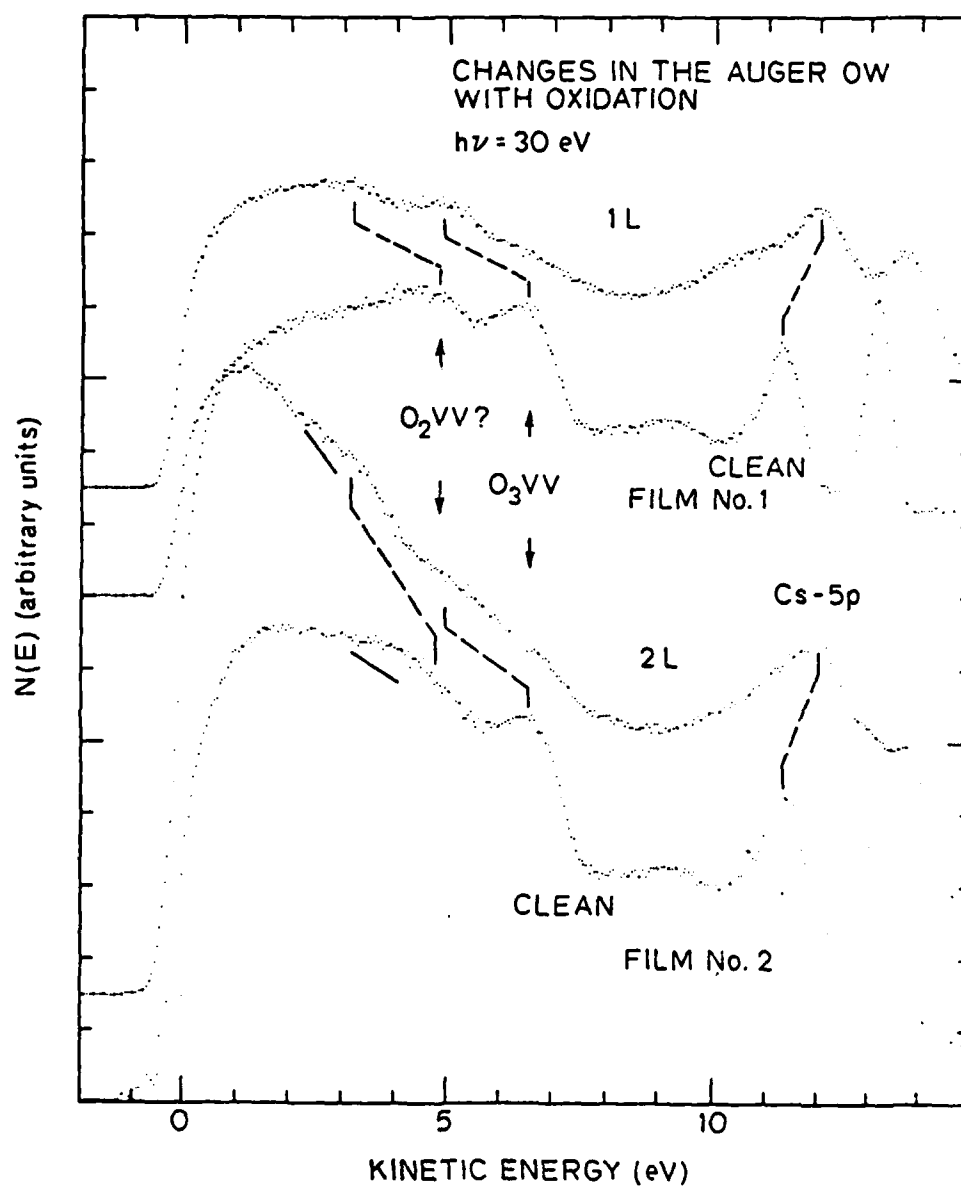


Figure 57: Changes in the OVV Auger transitions at low oxygen exposures. The Cs-5p levels are also included. We notice that the OVV transition and the 5p's shifted in the opposite direction after the oxygen exposures.

In fig. 54, O-2s is found at 19.4 eV BE throughout the whole exposure sequence. Whether state A gives a different O-2s level in the 1 L spectrum cannot be determined unambiguously because of the poor signal to noise ratio in that region. The O-2s level can also be seen in 30 eV spectra (fig. 50), but is obscured by the secondary tail so no accurate BE can be obtained there either.

4.5 RESULTS AND DISCUSSION - IDENTIFICATION OF THE OXYGEN SPECIES ADSORBED IN CS

The summary of oxygen induced features given in table 7 appears to be very complicated, as can be expected from the complicated Cs-O phase diagram. On the other hand, a rather simple picture of the sequence of oxygen states in table 7 emerges from examining the phase diagram. In table 4, we listed the known Cs-O compounds in the phase diagram together with the shortest O-O distance in each case.

The last column of table 9 suggests a simple picture: suboxides, Cs_7O , Cs_4O , Cs_{11}O_3 , Cs_3O , and the oxide Cs_2O , contain O^{2-} ions, the peroxide, Cs_2O_2 , contains O_2^{2-} ions, the sesquioxide, Cs_2O_3 , contains a mixture of O_2^{2-} and O_2^- ions, and the super oxide, CsO_2 contains O_2^- ions. Although in our experimental condition, formation of stoichiometric compounds with long range order such as those listed in table 9 may not be expected, an oxidation sequence with oxygen incorporated in surroundings locally similar to the structures of those compounds is very likely to occur. We therefore expect to obtain a series of spectra in our studies that are related to the various ionic species of oxygen; such correspondence between the oxygen adsorbed in Cs and various free-

TABLE 9

The nearest O-O distance in Cs-O compounds (a)

Compound	O-O distance (Å)	Oxygen Species
Cs ₇ O	3.92(b)	O ⁻²
Cs ₄ O	4.06	O ⁻²
Cs ₁₁ O ₃	4.04(b)	O ⁻²
Cs ₃ O		
Cs ₂ O	4.256	O ⁻²
Cs ₂ O ₂	1.49(c)	O ₂ ⁻² (c)
Cs ₄ O ₆	1.29(d)	2 O ₂ ⁻ + 1 O ₂ ⁻² . (d, f)
CsO ₂	1.29(e)	O ₂ ⁻ (d, f)

(a) Values without a reference are from Wyckoff [28]. (b) Ref. 8.

(c) Ref. 29. (d) Ref. 30. (e) Ref. 31.

(f) Confirmed by
magnetic measurements.

ion species of oxygen will be examined below in two separate steps: We will first compare the energy separations of the multiple features of each state in table 7 with the energy separations of the multiplets of an individual oxygen species (section 5.1), and then we will attempt to relate the binding energy of the lowest BE feature of a state to the first ionization energy of a corresponding oxygen species (section 5.2).

4.5.1 Multiplet structure

In fig. 58, we give the multiplet structures expected for ionizing, from top to bottom, O^{-2} , O_2^{-2} , and O_2^- . The energy position of the leading peak in each case is assigned as the energy zero, because only the energy separations will be compared with measured spectra. The relative height of the multiplets of an oxygen species indicated in fig. 58 is simply based on the spin-orbit degeneracy of the individual multiplets. The degeneracies are true measure of the relative intensity of these multiplets in a photoemission spectrum only when the ionization probabilities of all orbitals are equal.

In fig. 58, we have also indicated (with heavy short bars) the energy positions of the multiplets of three experimentally observed states: state A is compared to O^{-2} , state B is compared to O_2^{-2} , and state D is compared to O_2^- .

As has been discussed in detail in the last section, state A oxygen gives a single peak in the photoemission spectrum when the $O-2p$ subshell is photoionized. (The 4.4 eV and the 5.7 eV BE features in table 7 are plasmon losses.) The O^{-2} ion has a close shell configuration and gives a single peak when ionized (ignoring the very small spin-orbit splitting). The O^{-2} ion is the only oxygen species that gives a single peak in the photoemission spectrum when the $O-2p$ subshell is photoionized, hence it is identified with the state A oxygen adsorbed in Cs. (Neutral O atom gives three multiplets at ionization energies 2.4 eV, 4.25 eV, and 7.4 eV with an intensity ratio of 1:3.5:3 [32]; the O^- ion also gives three multiplets at ionization energies 1.5 eV, 3.5 eV, and 5.7 eV with an intensity ratio of 9:5:1.)

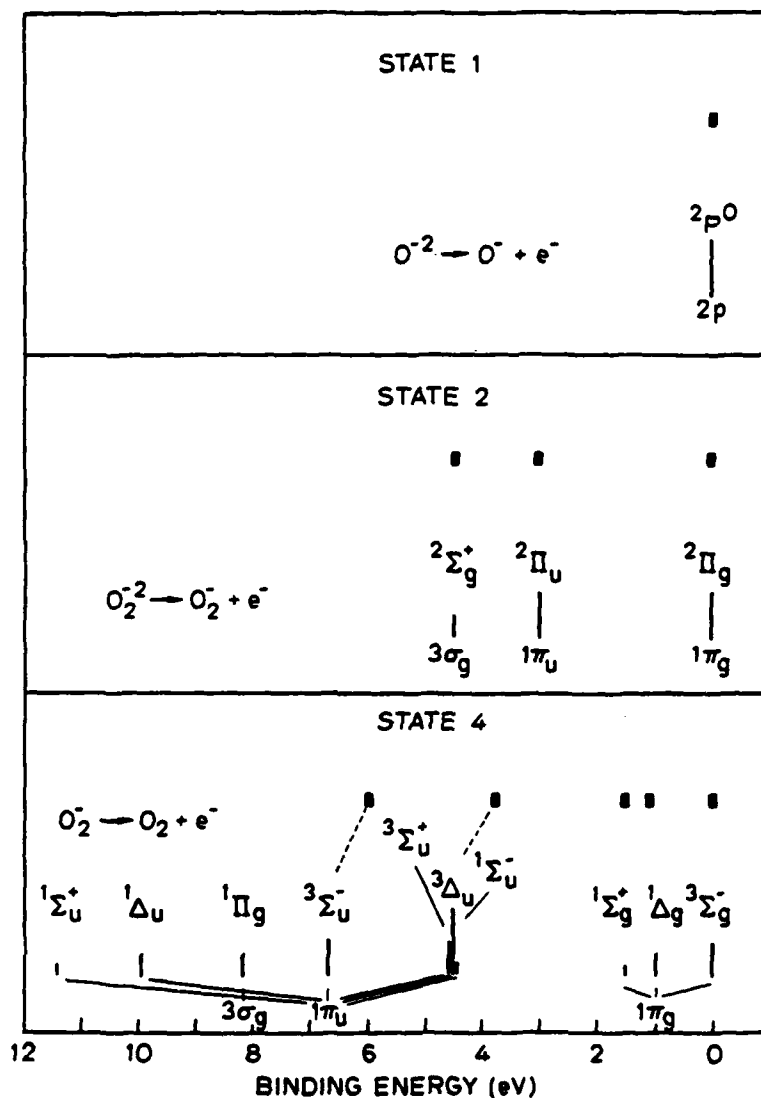


Figure 58: Comparison of the multiplet structures of free (thin lines) and adsorbed (short bars) oxygen species: O^{-2} with state A (top), O_2^{-2} with state B (center), and O_2^- with state D (bottom). Only energy separations are compared; in each case, the energy zero is chosen to be the energy position of the leading oxygen multiplet. Designation of the multiplets are indicated on top of the thin vertical lines, and the molecular orbital origin of each multiplet is also indicated below the lines.

A few words of explanation of the origins of the multiplets, and of the sources of information of the energy separations of the O_2^{-2} and the O_2^- ions will be given before evaluating their relations to state B and state D oxygen.

Since the O_2^{-2} ion has the close shell configuration $1\pi_u^4 3\sigma_g^2 1\pi_g^4$, it gives three features in the photoemission spectrum corresponding to ionizing the $3\sigma_g$ (leading to the $^2\Sigma_g^+$ multiplet), the $1\pi_u$ (leading to the $^2\Pi_u$ multiplet), and the $1\pi_g$ (leading to the $^2\Pi_g$ multiplet) orbitals. Energies of these multiplets given in fig. 58 are those calculated by Krauss et al [34] for O_2^- (the final state of the ionization process, $O_2^{-2} \rightarrow O_2^- + e^-$) using MCSCF method, which had also been included in the theoretical-experimental data compiled by Krupenie [34]. Other multiplets of O_2^- which arise from, for example, the configuration $1\pi_u^4 3\sigma_g^2 1\pi_g^2 3\sigma_u$, are not included in fig. 58. Such excited states of O_2^- are arrived at by ejection of one photoelectron and simultaneous excitation of another electron into the empty $3\sigma_g$ orbital; this type of process has low probability to occur and has been neglected in preparing fig. 58.

The energy positions of the multiplets of O_2 (the final state of the ionization process $O_2^- \rightarrow O_2 + e^-$) in fig. 57 was obtained from potential curves compiled by Krupenie [35] at an O-O distance of 1.30 Å; more recent GVB-CI calculations of Moss and Goddard [36] give values in close agreement with the compilation of Krupenie. The molecular orbitals from which the multiplets are originated are also indicated in fig. 58. Ionization of an $1\pi_g$ electron gives the $^3\Sigma_g^-$, $^1\Sigma_g^+$ and the $^1\Delta_g$ multi-

plets of the configuration $3\sigma_g^2 1\pi_u^1 1\pi_g^2$, of an $1\pi_u$ electron gives the $^1\Sigma_u^-$, the $^3\Delta_u$, the $^3\Sigma_u^+$, the $^3\Sigma_u^-$, the $^1\Delta_u$, and the $^1\Sigma_u^+$ multiplets of the configuration $3\sigma_g^2 1\pi_u^3 1\pi_g^3$, and of an $3\sigma_g$ electron gives the $^1\Pi_g$ multiplet (value for the $^3\Pi_g$ not available) of the configuration $3\sigma_g 1\pi_u^1 1\pi_g^3$.

We immediately see in the center panel of fig. 58 that an excellent agreement exists between the multiplet splitting of state B and those of the O_2^{-2} ion. In the bottom panel of fig. 58, we recognize the remarkable agreement in energy separations between the three leading peaks of state D and the three multiplets produced by ionizing the $1\pi_g$ orbital of O_2^- . The relative intensity of the three leading peaks of state D is also reasonably close to that given by the spin-orbit degeneracies of $^3\Sigma_g^-$, $^1\Delta_g$, and $^1\Sigma_g^+$. Multiplets $^1\Sigma_u^-$, $^3\Delta_u$, and $^3\Sigma_u^+$ are distributed within 0.33 eV and centered at 4.5 eV below the $^3\Sigma_g^-$ state; they can be related to the 8.7 eV BE peak (4.0 eV below the leading peak) of state D. The $^3\Sigma_u^-$ multiplet (6.7 eV below $^3\Sigma_g^-$) can be related to the 10.7 eV peak (6.0 eV below the leading peak) of state D. Multiplets $^1\Pi_g$, $^1\Delta_u$, and $^1\Sigma_u^+$, if occur in the spectrum of state 4, are degenerate with the Cs-5p levels and cannot be directly observed. A hint of the existence of these multiplets in the spectrum of state D, however, is given by the reversal of the relative height of the two 5p peaks as mentioned earlier (fig. 51). Overall, the identification of state D with O_2^- is well justified.

The nearly perfect agreement between the multiplet splittings of free O_2^{-2} and sorbed O_2^{-2} suggests that little differential relaxation has occurred for different molecular orbitals when inserting O_2^{-2} into a

solid state environment. This is believed to be due to the close-shell configuration of O_2^{-2} . Since all three molecular orbitals $3\sigma_g$, $1\pi_u$, and $1\pi_g$ are fully occupied, little interaction of these orbitals with the solid environment is expected. In contrast to the case of O_2^{-2} , significant differential relaxation of the multiplets of the O_2^- ion is observed when inserting O_2^- into solids (the bottom panel, fig. 58). This differential relaxation can be related to the open shell configuration of the O_2^- ion.

So far, the state C oxygen has not been associated with a particular oxygen species. Since state C appears at exposures intermediate to those required to produce state B (O_2^{-2} .) and state D (O_2^-), it might be related to Cs_2O_3 which table 9 has suggested to contain a mixture of O_2^{-2} and O_2^- ions. The presence of the 5.5 eV peak and the absence of the three leading peaks of state D in the spectrum of state C, however, prohibit the interpretation of state C being a mixture of O_2^{-2} and O_2^- . It is therefore interesting to re-examine the assignment of the oxygen species in Cs_2O_3 . In the work of Helms and Klemm [31] on the sesquioxide, although the measured magnetic susceptibility can well be explained by 2 O_2^- and 1 O_2^{-2} in the $Cs_4(O_2)_3$ formulae-unit, the structural study has shown O_2^- and O_2^{-2} to be geometrically equivalent. O_2^- and O_2^{-2} ions are known to have significantly different sizes: when the size is measured in terms of a rotational ellipsoid enclosing the $(O-O)^{-n}$ ion, O_2^- has a 2.02 Å long axis and a 1.51 Å short axis, and O_2^{-2} has a 2.56 Å long axis and a 1.67 Å short axis [31]. Such difference in size appears to be suppressed in the crystal lattice of Cs_2O_3 , so that no special site can be identified for either O_2^- or O_2^{-2} . It is therefore

not inconceivable that the oxygen species in Cs_4O_6 is also indistinguishable electronic-structure-wise and can be described by an average-of-configuration of O_2^{-t} , with t being a non-integral value between 1 and 2. An oxygen species with such an electronic structure is consistent with our data and we suggest it to be the identity of state C..

Overall we have seen in this subsection that the oxygen states observed in the oxidation of Cs films, with the exception of state C, can be well understood in terms of the multiplet structures of free oxygen ions. This demonstrates that the multiplet splitting, which is caused by the photoionization process, is not suppressed in a solid state environment.

4.5.2 The Binding Energies and the Ionization Energies

The comparison made in the previous subsection between free oxygen ions and oxygen species in solids were based on energy separations between different multiplets. A semiquantitative comparison of the absolute binding energies can also be made. In this subsection we will attempt to predict the binding energies of the highest lying levels of state A, B, and D from the first ionization energies of O^{-2} , O_2^{-2} , and O_2^- . Such attempt not only facilitates better identification of the oxygen species but also helps understand the binding force in cesium oxides.

The general equation

The binding energy of an electron on an ion in a solid, E_x , is related to the ionization energy of a free ion, E_{fi} , as

$$E_x = E_{fi} + E_b - E_r \quad (1)$$

E_r in eq.(1) is the extra-atomic relaxation energy introduced by the photoionization process in a solid, as has been discussed in 4.3 in conjunction with the Auger transitions. E_b in eq.(1) is the additional binding energy introduced by the solid state environment to the electron under consideration. To compare the calculated values with our measured binding energy referring to the Fermi level, eq.(1) has to be corrected for the work function, ϕ , of the solid in question.

$$E_{fx} = E_{fi} + E_b - E_r - \phi \quad (2)$$

In a pure ionic solid, E_b is mainly electrostatic:

$$E_b = \sum q_c / r_{oc} + \sum \sigma_c(r_{oc}) N_c \quad (3)$$

The first term on the right of eq.(3) is the lattice (Madelung) potential produced by all other ions in the crystal at the ion site in consideration. The second term on the right is the overlap repulsion energy between ions; it is generally an order of magnitude smaller than the lattice potential term [37] and will be neglected in our consideration, (i.e., we will use a point-charge approximation).

In the cases of an impurity ion dissolved in Cs metal, the change in kinetic, exchange and correlation energy of the free electron gas due to the renormalization of charge density around the negatively charged O^{-2} ion should be included in E_b '.

$$E_b = \sum q_c / r_{oc} + \mu_1 + \mu_2 \quad (4)$$

where μ_1 is the energy of inserting a negative charge from vacuum into the solid and μ_2 is the renormalization of the free electron gas in response to the negative charge. The relaxation energy in a metal, E_r , is essentially the change in kinetic, exchange and correlation energy due to a delocalized hole [38]. Since the integrated screening charge in the free electron gas due to the presence of O^{-2} has to be equal to 2, the change in energy due to renormalization of charge density can be regarded as the same as the relaxation energy for two delocalized holes. Hence, we take, for the purpose of estimate, $\mu_1 + \mu_2 = 2E_r$, and eq.(2) becomes

$$E_{fx} = E_{fi} + \sum q_c/r_{oc} + E_r - \frac{1}{2} \quad (5)$$

Eq.(5) is essentially identical to that derived by Helms and Spicer [39] through a more careful enumeration of the various energy terms involved. (Here we will neglect a small surface dipole term about 0.14 eV.)

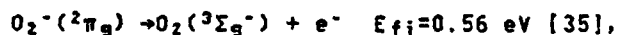
The lattice potential

To calculate the lattice potential term, knowledge of the lattice containing each of the O^{-2} , the O_2^{-2} , and the O_2^- ions is necessary. As stated in the beginning of this section, although the formation of crystalline oxides is not expected in our experimental condition, the local structure surrounding each type of oxygen ion is likely to be similar to that in the corresponding crystalline oxide. Thus in table 10 we have used the crystal structure of Cs_2O_2 and CsO_2 to calculate the lattice potential term for O_2^{-2} and O_2^- , respectively. For the O^{-2} ion we will consider three different cases: (1) O^{-2} as an impurity in Cs and occupying octohedral sites, (2) O^{-2} as impurity in Cs but existing in a $Cs_{11}O_3$

cluster which contains three octahedrons in close contact and has been suggested by Simon et al [8] to be the building unit for all Cs suboxides, and (3) O^{-2} in Cs_2O . All the three cases should lead to the same BE for the O^{-2} ion, because Simon et al [8] have found only one BE (2.7 eV) for the $O-2p$ level in two suboxides ($Cs_{11}O_3$ and Cs_7O) and the mono oxide Cs_2O .

In the case of an oxygen ion being dissolved in bulk Cs, the lattice potential in eq.(4) is simply the potential due to a cluster of positive ions surrounding the negative oxygen ion. The charges on the positive ion in the cluster are assigned in the way outlined by Helms and Spicer [39]. The lattice potential for Cs_2O , Cs_2O_2 , and Cs_2O_4 are calculated with an semi-empirical equation derived by Broughton and Bagus [40]. The calculated lattice potential energies are entered in the 4th row of table 10.

Values of work function listed in table 5 are from ref. 9. The free ion energies are obtained from the following ionization processes:



and

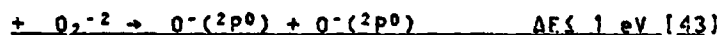


TABLE 10

Comparison of calculated and measured BE of oxygen levels of various oxygen species in Cs

Oxygen Species	O ⁻²	O ⁻²	O ⁻²	O ₂ ⁻²	O ₂ ⁻
Compound or cluster	Cs ₆ O in Cs	Cs ₁₁ O ₃ in Cs	Cs ₂ O	Cs ₂ O ₂	CsO ₂
E _{fi}	-6.5	-6.5	-6.5	-1.6	0.56
Φ	2.0	2.0	0.8	2.0	2.0
Lattice Potential	10.07	8.86	7.84	8.33	7.71
E' _{fx} (eq.6)	1.57	0.36	0.54	4.73	6.27
Other Binding Contribution	4.18	4.18	4.20	0	0
E _r	2.09	2.09	2.10	1.53	1.42
E _{fx}	3.66	2.45	2.64	3.20	4.85
E _{exp}	2.7	2.7	2.7	3.3	4.7

In order to see the relative importance of the different binding energy terms in eq.(1), we have first calculated the binding energy including only the lattice potential term in E_b, and not including the relaxation term E_r in eq.(2), i.e.

$$E'_{fx} = E_{fi} + \sum q_c/r_{oc} - \Phi \quad (6)$$

and the results are listed in table 10.

Eq.(6) should always predict a binding energy higher than the measured value if Madelung energy is the principal contributor to the binding

energy of the oxygen species in question. However, when the values of the E'_{fx} 's in table 10 are compared to the measured values, we clearly distinguish two cases. For Cs_6O , $Cs_{11}O_3$ clusters and Cs_2O , the calculated values are lower than the measured values, whereas the opposite is true for Cs_2O_2 and Cs_2O_4 . In the case of Cs_2O_2 and Cs_2O_4 , we also notice that the difference between the calculated values and the measured values is close to the typical value of relaxation energy found in ionic solids [44,45]. For the case of O^{-2} in Cs, inclusion of a relaxation term according to eq.(2) would result in unphysically low binding energies. Obviously this means that Madelung energy alone is not sufficient to stabilize the O^{-2} ion. Other important binding energy terms have to be included. For the cases of Cs_6O and $Cs_{11}O_3$ clusters in Cs, the extra binding energy term comes from the response of the free electron gas to the O^{-2} impurity, as discussed above in introducing eq.(5). Cs_2O is insulating in the sense that all available valence charges are localized on oxygen, hence the free electron contribution to the binding energy is not important. The polarization of Cs-5p electrons reported by Tsai et al [26], which we have discussed in subsection 4.3, gives an increase in the binding energy of the valence electrons on O^{-2} ions, i.e., the polarization introduces an additional term in E_b . Hence we rewrite eq.(4) as

$$E_b = \sum q_c/r_{oc} + E_{po}\epsilon d l. \quad (7)$$

The same polarizability of Cs-5p electrons should also be the major contributor to the extra-atomic relaxation energy, hence in analogy with eq.(5) we have $E_{po}\epsilon d l. \approx 2E_r$ and

$$E_{fx} = E_{fi} + \sum q_c/r_{oc} + E_r - \frac{1}{2} \quad (8)$$

The relaxation energy

We now proceed to calculate the term E_r the various cases considered in table 10.

For the cases of Cs_6O and Cs_{11}O_3 clusters in Cs, the extra atomic relaxation is essentially that of pure Cs. The term E_r of Cs can be determined by the difference in ionization energy between Cs atom and Cs metal according to

$$E_i(\text{metal}) = E_i(\text{atom}) + E_c - E_r \quad (9)$$

where E_c is the cohesive energy per atom of Cs metal (0.827 eV [46]). Eq.5 is in analogy with eq.1. The ionization energy of atomic Cs is 3.893 eV [42]. The ionization energy of metal is defined as

$$E_i(\text{metal}) = \phi + 2/5 (E_0 - E_f) \quad (10)$$

where ϕ is the work function of Cs (2.0 eV [9]), and $(E_0 - E_f)$ is the width of the valence band of Cs (1.58 eV). $2/5(E_0 - E_f)$ is the position of the center of gravity of the valence band referring to the Fermi level. Thus we have $E_r = 2.09$ eV. When the correction of E_r is made according to eq.(5), a more reasonable BE of 3.66 eV and 2.5 eV are obtained for the Cs_6O cluster. For comparison with the lattice potential term and the relaxation energy term, we have also listed $\mu_1 + \mu_2 = 2E_r$ in table 10 under the entry of 'other binding contribution'. The apparent better agreement between the calculated and the measured BE's of the Cs_{11}O_3 cluster does not necessarily imply that it describes the reality better than the Cs_6O cluster does, considering the approximations involved. Better theoretical considerations are required to resolve this uncertainty.

The relaxation energy in Cs_2O_2 and Cs_2O_4 were estimated according to a classical electrostatic treatment of Jost [47], who modeled the hole as a spherical cavity of radius R in a continuous medium of high frequency dielectric constant κ_0 , and found the polarization energy to be

$$E_p = \frac{1}{2} \cdot e^2 / R \cdot [1 - (1/\kappa_0)] \quad (11)$$

in which e is the electron charge, and R is the effective hole radius. R has been found [45,47] to be $0.9 a$ (a is the nearest neighbor distance) for hole on an anion site. The κ_0 's are calculated to be 2.17 and 1.96 for Cs_2O_2 and Cs_2O_4 respectively [43]. The shortest Cs-O distance is 2.95 \AA for both Cs_2O_2 and Cs_2O_4 . The resulting E_p 's are listed in table 4 under the entry for E_r . Substituting the E_r 's in eq. 1 yield binding energies which are rather too close to the measured values. We notice that no 'other binding contribution' is needed for either Cs_2O_2 or CsO_2 .

The value of E_r for Cs_2O again can be estimated using eq.(11) with a measured κ_0 of 4 [49]. The result of 2.1 eV brings a close agreement between the calculated and the measured BE.

For all cases considered here, the calculated values can be easily compared to the experimental results in the last two rows of table 10. The agreement is surprisingly good, considering all the approximations involved. The additional support rendered by table 10 to the interpretation that state A being O^{2-} , state B being O_2^{2-} , and state D being O_2^- , is gratifying.

Some Other Implications

The above simple calculation also gives a basis for speculating about the possible connections between the following observations:

- i) The binding energy of the O-2p level of the O^{-2} ion references to the Fermi level is the same (2.7 eV) whether in Cs metal (this work and Gregory [9]) or in suboxides (Cs_7O and $Cs_{11}O_3$) or in Cs_2O [8]. In Cs_2O , an oxygen level broader than that observed in suboxides has been observed by Simon et. al. [8]; the broadening cannot be explained by O-O overlap, because the O-O distance is larger in Cs_2O than in $Cs_{11}O_3$ and other suboxides (table 9).
- ii) The values of work function of the cesium suboxides are known to be lower than that of Cs, and the lowest work function has been suggested to occur on the Cs rich side of Cs_2O [8,9]. The decrease in work function, going from Cs to Cs suboxides containing $Cs_{11}O_3$ clusters, has been suggested by Burt and Heine [50] to be due to the confinement of free electrons by the repulsive potential of clusters of O^{-2} ions.
- iii) Clark [51] has predicted that, with increasing oxygen concentration in CsO_x , a Mott transition occurs at $x \approx 0.43$ (i.e., $Cs_{2.10}$).

We notice that in our calculation of the Cs_6O and $Cs_{11}O_3$ clusters in Cs, the terms E_F and ϕ in eq.(5) nearly cancel each other. The free electron contribution in E_F and ϕ actually have the same origin [38]. As

the concentration of O^{-2} increases, we expect both work function and the relaxation energy to decrease due to a reduction of the free electron density; the changes, however, cancel each other in eq. 4 so that O^{-2} ions would be stabilized to the same extent with respect to the Fermi level if the point-charge-cluster representing the adsorption complex remains the same. This picture appeared to connect points (i) and (ii) above, but it cannot be readily extended to higher oxygen concentration up to Cs_2O -- our calculation shows that in Cs_2O the term E_F (2.1 eV) does not cancel the work function term ϕ (0.8 eV) in eq.(8). The fact that the valence electrons on the O^{-2} ions are still stabilized to the same extent with respect to the Fermi level as are those of the O^{-2} ion dissolved in Cs, is due to a smaller lattice potential term for Cs_2O than that for $Cs_{11}O_3$ clusters in Cs (table 10). The decrease in the lattice potential term with increasing oxygen concentration in Cs may not be accidental. In our approximation of the electrostatic interaction between the negatively charged O^{-2} and the renormalized electron of Cs, we have replaced the exact charge density surrounding O^{-2} with a point-charge-cluster. When an impurity carrying a point charge $-Z$ is introduced into a free electron gas, the electrons are perturbed to produce a change in charge density [52]:

$$\rho(r) = Ze/r \cdot \exp(-kr)$$

The electrostatic energy at the impurity site is simply

$$\int \rho(r)/r \, dv = Ze^2/2 \int 4\pi \exp(-kr) dr = Ze/[2(1/k)]$$

Thus the electrostatic energy at the impurity site can simply be accounted for by positioning Ze positive charge on an "impurity sphere" of radius $2(1/k)$. Since the screening length k^{-1} increases with

decreasing free electron density, the Madelung energy of the point charge-cluster decreases when the concentration of O^{-2} becomes higher. This destabilizes the valence electrons on O^{-2} with respect to the Fermi level, hence the valence electrons become relatively delocalized. The delocalization would then give rise to a polarization energy, e. g. through distortion of the Cs-5p levels (which is the essence of a polaron), which stops the valence electrons from further delocalization. The work function measures the energy required to move an electron at the Fermi level to infinity, and hence it is determined by the properties of the free electrons in the system. The E_F term, which contains both free electron and polarization contribution, does not cancel the work function term in eq.(8). The difference between the two terms compensates the decrease in Madelung energy.

The polarization contribution to the E_F term reaches a maximum in Cs_2O , as does the delocalization of the valence electrons on the O^{-2} ions. This can be understood as if the average free-electron-character of the valence charges on O^{-2} is increased by freezing more free electrons onto O^{-2} . This point has been verified by Clark [51] in a more rigorous way: The radius of the polaron in Cs_2O is found to be 5.9 Å [51], which is greater than the Cs-Cs distance of 4.19 Å and the O-O distance of 4.26 Å, indicating the polarons are rather extended. Such delocalization of the valence electrons on O^{-2} implies a broadened oxygen level in the photoelectron spectrum of Cs_2O , as has been observed by Simon et al [8] on standard Cs_2O compound. The residual free electron character of the valence electron on O^{-2} suggests that the broadening may extend up to the Fermi level.

As stated earlier, the decrease in work function with increasing concentration of O^{2-} in Cs is determined by the change in the properties of the free electron in the system. At low concentration of O^{2-} (i.e., when an impurity picture apply), the decrease in work function with increasing O^{2-} concentration can be understood in terms of decreasing free electron density [38]. At higher concentration of O^{2-} (such that formation of suboxides with definite structure occurs), the picture of confinement of free electrons may apply [50]. In the latter picture, it is not surprising to see the point of minimum work function coincides with the point of Mott transition at approximately Cs_2O . Because a Mott transition occurs when the free electrons become localized, i.e., the confinement of free electrons reaches a maximum. This maximum confinement of free electrons in Cs_2O is reflected in our calculation in the full replacement of the free electron contribution to E_F by the polarization contribution.

4.6 THE OXIDATION PROCESS

Having identified the adsorbed oxygen species, a brief discussion of the actual oxidation mechanism follows.

From the phase diagram one expects the oxidation to proceed from the formation of suboxides to the formation of peroxides as the oxygen exposure increases. On the other hand, the adsorption of O^{2-} ions requires the dissociation of oxygen molecules, and it is not obvious that this should occur before the non-dissociative adsorption of O_2^{2-} or O_2^- ions. Our observation of the adsorption of O^{2-} ions prior to the O_2^{2-} and O_2^- ions therefore suggests that clean Cs is capable of removing or lowering

considerably the activation barrier of dissociating oxygen molecules. This is not surprising because of the easiness of transferring electrons from Cs to oxygen. The dissociated oxygen is dissolved in Cs as O^{-2} . The concentration of O^{-2} , however, is probably limited to a very narrow range, as will be discussed below. The O^{-2} ions did not go deep into the bulk of Cs because of their limited mobility at low temperatures ($\sim 160^\circ K$). The only possible driving force for O^{-2} to move farther than one or two layers below surface is a build-up of O^{-2} concentration in this region. The supply of O^{-2} ions, however, is cut off at increased oxygen exposure, because the capability of the Cs surface to dissociate oxygen molecules is gradually lost (due to loss of free electrons) when a concentration of O^{-2} ions is built up within the first few layers below the surface. This concentration may saturate far before turning the region occupied by O^{-2} into Cs_2O (the upper limit for the existence of O^{-2}), because the charge supply at the surface required for the formation of O_2^{-2} ions (the second oxygen species in the observed oxidation sequence) would be greatly impeded by an insulting layer of Cs_2O . Although a limited amount of charge may be made available through the space charge region in Cs_2O , physisorption of O_2 or adsorption of O_2^- would be more favorable than adsorption of O_2^{-2} under such condition. Thus the adsorption of O_2^{-2} commences before the free electron density in the surface region is reduced to zero, but after it is reduced substantially so that the dissociative sorption of O^{-2} is no longer competing effectively. This suggestion is consistent with the preservation of metallic character even after a mixture of about equal amount of O_2^{-2} is observed (fig. 47, the I L spectrum), although this can also be interpreted as due to inhomogeneity of the Cs film. Heimann et al [49], in

their microbalance mass study of the oxidation of Cs, have found that Cs_2O does not form through direct oxidation of Cs. Instead, they found the formation of Cs_2O_2 and Cs_2O_4 in two steps. A narrow range of suboxide formation or O^{2-} dissolution in the initial stage of oxidation would certainly escape the detection of mass measurement. Hence the results of Heimann et al [49] are consistent with our proposal that the saturation concentration of O^{2-} is smaller than monolayer. The limited concentration of O^{2-} in Cs should be contrasted to the case of Sr, where the diffusion of O^{2-} into the bulk of Sr is barrier-less and hence the surface remains metallic after building up a large concentration of O^{2-} [1].

After the surface Cs atoms are taken away by the incorporation of O_2^{2-} ions, the initially dissolved O^{2-} ions find new driving force to go farther into the bulk. The newly incorporated O_2^{2-} ions also separate the O^{2-} ions farther away from the surface. Thus the disappearance of the O^{2-} features in photoemission spectra at high oxygen exposures (>10 L) can be understood in terms of increased separation of O^{2-} ions from the surface rather than the conversion of the O^{2-} ions into other species. On the other hand, the decrease in intensity of O^{2-} features at higher oxygen exposures (>30 L) does not have to be explained as migration of O_2^{2-} away from the surface. Some O_2^{2-} may simply be converted to O_2^- by charge re-distribution and rearrangement of $\text{Cs}^+-\text{O}_2^{2-}$ ($1\text{In}12$) coordination in the same spatial region near surface. A saturation of the whole oxidation process can take place after the conversion of O_2^{2-} into O_2^- is near completion. The rate at which this final stage is reached depends on the sticking probability of O_2 on an insulating sur-

face and the easiness of migration of Cs^+ and O_2^{-n} ions to achieve proper cesium-oxygen coordination.

4.7 SUMMARY

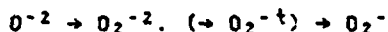
In summary, we have performed photoemission measurements on the adsorption of oxygen on thick Cs films at 140°K - 160°K. Four different states of oxygen were observed. Definitive identification of three of the four states of oxygen have been achieved through

- i) comparison of the multiplet structures in the photoemission spectra of free and adsorbed oxygen species (i.e., comparison of the energy separation of the multiplets only)
- ii) comparison of the experimentally measured binding energies of the various states of oxygen with calculated binding energies of known oxygen species inserted in Cs (based on the ionization energies of those free species).

The oxygen species identified are O^{-2} , O_2^{-2} and O_2^- . The multiplet splitting arising in the photoionization process is seen to be well preserved in a solid state environment. The multiplet structure of the photoemission spectrum of O_2^{-2} in Cs is identical to that expected for free O_2^{-2} without any differential relaxation in the orbital energies. In contrast to the case of O_2^{-2} , a significant differential relaxation in the orbital energies is observed for O_2^- in Cs. The difference is attributed to the close shell and open shell configurations of O_2^{-2} and O_2^- , respectively. The fourth oxygen state was produced with oxygen

exposures intermediate to those required to produce O_2^{-2} and O_2^- . It suggests the possible existence of an oxygen species like O_2^{-t} , with t being a non-integral value between 1 and 2. Such species may be related to the oxygen species found in the sesquioxide Cs_2O_3 . No simple interpretation of the multiplet structure of this state of oxygen, however, is available at the present.

The oxygen adsorption proceeds in the sequence



in good correspondence with the stable Cs-O compounds in the Cs-O phase diagram:



The range of concentrations which O^{-2} ions exist, however, is limited. Distinct spectroscopic changes, such as disappearance of plasmon loss features and emission near Fermi level, and sharp increase in the photoelectron yield, have been found to accompany the $O^{-2} \rightarrow O_2^{-2}$ transition.

Changes in the 4d, 5s and 5p core levels, and the N00 and OVV Auger transitions with oxygen adsorption have also been examined in detail. Clear evidence has been given showing that different responses to the changes in chemical environment of Cs atoms are found in the 5p's and 4d's; the difference has been explained by recognizing that the 5p is the outermost subshell of Cs^+ .

REFERENCE

1. C. R. Helms and W. E. Spicer, Phys. Rev. Lett. 28, 565(1972)
2. K. A. Kressand and G. J. Lapeyer, Phys. Rev. Lett. 28, 1639(1972)
3. K. Y. Yu, J. N. Miller, P. Chye, W. E. Spicer, N. D. Lang, and A. R. Williams, Pyhs. Rev. B 14, 1446(1976)
4. S. A. Flodstrom, L-G. Petersson, and S. B. M. Hagstrum, J. Vac. Sci. Technol. 13, 280(1976)
5. A. Barrie and J. Street, J. Electr. Spectr. Related Phenomena 7, 1(1975)
6. L-G. Petersson and S. E. Karlsson, Physica Scripta 16, 425(1977)
7. C. Wijers, M. R. Adriaens and B. Feuerbacher, Surf. Sci. 80, 317(1979)
8. A. Simon, in Structure and Bonding 36 pp.81 (Springer, N. Y. 1979)
9. P. E. Gregory, P. Chye, H. Sunami and W. E. Spicer, J. Appl. Phys. 46, 3525(1975)
10. B. Feuerbacher, in Proc. 7th Intern. Congr. & 3rd Intern. Conf. Solid Surfaces, 1149 (Vienna, 1977)
11. H. A. Engelhardt and D. Menzle, Surf. Sci. 57, 591(1976)
12. J. C. Fuggle, Surf. Sci. 69, 581(1977)
13. N. D. Lang, and A. R. Williams, Phys. Rev. Lett. 34, 531(1975); J. Harris and S. G. Painter, Phys. Rev. Lett. 36, 151(1976); .R. P. Messmer and D. R. Salahub, Phys. Rev. B 16, 3415(1977); I. P. Batra and S. Ciraci, Phys. Rev. Lett. 39, 774(1977)
14. See, for example, A. H. Sommer, Photoemission Materials, (Wiley, N. Y. 1968)
15. W. E. Spicer, Appl. Phys. 12, 115(1979) and references therein
16. W. E. Spicer, I. Lindau, C. Y. Su, P. W. Chye and P. Pianetta, Appl. Phys. Lett. 33, 934(1978)
17. S. J. Yang and C. W. Bates, Jr., Appl. Phys. Lett. 36, 675(1980)

18. N. V. Smith and G. B. Fisher, Phys. Rev. B 3, 3662(1971)
19. R. G. Oswald and T. A. Callcott, Phys. Rev. B 4, 4122(1971)
20. N. E. Christensen, in Proc. Intern. Symp. Photoemission, Noordwijk, Holland, 1976
21. P. Steiner, H. Hochst and Hufner, in Photoemission in Solids II: Case Studies, ed. by L. Ley and M. Cardona, Springer, N. Y. 1978
22. R. P. Gupta and A. J. Freeman, Phys. Lett. 59A, 223(1976)
23. Calculated according to the free electron equation
 $\omega_p = \sqrt{4\pi n e^2 / m}$ with a free electron density of $n = 0.91 \times 10^{22} \text{ cm}^{-3}$.
 See, for example, eq. 8-15 of C. Kittel, Introduction to Solid State Physics 4th ed., Wiley, N. Y., 1971
24. $\omega_p = \sqrt{4\pi n e^2 / \epsilon_{core} m}$ in which $\epsilon_{core} = 1.39$ for Cs, as calculated from the Claussius-Mossotti relation $\epsilon - 1 / (\epsilon + 2) = 4\pi n \alpha / 3$ with $\alpha = 3.02 \times 10^{-24} \text{ cm}^3$. See eq. 8-18, 13-35 and table 13-1 of C. Kittel, *ibid.*
25. C. D. Wagner and P. B. Biloen, Surf. Sci. 35, 82(1973)
26. K.-R. Tsai, P. M. Harris, and E. N. Lassette, J. Phys. Chem. 60, 338(1956)
27. See, for example, S. Chikazumi, Physics of Magnetism, Wiley, New York, 1965, p.157
28. R. W. G. Wykoff, Crystal Structure, 2nd ed., Wiley, N. Y., 1964
29. H. Foppl, Z. Anorg. Allg. Chem. 91, 12(1957)
30. V. A. Helms and W. Klemm, Z. Anorg. Allg. Chem. 242, 201(1939)
31. V. A. Helms and W. Klemm, Z. Anorg. Allg. Chem. 241, 97(1939)
32. N. Jonathan, A. Morris, M. Okuda, D. J. Smith and K. J. Ross in Electron Spectroscopy (ed. D. A. Shirley), North Holland, Amsterdam, 1972, p.345
33. M. Krauss, D. Neumann, A. C. Wahl, G. Das, and W. Zemke, Phys. Rev. A 7, 69(1973)
34. J. C. Slater Quantum Theory of Atomic Structure, vol. I, McGraw-Hill, N. Y., 1960, p.303
35. P. H. Kruperne, J. Phys. Chem. Ref. Data, 1, 423(1972)
36. B. J. Moss and W. A. Goddard III, J. Chem. Phys. 63, 3523(1975)

37. P. H. Citrin and T. D. Thomas, J. Chem. Phys. 57, 4446(1972)
38. E. R. McFeely, L. Ley, S. P. Kowalczyk, J. O. Jenkin, and D. A. Shirley, Phys. Rev. B 11, 600(1974)
39. C. R. Helms and W. E. Spicer, Phys. Rev. Lett. 31, 1307(1973)
40. J. Q. Broughton and P. S. Bagus, J. Electron. Spectr. and Related Phenomena, 20, 261(1980)
41. E. R. S. Winter, J. Chem. Soc. A 1968, 2889(1968)
42. Table 3-4, C. Kittel, *ibid.*
43. The O-O bond energy in an RO-OR complex is ~1.0 eV. T. L. Cottrell The strengths of chemical bonds, 2nd ed., Butterworth Sci. Pub., London, 1958
44. N. F. Mott and R. W. Gurney, Electronic Processes in Ionic Crystals, 2nd ed., Dover, N. Y., 1964
45. N. F. Mott and M. J. Littleton, Trans. Faraday Soc. 34, 485(1973), discussed in chap. 2 of Mott and Gurney, *ibid.*
46. Table 3-1, C. Kittel, *ibid*
47. W. Jost, J. Chem. Phys. 1, 466(1933), discussed by Mott and Gurney, chap 2, *ibid.*
48. Calculated using the Lorentz-Lorenz formula

$$(\kappa_0 - 1)/4\pi = N(\alpha_1 + \alpha_2)/[1 - 4/3 \cdot \pi N(\alpha_1 + \alpha_2)]$$
 (Mott and Gurney, pp.18, *ibid*), in which N is the number of ion pairs per unit volume, α_1 , α_2 are the polarizability of the two types of ions. We have taken $\alpha(\text{Cs}^+) = 3.02 \times 10^{-24} \text{ cm}^3$ and $\alpha(\text{O}_2) = 1.57 \times 10^{-24} \text{ cm}^3$, the polarizability of gaseous oxygen molecule (N. F. Hill et al, Dielectric Properties and Molecular Behavior, Nostrand, N. Y., 1969). The validity of using the polarizability of gaseous oxygen is checked by using it for F_2^{-2} ions in calculating the κ_0 's of CaF_2 , BaF_2 , and SrF_2 , in which cases measured values of κ_0 's are available; in all three cases, the deviation of the calculated values from the measured values are less than 4%.
49. W. Heimann, E.-L. Hoene, S. Jeric and E. Kinsky, Exp. Tech. Phys. 21, 193-207, 325-341, 431-436 (1973)
50. M. G. Burt and V. Heine, J. Phys. C: Solid State Phys. 11, 961(1978)
51. M. G. Clark, J. Phys. D: Appl. Phys. 8, 535(1975)
52. C. Kittel, Quantum Theory of Solids, pp.113, Wiley, N. Y., 1968

Chapter V

PHOTOEMISSION STUDIES OF THE INTERACTION OF (CS,O) WITH THE GaAs(110) SURFACE

5.1 INTRODUCTION

Co-adsorption of Cs and oxygen on GaAs surface is known to activate the GaAs surfaces to negative electron affinity (NEA) condition, which finds important application as the photocathode of the current-generation night-vision image intensifier [1], and as sources for spin-polarized electrons [2]. The methods of co-adsorbing Cs and oxygen, however, has so far been empirical, and a fundamental understanding of the interaction of the (Cs,O,GaAs) system has been lacking. In this chapter we present results of photoemission measurements of the interaction of cesium-oxygen with GaAs(110) surfaces.

Adsorption of oxygen on GaAs(110) has been a subject of many studies in recent years [3]. Photoemission studies of the oxidation of Cs has also become complete very recently [4]. With reference to knowledge of the O/GaAs and the O/Cs systems, we can address in this work the following questions: How does the presence of Cs affect the oxygen adsorption properties of the GaAs(110) surfaces, and how does the presence of the GaAs substrate affect the interaction of Cs and oxygen? Answers to these questions will not only provide basis for further understanding and improvement of the NEA surfaces, but also throw lights on the understanding of the oxygen adsorption properties of GaAs(110)

and Cs. Implications in the formal aspect will be given in detail elsewhere [5]. Here we concentrate on gaining fundamental understanding of the interaction of Cs and oxygen with GaAs(110) surfaces.

Results and discussion are divided into the following sections: As a reference for the Cs-O interaction on GaAs, we briefly summarize in section 3 the results from our previous photoemission studies of the oxidation of bulk Cs. Properties of the Cs-covered GaAs(110) surface are examined next in section 4. In section 5, we report the oxidation properties of monolayer-cesium-covered GaAs (110) surfaces. The interaction of such surfaces (monolayer-cesium-covered and subsequently oxidized GaAs(110)) with additional Cs treatments as well as the modification of the oxidation properties of such surfaces by additional Cs treatments are presented in section 6.

5.2 EXPERIMENTAL

The experiments were performed in a standard stainless steel ultra high vacuum ($\sim 7 \times 10^{-11}$ torr) chamber. Samples used were $6 \times 10^{17} \text{ cm}^{-3}$ Te-doped n-type, and 3.3×10^{18} Zn doped p-type GaAs. The cesium vapor in these experiments was supplied by cesium chromate channels. Cesium channels were mounted 5 inches away from GaAs samples and were enclosed in collimation shields which force the Cs vapor to deflect before reaching samples. Oxygen exposures were made with research grade oxygen through leak valves. The ion pump was completely valved off during exposures and oxygen pressures were measured with either a Redhead cold-cathode gauge (10^{-12} – 10^{-6} torr) or a Varian 860 cold-cathode gauge (10^{-8} – 10^{-3} torr). Exposures indicated have been corrected for gauge sensitivity.

Light sources used were synchrotron radiation in the range of 50 eV-200 eV from the Stanford Synchrotron Radiation Laboratory (SSRL) and He-I (21.2 eV) and He-II (40.8 eV) resonance lines from a monochromatized, differentially-pumped He discharge lamp. Energy analyses of the photoelectrons were performed by a double-pass cylindrical mirror analyzer (Physical Electronics).

The monolayer-Cs here is defined as the saturation coverage of Cs on the GaAs (110) surface at room temperature, i.e. the coverage at which any additional Cs atom will desorb by long pumping in ultra high vacuum. The absolute number of Cs atoms at this coverage has been estimated to be $4.6 \pm 0.4 \times 10^{14}$ atoms/cm². Thus, by our definition a monolayer contains about half of the total number of atoms in a GaAs (110) plane (8.85×10^{14} atoms/cm²). In this work the necessary Cs flux to reach monolayer coverage was established by monitoring Cs core levels (4d and/or 5p) to saturation in preliminary experiments of depositing Cs on clean GaAs (110). This calibrated Cs flux was then used to obtain the desired Cs coverage on different GaAs surfaces. An additional check of the Cs coverage is provided by comparing the relative intensity of core levels of Cs and GaAs. For the surfaces reported here, the relative intensity of the Ga-3d and the Cs-5p levels indicated the accuracy of the above procedure in controlling Cs coverages to be $\pm 20\%$.

5.3 PHOTOEMISSION SPECTRA OF OXIDIZED CS

In Fig. 1 we show photoemission spectra of oxidized bulk Cs from our earlier studies [4]. The spectrum for an individual oxygen species was obtained at a somewhat arbitrary oxygen exposure, and hence may contain mixtures of other states. The detailed justification for the separation and the identification of each state have been given Chapter III. Here only the conclusions are indicated. The correct features associated with each oxygen state are labeled according to the following: features A1, A2, and A3 belong to the spectrum of O^{-2} , with A1 being the only $O-2p$ related peak and A2 and A3 are plasma losses associated with A1 [4]; features B1, B2 and B3 belong to the spectrum of O_2^{-2} ; features C1, C2 and C3 belong to O_2^{-1} , with 11t12; features D1, D2, D3, D4 and D5 belong to O_2^- . The binding energy in Figure 1 is referred to Fermi level of the system. For Cs-O adsorbate complex formed on GaAs, this binding energy may not be a meaningful quantity. We therefore include Cs-5p levels in Figure 1 and will use the energy separation between Cs-5p levels and oxygen levels as a reference in comparing with the results of (Cs,O) on GaAs.

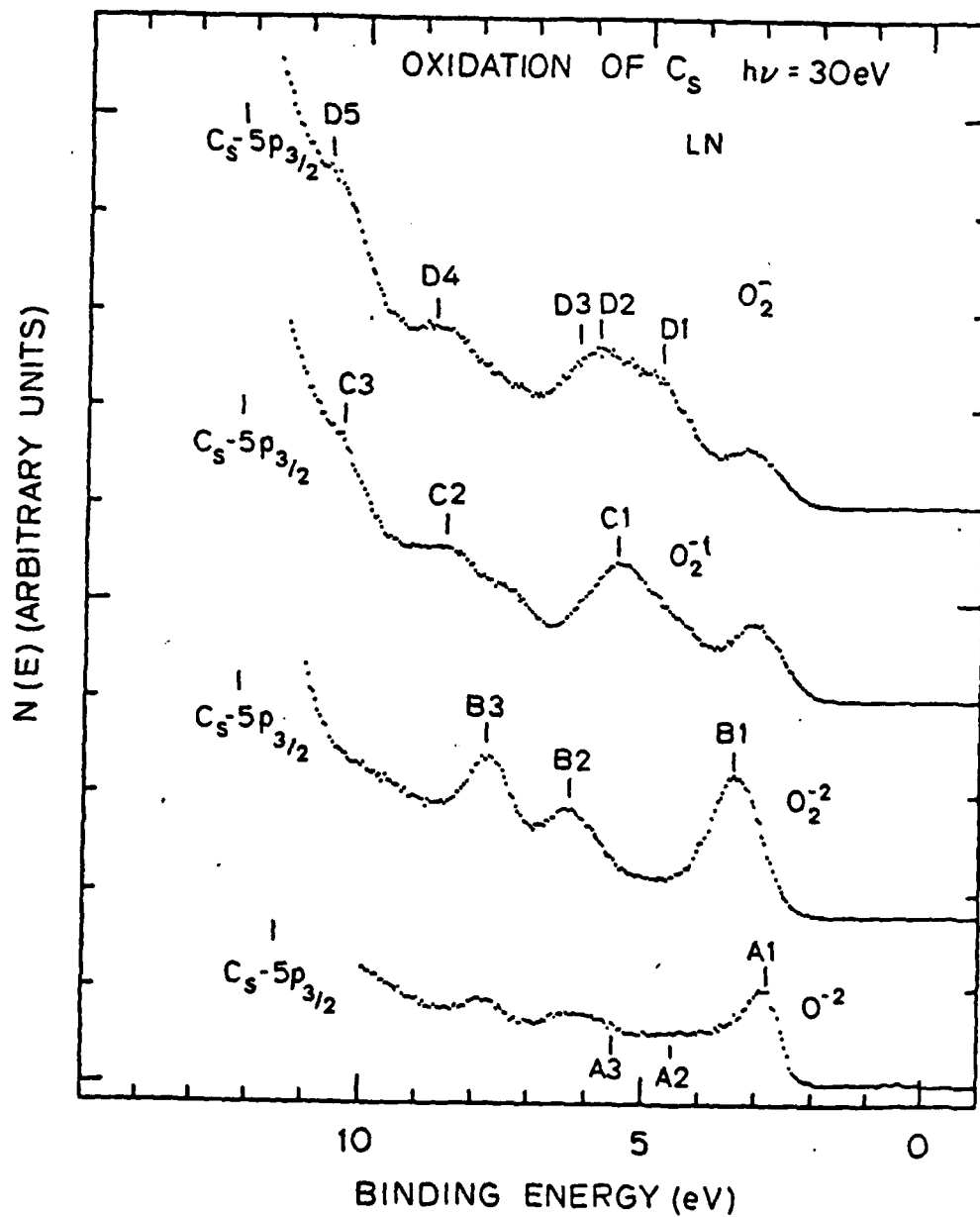


Figure 59: Spectra of various oxygen species in Cs, obtained from oxidizing thick Cs films.

5.4 RESULTS AND DISCUSSION - PROPERTIES OF THE CS OVERLAYER

Some characteristics of the monolayer Cs covered GaAs(110) surface are presented below to provide a basis for discussion of its oxidation properties.

Adsorption of Cs on GaAs is known to lower the work function of the GaAs surface [6]; such lowering of the work function is achieved by transferring the valence electrons ionized from the Cs atoms in the overlayer into the surface states or the space charge region of the GaAs substrate [6]. One indication in our results that Cs in the overlayer is in a state approaching the Cs^+ ion state, is given by the spin-orbit splitting of the Cs-5p levels: The splitting between the Cs-5p levels is 1.5 eV in this case as opposed to 1.9 eV in the case of bulk or atomic Cs, and we have demonstrated in our earlier work that such narrowing of the spin-orbit splitting of the Cs-5p's occurs whenever Cs is oxidized [4].

Gregory and Spicer, by assuming a simple two-dimensional dipole sheet at the Cs-GaAs interface, however, have shown that the Cs atoms need not to be completely ionized to explain the work function lowering observed [6]. Below, we point out some indications of the incomplete ionization of the Cs overlayer.

A monolayer of Cs has been reported [7,8] to form a $\text{C}(4 \times 4)$ ordered but out-of-registry overlayer on GaAs (110). LEED patterns of the surfaces reported here were not checked after Cs deposition.

Although it is not clear whether the ordered $C(4 \times 4)$ structure was achieved on the surfaces to be reported below. In a separate measurement, a $C(4 \times 4)$ LEED pattern was indeed observed on a similarly prepared Cs-covered GaAs (110) surface. The arrangement of the Cs atoms in the $C(4 \times 4)$ out-of-registry overlayer resembles that in the (111) plane of the bcc structure of Cs; this is indicative of significant Cs-Cs interaction within the Cs overlayer.

Photoemission spectra measured in this work also give the following indications that the Cs atoms in the overlayer are not completely ionized:

- i) emission near the top of valence band is increased relative to the other region of the valence band after Cs deposition, and the increase is higher for higher Cs coverage (see the bottom curves in figs. 64 and 65 below); a tailing emission is in fact found to extend into the band gap of GaAs and up to the Fermi level, although no sharp Fermi edge can be identified. This new emission near the valence band maximum of GaAs can be interpreted as due to valence electrons of Cs.
- ii) a tailing emission on the high binding energy side of the $Cs-4d_{3/2}$ is visible after the Cs deposition and before oxygen adsorption. This tailing emission can be interpreted as due to plasmon loss with the plasmon energy much reduced from the bulk metal value; it indicates the lack of true ionization of Cs, but a reduced "free electron" density compared to bulk Cs metal.

There is another comparison to be made between the monolayer Cs and bulk Cs. The binding energy of the Cs-5p_{3/2} level measured below Fermi level is nearly identical in the case of monolayer Cs and in the case of bulk metal. For both p-type and n-type samples, the 5p_{3/2} lies at 11.6 eV below VBM, or 12.2 eV below the Fermi level (the Fermi level of both n- and p-type GaAs are pinned at about 0.6 eV above VBM after Cs deposition). The binding energy of 5p_{3/2} measured for bulk Cs is 12.1 ± 0.1 eV below E_f [4]. The binding energy of the Cs-4d_{5/2} level, measured for n-type samples only, is 76.6 eV below VBM and 77.1 eV below E_f, which is also close to the 77.3 eV below E_f measured for bulk Cs [4].

Since the work function of monolayer-Cs-covered GaAs (≈1.2 eV [9]) is smaller than that of bulk Cs (2.0 eV), the binding energies of Cs core levels referred to the vacuum level are significantly lower in the case of monolayer Cs than in the case of bulk Cs. In our earlier work [4], we have seen that the Cs core levels shift to lower binding energy when forming Cs suboxides. Because in Cs suboxides the metallic character is retained and only the free electron density is reduced compared to that of bulk Cs, the lower BE's found for Cs core levels of the Cs overlayer as compared to those of bulk Cs therefore could be consistent with a partially ionized Cs overlayer.

5.5 RESULTS AND DISCUSSION - ADSORPTION OF OXYGEN ON MONOLAYER- CESIUM- COVERED GAAS (110)

This section concerns the oxidation properties of monolayer-Cs-covered GaAs. As mentioned in the introduction, the oxidation of cesi-

ated GaAs can differ from the oxidation of clean GaAs, and the oxidation of monolayer-thick Cs with the presence of GaAs can differ from the oxidation of bulk Cs. Such properties of the co-adsorption system will be determined in this section. The effect of additional Cs coverages will be examined in next section.

Results from three surfaces are presented here. Two p-type samples were studied mainly with the He-I radiation (21.2eV, figs. 64 and 65), and one n-type sample was studied with 120 eV synchrotron radiation (figs. 60 - 62). Consistent results were obtained on all surfaces studied. Results from the two p-type samples are reported here to illustrate effects of different Cs coverages (0.6 monolayer, fig. 64 and 1.0 monolayer, fig. 65). Experimental conditions used with He-I radiation also offer better energy resolution and signal-to-noise ratio for valence band spectra as well as the Cs-5p levels. High photon energy studies were made on n-type samples only. Chemical shifts in Ga-3d, As-3d (fig. 60) and Cs-4d (fig. 61) can be examined only in the high photon energy studies. In these figures, the cumulated oxygen exposures expressed in Langmuir ($1 \text{ L} = 10^{-6} \text{ torr} \times 1 \text{ sec.}$) are indicated together with each spectrum.

Presentation and discussion of the results will be further divided into two subsections. Description of photoelectron spectra and identification of oxygen induced features will first be presented. Discussion of the oxidation properties of monolayer-Cs-covered GaAs(110) surfaces then follows.

5.5.1 Identification of oxygen induced features

The dominant adsorption reaction on cesiated GaAs(110) surfaces is the bonding of oxygen to GaAs at an rate drastically increased over that of bare GaAs(110) surfaces. The bonding of oxygen to GaAs is evidenced by a chemically shifted As-3d peak and a broadened Ga-3d peak after exposing the cesiated surface to oxygen (fig. 60). The 3.0 eV shift in As-3d observed at oxygen exposures ≤ 20 L is characteristic of a chemisorption bonding of oxygen to As produced by exposing clean (uncesiated) cleaved GaAs(110) surfaces to unexcited molecular oxygen [3]. This suggests the formation, at the initial stage of oxygen adsorption on cesiated GaAs(110) surface, of a chemisorption phase similar to that found by adsorbing oxygen on bare GaAs (110) surfaces. The oxygen exposure required to form the chemisorption phase is ≤ 10 L for cesiated surface, and is 10^7 L for bare GaAs(110), hence the initial oxygen uptake of GaAs(110) is greatly enhanced when cesiated. Between 20 L and 40 L exposures, the value of chemical shift in As-3d increased from 3.0 eV to 3.6 eV; at higher exposures (≥ 40 L), the energy position of the shifted As-3d remained nearly stationary (fig.60). The intensity of the shifted As-3d also increased rapidly between 20 L and 40 L exposures, beyond 40 L it increased only slightly with increasing oxygen exposures. The ratios of intensity of the shifted to that of unshifted As-3d at exposures ≥ 40 L suggest that oxygen bonding to GaAs has advanced beyond the first layer of GaAs (see reference 10). Both the 3.6 eV shift and the intensity of the shifted As-3d indicate that at exposures ≥ 40 L the adsorption has proceeded beyond chemisorption to oxide formation. The 3.6 eV shift is consistent with the formation of As_2O_3 [11], or it could be a

surface oxide involving oxygen bridging over Ga and As and with each As seeing three such bridging oxygen; no definitive choice of these two possibilities can be offered here.

The Cs-5s and the O-2s levels are also included in the energy distribution curves (EDC's) in fig. 60, although they are not pronounced because of low photoionization cross sections. The energy position of the O-2s level falls in the region (exact position cannot be assessed due to its weak intensity) appropriate for oxygen bonded to GaAs (Pianetta et. al., ref. 9).

We have so far seen definitive evidence of the bonding of oxygen to GaAs for oxygen adsorbing on cesiated GaAs(110), it remains to be seen whether oxygen reacts with the Cs overlayer. In fig. 61, the Cs-4d levels are seen to shift to lower binding energy with increasing oxygen exposure; most of the shift ($\Delta \approx 0.6$ eV) occurs between 10 L and 40 L exposures, which is the same exposure range oxygen bonds rapidly to GaAs, and only small shift occurs between 40 L and 900 L which makes the total shift 0.8 eV toward lower binding energy. The gradual shift of the Cs-4d levels (and the Cs-5p levels, to be discussed below) toward lower BE is ambiguous in indicating whether oxygen is bonded to Cs or not, because in our previous studies of the oxidation of bulk Cs only discrete shifts in Cs core levels were observed for different oxidation states (e.g., $\Delta = 0.6$ eV toward lower BE when O⁻² is formed) - i.e., if the Cs overlayer were partially oxidized, one would observe two separate sets of Cs-4d levels (and Cs-5p levels) changing their relative strength

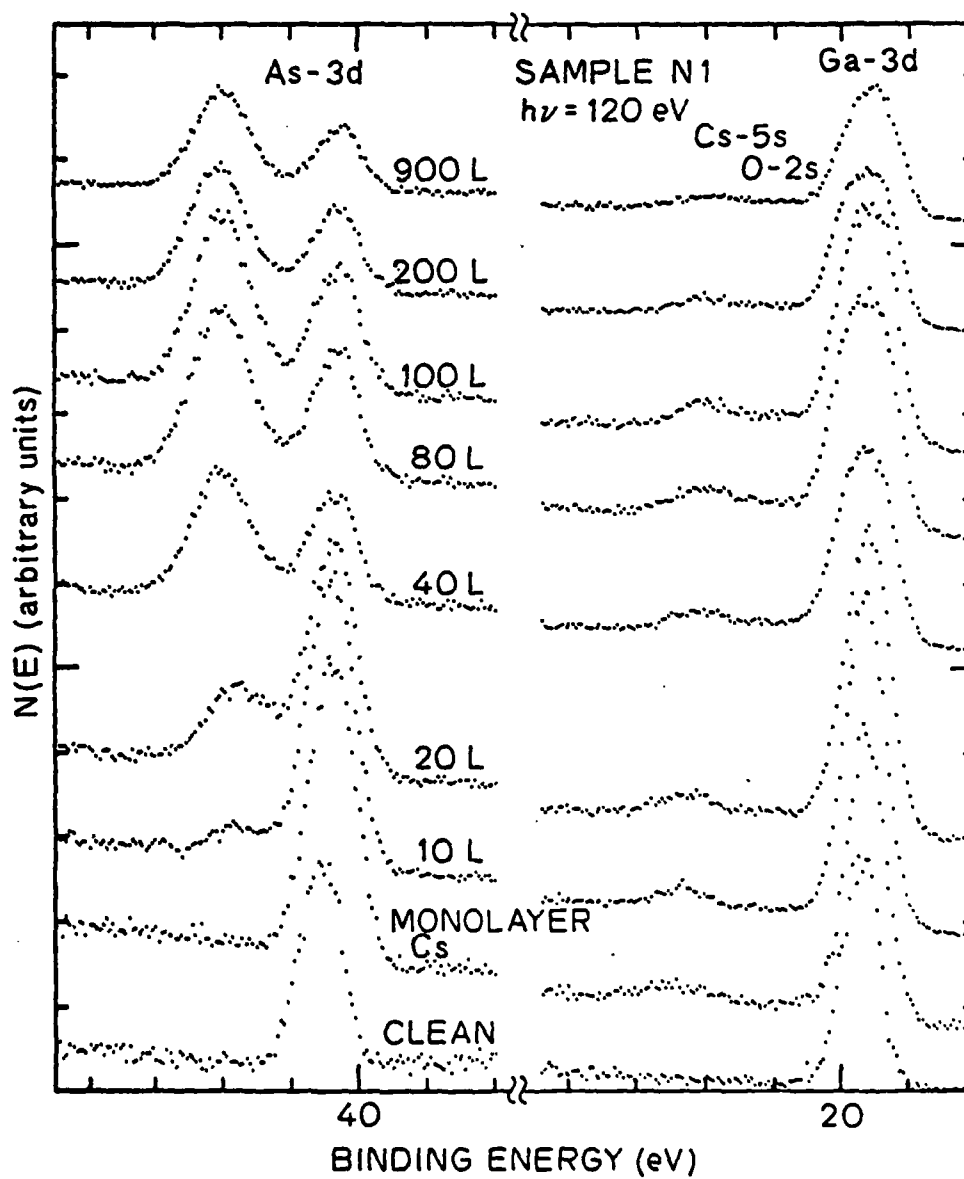


Figure 60: EDC's of As-3d, Ga-3d, Cs-5s and O-2s levels of clean, monolayer-Cs-covered and oxygen-exposed GaAs(110), $h\nu=120$ eV.

with increasing oxygen exposure instead of a single pair of gradually shifting Cs-4d's. Definitive evidence that oxygen does not bond to Cs at exposures below about 40 L is found in examining the valence band region of the EDC's, which we will discuss below.

Fig. 62 displays the Cs-5p levels and the valence band region of the EDC's taken on the same sample of figs. 60 and 61. At oxygen exposures below 20 L, the major oxygen induced features in the valence band region are a broad peak at 4.6 eV below the VBM and a broad shoulder on the high BE side of this peak. At exposures above 40 L, a new feature appeared at 2.8 eV below the 4.6 eV peak, and the peak shape of the 4.6 eV peak became distorted, which, as will be seen below, is better described as a new and relatively narrow peak superposed on the broad peak developed at lower exposures. It is clear from fig. 62 that throughout the whole exposure range we have studied (1 L - 1100 L) the O-2p related features of O⁻² at 2.7 eV below the Fermi level (A1 in fig. 59), and of O₂⁻² at 3.3, 6.4 and 7.8 eV below the Fermi level (B1, B2 and B3 in fig. 59) do not appear; the complex multiplet structure of O₂⁻ in Cs cannot be found in any of the spectrum either. Thus none of the three oxygen species, O⁻², O₂⁻² and O₂⁻, which are formed within 200 L oxygen exposure of bulk Cs, is produced in the Cs overlayer when adsorbing oxygen on monolayer-Cs-covered GaAs(110).

The nature of the oxygen induced features observed in fig. 62 are further examined in fig. 63. In fig. 63, we compare the 40 L EDC of the As-3d (from fig. 60) and the O-2p (from fig. 62) to the the corresponding EDC's of a bare GaAs(110) surface exposed to 10¹³ L oxygen. The

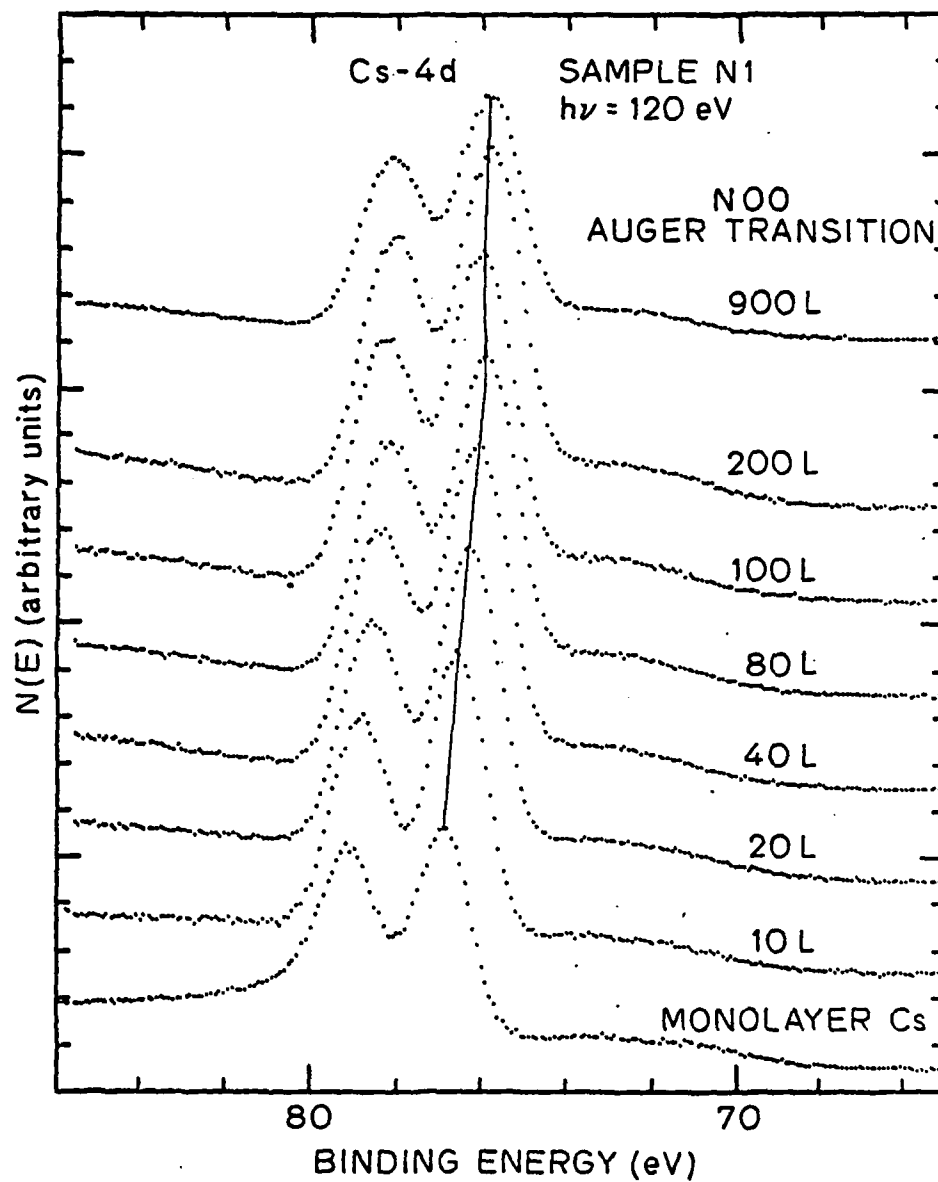


Figure 61: EDC's of Cs-4d and the N00 Auger transition of clean and oxygen-exposed monolayer-Cs on a GaAs(110) surface, at $h\nu=120$ eV.

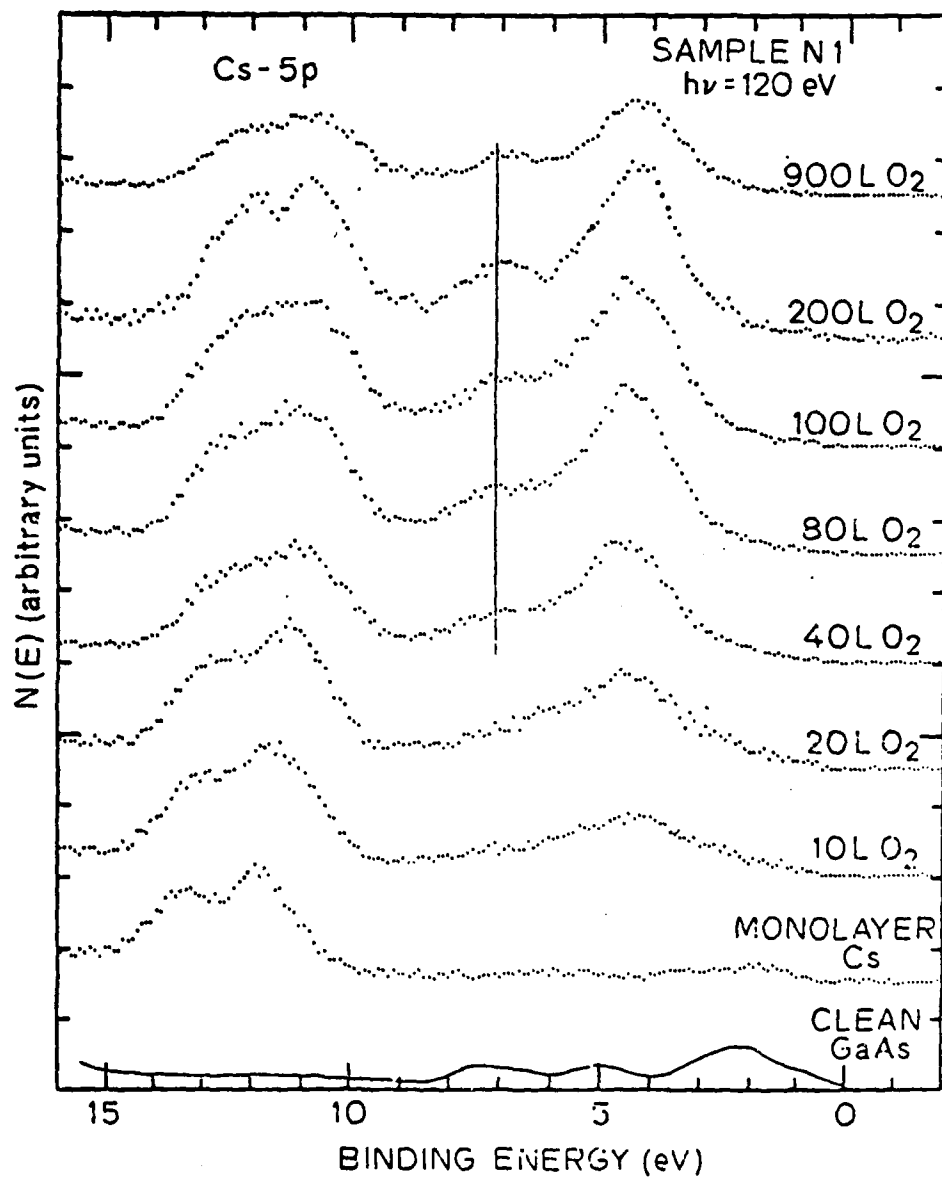


Figure 62: Cs-5p levels and the valence band region of the EDC's of clean, Cs-covered and oxygen exposed GaAs(110), $h\nu=120$ eV. Spectra were obtained on the sample of figs. 60 and 61.

two sets of EDC's are plotted with the total area under As-3d normalized to each other. Here we first recognize again the large enhancement in oxygen uptake of GaAs by the presence of a monolayer of Cs. The O-2p related features in the case of bare GaAs exposed to 10^{13} L oxygen are a broad peak at 4.6 eV below the VBM and a featureless shoulder on the high BE side of this peak, which are identical to the O-2p features observed for Cs-covered GaAs surfaces at exposures ≤ 20 L (fig. 62). After exposing the Cs-covered surface to 40 L oxygen, as has been mentioned before in conjunction with fig. 62 and is better seen here in the 40 L EDC of fig. 63, a relatively narrow peak at 4.6 eV BE, which overlaps with the broad peak due to oxygen bonded to GaAs, and a weaker peak at 2.8 eV on the low BE side of it are developed. These new pair of peaks cannot be found in the photoemission spectra of either oxygen chemisorbed on GaAs(110) or As_2O_3 [11] or Ga_2O_3 [12]; rather, the narrowness of the peaks are characteristic of oxygen bonded to Cs [4]. The 2.8 eV separation between the new pair of peaks is identical to the separation between the two leading peaks of the O_2^{-t} state shown in Figure 1. The small shoulder at 1.7 eV above the $5p_{3/2}$ peak found for the O_2^{-t} state in the oxidation of bulk Cs is not observed in the present case. The separation between the Cs- $5p_{3/2}$ peak and the leading oxygen peak (at 4.6 eV BE) appears to vary between 6.7 eV and 6.3 eV with increasing oxygen exposure. This agrees favorably with the 6.5 eV separation found for the O_2^{-t} state in Figure 1. In the oxidation of bulk Cs, O_2^{-t} state appear at oxygen exposures intermediate to those required to produce O_2^{-2} and O_2^{-} states [4], and it was suggested to be related to Cs_2O_3 so that $1 \leq t \leq 2$. The oxygen species in

the Cs overlayer found here may be a similar molecular ion with ionic charge intermediate between 1 and 2; we will designate this species O_2^{-n} ions (possibly $n \neq 1$). More justification of this assignment will be given in the next subsection where the oxygen adsorption process on cesiated GaAs(110) is discussed. It is important to point out here that reaction of oxygen with the Cs atoms in the monolayer-thick Cs overlayer indeed occurs, but only at high oxygen exposures after a significant amount of O-GaAs bonding is formed first and only one (O_2^{-n}) of the several possible oxygen species in Cs is formed.

In figs. 64 and 65, we show additional EDC's of the Cs-5p's and the valence band region of two p-GaAs(110) surfaces covered with different amount of Cs obtained with He-I radiation. The surface of fig. 64 was adsorbed with ~0.6 monolayer Cs prior to oxygen adsorption, whereas the surface of fig. 65 is covered with one monolayer Cs. The increment of oxygen exposure below 20 L made on these two surfaces is finer than that made on the surface of figs. 60, 61 and 62 which we have discussed above. In both figures we see again the gradual shift of Cs-5p's toward lower BE with increasing oxygen exposure. Two peaks are seen in the valence band region of the oxygen-exposed EDC's. The 4.6 eV BE peak which grows with increasing oxygen exposure is due to oxygen bonded to GaAs. The peak located at 2.3 eV below the 4.6 eV peak in these spectra is due to the 6.9 eV BE valence feature of bulk GaAs. This peak is seen in 21 eV spectra because of the large escape depth of the photoelectrons originated from this peak. For comparison, we show in fig. 66 the 21 eV EDC's of a bare p-type GaAs(110) surface subjected to two heavy oxygen exposures. The similarities between the valence band region of the EDC's in figs. 64 and 65 and those in fig. 66 are clear.

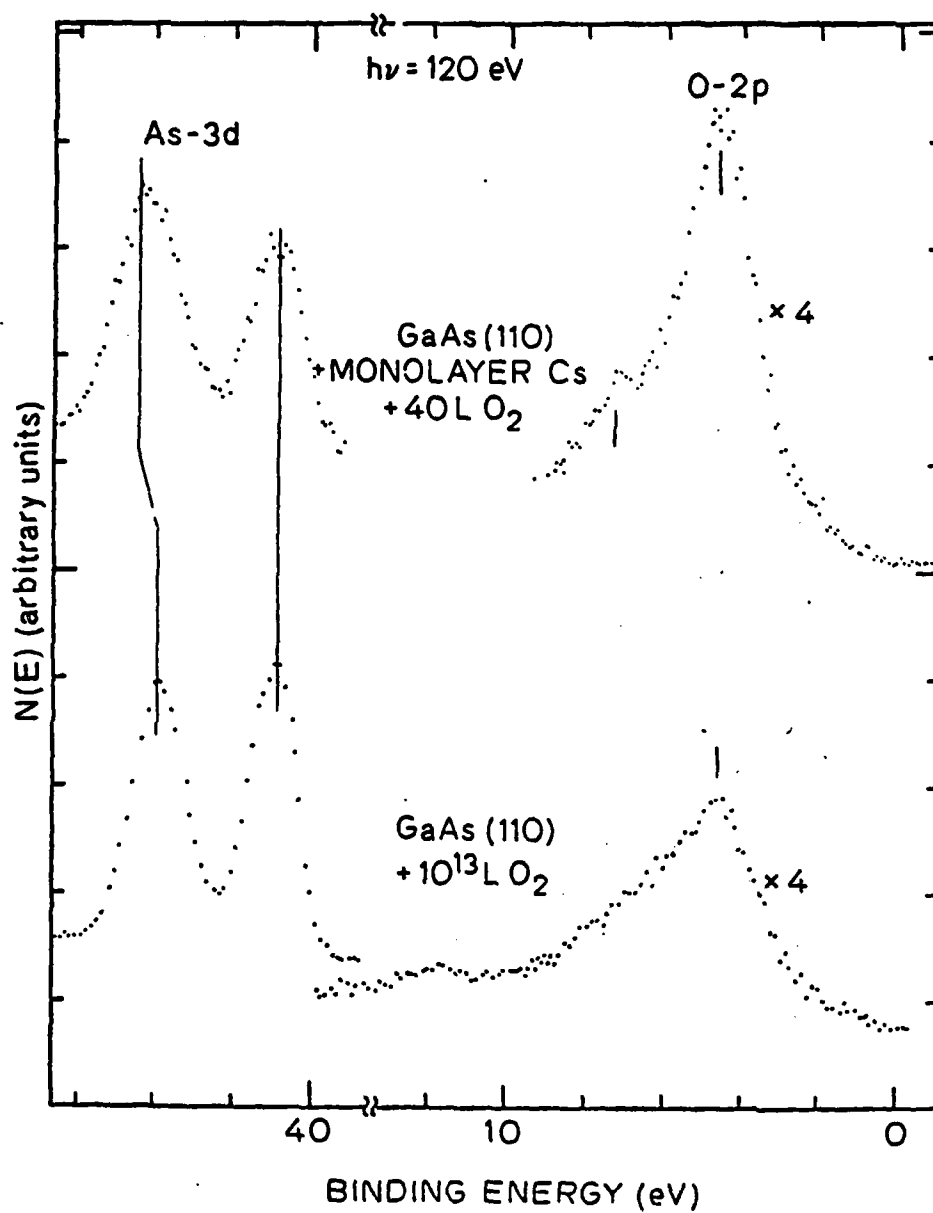


Figure 63: Comparison of oxygen induced feature in the spectra of oxygen adsorbed on a Cs-covered and a bare GaAs(110) surface.

The strength of the 4.6 eV oxygen peak relative to that of the 6.9 eV GaAs peak in the 1 L EDC of the monolayer-Cs-covered GaAs(110) surface in fig. 65, however, is higher than that in the 10^7 L EDC in fig. 66; the enhancement of the oxygen uptake of the GaAs(110) surface by the presence of monolayer of Cs is thus at least 10^7 times.

As can be seen in fig. 65, the oxygen induced feature at 2.8 eV below the 4.6 eV peak indicative of the incorporation of O_2^{-n} into the Cs overlayer (which has been discussed above) appeared at exposures ≥ 20 L. On the GaAs(110) surface covered with 0.6 monolayer Cs prior to oxygen adsorption, however, no clear trace of the features associated with the O_2^{-n} in Cs can be found in the EDC's (fig. 64) throughout the same oxygen exposure range as that made on the monolayer-Cs-covered GaAs(110) (0.5 L - 200 L).. Therefore the uptake of oxygen by the Cs overlayer is higher on the surface with higher Cs coverage. Comparison of the strength of the 4.6 eV oxygen peak in the corresponding EDC's in fig. 64 and fig. 65 reveals that the uptake of oxygen by the GaAs substrate is higher on the surface with higher Cs coverage. (Compare the 1 L curves in Figure 2 and Figures 3, and compare the depth of the valley between the oxygen peak and the substrate peak "A" for other exposures). We thus have established the Cs coverage dependence of the oxygen adsorption process on Cs-covered GaAs(110) surfaces.

Because oxygen bonds only to GaAs at exposure ≤ 20 L, the shift of Cs core levels toward lower BE in that exposure range (Cs-4d, fig. 61, and Cs-5p, figs. 62 and 65) cannot be caused by the direct bonding of oxygen with Cs; rather it must be caused by the indirect interaction of the

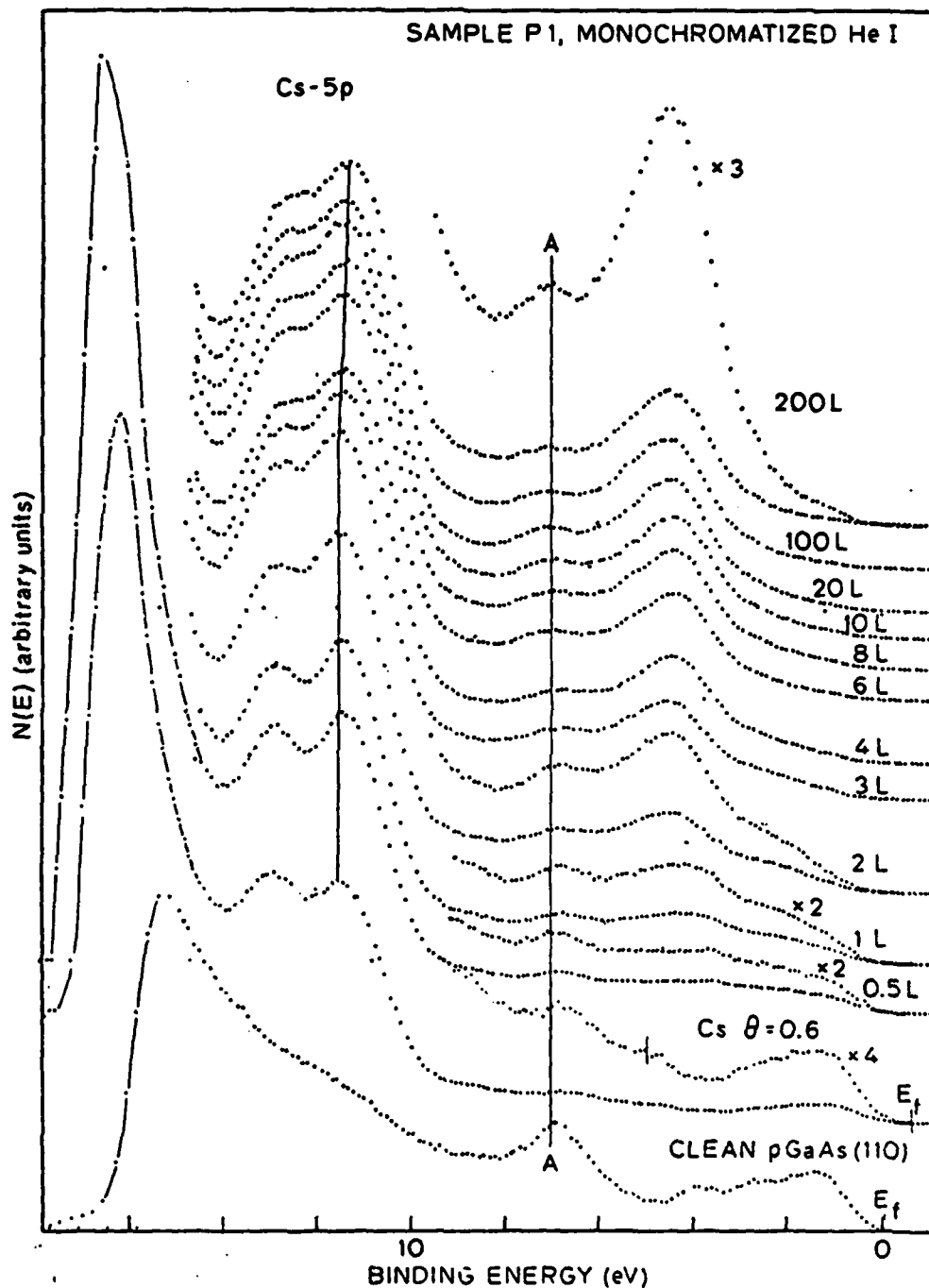


Figure 64: He-I spectra for sample P1 covered with 0.6 monolayer Cs and subsequently subjected to a series of oxygen exposures. Binding energy is referenced to the valence band maximum. Positions of Fermi level of clean and Cs covered surfaces are indicated.

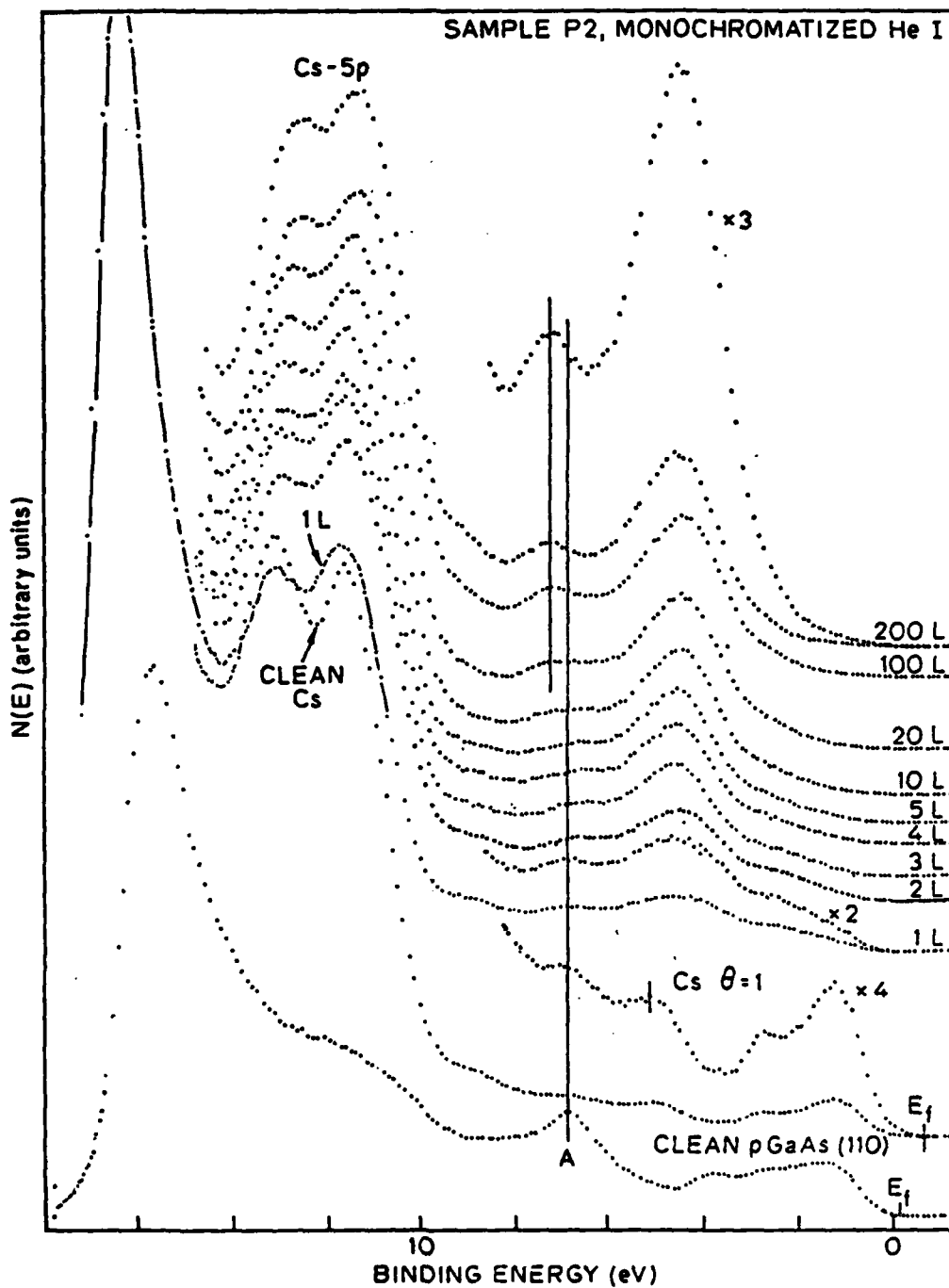


Figure 65: He-I spectra of sample P2 covered with one monolayer of Cs and subjected to a sequence of oxygen exposure.

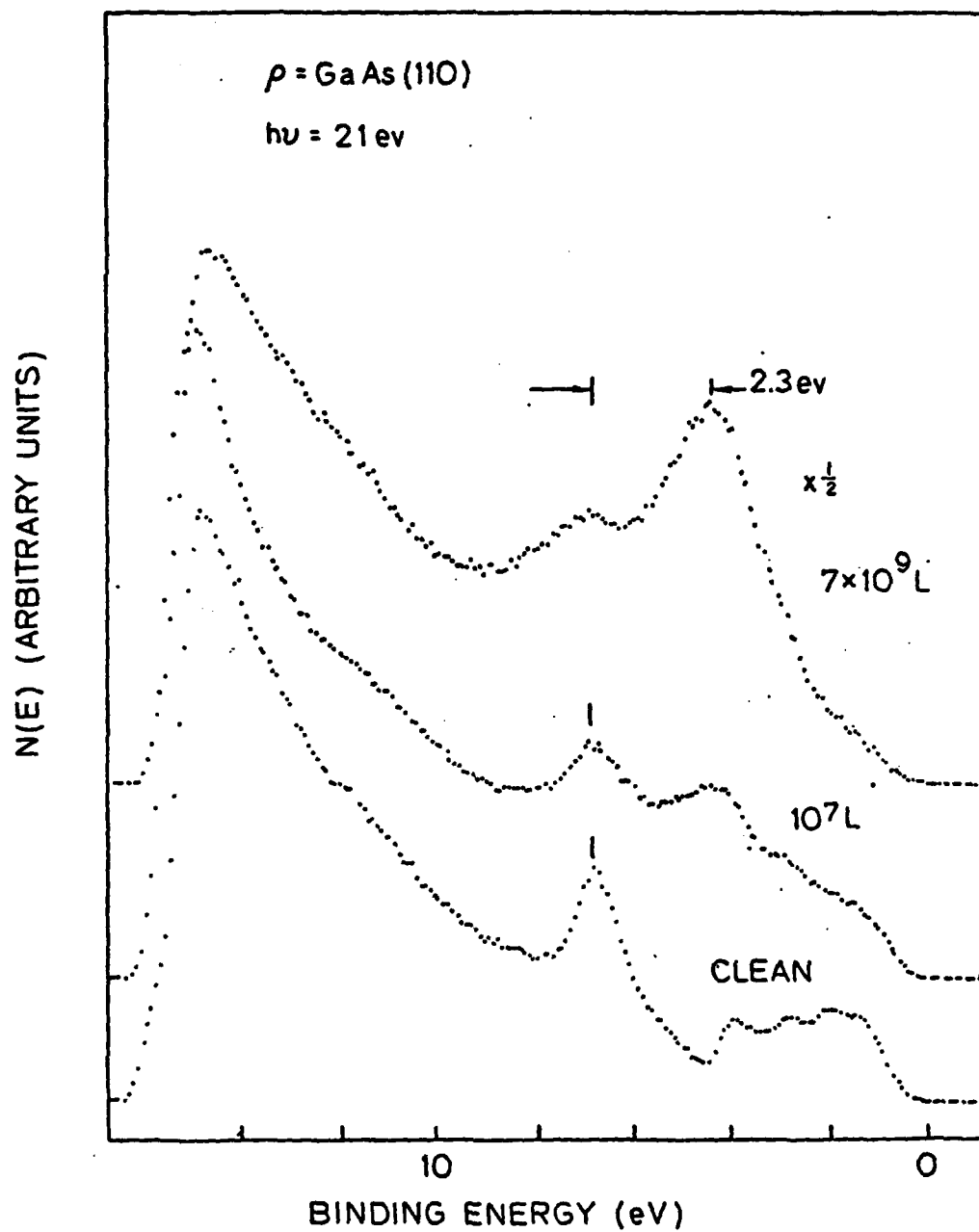


Figure 66: 21 eV spectra of a bare p-GaAs(110) surface subjected to two heavy oxygen exposures. The same O-2p related features are found in the spectra of Cs covered surfaces shown in figs. 64 and 65.

O-GaAs bonding with the Cs overlayer. One possibility is that the oxygen atoms, which are bonded to GaAs, disorder the Cs C(4x4) overlayer or provide screening between Cs atoms, such that the Cs-Cs interaction in the Cs overlayer is reduced; an indication of the depletion of "free electron" from Cs is the removal of the tailing emission on the high BE side of Cs core levels after oxygen exposure. It is not clear, however, whether the reduction in Cs-Cs interaction will cause Cs core levels toward lower BE. Another effect in play here may be the reduction of the dipole potential drop across Cs and GaAs (i.e., an increase in the work function of the (Cs,O,GaAs) composite surface with increasing oxygen exposure) caused by the disordering of the Cs core levels closer to the Fermi level (and hence the BE's of Cs core level, which are referenced to the Fermi level, are reduced). A more detailed picture of this dipole potential effect will be given in 6.2 below.

5.5.2 The Oxygen Adsorption Process on Cs-covered GaAs(110)

In this subsection we will provide explanations for the spectroscopic findings presented in the last subsection (5.1); description of the oxygen adsorption process on Cs-covered GaAs(110) will be based on these explanations.

The oxidation properties of Cs-covered GaAs(110) surfaces can be summarized as follows:

- i) No oxygen can be bonded to Cs before a significant amount of oxygen is bonded to the GaAs substrate. The exposure at which the bonding of oxygen to Cs begins decreases with increasing Cs

coverage. A lower limit of the oxygen exposure required to commence oxygen incorporation into a monolayer of Cs is 10 L.

- ii) The bonding of oxygen to GaAs is enhanced on Cs covered surfaces by at least 10^7 times as compared to that on bare surfaces. The enhancement increases with increasing Cs coverage.
- iii) The cesium-oxygen complex formed does not contain O^{2-} ions -- the oxygen species contained in cesium-suboxides and Cs_2O , but it contains a non-dissociated species, O_2^{-2} .
- iv) The bonding of oxygen to GaAs continues beyond the chemisorption stage to form more advanced oxide after passing the exposure at which oxygen begins to incorporate into Cs.

Result (i), the preferential bonding of oxygen to GaAs instead of Cs, should be compared with the thermodynamic quantities of the (Cs,O,GaAs) system. The heats of formation of Ga_2O_3 , As_2O_3 and As_2O_5 are 258, 156 and 364 Kcal/mole, respectively, are higher than the heat of formation of any of the cesium oxide (88 for Cs_3O , 76 for Cs_2O , 96 for Cs_2O_2 , 111 for Cs_2O_3 and 124 for CsO_2). In order to consider the thermodynamically favorable reaction of reacting a fixed amount of oxygen with Cs and GaAs, we compare in table 11 the standard free energies of reaction of reacting 1.5 mole oxygen with Cs, Ga, and As to form various possible oxides.. It is seen in table 11 that the free energy of reaction of Cs_3O is comparable to that of Ga_2O_3 ; the difference may be within experimental error. Comparison of the free energies of reaction for bulk

oxides, however, can be used only as a reference for the surface reactions being considered here. Special consideration given to the surface-reaction nature of the oxygen adsorption process makes the bonding of oxygen to GaAs even more favorable: A monolayer of Cs does not provide the Madelung energy necessary to stabilize various oxygen ions. Formation of cesium suboxides therefore requires migration of Cs atoms across the GaAs surface to form three dimensional islands. Such migration of Cs atoms is difficult because Cs atoms in submonolayer to monolayer coverages are strongly bonded to the GaAs substrate [13]. Similar consideration has to be applied to the formation of Ga_2O_3 , As_2O_3 , etc 'migration of Ga and As atoms is necessary. It is likely that oxygen forms bridge bond, Ga-O-As , or donor-acceptor bond, GaAs=O , or both with GaAs (see discussion in Chapter III). For such case the energetics to be considered are the following: the formation of Ga-O-As bond releases ~ 5.7 eV [14], and the formation of GaAs=O bond releases ~ 3.0 eV whereas the energy gained by forming $\text{Cs}^+-\text{O}^{2-}$ is ~ 2.0 eV (using the heats of formation of Cs_2O , Cs_3O , but subtracting the Cs/GaAs bonding energy of ~ 0.8 eV/atom [13]). Again, the oxygen clearly favors the bonding to GaAs.

Since the dissociation of oxygen molecules has been suggested both experimentally [17] and theoretically [14] to be the rate limiting step of oxygen adsorption on bare GaAs(110) surface, the great enhancement in the oxygen uptake of GaAs (result (ii) above) can be understood in terms of the availability of dissociated oxygen atoms. The ability of cesiated GaAs surfaces to dissociate molecular oxygen probably arises from barrier-less or low barrier charge transfer to impinging oxygen

TABLE 11

Heats of formation, standard entropies, and free energies of reaction of Cs, Ga, and As oxides

Reactions	$-\Delta H$ (kcal/mole)	S (cal/mole-°K)	$-\Delta G$ (kcal/mole)
Cs ¹	0	21.2	--
Ga ²	0	9.8	--
As ²	0	8.4	--
GaAs ²	19.5	15.4	--
9 Cs + 3/2 O ₂ → 3 Cs ₃ O ¹	264	123	221.9
6 Cs + 3/2 O ₂ → 3 Cs ₂ O ¹	227	97.2	196.9
3 Cs + 3/2 O ₂ → 3/2 Cs ₂ O ₂ ¹	144.3	46.6	117.3
2 Cs + 3/2 O ₂ → Cs ₂ O ₃ ¹	111.2	31.7	86.1
3/2 Cs + 3/2 O ₂ → 3/4 Cs ₂ O ₄ ¹	93.15	25.4	69.3
2 Ga + 3/2 O ₂ → Ga ₂ O ₃ ²	258.8	20.2	237.1
2 As + 3/2 O ₂ → As ₂ O ₃ ²	156.2	29.3	138.0
6/5 As + 3/2 O ₂ → 3/5 As ₂ O ₅ ²	218.5	25.2	184.5
1. Ref. 15	2. Ref. 16		

molecules. There are two possible sources of efficient charge transfer to impinging oxygen molecules:

- a. valence electrons in the Cs overlayer
- b. electrons in GaAs transferred through a surface barrier lowered by cesiation.

The evidence we have given at the beginning of section 4 that the degree of ionization of Cs atoms in the overlayer is low, suggests that mechanism (a) plays, at least at the initial stage of adsorption, an important role. Result (iv) above, that the bonding of oxygen to GaAs continues at high oxygen exposure, however, suggests that mechanism (b) should also be important.

At high oxygen exposures, the higher oxygen pressures used lead to higher impinging rate of oxygen molecules. Since non-dissociated oxygen does not bond to GaAs [3], it is incorporated into the Cs overlayer. This has motivated us to associate the new pair of O-2p related features appeared at high oxygen exposures to molecular oxygen ion, O_2^{-2} (section 5.1). At high oxygen exposures (>20 L), the O-GaAs bonding may weaken the binding force between Cs and the GaAs substrate to make Cs atoms relatively mobile, and hence the probability of incorporating oxygen species into the Cs overlayer increases.

The fact that the bonding of oxygen to GaAs can proceed beyond the surface layer to form more advanced oxide (result (iv) above) is worth emphasizing. This means the GaAs substrate can compete effectively for dissociated oxygen with the Cs overlayer over a wide range of oxygen exposures; this explains result (iii) above. The formation of substrate (GaAs) oxide beyond the first surface layer involves overcoming activation barriers such as the breaking of backbonds, the diffusion of oxygen atoms (and the migration of Ga and As atoms if bulk oxides like Ga_2O_3 and As_2O_3 are formed). The dissociated oxygen atoms appear to be energetic enough to overcome all these barriers.

The absence of O^{-2} ions in Cs throughout the whole range of oxygen exposures studied here should be contrasted to the case of thin layer of Cs on Ag. For a thin layer of Cs on Ag, Ebbinghaus et al [18] have shown that cesium-suboxide, i.e., O^{-2} ion, is formed readily by 10 L oxygen exposure at room temperature. The contrast offered by the case of Ag provides additional support to the general picture given to GaAs: (i) Oxygen bonding to Ag is weak compared to

cesium ($\Delta H(\text{Ag}_2\text{O}) = -7.3 \text{ Kcal}$ [15,16]), hence Ag does not compete for O^{2-} ions, (ii) Cs atoms in the Cs overlayer on Ag polarize less than on GaAs, i.e. the bonding between Cs and Ag is weak compared to the bonding between Cs and GaAs. Cs atoms may thus be mobile to form (oxygen-adsorption induced) islands and to achieve the necessary Madelung energy for the formation of cesium suboxides [19].

We conclude this subsection by giving the following brief description of the oxygen adsorption process on Cs-covered GaAs(110) surfaces: initially (i.e., at low oxygen exposure less than $\sim 20 \text{ L}$), the oxygen molecules which impinge on the cesiated GaAs(110) surface quickly dissociate by an efficient charge transfer from the low-work-function surface; the dissociated oxygen atoms cannot be stabilized by a thin layer of Cs, rather they find stable bonds with GaAs; as the amount of oxygen bonded to GaAs increases so that the mobility of Cs atoms in the Cs overlayer increases, the probability of the Cs layer to capture non-dissociated oxygen increases because the non-dissociated oxygen cannot find stable bonding with GaAs; the uptake of dissociated oxygen of the GaAs substrate slows down when the amount of oxygen bonded to GaAs increases beyond about one monolayer due to diffusion limited process, the bonding of O atom to GaAs, however, remains to be so favorable that no dissociated oxygen can be found in the Cs overlayer.

5.6 RESULTS AND DISCUSSION - EFFECTS OF ADDITIONAL CS TREATMENTS

One key factor determining the oxygen adsorption process on monolayer-Cs-covered GaAs(110) is the thinness of the Cs overlayer (monolayer is the highest stable Cs coverage achievable at room temperature before

adsorbing oxygen). For example, the sequence of oxygen species encountered in the oxidation of bulk Cs (section 3) does not occur in the adsorption process on Cs-covered GaAs surfaces due to (1) the insufficient Madelung energy provided by a thin layer of Cs, and (2) the proximity of the GaAs substrate which is a strong competitor for dissociated oxygen atoms. It is therefore interesting to ask that how much Cs is enough, in terms of both the thickness needed to provide enough Madelung energy for various oxygen ions and the thickness needed to separate the influence of the GaAs substrate, so that the oxidation of the Cs overlayer becomes similar to that of bulk Cs. We therefore have prepared surfaces with more than one monolayer of Cs by depositing additional Cs on the Cs/O-GaAs surfaces prepared in the way described in the previous section (sec. 5), and the oxygen adsorption properties of such "Cs-refreshed" surfaces are then examined; studies have been made on surfaces treated with up to three Cs-O cycles. In such experiments other questions can be asked, such as whether or not the Cs atoms supplied by the additional Cs treatment react with the oxygen in the O-GaAs bonding which was formed prior to the additional Cs deposition; question can also be asked whether or not the O_2^{-n} ions in Cs formed with 210 L oxygen exposure can be transformed into other oxygen species by the application of additional Cs.

The experimental data are spectroscopically complex. It is therefore appropriate to first list the important conclusions:

- i) the sequence of oxygen species, O^{2-} , O_2^{-2} , O_2^{-n} and O_2^- , which is encountered in the oxidation of bulk Cs, is observed with a total amount of Cs of ~3 monolayers.

- ii) the O_2^{-2} ion, if formed by oxygen exposure with 2monolayer Cs, is transformed into O^{-2} ion by a Cs treatment followed the oxygen exposure.
- iii) bonding of oxygen to GaAs continues with sufficiently high oxygen exposure even at the presence of more than one monolayer of Cs.
- iv) Cs atoms deposited after an oxygen exposure do not react with the oxygen atoms in the O-GaAs bonding.

We will again break the discussion into two subsections. The rather complex photoelectron spectra will be described first (6.1). A special subsection (6.2) is devoted to explaining the key phenomenon of dipole potential induced core level shifts. Explanations of the above conclusions will then follow (6.3).

5.6.1 The Photoelectron spectra

The EDC's of sample N2 subjected to alternating Cs and oxygen treatment are shown in figs. 67(Cs-4d), fig. 62(Cs-5p and O-2p related features) and fig. 60(Ga-3d, As-3d, Cs-5s and O-2s). Similar results obtained on sample N1 are also shown in fig. 70(Ga-3d, As-3d, Cs-5s and O-2s). The first Cs treatment resulted in monolayer coverage as defined in the previous bsection. Subsequent Cs treatments were with same flux but the actual coverage may be different due to different sticking coefficients of Cs on different surfaces. Only cumulative oxygen exposures between Cs treatments are entered in figs. 67 - 70.

The Cs Core Levels

Adsorption of oxygen shifts Cs core levels (5p, 5s, and 4d) to lower binding energy, whereas each "cesiation" brings Cs core levels to higher binding energy. The shift toward high BE (1.0 eV) produced by cesiation is slightly bigger than the toward low BE (0.7 eV) produced by adsorbing oxygen. After each fresh Cs treatment, a tailing emission can be seen on the high BE side of Cs-4d_{5/2} (fig. 67), and such tailing emission is removed after exposure to oxygen. This tailing emission indicates that, as has been discussed in section 4, the Cs overlayer deposited by each Cs treatment exhibits certain degree of metallic character, although the density of free electrons in the Cs overlayer must be lower than that of bulk Cs. Similar changes in the Cs-5p levels after Cs and oxygen treatment are also discernable (fig. 68).

O-2p Related Features

As has been described in section 5, O-2p related features produced by oxygen exposures after the first Cs treatment consist of two relatively narrow peaks at 4.6 eV and 7.4 eV below the VBM of GaAs, which are associated with O₂⁻ⁿ in Cs, superposed with a broad peak at 4.6 eV below VBM, which is due to oxygen bonded to GaAs. Cesiation shifts the pair of peaks (labeled 1 and 2 in fig. 68) of O₂⁻² to higher binding energy. The shift is equal to that of Cs core levels. The separation between the two peaks remain approximately the same after cesiation. The emission in the valley between the two peaks appears to be reduced after the second Cs treatment (curve c to curves d and e, fig.

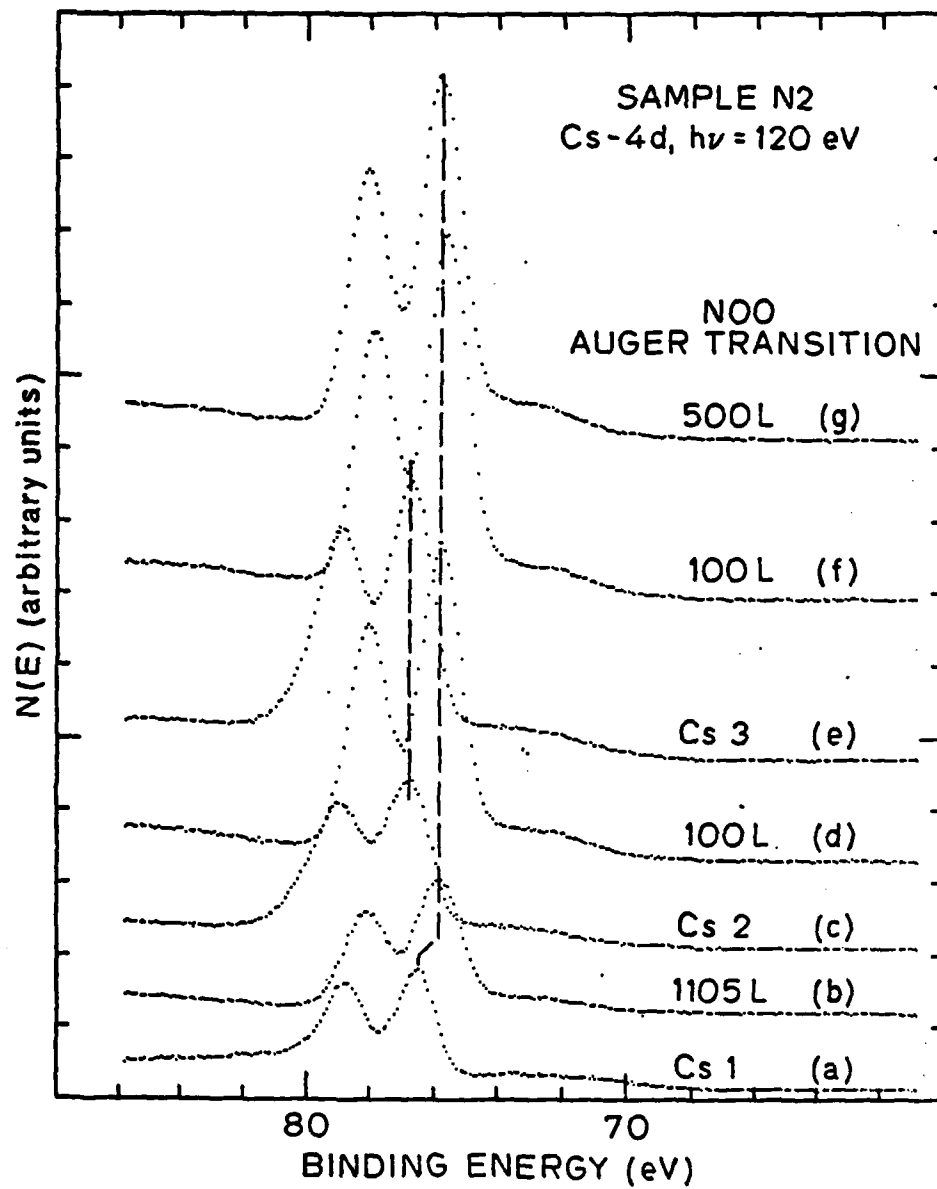


Figure 67: EDC's of the Cs-4d levels and the NOO Auger transition of sample N2 subjected to alternating Cs and oxygen treatments.

68). This indicates that the relative contribution from the oxygen in the O-GaAs bonding to the emission in the valence band region decreases after the second Cs treatment due to attenuation by the (Cs,O) overlayer with increasing thickness and due to increased amount of O_2^{-n} incorporated into Cs.

A new oxygen feature (labeled 3) appeared in curve d of fig. 68 after the 100 L oxygen exposure that followed the second Cs treatment; it is located at 2.2 eV below VBM. The separation of this peak from the Cs- $5p_{3/2}$ level is 8.6 ± 0.2 eV, close to that expected for either the O^{-2} ions (8.7 eV, fig. 59) or the leading peak of O_2^{-2} ions (8.6 eV, fig. 59). The expected positions for the other two peaks associated with O_2^{-2} ions are marked with arrows 3a and 3b in curves d of fig. 68. It is not clear whether there is feature above arrows 3a and 3b in curve d, because the positions of 3a and 3b overlap with peaks 1 and 2 due to O_2^{-n} . Peak 3 is also shifted to higher binding energy by cesiation as other levels of the overlayer are, but by a significantly smaller amount (0.6 eV, curves d and e, fig. 68). The smaller shift of peak 3 compared to other peaks by the third Cs treatment is explained below by the transformation of O_2^{-2} ions into O^{-2} ions, i.e., peak 3 in curve d (before the 3rd Cs treatment) is associated with O_2^{-2} , whereas peak 3 in curve e is associated with O^{-2} . The binding energy of the $O-2p$ level of O^{-2} ions, 2.7 eV below Fermi level, is 0.6 eV lower than the binding energy of the $2\pi_g$ multiplet of O_2^{-2} ions (3.3 eV below Fermi level). The transformation of O_2^{-2} to O^{-2} therefore introduces to peak 3 a shift 0.6 eV to lower BE, which superposes with the change of dipole potential induced by recesiation (to be discussed below

in 6.2) - a shift to higher binding energy by 1 eV for all energy levels. The net result is a shift of 0.4 eV of peak 3 toward higher binding energy after the 3rd Cs treatment. We therefore tentatively conclude here that O_2^{-2} in Cs can be formed with only about monolayers of Cs being present in the overlayer, but it is reduced to O^{-2} after recession.

The O_2^{-} ion in Cs was formed after the third Cs treatment and one high oxygen exposure (500 L, curve g of fig. 68). This is established by the similarity of the top spectrum in fig. 68 and the spectrum of O_2^{-} in fig. 59. The appearance of the O_2^{-} ion, the last oxygen species observed in the oxidation of bulk Cs (fig. 59, section 3), suggests that the oxidation behavior of Cs atoms becomes similar to that of Cs atoms in bulk Cs, after only about three monolayers of Cs being present in the overlayer.

The Ga-3d and the As-3d Core Levels

As explained in section 5, the oxygen adsorbed after the deposition of the 1st monolayer of Cs predominantly bonds to GaAs and induces a chemical shift in the As-3d level ($\Delta E=3.6$ eV) and a broadening in the Ga-3d level; these results are again seen in curve b of fig. 69. The shifted As-3d peak with ΔE (change in binding energy)=3.6 eV is moved by the second Cs treatment to have $\Delta E=4.6$ eV (curve c of fig. 69 and curve c of fig. 70). A shoulder with $\Delta E=3.2$ eV is also revealed by this treatment. The relative intensity of the shifted As-3d peak and the unshifted As-3d peak stayed constant before and after Cs treatment.

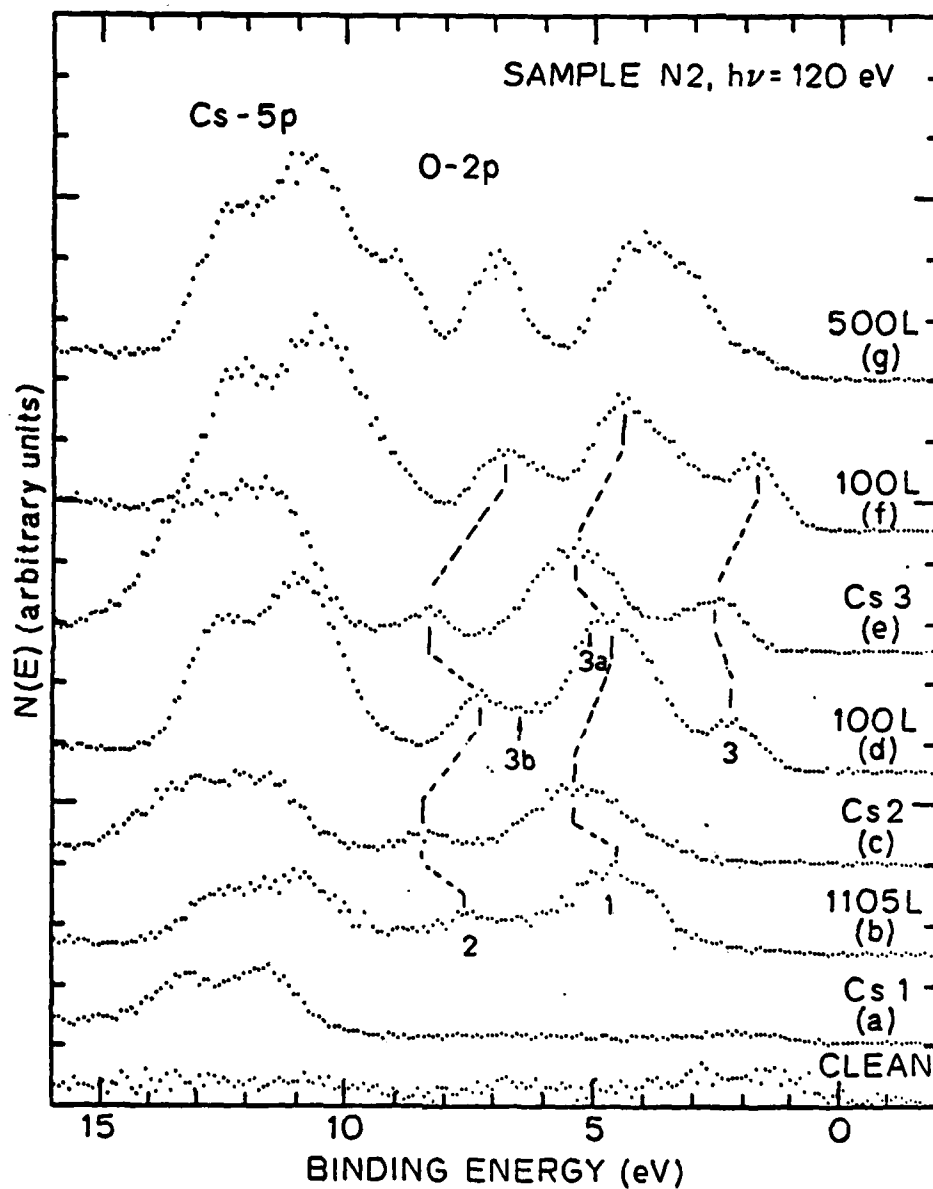


Figure 63: EDC's of the Cs-5p levels and the valence band region of sample N2 subjected to alternating Cs-O treatment.

This result is independent of the amount of shifted As-3d peak (compare curve c of fig. 69 and curve c of fig. 70). Oxygen exposures made after the second Cs treatment brought the shift back to $\Delta E = 3.6$ eV (curve d of fig. 69 and curve d of fig. 70). The shifted As-3d peak is, however, significantly narrower than before the 2nd Cs treatment (curve b, fig. 69), 1.7 eV vs. 2.2 eV FWHM. The GaAs substrate is further oxidized by oxygen exposures made after the second Cs treatment, as evidenced by the growth of the shifted As-3d peak relative to the unshifted As-3d peak (curve d of fig. 69 and curve d of fig. 70). Subsequent Cs and oxygen treatments on sample N2 switched the position of the shifted As-3d peak back and forth between $\Delta E = 4.6$ eV and $\Delta E = 3.6$ eV; the final oxygen exposure (500 L) moved the shifted As-3d peak slightly toward lower binding energy to give $\Delta E = 3.4$ eV (curve g, fig. 69).

The Ga-3d peak is also shifted by ~ 1.0 eV toward higher binding energy by the second Cs treatment (curve c of fig. 69 and curve c of fig. 70). The 100 L oxygen exposure followed moved the Ga-3d back to its position before the second Cs treatment (curve d, fig. 69). The effect on the Ga-3d generated by the rest Cs and oxygen treatments on sample N2 is difficult to assess because the Ga-3d is broad partly due to the rigid shift expected and partly due to the overlap with the newly emerged O-2s peak on the low BE side of Ga-3d.

In curve f of fig. 69, an O-2s peak related to cesium oxide clearly developed at 17.9 eV below VBM after the 100 L oxygen exposure that followed the third Cs treatment. The 6 eV separation between the Cs-5s

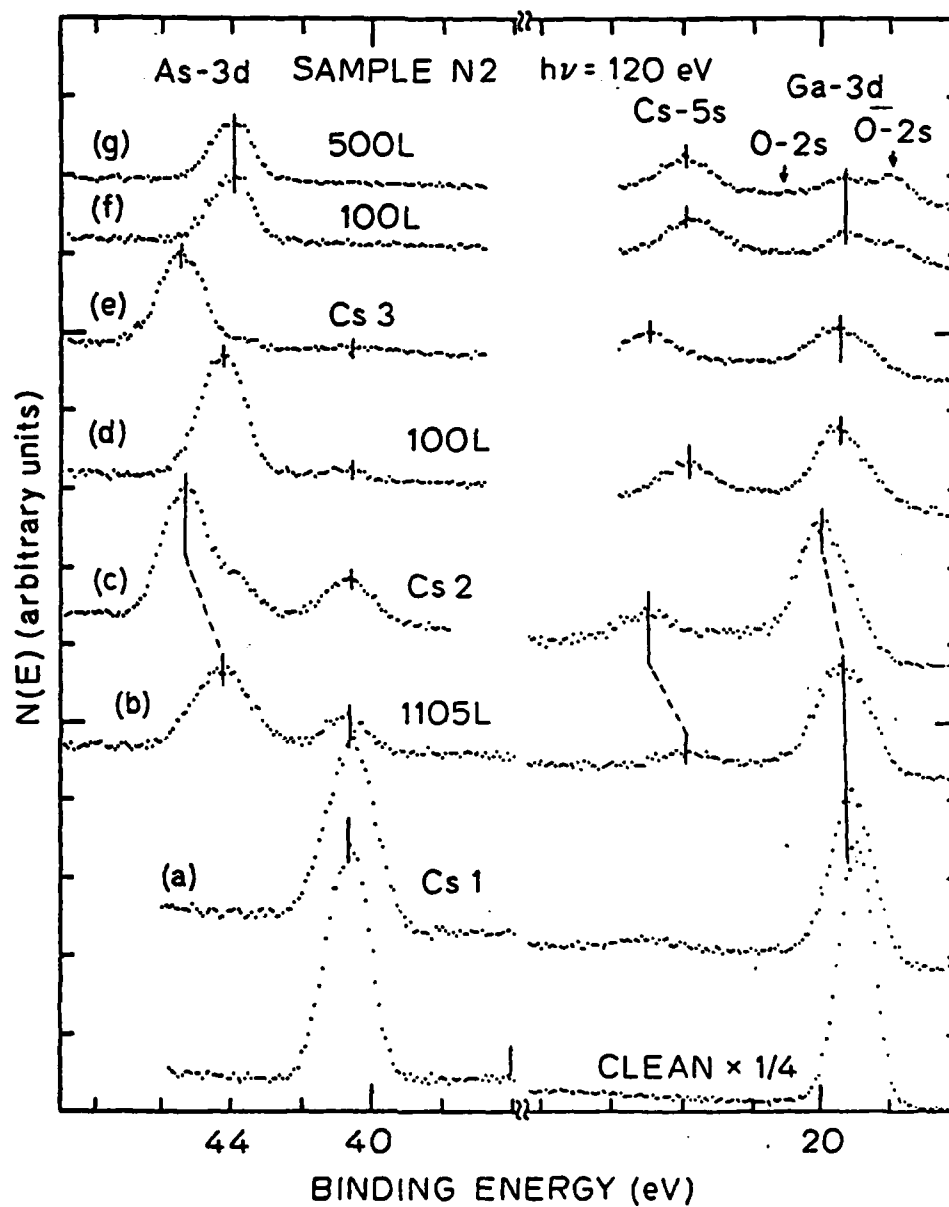


Figure 69: EDC's of Ga-3d, As-3d, Cs-5s and O-2s of sample N2 subjected to alternating Cs-O treatment. The level on the low BE side of the Ga-3d, seen in curves f and g, is due to oxygen incorporated in Cs, whereas the one on the high BE side of the Ga-3d is due to O-GaAs bonding.

peak and the O-2s peak is identical to that found in the oxidation of bulk Cs [4].

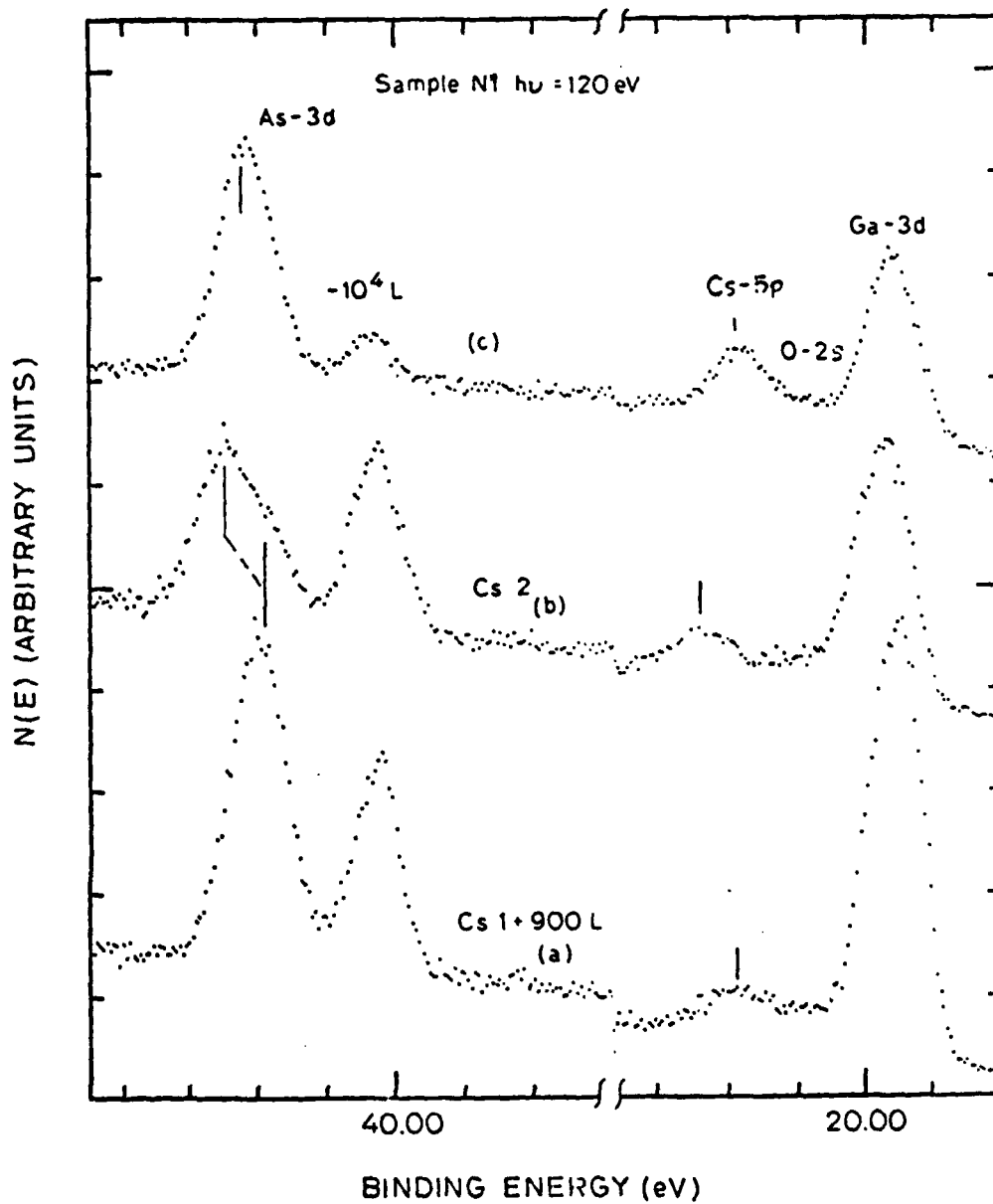


Figure 70: EDC's of As-3d, Cs-5s, O-2s, and Ga-3d spectra of sample N1 subjected to alternating Cs and O treatments.

5.6.2 Adsorbate Induced Surface Electrostatic Potential Change and the Shift of Adsorbate Core Levels

One key result to be understood in the above subsection is the complex shifts exhibited by various energy levels. Most of the shifts can be reasonably well explained by the change in the dipole potential across the overlayer. The possibility that the downward shifts occurred after each Cs treatment are caused by reactions of Cs with various oxides, however, cannot be immediately ruled out. The change of the chemical shift in As-3d levels between $\Delta E=3.6$ eV and $\Delta E=4.6$ eV by alternate cesium and oxygen treatments is rather intriguing. The shift of $\Delta E=3.6$ eV is close to the value expected for As_2O_3 [11], and the shift of 4.6 eV is close to the value expected for As_2O_5 [20]. It would then be tempting to associate the 4.6 eV shift with As_2O_5 and the 3.6 eV shift with As_2O_3 in the present case. To illustrate such possibility, we outline below one hypothetical way the Cs treatment could transform As_2O_3 to As_2O_5 .

We first notice that the ratio of the area under the shifted As-3d peak and that under the unshifted peak is the same before and after each Cs treatment (fig. 69). This result is independent of the absolute value of the ratio. In fig. 70, we have shown that consistent results were obtained on sample N1, which was initially oxidized to a less extent. Hence numbers of oxidized and unoxidized As atoms are the same before and after each Cs treatment. Additional oxygen atoms must be supplied for the transformation from As_2O_3 to As_2O_5 to occur. The most likely source is the release of O_2^{-n} ions from Cs. The

release could in principle be achieved by dissociating O_2^{-n} ions into O^{-2} ions using the excess charges supplied by fresh Cs; since As_2O_5 is thermodynamically more stable than As_2O_3 , formation of As_2O_5 from As_2O_3 would occur. Including all possible reactions, it is, however, thermodynamically more favorable to have Cs react with As_2O_3 , if it existed, to reduce it to free As, rather than to oxidize it to As_2O_5 ; free energies of reaction indicating this point are given in the Appendix. The most serious difficulty of the above interpretation is that the change of the shift from 4.6 eV back to 3.6 eV by oxygen exposures has to be understood as reduction of As_2O_5 to As_2O_3 by oxygen exposures. Such reduction is highly unlikely, if not impossible. The equality of the 4.6 eV shift observed here with the value expected for As_2O_5 is therefore merely coincidence. A mechanism other than the reaction of cesium with oxides must be sought to explain the shift.

The approximately equal shift (1 eV) of all overlayer-related levels relative to an substrate core level (As-3d of GaAs) indicates that one common mechanism is responsible for all shifts. We propose this mechanism to be the change of the dipole potential, induced by adsorption of Cs or oxygen, across the overlayer. The influence of the local electrostatic potential at the surface on the binding energy of adsorbate core levels has been theoretically considered by Gazuk [21]. The case that the binding energy of xenon core level is a constant when referenced to the vacuum level at the surface (instead of the Fermi level of the metal substrates) has been experimentally demonstrated by Fuggle and Menzle [22] who have measured the BE's of Xe-3d for Xe physisorbed on different metals with different work functions. In this work we

offer a case where the adsorbates themselves induce changes in the surface dipole potential which in turn cause proportional shift of the BE's of adsorbates core levels (and localized valence levels).

Fig. 71 schematically depicts this mechanism. Semiquantitative potential profiles near the surface region under different situations are shown. For simplicity, we have indicated only the As-3d (both shifted and unshifted) and the Cs-4d levels, other energy levels associated with the overlayer atoms follow the same change. The work function of GaAs (110) is taken from the value obtained by Gobeli and Allen [23] and corrected for the Fermi level pinning position. The lowering of work function by monolayer of Cs is from Clemens et. al. [9]. Electrons ionized from the Cs overlayer could reside either in the surface states or in the space charge region of GaAs, and can alter the band bending of GaAs. Such change in band bending is no more than 0.2 eV, hence we have ignored this change in preparing fig. 71. The dipole potential at the surface and the BE's of the core levels of the monolayer-Cs-covered GaAs(110) surface prior to oxygen exposure are shown in the left column. As a monolayer-Cs-covered surface is exposed to heavy oxygen exposure, one to two layers of O-GaAs bonding complexes are formed between Cs and GaAs (center column of fig. 71), which disorder the orientation of dipoles and may cause considerable weakening of the dipole. This mechanism of the weakening of the dipole is further aided by the incorporation of the O_2^{-n} ions into the Cs layer: Electrons are transferred from GaAs to O_2 molecules to form O_2^{-n} ions and the net dipole charges (between the GaAs substrate and the (Cs,O) overlayer) are reduced. Therefore most of the potential occurs

between the O-GaAs layer and the $\text{Cs}^+-\text{O}_2^{-n}$ layer, and only a small part falls over the O-GaAs layer. This reduction of the dipole strength raises the vacuum level at the surface; because the Cs core levels ride on the surface potential, their BE's referenced to the Fermi level are lowered. We have indicated, as an example, the shift of the Cs-4d level in fig. 71. In fig. 71, we have assumed that the shift in the Cs core levels is equal to the dipole potential change, i.e., we have assumed that the adsorption of oxygen in the Cs overlayer does not introduce chemical shift in the Cs core levels in addition to the dipole potential shift. This assumption is justified by (1) equal shift found in energy levels associated with different kinds of overlayer atoms, and (2) the lack of shift of Cs core levels when bulk Cs is oxidized to Cs_2O , Cs_2O_2 , Cs_2O_3 and CsO_2 [4].

The changes in the dipole potential and the BE's induced by recession are shown in the right column of fig. 71. Additional Cs treatment brings electrons that can be ionized from Cs and captured by GaAs (right column, Figure 14). The dipole potential is thus re-established between the GaAs substrate and the $\text{Cs}(\text{Cs}^+-\text{O}_2^{-n})$ layer. Because Cs^+ ion in the $(\text{Cs}^+-\text{O}_2^{-n})$ layer has a closer packing than Cs in the monolayer Cs on GaAs(110) (22 monolayers of Cs atoms are needed to pack one layer of Cs^+ ions in cesium oxides such as Cs_2O , Cs_2O_2 , Cs_2O_3 and CsO_2), part or all of the Cs atoms deposited by the 2nd Cs treatment may come into the same layer as the Cs^+ ions existed on the surface prior to the 2nd Cs treatment. Therefore the increase in the dipole potential mostly falls across the O-GaAs layer, and little falls within the $\text{Cs}(\text{Cs}^+-\text{O}_2^{-n})$ layer. Energy levels of all atoms in the overlayer,

including atoms in the O-GaAs layer, shift to higher BE with respect to the Fermi level by the same amount as the dipole potential increases. Re-exposure to oxygen leads to reduction in a manner similar to that depicted in the center column of fig. 7f, and re-cesiumation can resume the dipole strength in a manner similar to that depicted in the right column. Energy levels such as the shifted As-3d, Cs-4d, Cs-5p, and O-2p therefore switch between high and low binding energy with alternate Cs and oxygen treatment.

One important implication of the above picture is that it suggests that each Cs treatment is as effective in lowering the surface work function as the first Cs treatment applied to clean GaAs despite the existence of the intervening O-GaAs layers. This result, as reflected in core level shifts here, is consistent with the result of Gregory and Spicer [24] who have directly measured the charges in photoelectric thresholds. In their Cs-oxygen treatment Gregory and Spicer also used oxygen exposures much higher than normally used for activating the GaAs (110) surface. They have found that, however, by terminating an arbitrary sequence of Cs-O treatment that contained large oxygen exposure with a Cs treatment, it is possible to achieve the same photoelectric threshold as that achieved by applying Cs alone to clean GaAs(110), although the decrease in yield above threshold is obviously related to the increased thickness of the intervening oxides depicted in Figure 14. The oxide layer therefore can be considered as one possible origin of the "interfacial barrier" observed for photoemission from photocathodes [15]. The origin of this interfacial barrier, however, is entirely different from the heterojunction discussed by Uebbing and James [25], or the double dipole discussed by Fisher et al. [26].

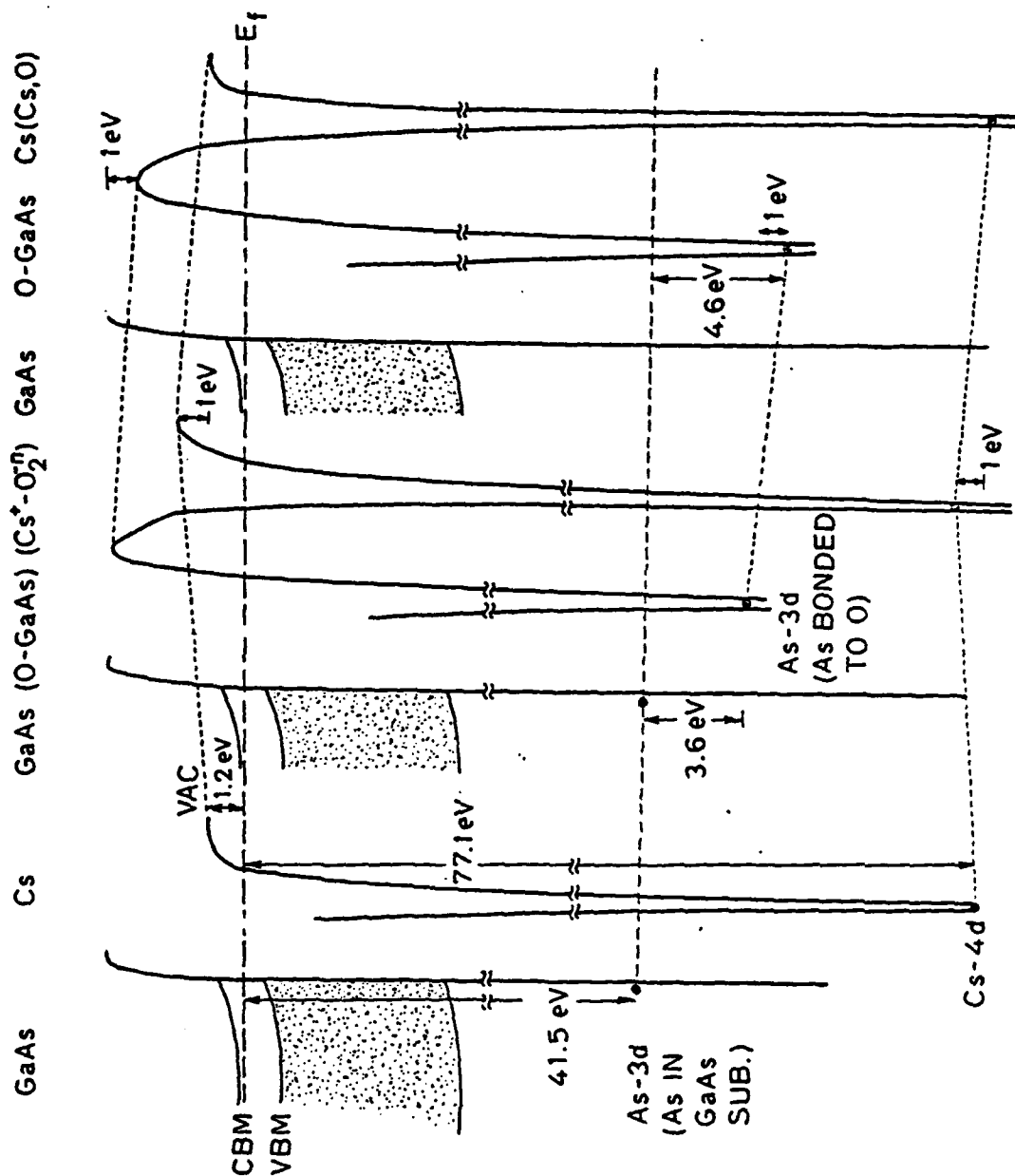


Figure 71: Schematic illustration of the changes in the surface dipole potential induced by oxygen or Cs adsorption. Such changes in the dipole potential are responsible for shifts of various energy levels displayed in figs. 67-70.

5.6.3 The Interaction Mechanisms

In this subsection we briefly give some explanations and implications of the spectroscopic findings, which have been summarized in the beginning of this section.

The fact that the oxidation property of Cs atoms in the overlayer becomes similar to that of bulk Cs (summary (i)) can be explained by the mobility of Cs atoms to form islands of cesium oxides and the reduction of the competition of the GaAs substrate for oxygen. The latter point is especially important in stabilizing O^{-2} ions in Cs. Reduction of the competing power of the GaAs substrate for dissociated oxygen may be achieved by two contributing factors: (a) increased thickness of a buffer layer of oxides (oxygen chemisorbed on GaAs(110) [3] or possibly As_2O_3 and Ga_2O_3 , and $Cs^+-O_2^{-n}$) so that the diffusion of oxygen atoms to the GaAs substrate is impeded; (b) increased amount of excess Cs so that the probability of stabilizing O^{-2} ions in Cs is increased. The relative importance of the two factors in stabilizing O^{-2} ions in Cs over a wide range of Cs coverages and oxygen exposures has not been determined in the present work. An optimum combination of the two factors for stabilizing O^{-2} ions may be pursued if the incorporation of O^{-2} ions in Cs on GaAs is desirable. Whether the O^{-2} ions are desirable or not for the

Result (ii) in the summary suggests that one way of obtaining Cs_2O or cesium suboxides is to reduce Cs_2O_2 by Cs. The result of section 5 shows that, however, Cs_2O_2 (or O_2^{-2} ions in Cs) cannot be obtained by

oxidizing a monolayer of Cs in direct contact with a GaAs substrate. It is necessary to deposit more than one monolayer of Cs.

Although the competing power of the GaAs substrate for dissociated oxygen is reduced and the oxidation of Cs atoms proceed nearly independent of the substrate after depositing more than one monolayer of Cs, the bonding of oxygen to GaAs still advances (summary (iii)). This indicates that the bonding of oxygen to GaAs is unavoidable even though different kinds of cesium oxides may be obtained on GaAs(110) by going to relatively thick Cs layers.

The fact that Cs does not react with oxygen in the O-GaAs bonding should again be contrasted to the case of (Ag₂O, Cs). It is a known method in preparing S-1 photocathode [15] (which is made of Ag, O and Cs) that Ag is first oxidized to form Ag₂O and then cesium vapor is then applied to reduce Ag₂O to produce Cs₂O. This method can not be extended to form Cs₂O on GaAs surfaces as indicated by our results. This difference is again explained by the relative stability of O-GaAs bonding over cesium oxides.

5.7 SUMMARY

In summary, we have examined the interaction of Cs and oxygen with the GaAs(110) surface from a fundamental point of view. The oxygen adsorption property of the GaAs(110) surface is found to be drastically modified by the presence of Cs, and the oxidation of the Cs atoms on GaAs(110) is found to be interfered by the chemically active substrate. The $\sim 10^7$ times enhancement in the rate oxygen bonds to GaAs with the presence of Cs suggests that the rate-limiting step of the oxygen

adsorption process on bare GaAs(110) surfaces is the dissociation of oxygen molecules. The fact that O^{-2} cannot be stabilized in a monolayer of Cs on GaAs is due to (1) the competition of the GaAs substrate for dissociated oxygen, and (2) insufficient Madelung energy in a two dimensional layer of Cs atoms. A non-dissociated oxygen species, O_2^{-n} , however, was found to incorporate into a monolayer of Cs on GaAs(110), because (1) it is easier to stabilize (free O^{-2} is 5.0 eV more unstable than neutral O atom, whereas O_2^{-} is 0.56 eV more stable than O_2) and (2) non-dissociated oxygen does not find stable bonds with GaAs thus it faces no competition from the substrate. Formation of O^{-2} was found after depositing two to three monolayers of Cs on GaAs; this result is not merely due to the increased number of Cs atoms, but also due to increased mobility of the newly added Cs atoms to form islands of Cs-oxygen complexes. The bonding of oxygen to GaAs continues, although at a slower rate, after the deposition of more than one monolayer of Cs.

The core level shifts of the overlayer atoms were found to reflect the change of surface dipole potential. The core shifts observed in experiments where the GaAs surface is subjected to alternating Cs-oxygen treatments revealed that each Cs recession is capable of achieving the same surface work function irrespective of the thickness of the O-GaAs layer built up by oxygen exposures and Cs treatments.

The results of this work also suggest the important considerations for co-adsorption studies - in the system we have studied, the interaction between adsorbates influence the adsorbate-substrate interaction and vice versa; neglect of any of the interactions would lead to failure of understanding the problem.

5.8 APPENDIX

For the purpose of reference we have calculated the standard free energies of reaction of adding cesium to various oxides. Results are listed in table 3. Thermodynamically, those reactions are most probable in which $-\Delta G$ are largest. As have been discussed in the text, before the second Cs treatment, the surface is oxidized to contain Ga_2O_3 , As_2O_3 , and one type of cesium oxide which is known definitely to have lower oxygen content than Cs_2O_4 .

Table A1 therefore suggests the following most probable sequence of reduction reactions by the second and the third Cs treatments:



If Cs_2O_3 was indeed the starting point of the reduction reaction, the amount of Cs supplied by the second Cs treatment would be enough to proceed at least to the second step in the above sequence. The amount of Cs, however, is not the reason that we do not observe the above reaction sequence (with the exception of O_2^{-2} to O^{-2}) -- as has been discussed in the text, the tailing emission on the high binding energy side of the $Cs-4d_{3/2}$ level (curve e, fig. 67), which also appeared after deposition of monolayer Cs on clean GaAs, suggests that there are actually excess or unreacted Cs in the overlayer after each recession. Other kinematic barriers may exist, or the O-GaAs bonding complex formed is a surface oxide involving Ga-O-As bridge bonds which may be more stable than As_2O_3 .

TABLE 12

Heats of formation and free energies of reaction of adding Cs to various oxides

Reactions	$-\Delta H$ (kcal/mole)	$-\Delta G$ (kcal/mole)
reactions with cesium oxides ¹		
1 $3 \text{ Cs}_2\text{O}_4 + 2 \text{ Cs} \rightarrow 4 \text{ Cs}_2\text{O}_3$	72.2	67.1
2 $\text{Cs}_2\text{O}_4 + 2 \text{ Cs} \rightarrow 2 \text{ Cs}_2\text{O}_2$	68.0	63.9
3 $1/3 \text{ Cs}_2\text{O}_4 + 2 \text{ Cs} \rightarrow 4/3 \text{ Cs}_2\text{O}$	59.8	55.3
4 $2 \text{ Cs}_2\text{O}_3 + 2 \text{ Cs} \rightarrow 3 \text{ Cs}_2\text{O}_2$	66.2	62.4
5 $\text{Cs}_2\text{O}_2 + 2 \text{ Cs} \rightarrow 2 \text{ Cs}_2\text{O}$	55.6	53.0
6 $2 \text{ Cs}_2\text{O} + 2 \text{ Cs} \rightarrow 2 \text{ Cs}_3\text{O}$	24.2	18.5
reactions with gallium oxide ²		
7 $4/3 \text{ Ga}_2\text{O}_3 + 2 \text{ Cs} \rightarrow 8/3 \text{ Ga} + \text{Cs}_2\text{O}_4$	-221	-224
8 $\text{Ga}_2\text{O}_3 + 2 \text{ Cs} \rightarrow 2 \text{ Ga} + \text{Cs}_2\text{O}_3$	-148	-151
9 $2/3 \text{ Ga}_2\text{O}_3 + 2 \text{ Cs} \rightarrow 4/3 \text{ Ga} + \text{Cs}_2\text{O}_2$	-76	-80
10 $1/3 \text{ Ga}_2\text{O}_3 + 2 \text{ Cs} \rightarrow 2/3 \text{ Ga} + \text{Cs}_2\text{O}$	-10	-13
reactions with arsenic oxides ²		
11 $4/3 \text{ As}_2\text{O}_3 + 2 \text{ Cs} \rightarrow 8/3 \text{ As} + \text{Cs}_2\text{O}_4$	-84	-91
12 $\text{As}_2\text{O}_3 + 2 \text{ Cs} \rightarrow 2 \text{ As} + \text{Cs}_2\text{O}_3$	-45	-52
13 $2/3 \text{ As}_2\text{O}_3 + 2 \text{ Cs} \rightarrow 4/3 \text{ As} + \text{Cs}_2\text{O}_2$	-8	-13
14 $1/3 \text{ As}_2\text{O}_3 + 2 \text{ Cs} \rightarrow 2/3 \text{ As} + \text{Cs}_2\text{O}$	24	20
15 $2 \text{ As}_2\text{O}_5 + 2 \text{ Cs} \rightarrow 2 \text{ As}_2\text{O}_3 + \text{Cs}_2\text{O}_4$	-0.5	-0.6
16 $3/2 \text{ As}_2\text{O}_5 + 2 \text{ Cs} \rightarrow 3/2 \text{ As}_2\text{O}_3 + \text{Cs}_2\text{O}_3$	17.7	16.3
17 $\text{As}_2\text{O}_5 + 2 \text{ Cs} \rightarrow \text{As}_2\text{O}_3 + \text{Cs}_2\text{O}_2$	33.8	31.7
18 $1/2 \text{ As}_2\text{O}_5 + 2 \text{ Cs} \rightarrow 1/2 \text{ As}_2\text{O}_3 + \text{Cs}_2\text{O}$	44.7	42.4
19 $4/5 \text{ As}_2\text{O}_5 + 2 \text{ Cs} \rightarrow 8/5 \text{ As} + \text{Cs}_2\text{O}_4$	-51	-55
20 $3/5 \text{ As}_2\text{O}_5 + 2 \text{ Cs} \rightarrow 6/5 \text{ As} + \text{Cs}_2\text{O}_3$	-20	-25
21 $2/5 \text{ As}_2\text{O}_5 + 2 \text{ Cs} \rightarrow 4/5 \text{ As} + \text{Cs}_2\text{O}_2$	8.8	4.4
22 $1/5 \text{ As}_2\text{O}_5 + 2 \text{ Cs} \rightarrow 2/5 \text{ As} + \text{Cs}_2\text{O}$	32.2	28.7
1. Ref. 15	2. Ref. 16	

REFERENCES

1. W. E. Spicer, Appl. Phys. 12, 115(1977)
2. M. Erbudak and B. Reihl, Appl. Phys. Lett. 33, 584(1978); D. T. Pierce, G. C. Wang and R. J. Celotta, Appl. Phys. Lett. 35, 220(1979)
3. see Chapter III
4. see Chapter IV
5. see Chapter VI
6. P. E. Gregory and W. E. Spicer, Phys. Rev. B 12, 2370(1975)
7. A. J. von Bommel and J. E. Crombeen, Surf. Sci. 45, 308(1974); Surf. Sci. 57, 109(1976)
8. A. Ya. Mityagin, V. D. Orlov, V. V. Panteleev, K. A. Khronopulo, and N. Ya. Cherevatskii, Soviet Phys.-Solid State, 14, 623(1973)
9. H. J. Clemens, J. V. Wienskouski and W. Monch, Surf. Sci. 78, 648(1978)
10. Pianetta et. al. have shown that, by assuming reasonable values of escape depth for photoelectrons excited by 100 eV photon, a monolayer oxygen coverage on GaAs(110) is obtained when the shifted and the unshifted As-3d have about equal strength. P. Pianetta, I. Lindau, C. M. Garner and W. E. Spicer, Phys. Rev. B 18, 2792(1978)
11. see Appendix B of Chapter III
12. see Appendix A of Chapter III Ga₂O₃
13. J. Derrien, F. Arnaud d'Avitaya, and M. Bienfait, Solid State Commun. 20, 557(1976); Surf. Sci. 65, 668(1977)
14. J. J. Barton, W. A. Goddard III and W. E. Spicer, J. Vac. Sci. Technol. 16, 1178(1979)
15. W. Heiman, E.-L. Hoene, S. Jeric, and E. Kinsky, Exper. Tech. Phys. 21, 193-207, 325-341, 431-436(1973)
16. O. Kubaschewski and C. B. Alcock, Metallurgical Thermochemistry, 5th ed., Pergmon Press, N. Y., 1979

17. I. Lindau, P. Pianetta, W. E. Spicer, P. E. Gregory, C. M. Garner and P. W. Chye, J. Electr. Spectr. Related Phenom. 13, 155(1978)
18. G. Ebbinghaus, W. Braum, A. Simon and K. Berresheim, Phys. Rev. Lett. 37, 1770(1976)
19. A. Simon, in
 . us Structure and Bonding 36 pp. 81(Springer, N. Y., 1979)
20. M. K. Bahl, R. O. Woodall, R. L. Watson and K. J. Irgolic, J. Chem. Phys. 64, 210(1976)
21. J. W. Gazuk, Phys. Rev. B 14, 2267(1976)
22. J. C. Fuggle and D. Menzel, Surf. Sci. 53, 21(1975)
23. G. W. Gobli and F. G. Allen, chap 11 in Semiconductors and Semimetals vol. 2, Academic Press, 1966
24. P. E. Gregory and W. E. Spicer, J. Appl. Phys. 47, 510(1976)
25. J. J. Uebbing and L. W. James, J. Appl. Phys. 41, 4505(1970)
26. D. G. Fisher, R. E. Enstrom, J. S. Esher, and B. F. Williams, J. Appl. Phys. 43, 3815(1972)

Chapter VI

PHOTOELECTRON SPECTROSCOPIC DETERMINATION OF THE STRUCTURE OF (Cs,O) ACTIVATED GAAS(110) SURFACES

6.1 INTRODUCTION

Negative electron affinity (NEA) refers to the condition that the vacuum level at the surface of a semiconductor lies below the conduction band minimum in the bulk. The first NEA condition was demonstrated on p-type GaAs by Scheer and Van Laar [1] by treating vacuum cleaned (110) surfaces with Cs. Later Turnbull and Evans [2] have demonstrated that even lower vacuum level and greater stability in photoemissive yields can be obtained by applying Cs and O alternately on GaAs (110) surfaces. Since these initial discoveries, extensive attempts have been made to achieve the NEA condition on other III-V semiconductors with narrower band gaps than GaAs [3,4,5]. The driving force has been to find high efficiency photocathodes for a number of IR systems at wavelengths near or longer than 1 μm [6]. Photocathodes used in the current generation of night-vision image intensifiers are (Cs,O) activated GaAs. The GaAs-(Cs,O) cathodes also find extensive use as sources of spin polarized electrons [8].

Despite the successful development of the NEA photocathode technology [3], fundamental understanding of the lowering of the potential barrier at the semiconductor surface by (Cs,O) treatment has been lacking. The method of (Cs,O) treatment, the so-called "yo-yo" technique [3-5], has

so far remained empirical. The overall quantum yield of a photocathode can be analyzed in terms of the 3-step model of photoemission developed by Spicer [9,10] and the final step in such analysis involves the surface potential barrier which is, in part, determined by the nature of the (Cs₂O) activating layer. Two different types of surface potential barrier have been proposed and both types have successfully accounted for the experimental spectral yield data for NEA photocathodes with a wide range of band gaps. The nature of the two types of barrier, however, is qualitatively distinct from each other. In the dipole model [11-13], the surface potential barrier is determined by a dipole layer with a width of one or two atomic layers. In the heterojunction model [3,6,14-16], the major escape barrier is determined by the heterojunction between the n-type semiconducting Cs₂O and the III-V compound substrate; the heterojunction height also controls the band bending in Cs₂O and hence the position of the vacuum level at the final Cs₂O surface, which is another factor in determining the surface escape probability. The major consequence of the above difference between the two models is that the heterojunction model predicts limitation of extending the high yield threshold below 1.2 eV by using narrow band gap III-V compounds, whereas such limitation is not clearly predicted by the dipole model. The findings of Uebbing and James [15,17] that, for example, on activated GaSb the high yield threshold is set by a value higher than the band gap of GaSb, appears to support the existence of an "interfacial barrier". Such findings have prompted the development of the (field-assisted) transfer-electron photocathodes [18] where escape of photoelectrons into vacuum originates from valleys of the conduction band lying

at energy higher than the Γ point (the lowest energy valley of the conduction band of all direct-gap III-V compounds). The physical origin of the interfacial barrier, however, has not been identified and possible improvement of non-transfer type photocathodes has not been successfully pursued.

Clark [19] has attempted to provide a more general theoretical basis for possible types of activating layer. After showing that a Mott transition occurs in amorphous Cs_2O at $x \approx 0.1$, a wide range of experimental results on Cs-O activation layer on III-V semiconductor were explained in terms of either the Schottky or the heterojunction mode of activation.

The relevance of the unifying theoretical picture of Clark, as well as the resolution of the disputes between the two models, clearly requires experimental data other than yield measurements. A few compositional and structural studies have been made in the past. Sommer et. al. [11], using atomic absorption analysis, have determined the Cs content in the Cs-O activation layer on GaAs, to be 4.7 monolayer (1 monolayer = 4×10^{14} atoms/cm²). The oxygen content, however, cannot be determined in the atomic absorption analysis, hence the suggestion of the 4.7 monolayer Cs being equivalent to 1 monolayer of Cs plus one monolayer of Cs_2O by Sommer et. al. [11] requires further justification. Goldstein [20] has made LEED, AES, and thermal desorption studies of Cs-O activating layer on GaAs (111) and (100) surfaces. The major findings of this work are that the (Cs,O) activation layer is disordered and that there is no clear correlation between photoemission sensitivity and

the amount of Cs and O adsorbed. Flash desorption has shown that O desorbs after desorption of Cs is completed. Similar studies have also been made by Stocker [21]. The major concern in Stocker's work is the understanding of a two-stage activation process. In a two-stage process the initial "yo-yo" activation is followed by heating to elevated temperatures (520°C-580°C) and a second activation; the second activation normally gives 30% higher photoemission sensitivity[21,22]. To date the highest reflection yield reported on activated GaAs was obtained by the two-step activation process [22]. Stocker [21] found that the heating prior to the second activation desorbs nearly all Cs in the activating layer and causes no change in the amount of oxygen. Gregory and Spicer [23] have compared UPS spectra ($h\nu < 11.6\text{eV}$) of thick cesium-oxide film with those of Cs-O activation layer on GaAs(110) surfaces. There they found no similarity between the Cs-O activation layer achieving the NEA condition and thick cesium oxides.

The structural and compositional studies reviewed above point to a picture much more complicated than models based on yield measurements. The result of Goldstein [20] and Stocker [21] of disordered (Cs,O) activation layer does give some support to Clark's picture of an amorphous activating layer. The existence of suboxides, Cs_{2+x}O , however, can be questioned by comparing the photoemission studies of bulk suboxides by Ebbinghaus et. al. [24] with the results of Gregory and Spicer [23]. A more serious implicit assumption common to all early studies is the inertness of III-V substrates in the Cs-O reaction, although the desorption results of Goldstein [20] and the two-stage activation results of Stocker [21] clearly require invoking oxygen-GaAs bonding.

We have recently performed photoelectron spectroscopic studies of the interaction of Cs and oxygen with GaAs(110) surfaces [25,26]; in those non-activation experiments (i.e., Cs and oxygen were applied to GaAs surfaces without following the yo-yo procedure) we were able to determine several properties to be considered fundamental to the (Cs,O,GaAs) system, the most important one being perhaps the drastically enhanced rate (10^7 times) of bonding of oxygen to GaAs with the presence of Cs which questions the assumption of the inertness of the GaAs substrate in the activation process. More of these fundamental properties will be summarized in section 3 after describing experimental details in section 2. In this work we have performed photoelectron spectroscopic measurements on GaAs(110) surfaces activated to known white light sensitivity. The results of such experiments are compared to the fundamental properties concluded from the non-activation experiments and a new physical model of the activated GaAs surface will be given (section 4). As a by-product of this study, we have also found contamination of the activation layer by OH ion and we will discuss its effect on the activated surface in section 5.

6.2 EXPERIMENTAL

Experiments were performed in a standard stainless-steel ultra high vacuum chamber with a base pressure of $3-5 \times 10^{-11}$ torr. Energy analyses of the photoelectrons were performed by a double-pass cylindrical mirror analyzer (Physcial Electronics). Light sources used were monochromatized He-I (21.2 eV) and He-II (40.8 eV) radiation from a differentially pumped discharge lamp.

Samples used were Zn-doped $1.4 \times 10^{18} \text{ cm}^{-3}$ p-type GaAs. The doping concentration and the quality of the crystal may not be that used to make optimum NEA photocathodes. Cs vapor was supplied either by channels or by metallic source with no systematic difference in the final photoemission. It was found, however, easier to obtain activated surfaces with metallic source, hence the major part of this type of studies was made with metallic Cs source. Preparation and arrangement of the metallic Cs source have been described elsewhere [27]. The copper side arm used in ref. 27 was replaced by a glass tube, with Cs sealed off in one end of the tube. The source warmed to 45°C to give a controllable rate. For ease of control, oxygen exposures were made with ion pump only partially valved off, and oxygen pressures were maintained at 2×10^{-9} torr over a base pressure of 5×10^{-11} torr. Two types of "yo-yo" techniques were used. In one case the Cs and oxygen were applied alternately to peak the white light sensitivity. (In order to obtain a well defined peak in the white light sensitivity, Cs or O flux were in practice terminated after the sensitivity dropped 5%-10% below the peak value). In the other case, Cs flux was maintained continuously during the whole activation procedure, and O was applied on and off to peak the white light sensitivity. No systematic difference was found between the two techniques of activation. A calibrated tungsten light source operated at $\approx 2800^\circ\text{K}$ and focused to 2mm diameter was used to measure the white light sensitivity.

6.3 SUMMARY OF SOME FUNDAMENTAL PROPERTIES OF THE (CS,O,GAAS) SYSTEM

In an earlier study of co-adsorption of Cs and oxygen on the GaAs(110) surface (Chapter III), we have considered the following problems: (1) how does the presence of Cs (monolayer or sub-monolayer coverages) on the GaAs surface change the oxygen adsorption properties of GaAs(110), (2) how does the presence of the GaAs substrate influence the oxidation properties of the Cs overlayer, and (3) how does the Cs-oxygen interaction depend on the Cs coverage. Important results from that study that are relevant to the activation of GaAs surfaces are summarized below:

- i) The rate of oxygen bonding to GaAs is enhanced by at least 10^7 times in the presence of one monolayer (4.6×10^{14} atoms/cm²) of Cs
- ii) With one only one monolayer Cs on GaAs(110) surfaces, no oxygen can be incorporated into the Cs layer for oxygen exposure below 10 L; the only oxygen species that can be incorporated into the Cs layer (one monolayer or less) is not O⁻², the oxygen species contained in cesium suboxide, but is a non-dissociated oxygen species. We notice that in a normal activation procedure the total oxygen exposure is no more than 10 L [4,5,10,11,21].
- iii) with only about two to three monolayers of Cs on GaAs(110) the oxidation of the Cs overlayer becomes similar to that of bulk Cs, i.e., O⁻² can be stabilized in the Cs layer at low exposure, and other oxygen species in Cs, such as O₂⁻², and O₂⁻, also occur at high oxygen exposures.

iv) O_2^{-2} in Cs, if formed, can be reduced to O^{-2} by fresh Cs treatment; O_2^{-} can be formed only with the presence of more than two monolayers of Cs and oxygen exposures ≥ 100 L. This result, together with (ii), suggests that O^{-2} is the only species in Cs to be considered for a GaAs surface activated with (Cs,O) yo-yo treatment.

v) with the presence of more than two monolayers of Cs on GaAs, the bonding of oxygen to GaAs still continues (although at a slower rate than with only one monolayer of Cs).

The most important implication of the above results from the non-activation experiments is that O-GaAs bonding should play an important role in the activation of GaAs surfaces, which has been ignored in all previous work. The specific conditions under which these implications are applicable to surfaces activated with yo-yo technique will be the subject of the rest of this paper.

6.4 RESULTS AND DISCUSSION - MODEL OF THE (CS,O) ACTIVATED GAAS(110) SURFACE PREPARED BY THE "YO-YO" TECHNIQUE

Activation of GaAs(110) surfaces with conventional "yo-yo" techniques have been attempted. As has been mentioned in the Introduction section, it is difficult to quantitatively specify the activation process. Therefore by no means can we suggest the composition and structure determined here for our activated surfaces to be exactly applicable to the typical activated surfaces obtained in other laboratories. The small oxygen exposures and the repeated Cs treatments are, however, closer to

the conditions common to most yo-yo processes than the extreme conditions studied in our non-activation experiments (sec. 3). Therefore the activated surfaces studied here in conjunction with the fundamental properties concluded from the non-activation experiments, which we have summarized in section 3, do offer general understanding of the "yo-yo" technique.

Discussion in this section will be divided into two subsections: Photoelectron spectra obtained on typical activated surfaces will first be analyzed and the qualitative ingredients, as well as semiquantitative estimates of several parameters, of the model of activated surfaces will be given (4.1). Some implications of the new model will be discussed in 4.2.

6.4.1 The Model

The photoelectron spectra

In the lower curve of fig. 72, we show the He-II ($h\nu=40.8$ eV) spectrum of a p-GaAs(110) surface activated with (Cs,O) to have white light sensitivity of $880 \mu\text{A/l}$. This spectrum is typical of several surfaces activated to have comparable sensitivity. Although the $880 \mu\text{A/l}$ white light sensitivity is less than half of the highest value observed to date, it is achievable only if the NEA condition is reached (NEA condition is reached if white light sensitivity is $\geq 400 \mu\text{A/l}$ [20]). The relatively low value of the white light sensitivity could be caused by non-optimum choices of doping concentration, which influences the band bending and, to less extent, the diffusion length of electrons, and the

quality of crystal which seriously influences the diffusion length. These bulk properties of GaAs are not of concern here.

There are two major O-2p related features in the energy distribution curve (EDC) obtained on activated surface: Peak 1a at 3.3 eV below VBM and peak 1b at ~4.6 eV below VBM. (There are also two weak peaks, 2 and 3, at ~5.0 eV and ~9.0 eV below VBM, respectively. They are due to minor OH contamination which will be ignored here; more discussion of the role of OH⁻ will be given in section 5.)

Peak 1 can be attributed to O⁻² ion, which has a single O-2p related feature in the photoemission spectrum [27]. The binding energy of peak 1 is 1.1 eV higher than that observed for O⁻² ions in bulk Cs [27]. As explained in our earlier paper on the non-activation experiments [26], since adsorption of Cs and oxygen often produce large change in the dipole potential across the overlayer, energy levels associated with the overlayer atoms which ride on the dipole potential may not have a constant binding energy referenced to the Fermi level. Further justification of the assignment of peak 1 to O⁻² will be seen below (fig. 77) where we observe the BE of the O-2p of O⁻² ion in a thick Cs film on GaAs gradually move from 2.7 eV below the Fermi level (the value observed for O₆min.² in bulk Cs [27]) to higher BE as the photoemission sensitivity of that surface increases due to the adsorption of OH⁻.

Peak 1b is assigned to oxygen bonded to GaAs. Crude decomposition of the EDC and comparison with the spectrum of oxygen adsorbed on bare GaAs(110) (the upper curve of fig. 72) supports this assignment. Separate heating experiments done on unsuccessfully activated surfaces better reveal the O-GaAs bonding. In fig. 8heat., we show the EDC's of a

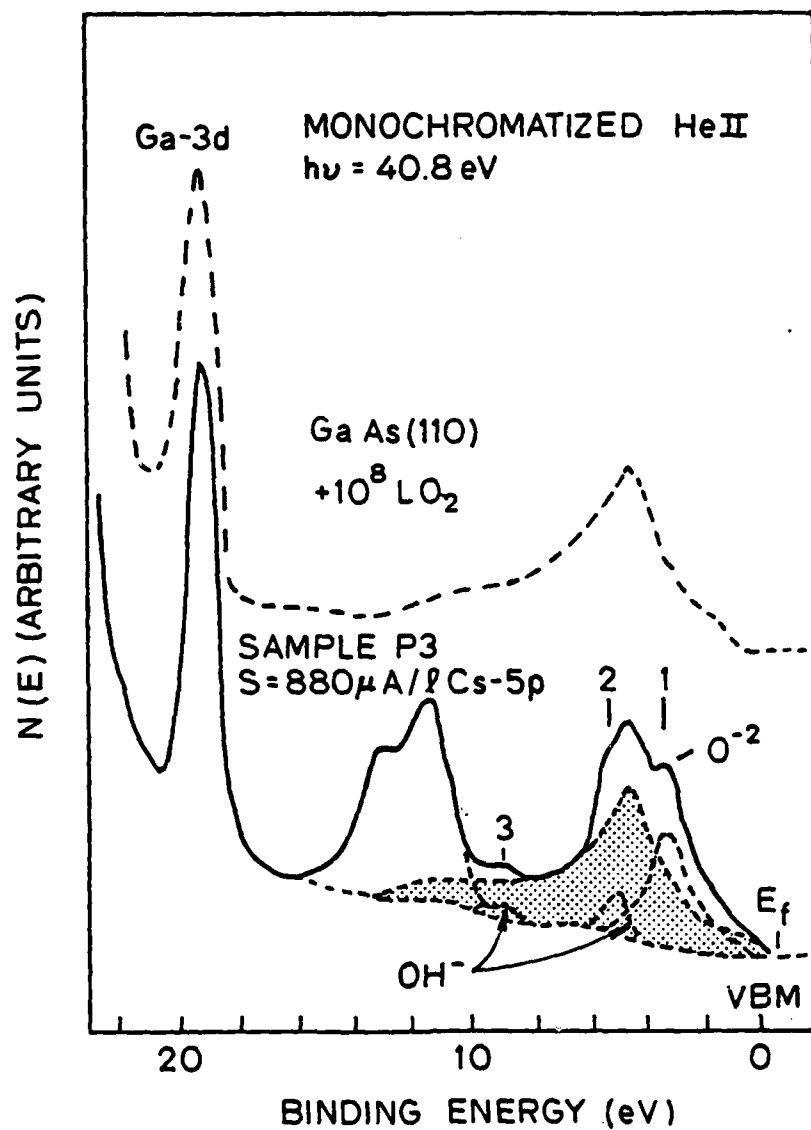


Figure 72: The He-II spectrum of a typical activated p-GaAs surface (the lower curve) compared to the He-II spectrum of a bare GaAs surface exposed to 10^8 L oxygen (the upper curve)

p-GaAs(110) surface activated to 280 $\mu\text{A/l}$ sensitivity (the lower curve) and after heating at 385°C for 10 min. (the upper curve). In the EDC before heating we see a small shoulder at ~3.0 eV below VBM due to O^{-2} and a pair of strong peaks due to OH^- . As will be explained later, the low sensitivity is due to excess OH adsorbed. After heating, the majority of the Cs atoms in the activation layer desorbs as evidenced by the decrease in the intensity of the Cs-5p levels. O-2p related features due to O^{-2} and OH^- , which are associated with Cs, disappear completely after heating; the broad O-2p peak revealed after heating is characteristic of oxygen bonded to GaAs.

We thus have confirmed that GaAs surfaces activated with (Cs,O) yo-yo treatments contain both oxygen bonded to GaAs and O^{-2} incorporated in Cs. This is expected from the findings of the non-activation experiments (sec. 3) - the yo-yo process does not introduce any peculiar behavior that is inconsistent with the fundamental properties governing the interaction of (Cs,O,GaAs). We have therefore found two essential qualitative ingredients of the activated surface: O-GaAs bonding layer and $(\text{Cs}^+, \text{O}^{-2})$ layer. Such a model is depicted in fig. 74(a). The O-GaAs layer is shown in fig. 74(a) to contain Ga-O-As=O bonding complex which is the bonding configuration proposed for oxygen adsorbed on bare GaAs(110) surfaces [28]. A $\text{Cs}^+ - \text{O}^{-2} - \text{Cs}^+$ sandwich structure is proposed for the $(\text{Cs}^+, \text{O}^{-2})$ layer; this is because O^{-2} is highly unstable (6.5 eV unstable with respect to neutral O atom) and requires positive ions on both sides to provide a large stabilizing electrostatic energy. Thickness of the individual layer is estimated in below.

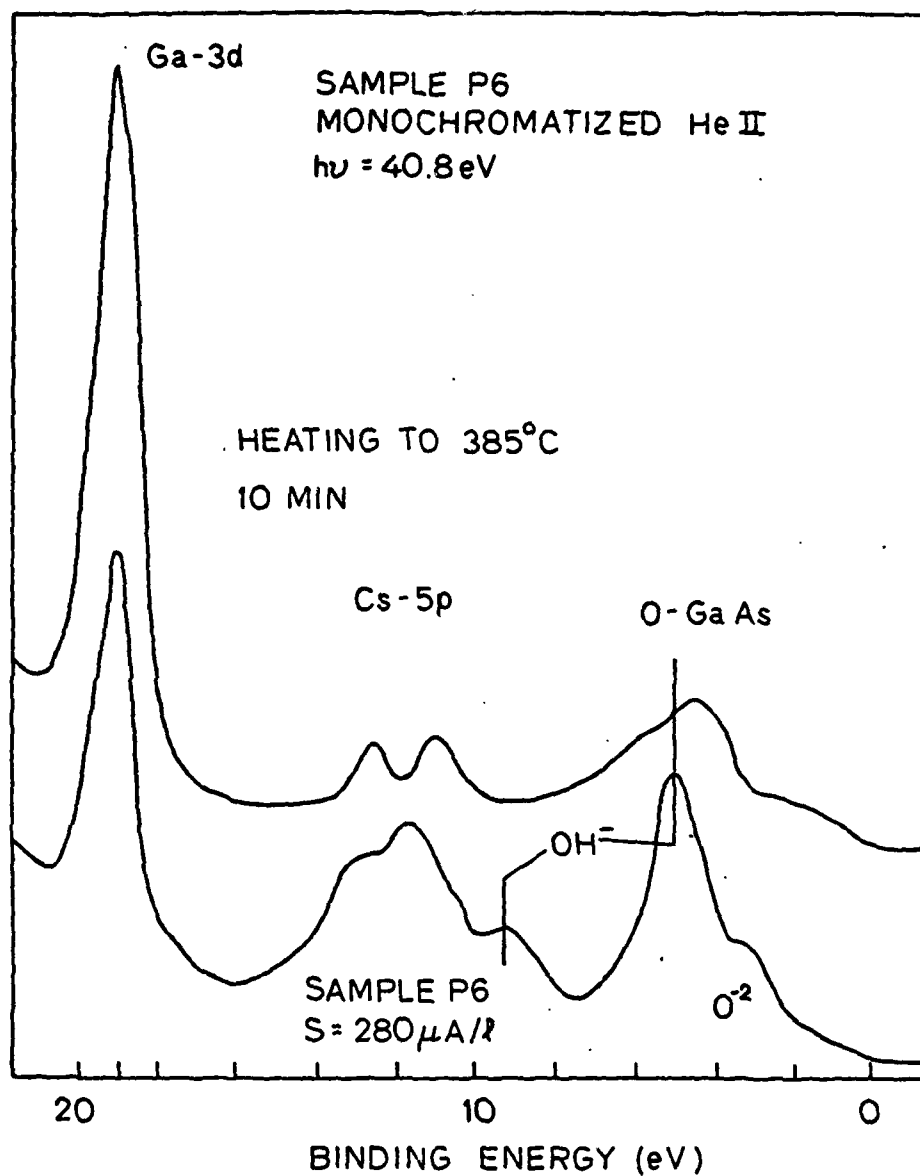


Figure 73: EDC's of an unsuccessfully activated p-GaAs(110) surface before and after heating at 385°C for 10 min.

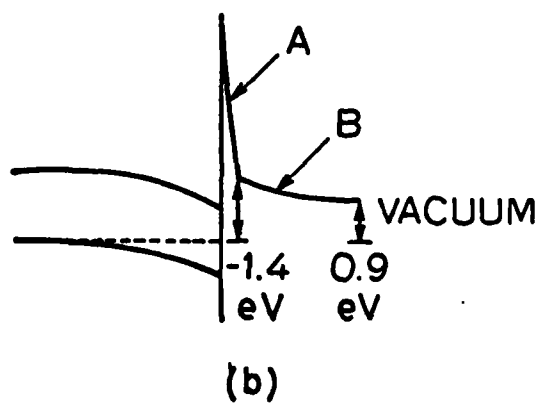
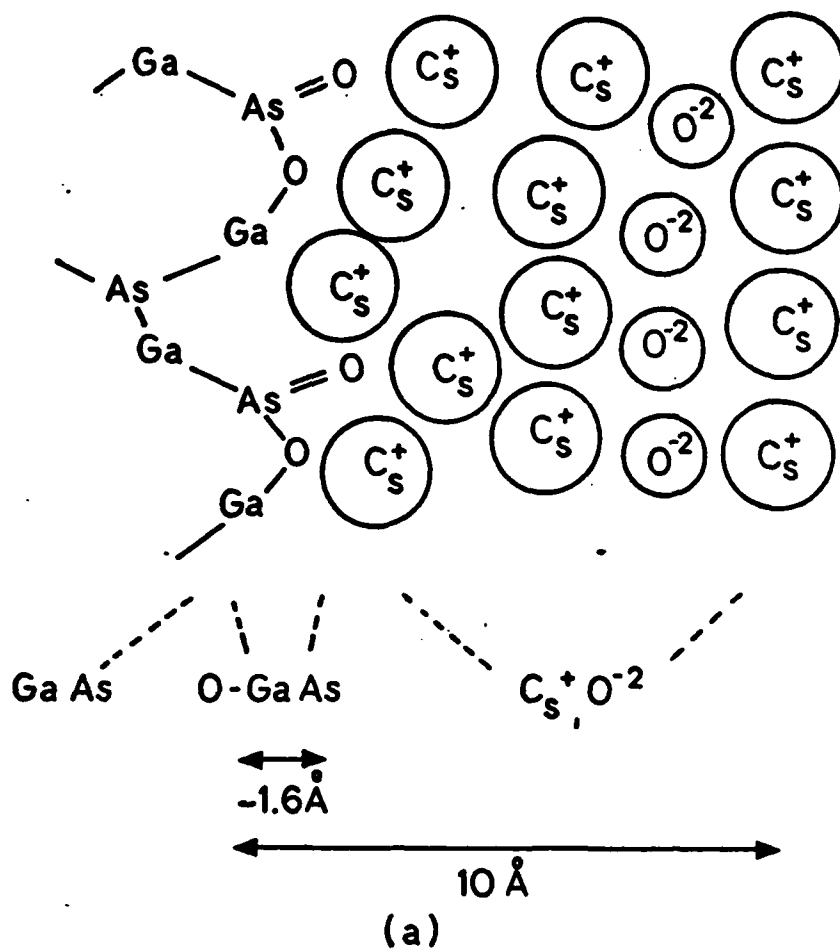


Figure 74: Structural model typical activated GaAs surfaces (a) and the corresponding potential profile (b)

Semiquantitative Estimates of the Structural and Compositional Parameters of Typical Activated Surfaces

Semi-quantitative estimates of a few structural and compositional parameters of typical activated surfaces can be done in the following ways:

- i) The thickness of the $(\text{Cs}^+, \text{O}^{2-})$ layer can be estimated from the ratio of the intensity of the Ga-3d before activation to that after activation (which has contribution from both the GaAs substrate and the O-GaAs layer). Such ratio ranges from 0.25 to 0.14 for typical activated surfaces (sensitivity $2680\mu\text{A}/1$); by assuming an escape depth of $\sim 5 \text{ \AA}$ (corrected for the geometry of the energy analyzer) for photoelectrons originated from the Ga-3d level, the thickness of the $(\text{Cs}^+, \text{O}^{2-})$ layer is found to range from $7\text{--}10 \text{ \AA}$.
- ii) The amount of Cs atoms can be estimated from the intensity of the Cs-5p levels of activated surfaces normalized to that of an oxidized monolayer Cs (i.e. a monolayer Cs on GaAs(110) exposed to 200 L oxygen). Such normalized intensity for a few typical activated surfaces studied here ranges from 1.7 to 2.3. To translate these intensities into numbers of Cs atoms, certain assumption about the structure of the $(\text{Cs}^+, \text{O}^{2-})$ layer must be made. We have assumed the sandwich structure shown in fig. 74 in which the second layer of Cs atoms are at an average distance of $\sim 6 \text{ \AA}$ away from the first layer. (This is consistent with the sandwich structure, knowing the ionic radius of O^{2-}

to be 1.45 Å and that of Cs^+ to be 1.67 Å, and the 7-10 Å overall thickness of the Cs-O overlayer.) If we assume the numbers of Cs atoms on the two sides of the O^{2-} are equal, the number of Cs atoms is estimated to be $1.6\text{--}2.3 \times 10^{15}$ atoms/cm² (3.5 to 5 equivalent monolayers one monolayer = 4.6×10^{14} atoms/cm²). If we assume that the number of Cs atoms on the GaAs side of the O^{2-} ion is twice of that on the vacuum side (for reasons to be discussed below), the number of Cs atoms is seen to be about $1.4\text{--}2.1 \times 10^{15}$ atoms/cm² (3-4.5 equivalent monolayers). As an estimate we have simply put the number of Cs to be 3-5 equivalent monolayers in fig. 74. This number is in reasonably good agreement with that measured by Sommer et. al. [11]. Sommer et. al. have also pointed out that, if we assume that the packing density of Cs^+ ions in the $(\text{Cs}^+, \text{O}^{2-})$ layer is the same as that in Cs_2O , it requires 3.7 equivalent monolayers of Cs to complete one layer of $\text{Cs}^+ \text{--} \text{O}^{2-} \text{--} \text{Cs}^+$ [11]. Our estimate of the number of Cs atoms then implies that there is at most one layer of $\text{Cs}^+ \text{--} \text{O}^{2-} \text{--} \text{Cs}^+$ in a typical activated surface, as is shown in fig. 74.

- iii) The number of O^{2-} ions is difficult to assess; nevertheless it can be seen in the crude decomposition in the lower curve of fig. 72 that the peak due to O^{2-} is at most half as intense as that due to oxygen in the O-GaAs bonding. We therefore simply put the upper limit of the number of O^{2-} ions to be half of the oxygen atoms in the O-GaAs layer; The number of oxygen atoms in the O-GaAs layer, as will be discussed below, is ≤ 1 monolayer

(one monolayer being $\sim 10^{15}$ atoms/cm² according to the bonding model proposed in reference 28), hence there are at most 5×10^{14} O⁻² ions per square centimeter. This number implies that, based on (ii) above, there are Cs in excess of that needed by a full Cs⁺-O⁻²-Cs⁺ sandwich layer.

- iv) The number of oxygen atoms in the O-GaAs layer can be determined in two ways. One way is to make the crude decompositions of the EDC's of O-2p of activated surfaces as that shown in the lower curve of fig. 72, the area under the O-2p of oxygen in O-GaAs relative that under the Ga-3d is then compared to the same quantity obtained in adsorbing oxygen on bare GaAs(110) surfaces where the oxygen coverage is relatively well known [28]. Estimates made in this way give 0.7 - 1.0 monolayer of oxygen in the O-GaAs layer for a few typical activated surfaces ($S=680 - 880 \mu A/l$) studied here. Another way of estimate is based on fig. 75, where we have shown the EDC's of a monolayer-Cs-covered GaAs(110) surface subjected to a sequence of oxygen exposure up to 10 L (dotted curves) and a GaAs(110) surface exposed to $\sim 10^{10}$ L excited oxygen. As discussed in our earlier paper [26], on a monolayer-Cs-covered GaAs(110) surface subjected to oxygen exposure smaller than 10 L, oxygen bonds only to GaAs, hence the EDC's shown in fig. 72 do not suffer from interference by emission of other oxygen species and direct comparison with the EDC of oxygen adsorbed on bare GaAs(110) is possible. In the EDC's shown in fig. 75, peak A is the non-bonding O-2p and peak B is the sp hybrid band of the GaAs substrate, hence the relative intensity of peaks A and B is a

measure of the amount of oxygen bonded to GaAs. We see that the amount of oxygen bonded to GaAs on monolayer-Cs-covered GaAs(110) at 10 L exposure is comparable to that produced by exposing bare GaAs to $\sim 10^{10}$ L excited oxygen, which was determined to be approximately 0.8 monolayer. The total oxygen exposure in our, as well as other's [4,5,10,11,21], typical activation procedure is less than 10 L; the yo-yo process applies more than one monolayer Cs to the GaAs surface and the Cs layer is capable of capturing O^{-2} , therefore, with the same oxygen exposure, the amount of oxygen bonded to GaAs is less in a yo-yo process than in the accumulative adsorption onto monolayer-Cs-covered surface. We thus put one monolayer as the upper limit for the thickness of the O-GaAs layer in typical activated surfaces.

Potential profile

As mentioned in the Introduction, an important part of understanding an activated surface is obtaining the profile of potential barrier for electron escape into vacuum. Such a profile is proposed in fig. 74(b) based on the structural information we have obtained. The most important feature of this profile is the separation of the dipole potential drop at the surface into two parts: dipole A across the O-GaAs layer and dipole B across the $Cs^{+}-O^{-2}-Cs^{+}$ layer. Dipole A can be a GaAs-O-Cs dipole in which the Cs comes from the Cs in excess of that of forming a full layer of $Cs^{+}-O^{-2}-Cs^{+}$ (point (iii)) in the "semiquantitative esti-

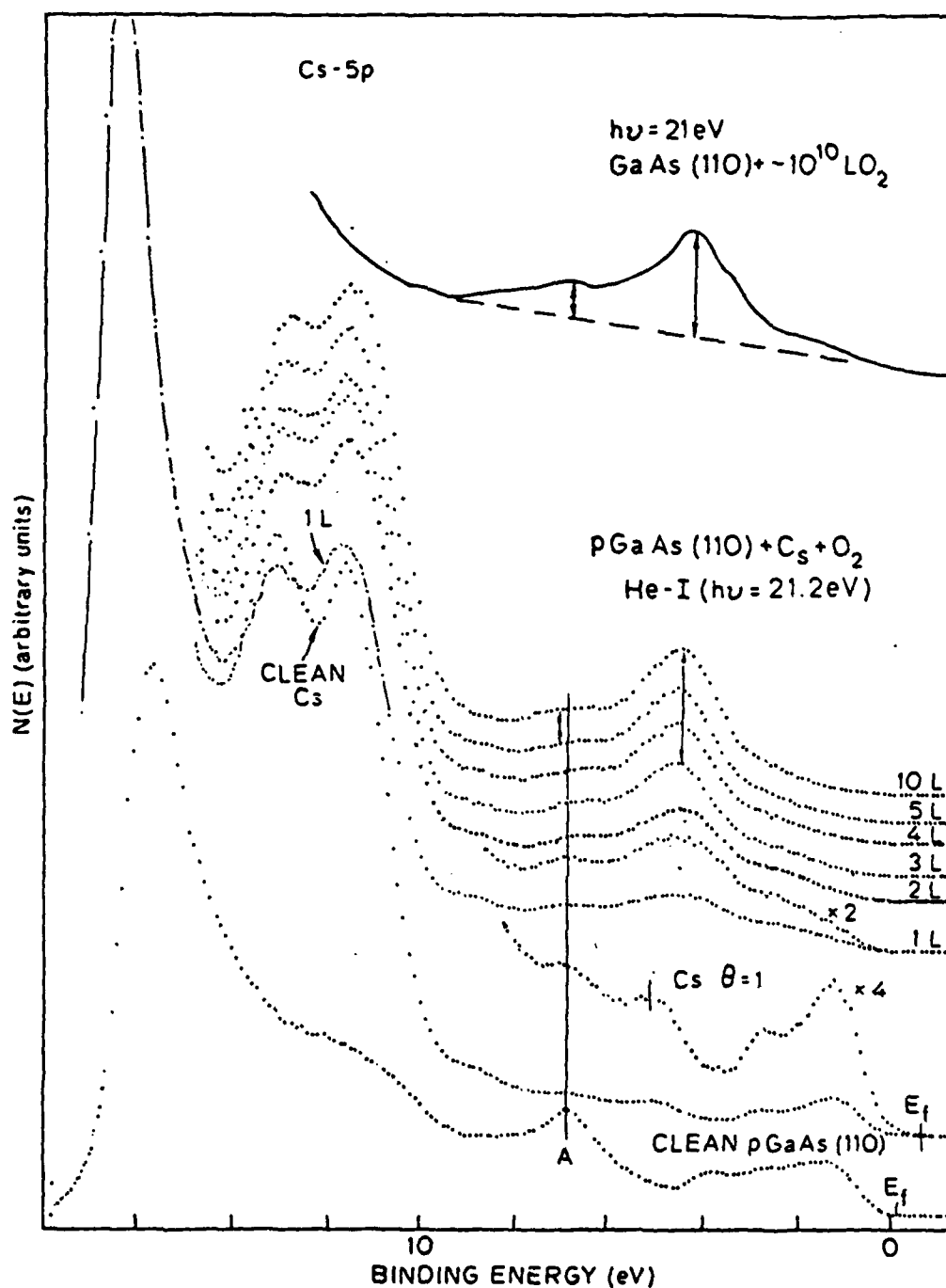


Figure 75: Comparison of the oxygen coverages using He-I spectra of a monolayer-Cs-covered GaAs surface exposed to a sequence of oxygen exposures up to 10 L and a bare GaAs surface exposed to $\sim 10^{10}$ L excited oxygen

mates"); this form of dipole A implies a $\text{GaAs-O-[Cs]-[Cs}^+\text{]-O}^{-2}\text{-Cs}^+$ overall structure (this was the reason we considered the case of a 2:1 ratio of the numbers of Cs atoms on the two sides of O^{-2} in point (ii) of the "semiquantitative estimates"). Clark, however, has argued that such a structure is thermodynamically unstable against homogenization into Cs_{2+x}O suboxide layer [19], which would then suggest a $\text{GaAs-O-(Cs}_{2+x}\text{O)}$ structure. Nevertheless the charges forming dipole A have to be supplied by excess Cs in the $(\text{Cs}^+, \text{O}^{-2})$ layer. We will use the notation $\text{GaAs-O-[Cs]:[Cs}^+\text{]-O}^{-2}\text{-Cs}$ to emphasize the existence of a GaAs-O-[Cs] dipole as far as charge distribution is concerned, but include the square brackets to indicate that [Cs] in the GaAs-O-[Cs] dipole may not be a well defined layer on top of the O-GaAs layer. We should also note that argument has been given that the Cs^+ and O^{-2} ions would favor a layer-like arrangement with Cs:Cs contact, similar to that found in Cs_2O [13]; the tendency to homogenize exists only when free electron is available in the layer as is the case for bulk cesium suboxides.

Accepting the $\text{GaAs-O-[Cs]:[Cs}^+\text{]-O}^{-2}\text{-Cs}^+$ structure, dipole B can be considered to result from a net polarization of electrons in the $[\text{Cs}^+]\text{-O}^{-2}\text{-Cs}^+$ layer toward the Cs:Cs region, as has been discussed by Fisher et. al. [13] based on the experimental finding of Tsai et. al. [31]. (Without the net polarization the $[\text{Cs}^+]\text{-O}^{-2}$ dipoles on the two sides of O^{-2} would cancel each other.) The strength of dipoles A and B cannot be determined in this work. Since the GaAs-O-[Cs] dipole is stronger than the GaAs-Cs dipole, we have assumed in fig. 74(b) that the GaAs-O-[Cs] dipole lowers the vacuum level to 11.4 eV, the cesiated work

function of p-GaAs [15], above the Fermi level. The final work function of a typical (Cs,O) activated surface is ~0.9 eV [13,15], hence the net dipole potential drop across the $[\text{Cs}^+]\text{-O}^{2-}\text{-Cs}^+$ layer is 10.4 eV.

Comparison with previous models

The model proposed above is similar to the double dipole model proposed by Fisher et. al. [13], except that barrier A is formed by the Cs-GaAs dipole in their model whereas it is formed by the Cs-O-GaAs dipole in our model. The importance of this difference is that, in the model of Fisher et. al., the width of dipole A can at most be the ionic radius of Cs (1.67 Å) and is negligible [13]. In our model the width of the dipole depends on the thickness of the O-GaAs layer and is estimated to be ~4Å (As=O bond length = 1.6 Å [28]) for typical activated surfaces which may not be completely transparent to electrons.

A double-barrier model has also been suggested by Chen [32] based on findings from the (Cs,O,W) system: the first barrier between the GaAs substrate and the (Cs,O) overlayer is proposed to be a GaAs-O-[Cs] dipole similar to our dipole A, and the second barrier between the (Cs,O) overlayer and vacuum is controlled by the band bending through a thick n-type $\text{Cs}_6\text{d}_2\text{O}$, the same as that assumed in the heterojunction model. The suggestion of the Cs-O-GaAs dipole is physically sound and is verified by this work; the thick n-type Cs_2O , however, has no physical basis in light of the present finding.

The heterojunction model was correct in predicting a barrier above the vacuum level, but since we found no evidence for the existence of a thick Cs_2O on activated surfaces, the model was wrong in identifying the

heterojunction between GaAs and Cs_2O as the interfacial barrier to electron escape. Rather, the semiconductor substrate-oxygen bonding layer is most likely to be the origin of the interfacial barrier revealed in the yield measurements.

6.4.2 Other Implications of the Model

The yo-yo process

The nature of the present model can be further illuminated by considering the conditions for obtaining optimized dipoles A and B. The first Cs treatment of the yo-yo procedure lowers the work function of p-GaAs to ~ 1.4 eV as mentioned above. The oxygen exposure followed introduces a small amount of oxygen bonded to GaAs; these oxygen atoms reduce the Cs-Cs interaction in the Cs layer [26] and increase the effective separation of a Cs^+ ion and its valence electrons residing in the GaAs substrate. The work function is thus further reduced. The reduction in work function and the increase in yield may soon slow down with increasing oxygen exposure because increased amount of oxygen in the O-GaAs bonding disorders the Cs layer which reduces the effective contribution of individual GaAs-O-[Cs] dipole. The disturbance of the Cs layer caused by the O-GaAs bonding, however, does allow higher packing density of Cs in the layer. More Cs thus can be deposited and the yo-yo process continues on. With a small amount of oxygen in the O-GaAs layer the average separation between Cs atoms and the GaAs substrate is increased, but is still small enough (within atomic radius of Cs) so that the charge transfer from the Cs to GaAs is not reduced; there is thus a net

increase in the dipole potential (charge density \times charge separation). At such small Cs-GaAs separation the degree of ionization of each Cs atom is a constant determined by the atomistic properties of Cs. At some larger Cs-GaAs separation the dipole potential drop from GaAs to the Cs layer becomes a constant, which is determined by the difference in the affinity of electrons, a macroscopic property, of the Cs layer and the GaAs substrate. In this range of Cs-GaAs separation, an increase in the thickness of the O-GaAs layer reduces the charge transferred from the Cs layer to the GaAs substrate so that the same dipole potential drop is maintained between the GaAs substrate and the Cs layer. It is advantageous to increase the O-GaAs layer thickness in such range of Cs-GaAs separation because, while maintaining the same strength for dipole A (GaAs-O-[Cs]), more O^{-2} ions can be stabilized in the $[Cs^+]-O^{-2}-Cs^+$ layer with the same number of Cs atoms due to extra electrons released from the GaAs-O-[Cs] dipole; the increased O^{-2} ions increase the polarization density of the $[Cs^+]-O^{-2}-Cs^+$ layer which in turn increases the strength of dipole B and lowers the vacuum level. A penalty in increasing the thickness of the O-GaAs, however, is soon reached because barrier A is no longer transparent to electrons.

We now recognize the weak point of the "yo-yo" technique: the GaAs-O-[Cs] (dipole A) and the $[Cs^+]-O^{-2}-Cs^+$ (dipole B) layer cannot be optimized independently. Oxygen atoms supplied by each oxygen exposure in the yo-yo process is distributed between the O-GaAs layer and the $[Cs^+]-O^{-2}-Cs^+$ layer. Such distribution is dictated by the thermodynamical properties of the system and a relative gain in yield in each Cs-O cycle, not by the requirement to obtain the absolute optimum in photoca-

thode performance. For example, at an intermediate (Cs,O) cycle of the yo-yo process Cs coverage is relatively low so that most oxygen atoms are bonded to GaAs. Further increase in the O-GaAs layer thickness at this stage does not increase the photoelectron yield, the oxygen exposure is terminated. Suppose that the next Cs treatment is just (hypothetically) enough to reverse the distribution of oxygen between the O-GaAs layer and the $[\text{Cs}^+]\text{-O}^{2-}\text{-Cs}^+$ layer so that initially most oxygen is used in forming O^{2-} in Cs, the oxygen exposure would be terminated after achieving the maximum allowable amount of O^{2-} and a "local" maximum in yield (due to a temporary saturation of the polarization through the $[\text{Cs}^+]\text{-O}^{2-}\text{-Cs}^+$ layer). Were the oxygen exposure not terminated after achieving the "local" maximum of yield, oxygen atoms would first be used in stealing Cs from the Cs-O-GaAs dipole which weakens dipole A, and would then be used in bonding to GaAs; the increase in the amount of O-GaAs bonding at the expense of a "local" maximum may be desirable in the long run due to reasons stated in the last paragraph. It is not clear, however, if the weakened dipole A may be recovered by the next Cs treatment. Therefore the pursuit of "local" maxima in photoelectron yield in a yo-yo process may leave the optimum thickness of the O-GaAs layer, which corresponds to a "global" maximum in photoelectron yield, unrealized.

The two-stage activation process

We recognize from the above discussion that the capability of forming the O-GaAs layer and the $[\text{Cs}^+]\text{-O}^{2-}\text{-Cs}^+$ layer independently is highly desirable. Such a technique indeed exist in the literature without

being well understood. As mentioned in the Introduction, to date the highest reflection yield reported on GaAs has been obtained by the two-stage activation process [22], in which a GaAs surface is first activated to have optimum yield by a normal yo-yo process and then followed by a heating to high temperature and a second yo-yo treatment. The heating after the first yo-yo process was found to desorb about 85% Cs while retaining all oxygen [21]. Clearly, the heating transfers most oxygen atoms to react with the GaAs substrate. Re-activation after the heating achieves a white light sensitivity about 1.4 times higher [21,22] than that achieved by the first activation. In light of the model discussed here, the heating prepares a relatively thick O-GaAs layer and creates a new initial point for a second (Cs,O) activation process. The activation followed the heating does not affect the O-GaAs layer. Oxygen supplied in this activation goes mostly into the Cs layer. The dipole drop across the O-GaAs layer may be equal to that achieved in the first activation, but is achieved with fewer dipole charges which enables incorporation of more O^{-2} ions with the same amount of Cs atoms. This description of the two-stage activation process is confirmed by the findings of Stocke [21] that (1) Cs and oxygen increases at an approximately equal rate (as measured by the Auger signals) after each (Cs,O) cycle in the second activation, a condition not achievable in the first activation, and (2) the total amount of Cs was found to be the same in the first and the second activation, while the total amount of oxygen was found to be higher at the end of the second activation. The successful explanation of Stocker's results in terms of our model can be regarded as strong support for the notion of an optimum O-GaAs layer.

The heating between the two stages of activation clearly improves the yield by bringing the thickness of the O-GaAs layer closer to the optimum value, but the question of, how close is unanswered at present. A systematic search of the optimum thickness of the buffer layer, by producing a wide range of oxide thickness through direct oxidation of GaAs, may therefore be of great interest for future work.

Crystallographic face dependence of the yield and the activated surfaces of narrow band gap III-V compounds

Dependence of the photoelectron yield on the crystallographic orientation of the GaAs surface has been reported [33]; the (111)B was shown to give the highest yield after activation. Part of this effect can be explained by the bulk electronic structure of GaAs: Burt and Inkson have shown that, by assuming identical potential barrier at the surface and by taking into account the Bloch nature of the wavefunction of photoexcited electrons, the transmission coefficient is twice higher on the (111)B surface than on the (111)A surface [34]. In light of the importance of the O-GaAs layer suggested by our model, part of the crystallographic face dependence could come from the different oxygen adsorption properties of the different surfaces of GaAs. The difference in adsorption property could be in the rate of adsorption, which influences the thickness of the O-GaAs layer, and/or in the O-GaAs bonding configuration, which influences the effectiveness of the orientation of the GaAs-O-[Cs] dipole.

Different spin-polarization efficiencies have also been observed on activated (110) and (100) surfaces of GaAs (Pierce, ref. 8). Again part of this difference could be explained by different channels of spin relaxation within bulk GaAs, but possible differences in the structure and composition of the activated surface due to different oxygen adsorption properties between the (110) and the (100) surfaces should not be excluded.

By the same notion of oxygen-substrate interaction, we can suggest reasons why some narrow band gap III-V compounds are difficult to activate. For example, GaSb was found to oxidize (direct formation of Ga_2O_3 and Sb_2O_3) after exposure to molecular oxygen at room temperature whereas GaAs does not [35]; it is thus possible that during the (Cs,O) treatment on GaSb surfaces thick layers of bulk oxides of Ga and Sb are formed, which are responsible for the interfacial barrier observed [15]. There may exist a general trend among III-V compounds: the narrower the band gap the easier is the oxidation and hence the more difficult is the elimination of the interfacial barrier in a yo-yo process.

Another special point to be remembered for narrow band gap III-V compounds is that dipole A, even after achieving the optimum substrate-oxygen bonding layer, may still be above the threshold set by the band gaps, optimization of dipole B then becomes very critical.

6.4.3 The Influence of OH^- on Activated Surfaces

Fig. 76 gives He-II spectra of three activated surfaces (the top solid curves) with their white-light sensitivity indicated. Peaks 2 and 3 in

the EDC's of samples P4 and P5 are much more prominent than those in the EDC of sample P3. The bottom dashed curve in fig. 76 shows the spectrum of OH⁻ on K obtained by Petersson and Karlson [36] by adsorbing H₂O on thick potassium film at liquid nitrogen temperature. (Note the He-II radiation used by Petersson and Karlson was not monochromatized, hence the peak with higher binding energy (10.9 eV below the Fermi level) in this spectrum contains excitation of the K-3p peak by the 48 eV line and thus appears stronger than it should be.) The binding energies of the two peaks in the spectrum of OH⁻ on K are at 6.7 eV and 10.9 eV below Fermi level. Both the separation and the relative intensity of the two peaks are close to those of peaks 2 and 3 in the EDC's of samples P4 and P5. We therefore conclude that serious contamination with OH had occurred in some of our activated surfaces. In contrast to the results here, no OH⁻ contamination was found in the non-activation experiments (sec. 3 and refs. 25,26); a few favorable conditions in our activation experiments for the formation of (OH)⁻ ions should be pointed out. The highest oxygen pressure used in activation experiments was 2×10^{-9} torr, whereas the lowest oxygen pressured used for the non-activation experiments was 1×10^{-8} torr. The competition from background H₂O and OH gas to react with Cs is much more severe in activation experiments than in the non-activation experiments. During the oxygen exposure, the partially open ion pump may have a high hydrogen background that can react with O₂ and deliver H₂O or OH to the main chamber. The adsorption of (OH)⁻ ions was found unavoidable on many surfaces, successfully activated or not, from three separate runs, so long as oxygen exposures were made in the way described above. It is not surprising, however, to have

successfully activated surfaces even with the presence of $(OH)^-$ ions. Uebbing and Bell [37] have demonstrated that $In_{0.11}Ga_{0.89}As$ surfaces can be activated with alternating Cs- H_2O treatment to have as good yield as, if not better than that activated with Cs- O cycles. Because we expect H_2O to decompose into OH and O, the surfaces activated by Cs and H_2O should contain a mixture of OH^- and O^{-2} , similar to the activated surfaces contaminated with OH in this work. A more general discussion of the use of CsOH as a low work function coating has been given by Uebbing and James [15]. Although unintended, the adsorption of OH under our experimental condition was controllable in the sense that the partial pressure of OH was decreased and increased together with the partial pressure of O_2 according to the white light sensitivity monitored during the yo-yo process. Adsorption of OH from the residual gas after the completion of the activation is also possible and is uncontrollable, and hence may have different effect on the photoelectron yield which will be seen below. We note that ion pumping and $\sim 10^{-10}$ torr base pressure, similar to our experimental conditions, have been the environment of fabricating many practical photocathodes, hence the problem of OH "contamination" facing us here should be of general concern.

The most obvious correlation of differences in the EDC's in fig. 76 to differences in white-light sensitivity appears to be the relative height of the OH peak and the O^{-2} peak. The amount of OH is clearly smallest on sample P3 which has the highest white-light-sensitivity. This, however, does not imply the amount of O^{-2} should be arbitrarily high in order to have high yield. The only place a strong O^{-2} peak was obtained was by overcesiating at each Cs- O cycle, i.e., by peaking the

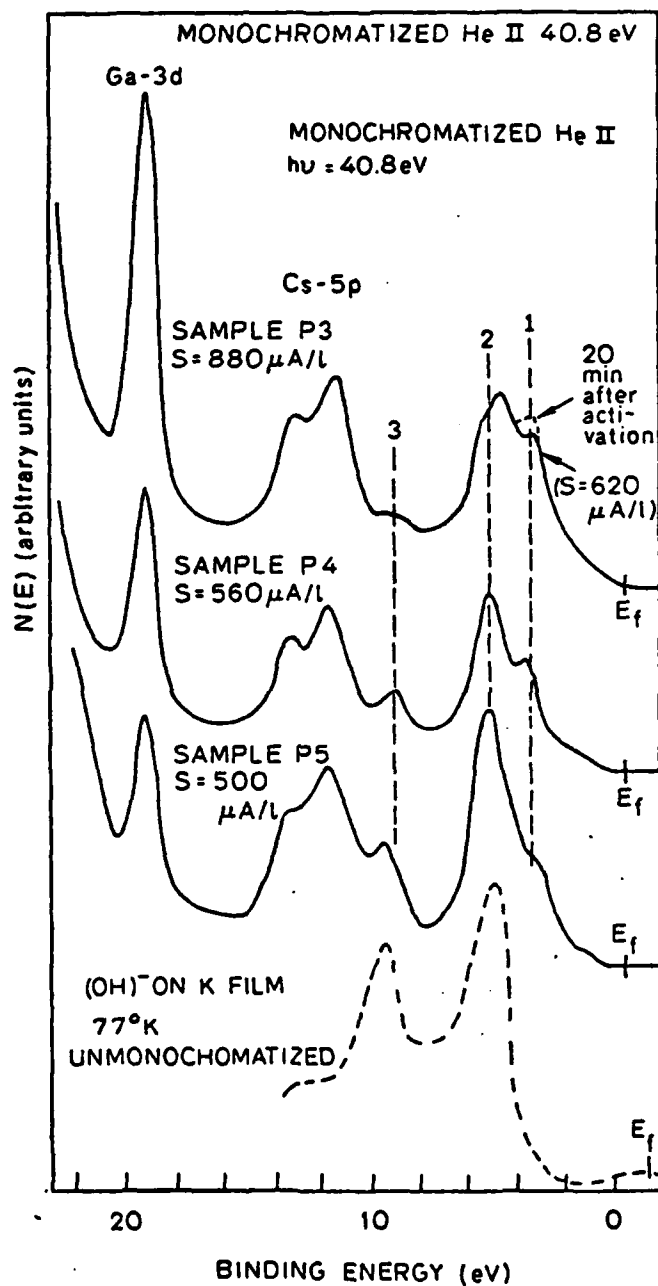


Figure 76: EDC's of three p-GaAs surfaces activated to different white light sensitivity, $h\nu = 40.8 \text{ eV}$ (He-II). The bottom dashed curve shows the spectrum of OH^- on K film for comparison.

white light sensitivity with oxygen but continuing the Cs flux beyond the peak sensitivity point until the sensitivity dropped more than 60% of the peak sensitivity. A thick (Cs,O) layer with very low white light sensitivity resulted from such treatment, as evidenced by the barely visible Ga-3d level in the spectra of fig. 77. Assuming an escape depth of $\sim 5 \text{ \AA}$ in the (Cs,O) overlayer for photoelectrons from the Ga-3d level, the thickness of the (Cs,O) overlayer is estimated to be of the order of 20 \AA . The white light sensitivity was very low at the end of this treatment and the OH peaks are seen to be weaker than the O^{-2} peak. As this surface was aged in vacuum, the OH peaks grew and the white light sensitivity increased, opposite to the trend seen in fig. 76. Part of the increase in yield can be attributed to the deduction in metallic character of the overlayer by the incorporation of OH ions: Right after the treatment, the overlayer is Cs rich as evidenced by the rather strong tailing emission on the high binding energy side of the $5p_{1/2}$ level (bottom curve, fig. 77). Electron scattering is strong in metal, hence a thick overlayer with metallic character results in a significant loss in the number of photoelectrons escaping from GaAs. Increasing the ionic character of the overlayer therefore enhances the yield. The other part of the increase in yield comes from the lowering of the surface work function: In fig. 77 we see the O^{-2} peak shift to higher binding energy (from 2.2 eV below VBM to 2.7 eV below VBM, or from 2.7 eV below the Fermi level to 3.2 eV below the Fermi level) as the amount of OH is increased. The Cs-5p levels also show a shift in the same direction, although the magnitude of shift is smaller. According to the model we developed in our early work [26], this shift indicates an

increase in the dipole potential drop across the region of the overlayer containing the O^{-2} ions. We interpret the initially broad O^{-2} peak as due to O^{-2} ions distributed throughout the overlayer, similar to the situation of O^{-2} in bulk cesium suboxide (and this is the reason the initial BE of the $O-2p$ peak is the same as that found in the oxidation of bulk Cs [27] and standard bulk suboxides [24]). The adsorption of OH forces O^{-2} ions to be confined within one or two outer layers which give an effective $[Cs^{+}]-O^{-2}-Cs^{+}$ dipole contribution to the lowering of the surface work function. The fact that the mild heating at $85^{\circ}C$ for 3 minutes (top curve, fig. 77) gave the largest increase in white-light-sensitivity appears to support the importance rearranging O^{-2} ions in enhancing the yield. Even after the undesirable thick, Cs rich suboxide is replaced by ionic CsOH layer and a $[Cs^{+}]-O^{-2}-Cs^{+}$ dipole is provided at the outer surface, the white-light sensitivity is still far below that expected for the NEA condition ($2400 \mu A/l$). The thickness of the overlayer in this case is of the order of that discussed for either a CsOH or a Cs_2O overlayer in the heterojunction model [15]. Such thickness is considered inappropriate based on the present results.

A case of contrast is given in fig. 78. When sample P5 was aged in vacuum overnight, the O^{-2} peak disappeared completely and the white light sensitivity dropped by a factor of 10. The overlayer is clearly thinner than that on sample P6 (fig. 77) both before and after aging, but the white-light sensitivity is only comparable to that of sample P6 after mild heating (top curve, fig. 77). We therefore conclude that O^{-2} is essential for achieving good yield. The OH ion is useful in "neutralizing" excess Cs and providing an ionic low work function coating on

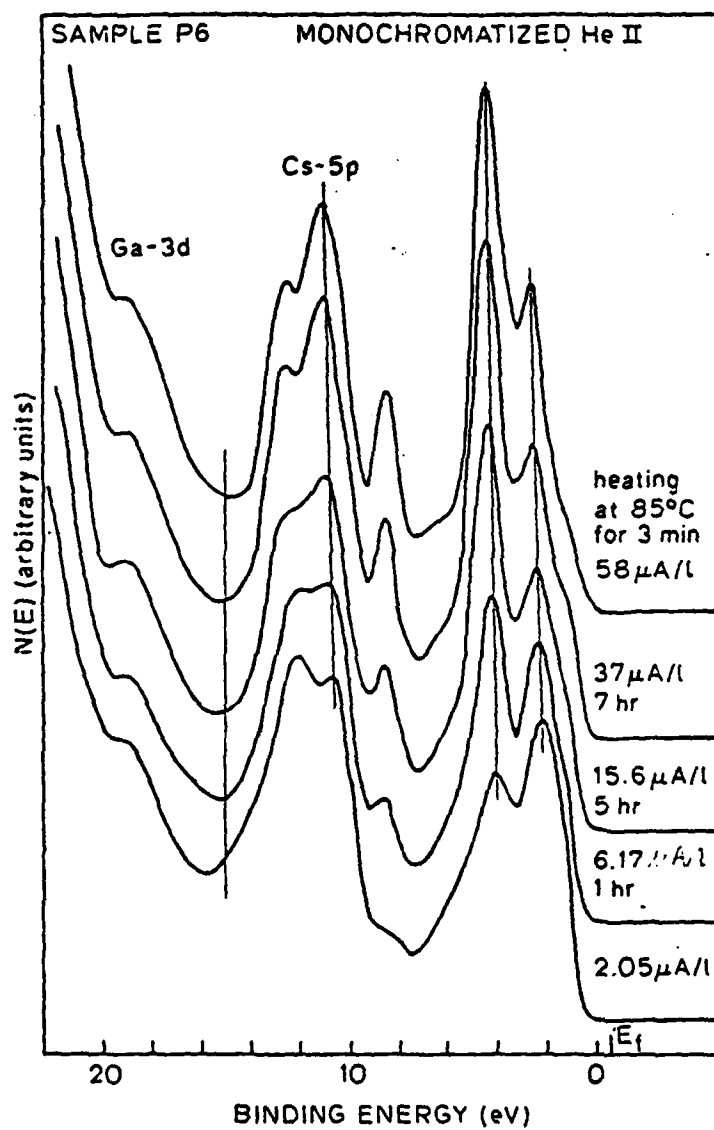


Figure 77: Evolution of a thick (Cs, O, OH) overlayer on sample P6 in ultra high vacuum as recorded in He-II photoemission spectra.

GaAs surfaces, but CsOH layer does not offer the polarizability the $[\text{Cs}^+]\text{-O}^{2-}\text{-Cs}^+$ layer possesses. (This is because OH^- does not favor a layer-like arrangement with Cs^+ whereas O^{2-} favors a layer-like arrangement with Cs^+ , for example, in Cs_2O) Over adsorption of $(\text{OH})^-$ ions at the expense of O^{2-} ions is therefore one of the degradation mechanisms of an activated surface.

The replacement of O^{2-} by OH in the Cs layer is also expected from considerations of heats of formation. In tabel 13, we listed the heats of reaction of OH with Cs, Cs_3O and Cs_2O . CsOH is clearly more stable than any of the O^{2-} containing compounds; OH will eventually replace all oxygen in the Cs layer over a long time.

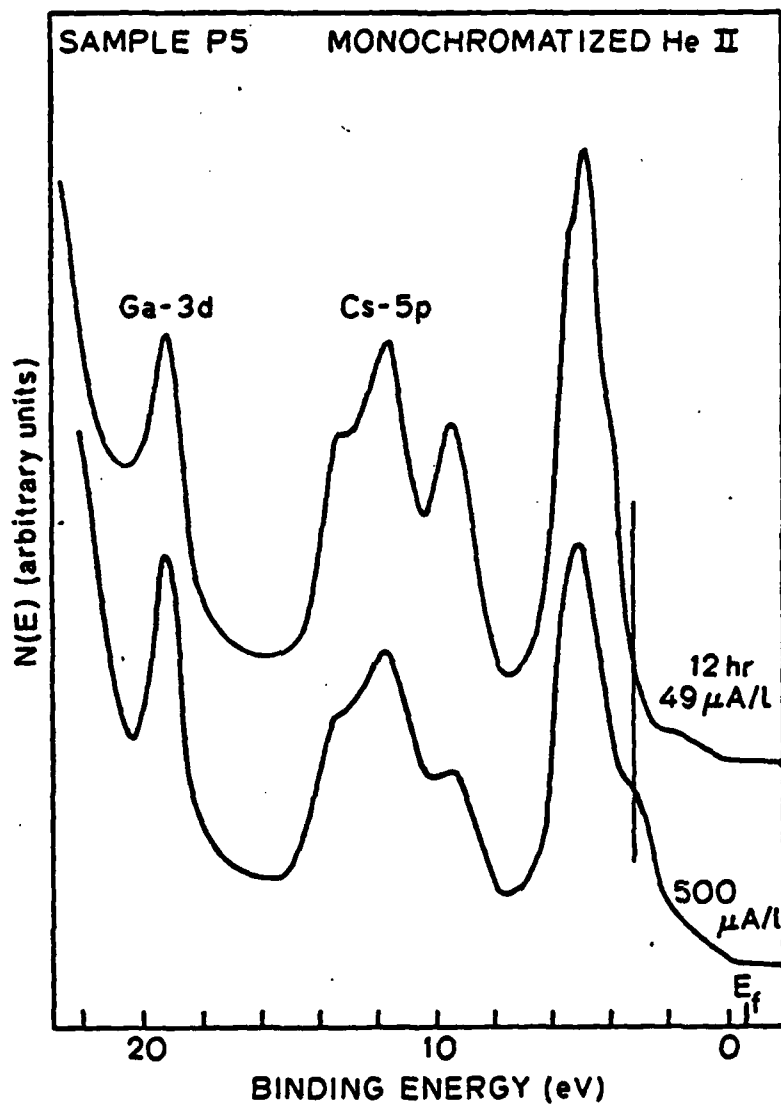


Figure 78: Overnight degradation of an activated surface as recorded in He-II photoemission spectra.

TABLE 13

Heats of formation of OH compounds

Reactions	$-\Delta H(\text{kcal/mole})^\dagger$
$\text{Cs} + \text{OH} \rightarrow \text{CsOH}$	97
$\text{Cs}_2\text{O} + \text{OH} \rightarrow \text{Cs}_2\text{O} + \text{CsOH}$	88
$2 \text{Cs}_2\text{O} + 2 \text{OH} \rightarrow \text{Cs}_2\text{O}_2 + 2 \text{CsOH}$	141
† Ref. 38	

6.5 CONCLUSION

In conclusion, we have established a physical model for GaAs surfaces activated with (Cs,O) yo-yo treatment, based on photoelectron spectroscopic measurements made on such surfaces. Two dipole layers, a GaAs-O-[Cs] layer and a $[\text{Cs}^+]\text{-O}^{-2}\text{-Cs}^+$ layer, are found in the model to contribute to the lowering of work function on activated surfaces. The identification of a layer of oxygen bonded to GaAs greatly clarifies the physical nature of the "interfacial" barrier to electron escape observed in earlier yield measurements. The failure of a normal yo-yo procedure to optimize the O-GaAs layer at the same time it forms the (Cs,O) layer is considered as a drawback of this activation technique. The two-stage activation procedure is shown to improve the yield of a photocathode by preparing the O-GaAs layer and the $(\text{Cs}^+, \text{O}^{-2})$ layer separately. The findings of this work indicate that a systematic search of the optimum O-GaAs layer with the aid of surface characterization tools, such as the photoelectron spectroscopic technique used here, will be of great value; extension of such work to III-V compounds with bandgaps narrower

than GaAs is especially crucial to the future photocathode technology utilizing those materials.

REFERENCES

1. J. J. Sheer and J. van Laar, Solid State Commun. 3, 189(1965)
2. A. A. Turnbull and G. B. Evans, Brit. J. Appl. Phys. 1, 155(1968)
3. W. E. Spicer, Appl. Phys. 12, 115(1977)
4. D. G. Fisher, R. E. Enstrom, J. S. Esher, H. F. Gossenberger, J. R. Appert, IEEE Trans. Electr. Devices, ED21, 641(1974) and references therein
5. L. W. James, G. A. Antypas, J. J. Uebbing, T. O. Yep, and R. L. Bell, J. Appl. Phys. 42, 580(1971) and references therein.
6. R. L. Bell Negative Electron Affinity Devices (Clarendon, Oxford, 1973)
7. G. A. Antypas and J. Edgecombe, Appl. Phys. Lett. 37(1975)
8. M. E. Erbudak and B. Reihl, Appl. Phys. Lett. 33, 584(1978); D. T. Pierce, G. C. Wang and R. J. Celotta, Appl. Phys. Lett. 35, 220(1979)
9. W. E. Spicer, Phys. Rev. 112, 114(1958); C. N. Berglund and W. E. Spicer, Phys. Rev. 136, A1030(1964)
10. L. W. James, J. L. Moll, and W. E. Spicer, Inst. Phys. Conf. Ser. 7, 230(1968)
11. A. H. Sommer, H. H. Whitaker, and B. F. Williams, Appl. Phys. Lett. 17, 273(1970)
12. B. F. Williams and J. J. Tietjen, Proc. IEEE 59, 1489(1971)
13. D. G. Fisher, R. E. Enstrom, J. S. Esher, and B. F. Williams, J. Appl. Phys. 43, 3815(1972)
14. H. Sonnenberg, Appl. Phys. Lett. 14, 239(1969)
15. J. J. Uebbing and L. W. James, J. Appl. Phys. 41, 4505(1970)
16. A. F. Milton and A. D. Baer, J. Appl. Phys. 42, 5095(1971)
17. L. W. James and J. J. Uebbing, Appl. Phys. Lett. 16, 370(1971)

18. J. S. Esher, R. D. Fairman, G. A. Antypas, R. Sankaran, L. W. James and R. L. Bell, CRC Crit. Rev. Solid State. Phys. p. 577 (1975); R. Sahai, J. S. Harris, R. C. Eden, L. O. Bubulac and J. C. Chu, CRC. Crit. Rev. Solid State Phys., p.565 (November, 1975) D. G. Fisher, R. E. Enstrom and B. F. Williams, Appl. Phys Lett. 18, 371(1971)
19. M. G. Clark, J. Appl. Phys. D: Appl. Phys. 8, 535(1975)
20. B. Goldstein, Surf. Sci. 47, 143(1975); B. Goldstein and D. J. Szostak, Appl. Phys. Lett. 26, 111(1975)
21. B. J. Stocker, Surf. Sci. 47, 501(1975)
22. G. H. Olsen, D. J. Szostak, T. J. Zamerowski, and M. Ettenberg, J. Appl. Phys. 48, 1007(1977)
23. P. E. Gregory and W. E. Spicer, J. Appl. Phys. 47, 510(1976)
24. G. Ebbinghaus, W. Braum, A. Simon and K. Berresheim, Phys. Rev. Lett. 37, 1770(1976)
25. W. E. Spicer, I. Lindau, C. Y. Su, P. W. Chye, and P. Pianetta, Appl. Phys. Lett. 33, 934(1978); C. Y. Su, P. W. Chye, P. Pianetta, I. Lindau and W. E. Spicer, Surf. Sci. 86, 894(1979)
26. see Chapter V
27. see Chapter III
28. see Chapter III
29. A. Simon, in Structure and Bonding 36, pp. 31(Springler, N. Y., 1979)
30. A. Kahn, D. Kanani, P. Mark, P. W. Chye, C. Y. Su, I. Lindau and W. E. Spicer, Surf. Sci. 87, 325(1979)
31. K.-R. Tsai, P. M. Harris and E. N. Lassetre, J. Phys. Chem. 60, 338(1956)
32. J. M. Chen, Surf. Sci. 25, 457(1971)
33. L. W. James, G. A. Antypas, J. Edgecumbe, R. L. Moon and R. L. Bell, J. Appl. Phys. 42, 4976(1971)
34. M. G. Burt and J. C. Inkson, Appl. Phys. Lett. 28, 5(1976)
35. P. Pianetta, I. Lindau, C. M. Garner, and W. E. Spicer, Phys. Rev. B 18, 2792(1978);
36. P. E. Gregory and W. E. Spicer, Phys. Rev. B 12, 2370(1975)
37. G. Ebbinghaus, W. Braun, A. Simon, and K. Berresheim

38. G. W. Gobeli and F. G. Allen, chap. 11 in Semiconductors and Semimetals vol. 2, Academic Press, 1966
39. L.-G. Petersson and S. E. Karlsson, Physica Scripta 16, 425(1977)
40. J. J. Uebbing and R. L. Bell, Proc. IEEE, p.1264 (Sept. 1968)
41. O. Kubaschewski and C. B. Alcock, Metallurgical Thermochemistry, 5th ed., Pergmon Press, N. Y., 1979

Chapter VII

CONCLUSIONS: LOOKING AHEAD

The major conclusions of this dissertation have been given in the summary section of each chapter. Therefore we will not re-iterate these conclusions in this final chapter. Instead, we will discuss possible extensions of this work based on the findings given in the preceding chapters.

7.1 ADSORPTION OF OXYGEN ON SI AND GAAS SURFACES

Chapters II and III are concerned with the adsorption of oxygen on Si and GaAs surfaces. The major effort of this work has been to determine the oxygen-semiconductor bonding configuration. To do so, we have heavily relied on the interpretation of the density of valence states. One limitation in those interpretations is that in angle-integrated photoemission spectrum the bonding band is broad and overlaps with substantially with the non-bonding band (see Chapter III) which make comparison with theoretical calculations a prohibitive task. Use of polarized synchrotron radiation in conjunction with angle-resolved photoelectron analyzer will overcome this problem. For example, if oxygen is in a bridge bonding configuration, say, Ga-O-As, the bonding band should split into a σ and a π component, such splitting is not resolved in angle-integrated photoemission measurements; in an angle integrated measurement, however, by choosing the polarization of the synchrotron radiation par-

allel with or perpendicular to the GaAs surface, the π or the σ component could be preferentially enhanced. Parameters such as the σ - π splitting can thus be obtained and readily compared to theoretical values.

Another interesting suggestion raised by the results of this dissertation is that dissociation of molecular oxygen on semiconductor surfaces does not necessarily occur through interaction with defect sites on the surface. Such suggestions were inferred from the bonding configuration determined. There are other possible sources of dissociated oxygen atom which may involve different energetics and thus lead to different oxygen-semiconductor bonding configurations. Comparative studies made on such systems may provide very important information for both the dissociation mechanism and the bonding configuration of adsorbing molecular oxygen on semiconductor surfaces. A few alternative sources providing different oxygen species are listed below:

- i) O_3 , the energy (0.7 eV) required to dissociate O_3 into O_2 and O is lower than that required to dissociate O_2 (4.6 eV).
- ii) N_2O . The complication could arise from adsorbing N_2O on either Si or GaAs is the possible interaction of nitrogen with the semiconductor surfaces. On Si surfaces, however, nitridation of Si is itself a subject of great practical significance.
- iii) Illumination of GaAs or Si surfaces with UV light (use, for example, mercury lamp) during oxygen exposure. The light energy should be just enough to excite electrons from semicon-

ductor into vacuum, and it should also be close to that required to excite singlet molecular oxygen. The combined effect of the formation of the singlet state and the charge transfer from semiconductor could lead to a charged singlet which will easily fragment into atomic oxygen.

7.2 THE (Cs,O) ACTIVATED GAAS SURFACES

In the area of (Cs,O) activated GaAs, the major inroad to be made is obvious. In this work we have only characterized activated surfaces prepared by conventional techniques. The finding of the existence of the O-GaAs bonding layer suggests that the activation layer should be systematically synthesized to achieve optimum structure and composition. The capability to characterize the activation layer with surface analytical tools, such as the photoelectron spectroscopic techniques used in this work, is essential to the search for optimum O-GaAs layer and (Cs⁺,O⁻²) layer. One weak point in the present work is that the As-3d level, which gives the best indication of the O-GaAs bonding, was not included in the measurements of the activated surfaces. Inclusion of the As-3d level by using 100 ~ 120 eV synchrotron radiation is highly desirable in future work. Measurement of the yield vs. photon energy of a activated surface in addition to the white light sensitivity would also add to the characterization capability.

Extension of the present studies to other surfaces of GaAs, as well as other narrow band gap III-V compounds, is important from an applica-

tion point of view. Investigation of the spin polarization efficiency of activated surfaces should also be considered, due to a potentially large demand for sources of spin-polarized electrons from many different branches of scientific activities.